UNIVERSITY OF CALIFORNIA
RIVERSIDE

Impact of Emission Control Systems and Alternative Fuels on Off-Road and On-Road Internal Combustion Engines

A Dissertation submitted in partial satisfaction
of the requirements for the degree of

Doctor of Philosophy

in

Mechanical Engineering

by

Cavan McCaffery

March 2021

Dissertation Committee:

Dr. Georgios Karavalakis, Co-Chairperson
Dr. Heejung Jung, Co-Chairperson
Dr. Roya Bahreini
Dr. Alex Greaney

The Dissertation of Cavan McCaffery is approved:

_____

_____

_____

Committee Co-Chairperson

_____

Committee Co-Chairperson

University of California, Riverside

Acknowledgements

I would like to thank many individuals for making this dissertation possible. I would like to thank my advisors Dr. Georgios Karavalakis and Dr. Heejung Jung for their support and guidance throughout my Ph.D. program. I would like to show my appreciation and gratitude to Dr. Georgios Karavalakis, Dr. Thomas Durbin, and Dr. Kent Johnson for giving me the opportunity to join the emissions and fuel research group at CECERT, providing financial support to make it possible for me to continue my education, and for being the best mentors I could have asked for. I would like to thank Dr. Roya Bahreini and Dr. Alexander Greaney for their participation in my final dissertation committee. I want to thank Dr. Wayne Miller for his help and guidance throughout my PhD.

I would also like to thank the team members of the emissions and fuels research group including Mr. Mark Villela, Mr. Daniel Gomez, Mr. Kurt Bumiller, Mr Daniel Sandez, Mr. Victor Olivares Moran and Mr. Andrew McCaffery for their help with various light-duty, heavy-duty, marine, and PEMS tests. I want to show my appreciation to my close team members for all their support Dr. Chengguo Li, Dr. Weihan Peng, Mr. Hanwei Zhu, Mr. Tianbo Tang, Mr. Ma Tiany, Mr. Qi Li, and Mr. Tom Eckel. I would also like to thank former graduate students Dr. Jiacheng (Joey) Yang and Dr. Yu Jiang for their mentorship. I would also like to thank previous undergraduates Mr. Taymour Mohammed, Mr. Brian Estrada, Mr. Daniel Zaragoza, Mr. Miguel Robledo, Mr. Nathaniel Wilde, Ms. Grace Johnson, and Mr. Franklin Ippolito for all their contributions to the studies.

I want to show gratitude to Southern California Air Quality Management District (SCAQMD), California Air Resources Board (CARB), Coordinating Research Council

(CRC), the California Energy Commission (CEC), Southern California Gas Company (SoCalGas), and Manufacturers of Emissions Controls Association (MECA) for their financial support. I would like to thank MECA for providing the catalyzed GPFs for studies and for their technical support and guidance. I want to thank Neste Corporation for providing the HVO fuel for parts of this thesis. I also want to thank Pegasor Oy for providing in-kind the Pegasor MI3 unit to obtain PM mass and number emissions.

The text of Chapter 2 of this dissertation, in part, is reprinted from SAE Technical Paper Series; Cavan McCaffery, Georgios Karavalakis, Thomas D. Durbin, Heejung Jung and Kent C. Johnson; Engine-Out Emissions Characteristics of a Light Duty Vehicle Operating on a Hydrogenated Vegetable Oil Renewable Diesel, Copyright (2020), with permission from SAE.

The text of Chapter 4 of this dissertation, in part, is reprinted from Science of the total Environment, Vol. 710; Cavan McCaffery, Hanwei Zhu, Chengguo Li, Thomas D. Durbin, Kent C. Johnson, Heejung Jung, Rasto Brenzy, Michael Geller, and Georgios Karavalakis; On-Road Gaseous and Particulate Emissions from GDI Vehicles with and without Gasoline Particulate Filters (GPFs) Using Portable Emissions Measurements Systems (PEMS), Copyright (2020), with permission from Elsevier.

The text of Chapter 7 of this dissertation, in part, is reprinted from Atmospheric Environment, Vol. 245; Cavan McCaffery, Hanwei Zhu, Georgios Karavalakis, Thomas D. Durbin, J. Wayne Miller, and Kent C. Johnson; Sources of Air Pollutants from a Tier 2 Ocean-Going Container Vessel: Main Engine, Auxiliary Engine, and Auxiliary Boiler, Copyright (2021), with permission from Elsevier.

Dedication

I would like to dedicate this work to my parents Drew and Donna McCaffery, my brothers Shane McCaffery, Justin McCaffery, and Chance McCaffery, my sister Meaghan McCaffery, all my nieces and nephews, and my girlfriend Celina Nguyen for their endless love and support throughout the entire duration of my academic career.

Abstract of the Dissertation

Impact of Emission Control Systems and Alternative Fuels on Off-Road and On-Road Internal Combustion Engines

by

Cavan McCaffery

Doctor of Philosophy, Graduate Program in Mechanical Engineering
University of California, Riverside, March 2021
Dr. Georgios Karavalakis, Co-Chairperson
Dr. Heejung Jung, Co-Chairperson

Internal combustion engines (ICEs) represent one of the largest sources of emissions leading to air pollution in the united states. Emissions from ICEs pose large concerns due to human health and environmental effects, but they can be controlled. This dissertation is an investigation into the pollutants emitted from ICEs for a range of applications and the usefulness of available emission control strategies and different fuel sources. The range of ICEs includes small off-road diesel engines, light duty gasoline and diesel engines, heavy duty diesel and alternative fuel engines, and large marine engines. The control technologies included gasoline particulate filters (GPFs), selective catalytic reduction (SCR), and diesel particulate filters (DPFs), and the alternative fuels included hydrogenated vegetable oil (HVO), biodiesel HVO fuel blends, natural gas (NG), liquefied petroleum gas (LPG), diesel-electric hybrids, marine gas oil (MGO) and ultra-low sulfur heavy fuel oil (ULSHFO).

As renewable fuel sources gain more attention for their ability to reduce the overall greenhouse gas impacts of ICEs, it is important to fully understand the emissions of new renewable fuel sources. This dissertation provides an investigation into the fuel impacts and engine impacts of a second-generation biofuel, HVO, and fuel blends of HVO and biodiesel in light duty and heavy-duty diesel engines. This dissertation also investigates the toxicity of pollutants from heavy duty diesel engines utilizing HVO and HVO biodiesel fuel blends.

Laboratory testing follows standardized and repeatable procedures that allow emissions of different models of vehicles to be compared to each other. In real-world driving however, there are many variables that can affect emissions which cannot be reproduced in a laboratory. For this reason, it is important to investigate and understand the emissions during real world driving. This dissertation provides an investigation into emissions formations of light duty gasoline direct injection (GDI) engines and heavy-duty vehicles during real world driving.

Off-road engines represent one of the largest sources of PM and NOx in California and nationwide. This dissertation investigated large ocean-going vessels (OGVs) utilizing two fuels and the feasibility of applying new stringent standards to small off-road diesel engines (SORDEs).

Table of Contents

List of Figures

List of Tables

1. Introduction

It has been over a century since the first internal combustion engine (ICE) was developed. Since then, constant improvements have paved the way to the implementation of ICE engines worldwide from small to large sizes. Today, ICEs represent the most prominent sources of power generation in the transportation sector, with compression and spark ignition engines utilizing diesel and gasoline fuel being the most popular. It is estimated that there are over 2 billion ICEs currently deployed in ground transportation and freight shipping (Heywood, 2018). The need for gasoline and diesel engines is expected to grow in coming years with some projections showing the demand growing 20% by 2040 (ExxonMobil, 2019).

Due to the widespread adoption of ICEs, the impacts of emissions have been amplified. ICEs are known to have a large environmental impact, representing one of the largest sources of particulate matter (PM), nitrogen oxides (NOx), and carbon dioxide (CO_2) in the United States (U.S.) (United States Environmental Protection Agency [EPA], 2020). Greenhouse gas emissions, such as CO_2, have been a high priority for reductions for regulatory agencies as greenhouse gas (GHG) emissions are known to effect global climate change. One way to reduce CO_2 is to make engines more efficient and use a smaller amount of fuel to create the same amount of power. Gasoline direct injection (GDI) engines have become a prominent engine technology for spark ignited engines due to the fuel savings and higher efficiencies when compared to more traditional port fueled injection (PFI) engines (Alkidas, 2007). One major drawback of GDI engines is the reduce amount of time

for mixing inside the combustion chamber, which can lead to increased formation of other pollutants such as PM (Karavalakis et al., 2015).

PM is a large concern when utilizing ICEs due to non-homogenous mixing leading to fuel rich areas during combustion in GDI and diesel engines (Heywood, 2018). The majority of PM emitted is classified as PM2.5, or PM with an aerodynamic diameter of less than 2.5 μm. PM2.5 can have long lasting health effects on humans and animals, as the small aerodynamic diameter particles can penetrate deeper into the lungs. This can lead to chronic illnesses such as cardiopulmonary diseases and lung cancer (Feng et al., 2016). In California and nationwide, PM2.5 is classified as a toxic air pollutant and there are many restrictions limiting the amount of PM2.5 emissions from mobile sources.

Another large concern for ICEs is the formation of NOx during the combustion phase due to high temperatures and pressures. NOx is formed when nitrogen and oxygen present in air are dissociated by high in-cylinder combustion temperatures. NOx has been a pollutant of high concern for California due to its harmful health effects as well as its ability to react with volatile organic compounds (VOCs) to form harmful tropospheric ozone (Sillman, 1999). This is a primary concern for densely populated areas such as the Los Angeles (LA) metropolitan area and New York where they are often in non-attainment for healthy ozone standards. Diesel engines typically emit more NOx than spark ignited engines due to the higher compression ratios leading to higher in-cylinder temperatures and less pathways for NOx to reduce once formed. Diesel and gasoline fueled engines represent about 77% of the U.S. transportation sector energy use, so it is imperative for reductions in these areas

to meet attainment for ozone standards (United States Energy Information Association (EIA), 2020).

This dissertation provides an evaluation and investigation of newer aftertreatment technologies and fuel sources in order to understand the best available strategies to reduce pollution formation and GHG emissions. Hydrogenated Vegetable Oil (HVO) is a second-generation biodiesel that has potential to reduce NOx emissions when compared to typical biodiesel but needs to be studied in more depth to understand engine impacts and unregulated pollutant formation in both light duty and heavy-duty diesel vehicles. Real-world driving emissions have also become a very important topic as real-world driving conditions can greatly change pollutant formation when compared to laboratory verification tests. As of now, small off-road diesel engines are certified to more lenient emissions standards and either do not require the use of aftertreatment systems or utilize less extensive aftertreatment system. However, with newer technology aftertreatment systems becoming more prominent, it may be feasible to apply to more stringent standards and regulations to these smaller engines that could promote more extensive use of aftertreatment for that category. Shipping emissions are generally accepted to be one of the largest sources of pollution in the world, but newer fuel types have the ability to greatly reduce the impact that these ocean-going vessels have on the environment. The rest of this introduction provides background to each of the main thesis topics and the last section provides a look into each of the thesis chapters.

1.1 Investigation of Emissions and In-Cylinder Characteristics of a Light-Duty Diesel Vehicle Utilizing Hydrogenated Vegetable Oil

Biodiesel is produced through a process called transesterification which processes vegetable oils into fatty acid methyl ester (FAME). Another way to process vegetable oil is to remove the oxygen from the structure and hydrogenate the double bonds in the triglyceride molecule. This is a popular pathway to produce HVO (also known as renewable diesel), which is a second-generation biofuel that could address the stability problems associated with conventional biodiesel described above. Similar to biodiesel, HVO is derived from vegetable oils, animal fats, waste cooking oils, and forest/biomass residues. A catalytic hydrogenation process converts triglycerides into alkanes by hydro-deoxygenation. Isomerization may also be incorporated to improve the low temperature operability or cold flow properties. HVO properties, including high cetane number, narrow distillation, high heating value on a mass basis, low aromatics, ultra-low sulfur content, and excellent oxidation stability, collectively contribute to lower emissions and better engine performance (Erkkila et al., 2011; Gomez et al., 2016; Rantanen et al., 2005; Singh et al., 2018).

A number of studies have shown that the use of neat or blended HVO with diesel fuel can reduce gaseous and particulate emissions compared to regular diesel and biodiesel fuels (Singer et al., 2015; Lehto et al., 2011; Bhardwaj et al., 2013; Na et al., 2015; No et al., 2014). Pflaum et al. (2010) reported that HVO can reduce particulate matter (PM) emissions up to 50% compared to diesel fuel due to the absence of aromatics, when using

a 2-liter, 4-cylinder diesel engine and a vehicle with the same engine over the New European Driving Cycle. They also found reductions in both total hydrocarbon (THC) and carbon monoxide (CO) emissions with HVO compared to diesel, but no significant variations in NOx emissions. Wu et al. (2017) tested HVO fuel and regular diesel using a Euro 5 direct injection diesel engine equipped with exhaust gas recirculation (EGR), an integrated diesel oxidation catalyst (DOC), and a diesel particle filter (DPF) aftertreatment system. They found significantly lower (50% or more) particle number emissions from HVO at a sampling location upstream of the exhaust aftertreatment system (engine out) due to no aromatics. They also showed lower THC and NO emissions with the HVO compared to diesel. The ignition delay of the HVO was shorter than the diesel fuel at lower engine speeds because of the high cetane number of HVO. Omari et al. (2017) showed that HVO as a drop-in fuel will likely result in an increased volumetric fuel consumption of about 2% due to the lower density of HVO. They also showed that NOx emissions were comparable to diesel, but CO, THC, and PM emissions were reduced by more than 50%. Bohl et al. (2018) showed no reductions in NOx emissions with HVO, but reductions in particle number emissions. They also showed lower CO and THC emissions with HVO due to better fuel-air mixing, absence of aromatics, and low boiling range components of HVO compared to diesel fuel.

With the expectation of the widespread employment of low carbon fuels, such as HVO, for Tier 3 type of vehicles, this study aims to characterize the engine-out gaseous and particulate emissions from a light-duty diesel truck operated on neat HVO and ULSD. The vehicle was exercised over the LA-92 driving cycle using a chassis dynamometer.

Additional testing was conducted over steady-state conditions at 30 miles per hour (mph) and 50 mph on different loads.

1.2 Evaluation of Heavy-Duty Diesel Engines Utilizing Renewable Diesel and Renewable Diesel/Biodiesel Blends

FAME are the most widely used biofuel used for diesel engines and it commonly referred to as Biodiesel (EIA 2020). biodiesel fuels are created through a process called transesterification. In this process feedstock triglycerides are mixed with methanol and introduced to an acidic catalyst. The glycerol is separated from the fatty acids and the fatty acids then react with the alcohol to form fatty acid methyl esters. Many studies have investigated the influence of biodiesel on engine performance, combustion, and emissions (Knothe et al., 2005; Mueller et al., 2009; Lapureta et al., 2007; Ozener et al., 2012; Qi et al., 2010). Biodiesel can provide several benefits over typical petroleum derived ULSD such as decreased PM emissions and superior lubricity (Knothe et al., 2005; Waynick, 2005; Ozener er al., 2012). However, Biodiesel does have many drawbacks as evidenced by several literature reviews of over 100 studies in biodiesel concluding that NOx formation increases while using biodiesel (Szybist et al., 2007; Xue et al., 2011; Basha et al., 2009). Mueller et al., (2009), showed that biodiesel NOx increases can be attributed to a longer residence times, higher peak temperatures, and air fuel ratios closer to stoichiometry. In addition to NOx increases, biodiesel faces storage stability issues and is susceptible to oxidation and fuel degradation (Waynick, 2005). These major issues have led to the need for finding another alternative fuel source that address the issues put forth

by biodiesel. Hydrogenated vegetable oil (HVO), also known as renewable diesel, is a second generation biofuel used in compression engines and is gaining popularity due to its improved cold temperature performance and increased storage stability compared to biodesiel and PM and NOx benefits compared to ULSD (Singh et al., 2018; Ogunkoya et al., 2015).

Although there are many studies characterizing combustion performance and emissions of HVO and biodiesel, there is a lack of literature on the emissions characterization of HVO-biodiesel fuel blend. In addition, the characterization of toxic pollutants from these fuel blends is limited and needs to be expanded. The purpose of this study is to further evaluate emissions and performance effects resulting for the use of renewable diesel and renewable diesel/biodiesel blends relative to CARB diesel in off-road legacy diesel engines and in new technology on-road diesel engines. Four fuels were utilized in this study including, neat CARB ULSD, neat renewable diesel (R100), and two renewable diesel-biodiesel blends of 65% renewable diesel and 35% biodiesel (R65/B35) and 50% renewable diesel and 50% biodiesel (R50/B50). Additional toxic emissions sampling was performed in addition to regulated pollutants.

1.3 Investigation of GPF Reduction Efficiency of GDI Engines During Real-World Driving

The share of GDI engines has grown rapidly in both the US and the EU. GDI technology enables both an increase in specific power and a better fuel economy (with simultaneous reduction in CO_2 emissions), compared to traditional PFI engines (Alkidas, 2007). However, GDI engines are known to produce higher PM mass, black carbon, and particle number emissions than PFI engines and modern technology diesel engines equipped with DPFs (Karavalakis et al., 2015; Saliba et al., 2017; Zinola et al., 2016). PM formation in GDI engines is due to partially evaporated liquid fuel leading to fuel rich regions in the combustion chamber that promote the generation of PM (Karlsson and Heywood, 2001; Piock et al., 2011). Studies have shown that most GDI PM emissions are formed during the cold-start phase and during highly transient operations (Chen et al., 2017; Koczak et al., 2016). The dynamic market penetration of GDI engines along with their elevated PM emissions create a growing public health concern in terms of PM exposures in urban areas. Concerns about the real-world performance of vehicles and the lack of real-world operation represented in chassis dynamometer tests are now being addressed with test protocols capable of characterizing real-world vehicle emissions. Portable emissions measurement systems (PEMS) have been widely used to measure vehicle gaseous and particulate emissions under real-world conditions (Weiss et al., 2011; Gallus et al., 2016; Kwon et al., 2017; Yang et al., 2018a). PEMS have proven to be an important tool for emission inventories because they enable testing under a wide variety of driving conditions,

including road gradients, altitude and environmental conditions variations, and strong accelerations (Zhang et al., 2019; Bishop et al., 2019; O'Driscoll et al., 2018). In the U.S., PEMS measurements are required for in-use compliance testing of heavy-duty diesel vehicles, while the EU has implemented PEMS-based type-approval testing for light-duty vehicles starting from the Euro 6 standards. Overall, previous work has shown that there are substantial differences in emissions measured on-road using PEMS compared to laboratory testing (May et al., 2014; Chossière et al., 2018; Fontaras et al., 2017; Andersson et al., 2014). Automotive manufacturers put considerable effort into developing engine maps that allow the vehicles to pass certification test cycles, but this may have side effects where vehicles will emit more emissions during on-road driving. A number of studies have been conducted on different types of vehicles using PEMS, including heavy-duty trucks (Mendoza-Villafuerte et al., 2017; Johnson et al., 2009) and light-duty diesel and gasoline cars (Valverde et al., 2019; Khan and Frey, 2018), and off-road equipment (Cao et al., 2016; Cao et al., 2018). Gallus et al. (2017) found CO_2 and NOx emissions were strongly correlated with driving parameters, showing increases with road grade. Wang et al. (2018) reported increases in CO, NOx, and particle number emissions at elevated altitude. Other PEMS studies have shown that real-world NOx and particulate emissions are affected by fuel type, aftertreatment control, and engine power (Quiros et al., 2016; Huang et al., 2013; Demuynck et al., 2017).

The introduction of more challenging test procedures, such as real driving emissions (RDE) for type approval in the EU, as well as stricter emission standards, such as the California LEV III PM mass limit of 1 mg/mile beginning in 2025 and the Euro 6a particle number

limit of 6×10^{11} particles/km, make the reductions in target pollutants more difficult to be met with engine improvements alone. While stricter solid particle number regulations in the EU may have led to the introduction of gasoline particulate filters (GPFs) in the passenger car fleet there, at this time it is not expected that GPFs will be widely adopted in the U.S. in the near term. Several studies have reported that the use of GPFs resulted in dramatic reductions in PM mass, number, and black carbon emissions from GDI vehicles (Yang et al., 2018b; Araji and Stokes, 2019). A recent study even showed that the use of catalyzed GPFs can reduce secondary organic aerosol formation (Roth et al., 2019). In addition, studies have shown reductions in particulate emissions and improved conversion efficiencies for CO and NOx emissions with the use of catalyzed GPFs under real-world conditions with minimal impact on CO_2 emissions (Schoenhaber et al., 2017; Yoshioka et al., 2019). Demuynck et al. (2017) investigated the deployment of GPFs on GDI vehicles using PEMS and found significant reductions in particle number emissions under RDE conditions. A similar study also showed reductions in particle number emissions with the use of GPFs, without any detectable increase in CO_2 emissions (Ogata et al., 2017).

The primary objective of this study was to improve our understanding of the particulate emissions from three current technology GDI light-duty vehicles under different driving conditions mimicking urban, rural, and highway driving patterns, and included changes in altitude, road grade, and environmental conditions. Emissions testing was conducted on two vehicles in the stock configuration as well as after replacing the OEM underfloor three-way catalyst (TWC) with a catalyzed GPF. The catalyst formulation on the GPF was typical of an underfloor catalyst on vehicles of the same class, however, no attempt was made to

exactly match the GPF catalyst formulation with that on the stock underfloor converter. Furthermore, the mileage accumulated on the GPF was not matched with the mileage of the TWC that it replaced. Therefore, the gaseous emissions are provided as observations for the purpose of relative comparison and are not intended to draw absolute conclusions. The results of this study will be useful in understanding real-world emissions from GDI vehicles and their contribution to air pollution in the Los Angeles Basin and other urban areas.

1.4 Investigation of NOx Emissions from Heavy-Duty Vehicles During Real-World Driving

In a response to the stricter emission standards for heavy-duty vehicles, engine and aftertreatment manufacturers introduced selective catalytic reduction (SCR) technology for reducing tailpipe NOx for 2010 and newer vehicles. SCR technology uses an aqueous urea solution, which hydrolyzes to ammonia (NH_3), leading to the conversion of NOx into nitrogen and water over a catalyst (Piumetti et al., 2015; Guan et al., 2014). NOx conversion is highly dependent on the catalyst temperature and therefore fairly sensitive to the operating conditions of the engine, as well as on catalyst material and urea dosing strategy. It has been demonstrated that at low load and low speed urban driving conditions tailpipe NOx emissions usually increase due to the reduced conversion efficiency of the SCR catalyst (Jiang et al., 2018; Sowman et al., 2018; Zhang et al., 2014). Thiruvengadam et al. (2015) showed elevated NOx emissions at exhaust temperatures below 250 °C when they tested heavy-duty diesel trucks equipped with SCR over the local and near-dock

drayage driving cycles in a chassis dynamometer. Misra et al. (2013) also found elevated NOx emissions during driving conditions where the SCR temperature was below its light-off operating range and during cold-starts.

An additional effort to lower NOx emissions from on-road heavy-duty vehicles in the transportation sector is the widespread use of natural gas-powered engines, and in particular the development of ultra-low NOx natural gas engines, capable of achieving 0.02 g/bhp-hr of NOx emissions (Zhu et al., 2020; Li et al., 2019). Stoichiometric natural gas engines are equipped with three-way catalysts (TWC) that control NOx, CO, and THC emissions. Previous studies have demonstrated NOx emissions reductions with stoichiometric natural gas engines compared to SCR-equipped diesel engines (Yoon et al., 2013; Quiros et al., 2016; Thiruvengadam et al., 2015). A recent study has shown dramatic reductions in NOx emissions from two ultra-low NOx natural gas heavy-duty vehicles when operated on different test cycles, concluding that the use of these engines in captive fleets and goods movement vehicles will contribute to the alleviation of ground-level smog formation (Zhu et al., 2020).

Controlling NOx emissions from heavy-duty vehicles remains a significant challenge, especially during real-world driving conditions. Heavy-duty engines are certified under controlled laboratory conditions over an engine dynamometer and using the Federal Test Procedure (FTP) cycle and the Supplemental Emissions Test (SET). Heavy-duty vehicles should also meet the in-use not-to-exceed (NTE) standard that controls NOx emissions under real-world, high-speed cruise operation (as specified in CFR Title 40 Parts 86 and

1065). Several studies have shown that NOx emissions measured from heavy-duty vehicles can significantly differ in real-world conditions compared to laboratory certification testing (Misra et al., 2017; Anenberg et al., 2017; Quiros et al., 2016; Dixit et al., 2017; Wu et al., 2012). Conditions such as urban driving, stop-and-go traffic, excessive idling, and low load/low speed operation can all affect SCR efficiency and tailpipe NOx (Yoon et al., 2017; Grigoratos et al., 2019; Mendoza-Villafuerte et al., 2017; Kotz et al., 2016).

For this study, in-use NOx emissions were measured from 50 heavy-duty vehicles of different vocations, engine type, and aftertreatment controls using portable emissions measurement systems (PEMS). This study is part of a larger and more comprehensive testing campaign executed in the South Coast Air Basin (SCAB) in the great LA area that included about 200 in-use heavy-duty vehicles tested for emissions under in-use conditions and on a chassis dynamometer, and monitored for activity. The goal was to better characterize and understand in-use NOx emissions that will affect efforts to meet future ambient ozone goals in SCAB and elsewhere, to identify technology benefits/shortfalls for a range in vehicles technologies in different vocations, and to provide information that can be used to guide future research and development initiatives, to develop future regulations and to improve emissions inventory estimates. The full study represents one of the largest studies of in-use emission rates of heavy-duty vehicles to date, and is being used as a key basis for the development of the next generation CARB's Emission Factor (EMFAC) model. Results are discussed as a function of engine technology, vocation, aftertreatment control, and emissions certification level.

1.5 Evaluation of Small Off-Road Diesel Engines and Aftertreatment Systems

The existing standard for Tier 4 off-road engines was developed based on a Regulatory Impact Analysis (RIA) conducted in 2004 (U.S. EPA, 2004). Emissions control strategies such as DPF and SCR were implemented into these standards, but to a lesser degree for smaller engines. PM and NOx aftertreatment was not widely implemented at this time, as such, there was considerable uncertainty as to how viable such aftertreatment devices would be for smaller sized engines. Hence, the adopted compliance standards were designed to be met without using aftertreatment controls for NOx emissions below 75 horsepower (hp) or for PM emissions below 25 hp. This left an important gap in the existing emissions regulations, as engines under 25 hp represented 18% of off-road engines sales, while engines from 25 to 75 hp represented 38% of engine sales back in the timeframe of the Tier 4 off-road regulations were developed (U.S. EPA, 2004). Since aftertreatment control devices for diesel vehicles and diesel-powered equipment are considerably more common now, the use of these strategies for small off-road diesel engines (SORDEs) may be considerably more viable than when the standards were last updated, which could warrant renewed consideration for adopting more stringent exhaust standards for these engines.

The application of DPF and SCR technologies to SORDEs is faced with several challenges. It is important that the aftertreatment systems can be maintained at a sufficiently high temperature to effectively reduce PM and NOx emissions, and to prevent the systems from

increasing backpressure. For example, SCR performance largely depends on exhaust temperature to ensure adequate SCR activity and NOx emissions reductions (Guan et al., 2014; Koebel et al., 2000). These conditions are usually achieved under high engine load/speed operation, where exhaust temperatures are high enough for NOx conversion (Jiang et al., 2018; Misra et al., 2013). This could be problematic in applications where the engines are operating under lower loads or idle conditions for long periods of time. Packaging and positioning are also important considerations, as the amount of space available for the engine and aftertreatment system on SORDE equipment can be very constrained, and the positioning of the catalyst can influence overall efficiencies (Blakeman et al., 2001). It is also important to fully understand the extent to which such aftertreatment systems will deteriorate in terms of emissions benefits or create additional engine wear over the course of the engine's useful life. Degradation of the aftertreatment performance can be impacted by different mechanisms, including thermal aging, sintering, and thermal collapse (Praveena et al., 2018). Williams et al. (2013) showed that SCR and DPF performance can be affected by impurities in the fuel deactivating catalytic sites on the wash coat of the SCR and DPF substrate. Sulfur and ash (trace metals) have also been shown to act as a catalytic inhibitor on aftertreatment systems (Zhao et al, 2009). These mechanisms can lead to decreased efficiencies and increased operational costs for the fleet when repairs are necessary. While some work to characterize the potential benefits and limitations of aftertreatment for smaller off-road engines, there are still many uncertainties as to how effective and practical such systems might be in real world applications.

This project was part of a larger study to evaluate the potential effectiveness, feasibility, and cost-effectiveness of implementing regulations on mobile off-road diesel engines with rated powers of less than 75 hp (i.e., 56 kW [kilowatt]) that could be achieved using advanced emission control strategies, such as DPFs and SCR. This project included a comprehensive review of available aftertreatment and other technologies, demonstration of selected aftertreatment technologies on actual engines, verification of the emissions performance of these devices through a series of emissions and durability tests, evaluation of the potential impacts of additional emissions controls on the emissions inventory, and evaluation of the cost implications of the added emissions control strategies. The focus of this thesis chapter is on the durability emissions testing results, and the emissions and cost benefit analysis. The information from this study could provide the background for a future round of more stringent emissions regulations for SORDE's, as these engines remain an important part of the emissions inventory.

1.6 Emissions Evaluation of Modern Ocean-Going Vessels on Modern Fuels

Ship emissions are influenced by several factors, including ship operation and fuel type. Different operations and speeds have different power requirements and hence different emission profiles. Ships maneuvering in port areas require slow speeds and transient operation, where engine loads may rapidly change. During cruising conditions on the open sea, the main engines are usually operating at intermediate loads, whereas typically low loads are applied when the ship is maneuvering in the port. Studies have shown that gaseous

and particulate emissions are highly dependent on engine operation, with engine load variations affecting combustion conditions and pollutant formation (Petzold et al., 2010; Hountalas et al., 2014; Zhang et al., 2016; Khan et al., 2012a). Chu-Van et al. (2018) found elevated emission factors of CO, THC, PM, and particle number during maneuvering at a port of a large bulk carrier compared to cruising conditions. Agrawal et al. (2008) showed higher NOx emissions when they tested an oceangoing container vessel at low speed and low load conditions compared to intermediate engine load at normal cruise speed. Khan et al. (2012b) also showed higher CO and SO_2 emissions at low engine loads from a Tier 1 large container vessel, but lower PM mass emissions at low engine loads.

Fuel type and composition are also important factors in gaseous and particulate emissions formation. Heavy fuel oil (HFO) contains residues and distillates from the fuel refining process, such as sulfur, aromatics, and metals, and is mainly used in the main engines used for propulsion. Significant improvements on fuel quality have been made with the aim to reduce emissions from ships, with fuel switching capabilities when entering Sulfur Emission Control Area (SECA) regions being the most important. A number of studies have shown that switching from HFO to marine gas oil (MGO), a middle distillate fuel used in auxiliary and main engines, could potentially result in lower gaseous and particulate emissions (Moldanova et al., 2013; Browning et al., 2012; Mueller et al., 2015; Khan et al., 2012). Gysel et al. (2017) tested an oceangoing vessel operating within ECAs on a novel low-sulfur heavy fuel oil (LSHFO) and a distillate ECA MGO fuel. They found higher NOx emissions with MGO than LSHFO, and higher PM and particle number emissions with LSHFO than MGO. Zetterdahl et al. (2016) found lower emissions of SO_2,

PM mass, total volatile organic compounds (VOCs), and polycyclic aromatic hydrocarbons (PAHs) from switching between HFO and distillate fuels on a ship operating in a SECA. Reda et al. (2015) showed increases in carbonyl emissions with HFO compared to a SECA diesel fuel using a single-cylinder diesel research engine, with formaldehyde and heavier carbonyls being predominant in the emissions of HFO. Similarly, Wu et al. (2018) showed higher PM and PAH emissions, as well as higher oxidative activity and cytotoxicity with HFO compared to diesel fuel when they tested emissions from a container ship.

In addition to main and auxiliary engines, ship emissions are also generated from boilers used for the production of hot water and steam, but in lower concentrations (Chen et al., 2017). Boilers are typically used when at berth or operating on low main engine loads to meet demands for heating on board (Zenczak, 2013; Starcrest, 2011). Unlike the main and auxiliary engines, regulations applicable to ship boilers are less restrictive, with ship boiler emissions being indirectly regulating by restricting the fuel sulfur content when used in ports and SECA regions. Hulskotte and Denier van der Gon, (2010) showed that while at-berth the majority of the fuel use oceangoing vessels, tankers, and container ships is in boilers. Additionally, they showed lower emission factors from boilers compared to reciprocating combustion engines. Agrawal et al. (2008b) investigated the emissions of an auxiliary boiler powered by HFO on a crude oil tanker operating at sea. They found PM and NOx emissions were lower in an auxiliary boiler compared to the main engine, while acetaldehyde was the primary carbonyl in the auxiliary boiler. Cooper, (2003) also showed lower NOx, THC, SO_2, and PAH emissions from boiler use compared to the main or auxiliary engines. Yau et al. (2012) also showed that boilers generally contribute less than

5% of the NOx, PM, and SO_2 emissions from oceangoing vessels in Hong Kong when compared to main and auxiliary engines.

As highlighted above, the body of literature on ship emissions characterization is rich and has primarily focused on older technology engines when operated on fuels with relatively high sulfur contents. The present study focuses on the characterization of gaseous and particulate emissions from a modern Tier 2 oceangoing vessel operating on a new generation ultra-low sulfur HFO suitable for use in SECAs. For the main engine, emissions were measured on-board for both fuels while the vessel was cruising from the Port of Long Beach to the Port of Oakland in California. For the auxiliary engine and the auxiliary boiler, emissions were measured on a very low sulfur MGO and a novel ultra-low sulfur (HFO) for both fuels while the vessel was at-berth at the Port of Long Beach and during loading and unloading cargo. In addition to the Tier 2 OGV, emissions were also characterized from the auxiliary boiler of a modern Panamax tanker. The results of this study are discussed as a function of fuel type and engine operation conditions.

1.7 Outline of Dissertation

Chapter 2 presents an investigation into the engine out emissions characteristics and combustion analysis of a light duty diesel vehicle utilizing hydrogenated vegetable oil renewable diesel. The experimental results showed reductions in engine-out THC and CO emissions with HVO over the LA-92 cycle at a statistically significant level. Engine-out hot-running and weighted NOx emissions also showed statistically significant reductions with HVO compared to ULSD. CO_2 emissions and carbon balance fuel economy did not

show any significant differences between the test fuels. The small differences in fuel economy suggest that modern light-duty diesel vehicles are not calibrated to account for the differences in fuel properties when operated with neat HVO. Engine-out PM mass, soot mass, and solid particle number emissions showed large, statistically significant reductions with HVO fuel compared to ULSD, which can be attributed to the absence of sulfur and aromatic soot precursors in the HVO. For the steady-state conditions, THC emissions were lower with the use of HVO, while CO emissions showed mixed results. Engine-out NOx emissions did not show big differences between the test fuels for the low and partial points; but at 100% load, the use of HVO resulted in noticeable NOx increases compared to ULSD. In general, the chemical composition of HVO appeared relevant with respect to gaseous and particulate engine-out emissions over transient testing (i.e., LA-92 cycle), but not always for the steady-state conditions. These phenomena can be explained by the fact that the engine was equipped with a common rail system in which the physical properties of fuels had little influence on injection timing, and also the fluidity of HVO is close to petroleum diesel resulting in little differences in injection properties. HVO showed lower peak temperatures and pressures compared to ULSD. The higher cetane number of HVO also lead to shorter ignition delays, and in some cases the need for a double pilot injection at high loads. This study suggests the potential benefits of utilizing HVO in light duty diesel vehicles.

Chapter 3 presents an investigation into the physical and chemical characteristics of gaseous and particulate emissions from a heavy-duty on-road and a heavy-duty off-road diesel engine utilizing renewable diesel and renewable diesel biodiesel blends. Testing was

conducted using an engine dynamometer and 4 different test cycles. Results show that the use of renewable diesel has the potential to reduce NOx, CO, THC, PM, and PN from older engines with no aftertreatment systems. The use of DOCs and DPFs masks the fuel effects of CO, THC and PM differences for the newer technology on-road engine. The use of renewable-biodiesel blends still showed NOx penalties for both engines, however. PM2.5 and PN in general showed reductions with increasing biodiesel. Carbonyls, monoaromatic VOCs, and PAHs also showed reductions while using renewable diesel and increasing biodiesel blends due to the more complete combustion of these fuels. As such, the ozone forming potential is generally reduced with increasing use of renewable diesel and renewable diesel biodiesel blends.

Chapter 4 presents an investigation of the on-road gaseous and particulate emissions from GDI vehicles with and without GPFs. Testing was conducted on 3 different current technology GDI vehicles on four test routes in the greater LA Basin and San Diego representing urban, rural, highway, and high-altitude driving patterns. Results revealed significant reductions in soot mass and solid particle number emissions with the catalyzed GPFs. Mountainous driving showed elevated PM emissions compared to driving on relatively flat roads. The highest PM emissions were seen for the urban routes where public exposure is highest. For all test routes, the highest soot mass and particle number emissions were recorded for the low and intermediate speed bins and high acceleration events. NOx emissions were lower with the catalyzed GPFs due to the additional catalytic volume compared to the original configuration, suggesting additional NOx reductions in real-driving conditions. Unlike NOx, CO emissions did not show any benefits with the GPFs.

Emissions of CO_2 were found to be a function of engine size and were greater for the urban routes, as well as for the uphill segment. The use of GPFs did not show a statistically significant penalty in CO_2 emissions and fuel economy during real-world operation.

Chapter 5 presents an investigation into the real-world NOx emissions from heavy-duty diesel, alternative fuels, and diesel electric hybrids using PEMS on California roadways. Testing was conducted on 50 heavy-duty vehicles from different vocations and engine technologies. Emissions testing included school buses, transit buses, refuse haulers, goods movement, and delivery vehicles equipped with diesel engines with and without SCR, CNG and LPG engines, as well as diesel electric hybrid powertrains. This information will significantly add to the body of literature available on in-use emission rates of different heavy-duty vehicle types and is being used as a basis for the development of the next generation EMFAC model. Our results showed reductions in real-world NOx emissions as the emission standards tightened, but generally higher NOx emissions compared to the FTP certification standards for each engine category. On average, in-use NOx emissions exceeded the FTP certification standards by 80%, 21%, 66%, 44%, and 34%, respectively, for the 0.2 diesel, 0.2 CNG, 0.02 CNG, 0.2 diesel hybrid electric, and 0.14 LPG vehicles. Overall, the certification NOx emissions alone were not an accurate predictor for the real-world NOx emissions, independent of vehicle vocation or engine technology. The results showed the potential benefits of different advanced technology vehicles, suggesting that a range of technologies could play an important role in meeting air quality targets in California and elsewhere. CNG-powered vehicles showed considerably lower average in-use NOx emissions, with reductions of 75% and 94%, respectively, for 0.2 and 0.02

certified CNG engines compared to their diesel counterparts. Newer LPG vehicles in the delivery vehicle category also showed solid NOx reductions compared to diesel vehicles, with average brake-specific NOx reductions of about 79%. Diesel hybrid electric vehicles showed distance-specific NOx emissions benefits relative to the conventional SCR-equipped diesel vehicles (70% lower NOx emissions), but higher distance-specific NOx compared to CNG and LPG vehicles.

Chapter 6 presents an evaluation of small off-road diesel engine emissions and the feasibility and cost effectiveness of utilizing aftertreatment systems. This study assessed the impact and deterioration of applying new technology after-treatment systems to 4 engines in the SORDE category. Two engines under 25 hp were tested with a DPF and 2 engines between 25 and 75 hp were tested with an SCR. The DPFs showed >98% PM reductions for a baseline degreened and 1,000-hour aging tests. The NOx aftertreatment systems provided reductions ranging from 70 to 91% for a steady-state C1 cycle. Lower NOx reductions from 26 to 65% were seen for hot and cold start NRTC tests, as the exhaust temperature was below that required to begin dosing during the initial parts of these cycles. No significant deterioration was seen after the 1,000-hour durability testing with some aftertreatment systems providing better emissions reductions after the durability tests. Emissions inventory estimates suggest that the adoption of new standards can provide a PM reduction of 3.8% and a NOx reduction of 8.8-13.7% for the total off-road equipment emissions inventory. A cost benefit analysis indicated that the price of implementing DPFs on engines below 25 hp would cost a total of $15.29 per pound of PM saved, while the price of implementing SCRs on engine between 25-75 hp would cost between $0.38 - $0.59

per pound of NOx saved, which compares very favorably to other rulemakings adopted by CARB. While the results of this study are promising, it should be noted that given the wide variety of applications for off-road engines, the practicality of implementing such aftertreatment systems could vary between applications depending on the potential to transition to electric motors or gasoline engines, the cost of the aftertreatment system relative to the overall cost of the equipment it is being used in, and the complexity of the controls that would be required to manage the aftertreatment system for different applications.

Chapter 7 presents an evaluation of the air pollutant emissions from a tier 2 container vessel and a Panamax tanker vessel. Emission measurements were performed on the main and auxiliary engines, as well as on 2 different auxiliary boilers. For the auxiliary boiler testing, carbonyl emissions and the inorganic composition of PM2.5 (i.e., trace metals and elements) were investigated. The results revealed higher NOx and PM2.5 emissions for the main and auxiliary engines. For the auxiliary boiler, NOx emissions showed a statistically significant increase for the ULSHFO compared to MGO. For the larger auxiliary boiler, NOx emissions showed increases of around 50%. The higher PM2.5 emissions for the ULSHFO compared to MGO could be attributed to fuel properties such as viscosity, density, and carbon residue. Low engine load conditions generally resulted in higher NOx, PM2.5, and black carbon emissions. This finding can potentially have important environmental and health implications since marine engines are optimized for higher loads (typically 70-90%) when cruising at-sea. When at-berth or during maneuvering, the required low engine loads will contribute to total emissions and affect local air quality and

associated health effects in coastal communities. Formaldehyde and acetaldehyde emissions were the major aldehydes for both auxiliary boilers. Both aldehydes are known for their deleterious health effects, which could have an important contribution to air quality on a local scale when the ship was hoteling. The results also demonstrated that auxiliary boiler PM2.5 composition was dominated by sulfur, vanadium, iron, and nickel, which were derived from the lubrication oil and fuel, and were likely present in the PM2.5 emissions in the form of metal oxides.

1.8 References

Aatola, Hannu, et al. "Hydrotreated Vegetable Oil (HVO) as a Renewable Diesel Fuel: Trade-off between NOx, Particulate Emission, and Fuel Consumption of a Heavy Duty Engine." *SAE International Journal of Engines*, vol. 1, no. 1, 2008, pp. 1251–1262., doi:10.4271/2008-01-2500.

Agrawal, H., et al., "In-use gaseous and particulate matter emissions from a modern ocean going container vessel" Atmospheric Environment 2008a, 42, 5504-5510.

Agrawal, H., et al., "Emission measurements from a crude oil tanker at sea" Environ. Sci. Technol. 2008b, 42, 7098-7103.

Alkidas AC. "Combustion advancements in gasoline engines" Energy Conversion and Management 2007;48:2751-2761.

Andersson J, et al., "On-road and chassis dynamometer evaluations of emissions from two Euro 6 diesel vehicles" SAE Technical Paper 2014, 2014-01-2826.

Anenberg, S.C., et al., "Impacts and mitigation of excess diesel-related NOx emissions in 11 major vehicle markets" Nature 2017, 545, 467-471.

Araji F, Stokes J. "Evaluation of emissions from light duty trucks with and without the use of a gasoline particulate filter" SAE Technical Paper 2019, 2019-01-0971.

Basha, Syed Ameer, et al. "A Review on Biodiesel Production, Combustion, Emissions and Performance." *Renewable and Sustainable Energy Reviews*, vol. 13, no. 6-7, 2009, pp. 1628–1634., doi:10.1016/j.rser.2008.09.031.

Bhardwaj, O. et al., "Potential of Hydrogenated Vegetable Oil (HVO) in Future High Efficiency Combustion System," *SAE Int. J. Fuels Lubr.* 6(1):157-169, 2013, doi:10.4271/2013-01-1677.

Bishop JDK, et al., "Using portable emissions measurement systems (PEMS) to derive more accurate estimates of fuel use and nitrogen oxides emissions from modern Euro 6 passenger cars under real-world driving conditions" Applied Energy 2019;242:942-973.

Blakeman, P. G., et al. "Investigations into NOx Aftertreatment with Urea SCR for Light-Duty Diesel Vehicles." *SAE Technical Paper Series*, 2001, doi:10.4271/2001-01-3624.

Bohl, T., et al., "Particulate Number and NOx Trade-Off Comparisons between HVO and Mineral Diesel in HD Applications," *Fuel* 215:90-101, 2018.

Browning, L., et al., "Demonstration of fuel switching on oceangoing vessels in the Gulf of Mexico" J. Air Waste Manage Assoc 2012, 62, 1093-10101.

Cao T, et al., "Evaluations of in-use emission factors from off-road construction equipment" Atmospheric Environment 2016; 147:234-245.

Cao T, et al., "Characterization of the emissions impacts of hybrid excavators with a portable emissions measurement system (PEMS)-based methodology" Science of the Total Environment 2018; 635:112-119.

Chen L, et al., "Characterizing particulate matter emissions from GDI and PFI vehicles under transient and cold start conditions" Fuel 2017;189:131-140.

Chen, D., et al., "High-spatiotemporal-resolution ship emission inventory of China based on AIS data in 2014" Science of the Total Environment 2017, 609, 776-787.

Chu-Van, T., et al., "R.J. On-board measurements of particle and gaseous emissions from a large cargo vessel at different operating conditions" Environmental Pollution 2018, 237, 832-841.

Cooper, D.A. Exhaust emissions from ships at berth. Atmospheric Environment 2003, 37, 3817-3830.

Demuynck J, et al., "Real-world emissions measurements of a gasoli e direct injection vehicle without and with a gasoline particulate filter" SAE Technical Paper 2017, 2017-01-0985.

Dixit, P., et al., "Differences between emissions measured in urban driving and certification testing of heavy-duty diesel engines" Atmospheric Environment 2017, 166, 276-285.

Erkkilä, K., et al., "Emission Performance of Paraffinic HVO Diesel Fuel in Heavy Duty Vehicles," SAE Technical Paper 2011-01-1966, 2011, doi:https://doi.org/10.4271/2011-01-1966.

Exxon Mobile, “2019 Outlook for Energy: a Perspective to 2040”, 2019, https://corporate.exxonmobil.com/-/media/Global/Files/outlook-for-energy/2019-Outlook-for-Energy_v4.pdf

Feng, Shaolong, et al. “The Health Effects of Ambient PM2.5 and Potential Mechanisms.” *Ecotoxicology and Environmental Safety*, vol. 128, 2016, pp. 67–74., doi:10.1016/j.ecoenv.2016.01.030.

Fontaras G, et al., “Fuel consumption and CO_2 emissions from passenger cars in Europe – Laboratory versus real-world emissions” Progress in Energy and Combustion Science 2017;60:97-131.

Gallus J, et al., “Impact of driving style and road grade on gaseous exhaust emissions of passenger vehicles measured by a Portable Emission Measurement System (PEMS)” Transportation Research Part D 2017;52:215-226.

Gallus J, et al., “On-road particle number measurements using a portable emission measurement system (PEMS)” Atmospheric Environment 2016;124:37-45.

Gomez, A., et al., “Evaluation of Sooting Tendency of Different Oxygenated and Paraffinic Fuels Blended with Diesel Fuel,” *Fuel* 184:536-543, 2016.

Grigoratos, T., et al., “Real world emissions performance of heavy-duty Euro VI diesel vehicles” Atmospheric environment 2019, 201, 348-359.

Guan, B., et al., “Review of state of the art technologies of selective catalytic reduction of NOx from diesel engine exhaust” Applied Thermal Engineering 2014, 66, 395-414.

Guan, Bin, et al. “Review of State of the Art Technologies of Selective Catalytic Reduction of NOx from Diesel Engine Exhaust.” *Applied Thermal Engineering*, vol. 66, no. 1-2, 2014, pp. 395–414., doi:10.1016/j.applthermaleng.2014.02.021.

Gysel, N.R., et al., “Detailed analysis of criteria and particle emissions from a very large crude carrier using a novel ECA fuel” Environ. Sci. Technol. 2017, 51, 1868-1875.

Hajbabaei M, et al. Impacts of biodiesel feedstock and additives on criteria emissions from a heavy-duty engine. Fuel Processing Technology 2014;126:402-414.

Heywood, J.B. (2018). Internal Combustion Engine Fundamentals

Hountalas, D.T., et al., “Comparative evaluation of various methodologies to account for the effect of load variation during cylinder pressure measurement of large two-stroke diesel engines” Applied Energy 2014, 113, 1027-1042.

Huang, C., et al., “Emission factors of particulate and gaseous compounds from a large cargo vessel operated under real-world conditions” Environmental Pollution 2018, 242, 667-674.

Huang C, et al., “a PEMS study of the emissions of gaseous pollutants and ultrafine particles from gasoline- and diesel-fueled vehicles” Atmospheric Environment 2013;77:703-710.

Hulskotte, J.H.J., Denier van der Gon, H.A.C. “Fuel consumption and associated emissions from seagoing ships at berth derived from an on-board survey” Atmospheric Environment 2010, 44, 1229-1236.

Jiang, Yu, et al. “Characterizing Emission Rates of Regulated Pollutants from Model Year 2012 + Heavy-Duty Diesel Vehicles Equipped with DPF and SCR Systems.” *Science of The Total Environment*, vol. 619-620, 2018, pp. 765–771., doi:10.1016/j.scitotenv.2017.11.120.

Jiang, Y., et al., “Characterizing emission rates of regulated pollutants from model year 2012+ heavy-duty diesel vehicles equipped with DPF and SCR systems” Science of the Total Environment 2018, 619-620, 765-771.

Karavalakis G, et al., “Evaluating the effects of aromatics content in gasoline on gaseous and particulate matter emissions from SI-PFI and SI-DI vehicles” Environ. Sci. Technol. 2015;49:7021-7031.

Karlsson RB, Heywood JB. “Piston fuel film observations in an optical access GDI engine” SAE Technical Paper 2001; 2001-01-2022.

Khan T, Frey HC. “Comparison of real-world and certification emission rates for light duty gasoline vehicles” Science of the Total Environment 2018;622-623:790-800.

Khan. Y.M., et al., “Greenhouse gas and criteria emission benefits through reduction of vessel speed at sea” Environ. Sci. Technol. 2012, 46, 12600-12607

Khan, M.Y., et al., “Benefits of two mitigation strategies for container vessels: cleaner engines and cleaner fuels” Environ. Sci. Technol. 2012, 46, 5049-5056.

Koczak J, et al., “Particulate emissions in GDI vehicle transients: An examination of FTP, HWFET, and US06 measurements” SAE Technical Paper 2016; 2016-01-0992.

Koebel, M, et al. “Urea-SCR: a Promising Technique to Reduce NOx Emissions from Automotive Diesel Engines.” *Catalysis Today*, vol. 59, no. 3-4, 2000, pp. 335–345., doi:10.1016/s0920-5861(00)00299-6.

Kotz, A.J., et al., “Lagrangian hotspots of in-use NOx emissions from transit buses” Environ. Sci. Technol. 2016, 50, 5750-5756.

Knothe, Gerhard, et al. “Exhaust Emissions of Biodiesel, Petrodiesel, Neat Methyl Esters, and Alkanes in a New Technology Engine†.” *Energy & Fuels*, vol. 20, no. 1, 2006, pp. 403–408., doi:10.1021/ef0502711.

Kwon S, et al., “Characteristics of on-road NOx emissions from Euro 6 light-duty diesel vehicles using a portable emissions measurement system” Science of the Total Environment 2017;576:70-77.

Lapuerta, M, et al. “Effect of Biodiesel Fuels on Diesel Engine Emissions.” *Progress in Energy and Combustion Science*, vol. 34, no. 2, 2008, pp. 198–223., doi:10.1016/j.pecs.2007.07.001.

Lehto, K., et al., “Emission Reduction Using Hydrotreated Vegetable Oil (HVO) with Miller Timing and EGR in Diesel Combustion,” SAE Technical Paper 2011-01-1955, 2011, doi:https://doi.org/10.4271/2011-01-1955.

Li, C., et al., “Emissions from advanced ultra-low NOx heavy-duty natural gas vehicles” SAE Technical Paper 2019, 2019-01-0751.

May J, Bosteels D, Favre C. An assessment of emissions from light-duty vehicles using PEMS and chassis dynamometer testing. SAE Technical Paper 2014, 2014-01-1581.

Mendoza-Villafuerte, et al., “NOx, NH3, N2O and PN real driving emissions from a Euro VI heavy-duty vehicle. Impact of regulatory on-road test conditions on emissions” Science of the Total Environment 2017, 609, 546-555.

Misra, Chandan, et al. “In-Use NOxEmissions from Model Year 2010 and 2011 Heavy-Duty Diesel Engines Equipped with Aftertreatment Devices.” *Environmental Science & Technology*, vol. 47, no. 14, 2013, pp. 7892–7898., doi:10.1021/es4006288.

Moldanova, J., et al., “Physical and chemical characterization of PM emissions from two ships operating in European emission control areas” Atmos. Meas. Tech. 2013, 6, 3577-3596.

Mueller, L., et al., “Characteristics and temporal evolution of particulate emissions from ship diesel engine” Applied Energy 2015, 155, 204-217.

Mueller, Charles J., et al. “An Experimental Investigation of the Origin of Increased NOx Emissions When Fueling a Heavy-Duty Compression-Ignition Engine with Soy Biodiesel.” *SAE International Journal of Fuels and Lubricants*, vol. 2, no. 1, 2009, pp. 789–816., doi:10.4271/2009-01-1792.

Na, K., et al., “Impact of Biodiesel and Renewable Diesel on Emissions of Regulated Pollutants and Greenhouse Gases on a 2000 Heavy Duty Diesel Truck,” *Atmospheric Environment* 107:307-314, 2015.

No, S.Y., “Application of Hydrotreated Vegetable Oil from Triglyceride Based Biomass to CI Engines - A Review,” *Fuel* 115:88-96, 2014.

O'Driscoll R, et al., "Real world CO_2 and NOx emissions from 149 Euro 5 and 6 diesel, gasoline and hybrid passenger cars" Science of the Total Environment 2018;621:282-290.

Ogata T, et al., "Particle number emission reduction for GDI engines with gasoline particulate filters" SAE Technical Paper 2017, 2017-01-2378.

Ogunkoya, Dolanimi, et al. "Investigation of the Effects of Renewable Diesel Fuels on Engine Performance, Combustion, and Emissions." *Fuel*, vol. 140, 2015, pp. 541–554., doi:10.1016/j.fuel.2014.09.061.

Omari, A., et al., "Improving Engine Efficiency and Emission Reduction Potential of HVO by Fuel-Specific Engine Calibration in Modern Passenger Car Diesel Applications," SAE Technical Paper 2017-01-2295, 2017, doi:https://doi.org/10.4271/201701-2295.

Özener, Orkun, et al. "Effects of Soybean Biodiesel on a DI Diesel Engine Performance, Emission and Combustion Characteristics." *Fuel*, vol. 115, 2014, pp. 875–883., doi:10.1016/j.fuel.2012.10.081.

Pflaum, H., et al., "Potential of Hydrogenated Vegetable Oil (HVO) in a Modern Diesel Engine," SAE Technical Paper 2010-32-0081, 2010, doi:https://doi.org/10.4271/2010-32-0081.

Piock W, et al., "Strategies towards meeting future particulate matter emission requirements in homogeneous gasoline direct injection engines" SAE Int. J. Engines 2011;4:1455-1468.

Piumetti, M., et al., "Catalysis in diesel engine NOx aftertreatment: a review. Catalysis, Structure & Reactivity" 2015, 1, 155-173.

Praveena, V., and M. Leenus Jesu Martin. "A Review on Various after Treatment Techniques to Reduce NOx Emissions in a CI Engine." *Journal of the Energy Institute*, vol. 91, no. 5, 2018, pp. 704–720., doi:10.1016/j.joei.2017.05.010.

Quiros, D. C., et al., "Real-World Emissions from Modern Heavy-Duty Diesel, Natural Gas, and Hybrid Diesel Trucks Operating Along Major California Freight Corridors" Emission Control Science and Technology 2016, 2, 156-172.

Rantanen, L., et al., "NExBTL - Biodiesel Fuel of the Second Generation," SAE Technical Paper 2005-01-3771, 2005, doi:https://doi. org/10.4271/2005-01-3771.

Reda, A.A., et al., "Gas phase carbonyl compounds in ship emissions: differences between diesel fuel and heavy fuel oil operation" Atmospheric Environment 2015, 112, 370-380.

Roth P, et al., "Catalyzed gasoline particulate filters reduce secondary organic aerosol production from gasoline direct injection vehicles" Environ. Sci. Technol. 2019;53:3037-3047.

Saliba G, et al., “Comparison of gasoline direct-injection (GDI) and port fuel injection (PFI) vehicle emissions: Emission Certification standards, cold-start, secondary organic aerosol formation potential, and potential climate impacts” Environ. Sci. Technol. 2017;51:6542-6552.

Schoenhaber J, et al., “Impact of European real-driving-emission legislation on exhaust gas aftertreatment systems of turbocharged direct injected gasoline vehicles” SAE Technical Paper 2017, 2017-01-0924.

Sillman, Sanford. “The Relation between Ozone, NOx and Hydrocarbons in Urban and Polluted Rural Environments.” *Atmospheric Environment*, vol. 33, no. 12, 1999, pp. 1821–1845., doi:10.1016/s1352-2310(98)00345-8.

Singer, A., et al., “Aging Studies of Biodiesl and HVO and Their Testing as Neat Fuel and Blends for Exhaust Emissions in Heavy-Duty Engines and Passenger Cars,” *Fuel* 153:595-603, 2015.

Singh, D., et al., “Combustion and Emission Characteristics of a Light Duty Diesel Engine Fueled with Hydro-Processed Renewable Diesel,” *Energy* 154:498-507, 2018.

Singh, Devendra, et al. “Comprehensive Review of Combustion, Performance and Emissions Characteristics of a Compression Ignition Engine Fueled with Hydroprocessed Renewable Diesel.” *Renewable and Sustainable Energy Reviews*, vol. 81, 2018, pp. 2947–2954., doi:10.1016/j.rser.2017.06.104.

Sowman, J., et al., “In-use emissions testing of diesel-driven buses in Southampton: is selective catalytic reduction as effective as fleet operators thing?” IET Intell. Transp. Syst. 2018, 12, 521-526.

Starcrest Consulting Group, LLC. Port of Los Angeles inventory of air emissions-2010. Starcrest, 2011.

Sugiyama, Kouseki, et al. “Effects of Hydrotreated Vegetable Oil (HVO) as Renewable Diesel Fuel on Combustion and Exhaust Emissions in Diesel Engine.” *SAE International Journal of Fuels and Lubricants*, vol. 5, no. 1, 2011, pp. 205–217., doi:10.4271/2011-01-1954.

Szybist, James P., et al. “Biodiesel Combustion, Emissions and Emission Control.” *Fuel Processing Technology*, vol. 88, no. 7, 2007, pp. 679–691., doi:10.1016/j.fuproc.2006.12.008.

United States Environmental Protection Agency, “Air Pollutant Emissions Trends Data.”, 30 Apr. 2020, www.epa.gov/air-emissions-inventories/air-pollutant-emissions-trends-data

United States Environmental Protection Agency, 2004, Final Regulatory Analysis: Control of Emissions from Nonroad Diesel Engines, Document # EPA420-R-04-007, May.

"U.S. Energy Information Administration - EIA - Independent Statistics and Analysis." *Use of Energy for Transportation - U.S. Energy Information Administration (EIA)*, 2020, www.eia.gov/energyexplained/use-of-energy/transportation.php.

Valverde V, et al., "Emission factors derived from 13 Euro 6b light-duty vehicles based on laboratory and on-road measurements" Atmosphere 2019;10:243.

Wang H, et al., "The real driving emission characteristics of light duty diesel vehicle at various altitudes" Atmospheric Environment 2018; 191:126-131.

Waynick, J. "Characterization of Biodiesel Oxidation and Oxidation Products." *SwRI Report*, 2005, doi:10.2172/909194.

Weiss M, et al., "On-road emissions of light-duty vehicles in Europe" Environ. Sci. Technol. 2011;45:8575-8581.

Williams, Aaron, et al. "Impact of Fuel Metal Impurities on the Durability of a Light-Duty Diesel Aftertreatment System." *SAE Technical Paper Series*, 2013, doi:10.4271/2013-01-0513.

Wu, Y., et al., "Investigation of Combustion and Emission Performance of Hydrogenated Vegetable Oil (HVO) Diesel," SAE Technical Paper 2017-012400, 2017, doi:https://doi.org/10.4271/2017-01-2400.Wu, D., et al., "Primary particulate matter emitted from heavy fuel and diesel oil combustion in a typical container ship: characteristics and toxicity" Environ. Sci. Technol. 2018, 52, 12943-12951.

Wu, Y., et al., "The challenge to NOx emission control for heavy-duty diesel vehicles in China" Atmos. Chem. Phys. 2012, 12, 9365-9379.

Xue, Jinlin, et al. "Effect of Biodiesel on Engine Performances and Emissions." *Renewable and Sustainable Energy Reviews*, vol. 15, no. 2, 2011, pp. 1098–1116., doi:10.1016/j.rser.2010.11.016.

Yang J, et al., "A comparison of a mini-PEMS and a 1065 compliant PEMS for on-road gaseous and particulate emissions from a light duty diesel truck" Science of the Total Environment 2018a;640-641:364-376.

Yang J, et al., "Gasoline particulate filters as an effective tool to reduce particulate and PAH emissions from GDI vehicles: A case study with two GDI vehicles" Environ. Sci. Technol. 2018b;52:3275-3284.

Yau, P.S., et al., "Estimation of exhaust emission from ocean-going vessels in Hong Kong" Science of the Total Environment 2012, 431, 299-306.

Yoon, S., et al., "Criteria pollutant and greenhouse gas emissions from CNG transit buses equipped with three-way catalysts compared to lean-burn engines and oxidation catalyst technologies" J Air Waste Manag Assoc 2013, 63, 923-933.

Yoon, S., et al., “In-use emissions from 2010-technology heavy-duty trucks” Transportation Research Record 2017, 2627, 1-8.

Yoshioka F, et al., “Performance of next generation gasoline particulate filter materials under RDE conditions” SAE Technical Paper 2019, 2019-01-0980.

Zenczak, W. “The possibilities of limiting the toxic compound emission from diesel engines and boilers during ship’s stay in harbour” Scientific Journals 2013, 36, 190-195.

Zetterdahl, M., et al., “Impact of the 0.1% fuel sulfur content limit in SECA on particle and gaseous emissions from marine vessels” Atmospheric Environment 2016, 145, 338-345.

Zhang, F., et al., “Emissions factors for gaseous and particulate pollutants from offshore diesel engine vessels in China” Atmos. Chem. Phys. 2016, 16, 6319-6334.

Zhang, S., et al., “Can Euro V heavy-duty diesel engines, diesel hybrid and alternative fuel technologies mitigate NOx emissions? New evidence from on-road tests of buses in China” Applied Energy 2014, 132, 118-126.

Zhang L, et al., “Comparison of real-world emissions of LDGVs of different vehicle emission standards on both mountainous and level roads in China” Transportation Research Part D 2019;69:24-39.

Zhao, Hong, et al. “Effects of Fuel Sulfur Content and Diesel Oxidation Catalyst on PM Emitted from Light-Duty Diesel Engine.” *Energy & Fuels*, vol. 24, no. 2, 2010, pp. 985–991., doi:10.1021/ef900982c.

Zhu, H., et al., “Characterizing emission rates of regulated and unregulated pollutants from two ultra-low NOx CNG Heavy Duty Vehicles” 2020

Zinola S, et al., “Persistent particle number emissions sources at the tailpipe of combustion engines” SAE Technical Paper 2016; 2016-01-22

2. Engine-Out Emissions Characteristics of a Light Duty Vehicle Operating on a Hydrogenated Vegetable Oil Renewable Diesel

2.1 Abstract

We assessed the engine-out emissions of an ultra-low sulfur diesel (ULSD) and a neat hydrogenated vegetable oil (HVO) from a light-duty diesel truck equipped with common rail direct injection. The vehicle was tested at least twice on each fuel using the LA-92 drive cycle and at steady-state conditions at 30 mph and 50 mph at different loads. Results showed reductions in the engine-out total hydrocarbon (THC), carbon monoxide (CO), nitrogen oxide (NOx), and particulate emissions with HVO. The reductions in soot mass, solid particle number, and particulate matter (PM) mass emissions with HVO were due to the absence of aromatic and polyaromatic hydrocarbon compounds, as well as sulfur species, which are known precursors of soot formation. Volumetric fuel economy, calculated based on the carbon balance method, did not show statistically significant differences between the fuels. Steady-state testing at 30 mph and 50 mph revealed reductions in engine out THC emissions with HVO, but mixed results for CO emissions. Steady-state testing with HVO showed higher NOx and soot mass emissions for the higher load points compared to ULSD.

2.2 Introduction

As global demand continues to increase consumption of traditional petroleum-derived transportation fuels, biofuels have gained interest as a viable alternative to supplement existing petroleum supplies. In addition, low carbon fuel legislation efforts promoting biofuel use have expanded globally. For example, alternative fuels such as fatty acid methyl esters (FAME) and hydrogenated vegetable oils (HVO) are being considered as viable solutions for compression ignition (i.e., diesel) engine applications. FAME (commonly known as biodiesel) is the most widely used biofuel for diesel engines. It is produced from the transesterification of vegetable oils, animal fats, and waste cooking oils. The ester group of biodiesel provides superior lubricity compared to ultra-low sulfur petroleum diesel (ULSD) but is more susceptible to poor oxidative and storage stability (Hoekman et al., 2011).

Another way to process vegetable oil is to remove the oxygen from the structure and hydrogenate the double bonds in the triglyceride molecule. This is a popular pathway to produce HVO (also known as renewable diesel), which is a second-generation biofuel that could address the stability problems associated with conventional biodiesel described above. Similar to biodiesel, HVO is derived from vegetable oils, animal fats, waste cooking oils, and forest/biomass residues. A catalytic hydrogenation process converts triglycerides into alkanes by hydro-deoxygenation. Isomerization may also be incorporated in order to improve the low temperature operability or cold flow properties. HVO properties, including high cetane number, narrow distillation, high heating value on a mass basis, low aromatics, ultra-low sulfur content, and excellent oxidation stability, collectively

contribute to lower emissions and better engine performance (Erkkila et al., 2011; Gomez et al., 2016; Rantanen et al., 2005; Singh et al., 2018).

A number of studies have shown that the use of neat or blended HVO with diesel fuel can reduce gaseous and particulate emissions compared to regular diesel and biodiesel fuels (Singer et al., 2015; Lehto et al., 2011); Bhardwaj et al., 2013; Na et al., 2015; No et al., 2014). Pflaum et al. (2010) reported that HVO can reduce particulate matter (PM) emissions up to 50% compared to diesel fuel due to the absence of aromatics, when using a 2-liter, 4-cylinder diesel engine and a vehicle with the same engine over the New European Driving Cycle. They also found reductions in both total hydrocarbon (THC) and carbon monoxide (CO) emissions with HVO compared to diesel, but no significant variations in nitrogen oxide (NOx) emissions. Wu et al. (2017) tested HVO fuel and regular diesel using a Euro 5 direct injection diesel engine equipped with exhaust gas recirculation (EGR), an integrated diesel oxidation catalyst (DOC), and a diesel particle filter (DPF) aftertreatment system. They found significantly lower (50% or more) particle number emissions from HVO at a sampling location upstream of the exhaust aftertreatment system (engine out) due to no aromatics. They also showed lower THC and NO emissions with the HVO compared to diesel. The ignition delay of the HVO was shorter than the diesel fuel at lower engine speeds because of the high cetane number of HVO. Omari et al. (2017) showed that HVO as a drop-in fuel will likely result in an increased volumetric fuel consumption of about 2% due to the lower density of HVO. They also showed that NOx emissions were comparable to diesel, but CO, THC, and PM emissions were reduced by more than 50%. Bohl et al. (2018) showed no reductions in NOx emissions with HVO, but

reductions in particle number emissions. They also showed lower CO and THC emissions with HVO due to better fuel-air mixing, absence of aromatics, and low boiling range components of HVO compared to diesel fuel.

With the expectation of the widespread employment of low carbon fuels, such as HVO, for Tier 3 type of vehicles, this study aims to characterize the engine-out gaseous and particulate emissions from a light-duty diesel truck operated on neat HVO and ULSD. The vehicle was exercised over the LA-92 driving cycle using a chassis dynamometer. Additional testing was conducted over steady-state conditions at 30 miles per hour (mph) and 50 mph on different loads.

2.3 Experimental

2.3.1 Test Fuels

Two fuels were used in this study. An Ultra-Low Sulfur Diesel (ULSD) was used as the baseline fuel that was supplied by Gage Products Company. In addition, a hydrogenated vegetable oil (HVO) or renewable diesel, blended with 1.5% volume of petroleum diesel was supplied by Neste US, Inc. The ULSD was selected to have properties typical of those found in most automotive diesel fuels across the US. HVO is generally paraffinic in nature and typically has a cetane number greater than 70. HVO contains very low concentrations of sulfur and aromatic compounds. However, HVO has poor lubricity and a low volumetric energy content (Hartikka et al., 2012). A comparison of the test fuels is listed in Table 2-1.

Table 2-1: Properties of the test fuels

Properties		ULSD	HVO
Carbon Content (wt. %)	ASTM D5291	86.0	84.8
Hydrogen Content (wt. %)	ASTM D5291	13.2	14.9
Nitrogen Content (ppm)	ASTM D4629_5762	1.1	2.3
Sulfur (mg/kg)	ASTM D2622	6	< 3
Gross Heat of Combustion (MJ/kg)	ASTM D4809	47.20	48.45
Net Heat of Combustion (MJ/kg)	ASTM D4809	44.32	45.18
Cold Filter Plugging Point (CFPP)°C	ASTM D6371	-34	-22
Density @ 15°C (g/cm^3)	ASTM D4052	0.8536	0.7794
Corrected Flash Point °F	ASTM D93	147	151
Kinematic Viscosity @ 104°F/ 40°C (mm^2/s)	ASTM D445	2.8	3.006
Monoaromatics by SFC (wt. %)	ASTM D5186	22.4	0
Polynuclear Aromatics by SFC (wt. %)	ASTM D5186	2.9	0
Total Aromatics by SFC (wt. %)	ASTM D5186	25.3	0
Initial Boiling Point (°C)	ASTM D86	174	131.6
10% Recovery (°C)	ASTM D86	215.5	265.6
50% Recovery (°C)	ASTM D86	266.2	282.2
90% Recovery (°C)	ASTM D86	320.4	293.7
Final Boiling Point (°C)	ASTM D86	345.2	308.6
IQT Derived Cetane Number	ASTM D6890	43.8	84.1

2.3.2 Test Vehicle

A 2012 model year Chevrolet Silverado 2500HD Duramax was used in this study. The vehicle was equipped with a 6.6L common-rail diesel engine, diesel oxidation catalyst (DOC), a diesel particulate filter (DPF), and selective catalytic reduction (SCR). The technical specifications of the test vehicle are shown in Table 2-2. Prior to the start of testing, the engine lubricating oil and oil filter on the test vehicle were replaced.

Table 2-2: Technical specification of the test vehicle

Engine	6.6L Turbo-diesel V8
Power	397 hp at 3,000 rpm
Fuel injection	Common-rail direct fuel injection
Torque	765 lb-ft at 1,600 rpm
Compression ratio	16.8:1
Aftertreatment	DOC/DPF/SCR
Miles at start of testing	53,866
Emissions standards	Tier 2 Bin5/LEVII

2.3.3 Test Sequence and Fuel Conditioning

The vehicle was tested using each fuel at least twice over the LA-92 emissions test cycle. The LA-92 test cycle or the California Unified Cycle (UC) is a dynamometer driving schedule for light-duty vehicles developed by the California Air Resources Board (CARB). The LA-92 test has a similar three-bag structure, but is a more aggressive driving cycle than the Federal Test Procedure (FTP-75) cycle, which is used for certification of passenger cars and light-duty trucks in the U.S. The LA-92 test is characterized by higher

speeds, higher accelerations, fewer stops per mile, and less idle time. As shown in Figure 2-1, the LA-92 cycle has three phases; namely, the cold-start phase or Bag 1, the hot-running/transient phase or Bag 2, and the hot-start phase or Bag 3.

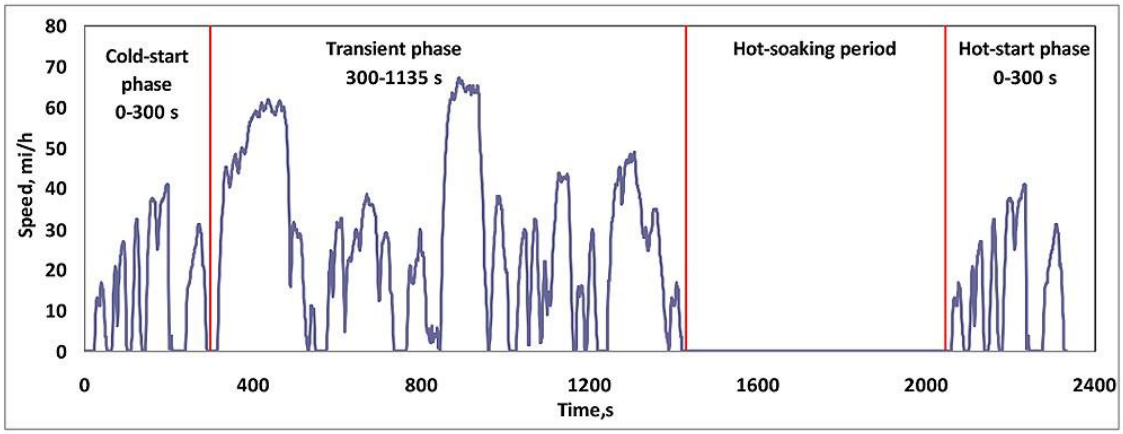

Figure 2-1: LA-92 Driving Cycle

After completing the initial duplicate LA-92 tests on each fuel, the data was evaluated to determine whether additional testing was required. A third test was performed if differences in LA-92 regulated emissions exceeded a predefined limit. This limit was defined using the same criteria as used in previous studies (Durbin et al., 2014; Painter et al., 1992). Specifically, a third test was performed if the difference between the LA-92 regulated emissions measurements exceeded the following repeatability criteria: THC 30%, NOx 50%, CO 50%, provided the absolute difference of the measurements was greater than 5 mg/mi. The emissions measurements for the third test also included particulate emissions measurements (soot mass, PM mass, and particle number).

Prior to testing, the vehicle was put through an oil conditioning procedure that included performing two US06 test cycles followed by an LA-4, followed by another US06 test cycle repeated twice on the given fuel, as illustrated in Figure 2-2. The existing fuel was drained from the vehicle and the tank flushed with the test fuel. The tank was filled to 40% capacity with the test fuel. Vehicle preconditioning was performed as specified in Figure 2-2 and included driving on an LA-4 cycle and two additional drain and fills at 40%. During the prep procedure, side fan cooling was applied to the fuel tank. Following the last prep cycle, the vehicle was idled for two minutes, then shut down in preparation for the soak.

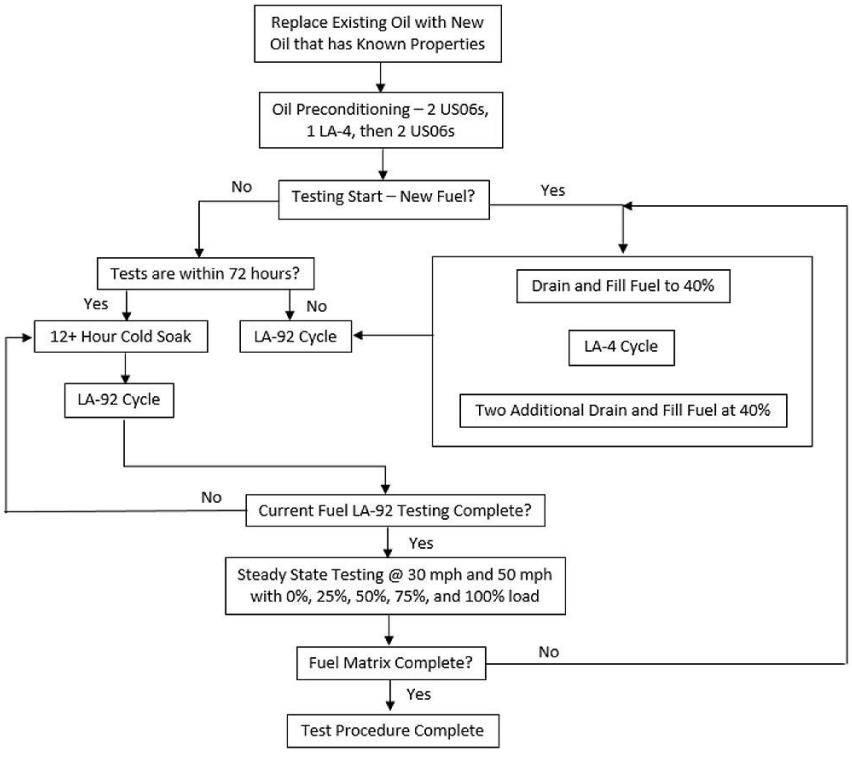

Figure 2-2: Test sequence for fuel change procedure and oil conditioning

After the 12-hour soak, the first LA-92 test cycle was performed. For the LA-92 test cycle, all specified engine-out gaseous emissions were collected along with instantaneous particulate number emissions. The test matrix was designed for the ULSD fuel to be tested first followed by the HVO fuel. Duplicates were run back to back. If an additional test for each test condition/fuel combination was needed, then a third test was applied immediately following. The data were evaluated after each set of replicate tests to determine whether a third test was required.

After completing the LA-92 tests on each vehicle/fuel combination, each fuel was evaluated at steady-state conditions at 30 miles per hour (mph) and 50 mph, at loads of 0, 25%, 50%, 75%, and 100%. For each test condition/fuel combination, combustion characteristics were monitored and recorded over the LA-92 and steady-state testing. These steps were repeated for each test fuel to verify the results of the testing after the fuel preconditioning was performed.

2.3.4 Emissions Testing

Vehicle emissions measurements were conducted in CE-CERT's Vehicle Emissions Research Laboratory (VERL), which utilizes a 48-inch Burke E. Porter single-roll electric chassis dynamometer, capable of testing vehicles weighing up to 12,000 lbs. For this project, emissions and fuel economy measurements were made only for the engine-out exhaust. The engine-out samples were collected inside the 4-inch exhaust pipe, prior to the catalyst and 16 inches downstream of a bend from the engine manifold. Since no modifications to the exhaust pipe were made, the length between the engine manifold bend and DOC is only 24 inches. This area was selected to be most representative of a well-

mixed exhaust sample. Insulated ¼ diameter sample probes were inserted into stainless steel half coupling pipe threads with stainless steel Swagelok fittings used to secure the probes. The gaseous sample probe was designed with a single hole and the PM sample probe was designed with an upstream facing sample and was inserted into the exhaust flow stream in such a manner that it was away from all other probes and away from boundary conditions where surface wall effects could impact sample quality.

An AVL Micro Soot Sensor 483 (MSS) with an AVL Exhaust Conditioning unit were used to measure real-time soot mass emissions. The MSS is an instrument that measures soot mass concentration at a frequency of one Hertz (Hz). The MSS uses a photo acoustic detection technique where the light absorbing PM components (such as soot particles) are exposed to laser light that is periodically modulated at the acoustical resonant frequency. The instrument is designed to measure soot concentrations down to approximately 5 $\mu g/m^3$, and operates at a flow rate of 2 L/min. The exhaust conditioning unit uses mass flow controllers to supply a constant dilution ratio to the MSS. Insulated ¼ inch stainless steel piping connected the sample probe to the dilution cell, which coupled the conditioning unit and MSS inlet.

A Pegasor Mi3 unit was used to measure PM mass and solid particle number (SPN) emissions. The Pegasor Mi3 utilizes electrical detection of particles using an ionization chamber to charge the particles, which are then measured with a sensitive electrometer. A heated sample line connected the exhaust inlet port directly to the inlet of the Pegasor Mi3 instrument.

For the gaseous emissions, including CO, CO_2 and NOx, a Horiba series 200 analyzer raw emissions unit was used. CO and CO_2 were measured using a non-dispersive infrared (NDIR) analyzer while a chemiluminescence (CLD) detector was used to measure NOx. A separate California Analytical Instruments Model 300-HFID HC analyzer was used to measure THC. A ¼ inch stainless steel tubing was used to connect the Horiba series 200 gas analyzer and flame ionization detector (FID) to the exhaust probes. A Sensors exhaust flow meter (EFM) was attached at the tailpipe and used to measure the mass flow rate of the exhaust gases. Two type K thermocouples were placed inside the exhaust pipe, one before the DOC/DPF and one after the aftertreatment system.

Real time combustion data of the fuels was measured and recorded using a dSPACE MicroAutoBox. The glow plugs inside the piston cylinders were replaced with BERU PSG Pressure sensor glow plugs. The combustion data (including piston cylinder pressure and heat release rate) was recorded every 0.2 milliseconds for the first minute of the test.

2.4 Results and Discussion

The results shown in the following figures represent the arithmetic average of all test runs completed on a given fuel. The weighted LA-92 cycle results were calculated using the same weighting factors utilized in determining the weighted FTP emissions using the cold-start transient, stabilized, and hot-start transient phases from the LA-92 cycle. For the steady-state tests, values presented in figures represent the arithmetic average for two tests on a given fuel for each load point and speed conditions. The error bars represent one standard deviation on the average values for each test point. Statistical analyses were

performed using a 2-tailed, 2-sample, equal-variance *t*-test. For the purpose of this discussion, results are considered to be statistically significant for p values ≤0.05 and marginally statistically significant for $0.05 \leq p < 0.1$.

2.4.1 THC and CO Emissions

The cold-start, hot-running transient phase, hot-start, and weighted LA-92 THC and CO emissions results are presented in Figure 2-3 and Figure 2-4, respectively. Engine-out THC emissions were found in lower concentrations for the HVO compared to the ULSD. For the weighted engine-out THC emissions, HVO showed a reduction of 29.6% relative to ULSD. The use of HVO also showed a reduction of 41.3% (p=0.048) in engine-out THC emissions for the cold-start segment of LA-92 relative to ULSD. For the engine-out CO emissions, the use of HVO resulted in statistically significant reductions on the order of 41.4% (p=0.002), 24.9% (p=0.004), and 28.3% (p=0.005), respectively, for the cold-start, hot-running, and weighted LA-92 compared to ULSD.

Our results are in line with previous studies that have shown reductions in THC and CO emissions with the use of either neat or blended HVO fuels compared to petroleum diesel (Pellegrini et al., 2015; Napolitano et al., 2015; Millo et al., 2013; Kousoulidou et al., 2014; Aatola et al., 2008). It has been reported that the very high cetane number and the absence of aromatic compounds in HVO are the main factors leading to reductions in CO and THC emissions (Pflaum et al., 2010; Napolitano et al., 2015). Aromatics are expected to affect CO and THC formation as they have a lower reactivity (leading to a longer ignition delay) as compared to paraffins. The shorter ignition delay of HVO originating from its molecular composition reduces the severity of over-leaning during combustion.

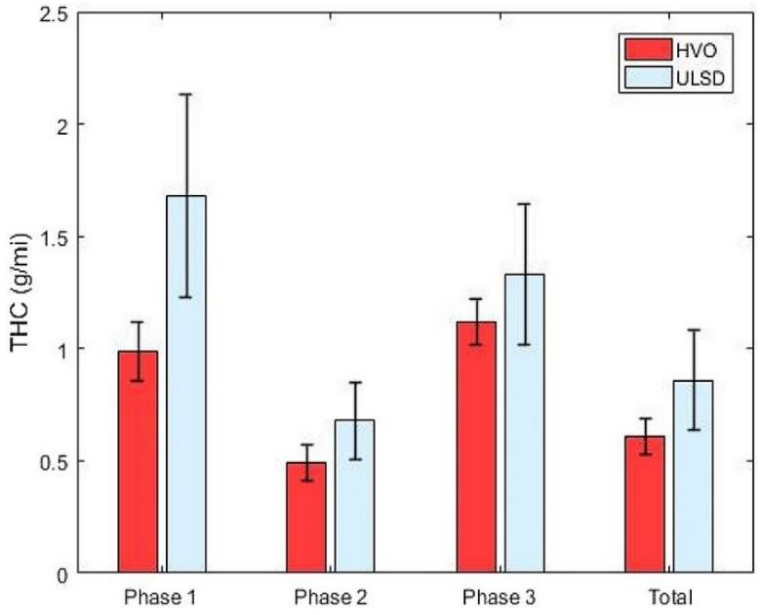

Figure 2-3: Engine-out THC emissions over the LA-92

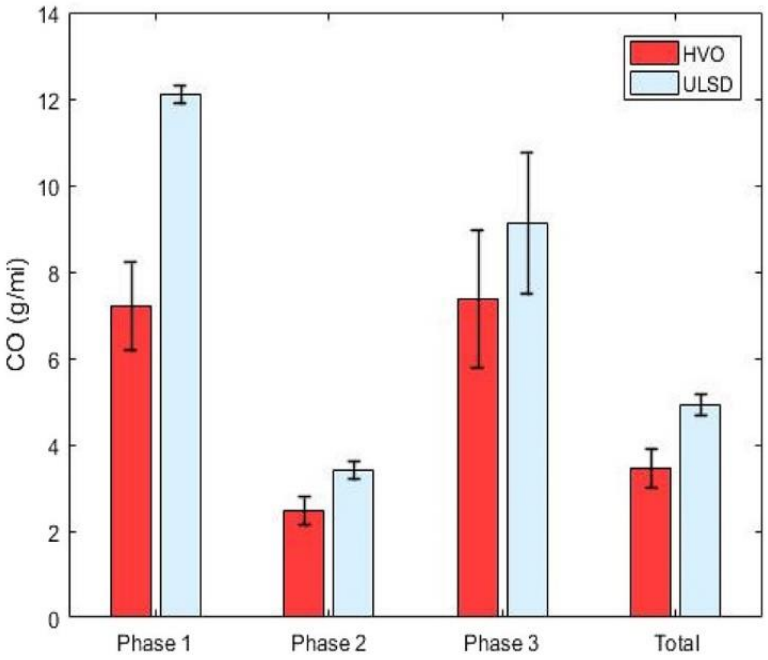

Figure 2-4: Engine-out CO emissions over the LA-92

2.4.2 NOx emissions

NOx emissions are shown in Figure 2-5. The use of HVO provided reductions in engine-out NOx of 14.8% (p=0.028) and 14.6% (p=0.048), respectively, for the hot-running and weighted LA-92 compared to ULSD. The large uncertainties of the HVO test results could be due to slight differences in the driving pattern and differences in fuel injection since the engine was not calibrated for HVO beforehand. HVO contains straight chain and branched hydrocarbons in the range of C10-C22. In addition to paraffins, a typical petroleum-derived ULSD also contains cyclic molecules (aromatics and naphthenes) that may boil over a wider temperature range. Due to the increased volumetric energy density, ULSD is expected to have higher in-cylinder temperatures and pressures during combustion, leading to higher NOx formation. Previous studies have shown that HVO combustion can lead to lower NOx emissions due to the shorter ignition delay period characteristic of its higher cetane number (Happonen et al., 2012; Heikkila et al., 2012; Kuronen et al., 2007; Murtonen et al., 2009). With HVO, NOx emissions are now comparable or slightly less than that of ULSD. This is important as typical biodiesel has been known to increase NOx emissions compared to ULSD. These results show that it is possible to now sell HVO in the market and meet low-carbon fuel legislation while maintaining attainment for NOx emissions standards.

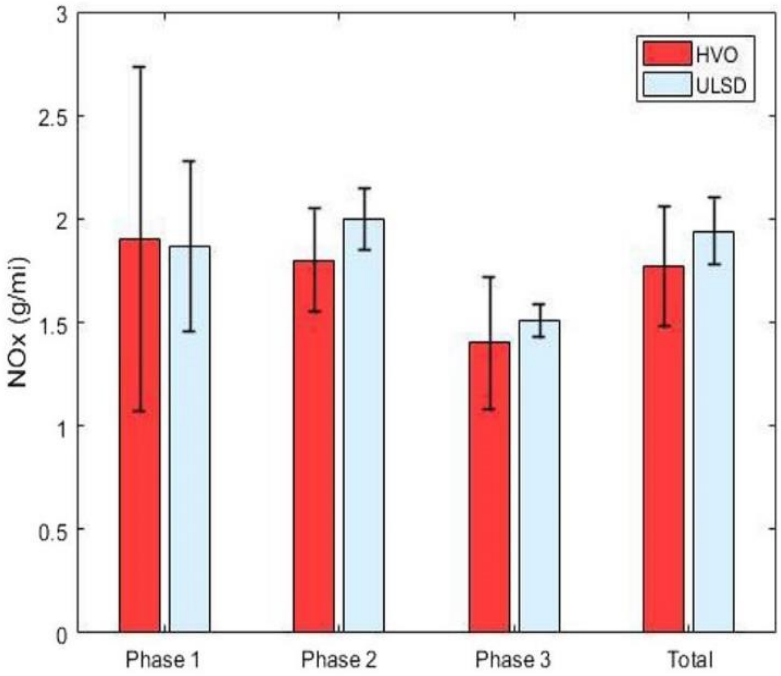

Figure 2-5: Engine-out NOx emissions over the LA-92

2.4.3 CO_2 Emissions and Fuel Economy

Engine-out CO_2 emissions are shown in Figure 2-6. CO_2 emissions did not show statistically significant fuel effects over either the weighted LA-92 cycle or its individual phases. Previous studies have shown that CO_2 emission levels decrease with HVO compared to the petroleum diesel due to a lower carbon content and lower C/H ratio of HVO (Kuronen et al., 2007; Murtonen et al., 2009; Singh et al., 2018; Napolitano et al., 2018).

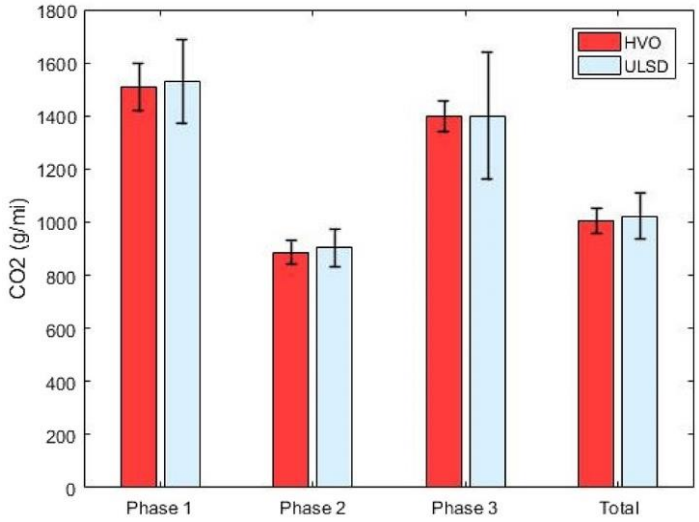

Figure 2-6: Engine-out CO_2 emissions over the LA-92

Fuel economy results are shown in Figure 2-7. Fuel economy was calculated based on the carbon balance method and the unique properties for each different test fuel, rather than the standard EPA equation. The carbon balance equation more directly accounts for the differences in energy content between different fuels, which are normalized out in the standard EPA fuel economy equation.

Although fuel economy trended lower for the HVO fuel, the differences in carbon balance fuel economy for the weighted LA-92 cycle and each individual phase were not statistically significant. Previous studies have reported lower volumetric fuel economy with HVO due to its lower density compared to petroleum diesel (Kousoulidou et al., 2014; Kuronen et al., 2007; Napolitano et al., 2018). On average the use of HVO resulted in an 8% fuel penalty when compared to ULSD. The insignificant differences in fuel economy under the present test conditions may indicate that modern diesel vehicles are not calibrated to account for the differences in fuel properties when operated with HVO.

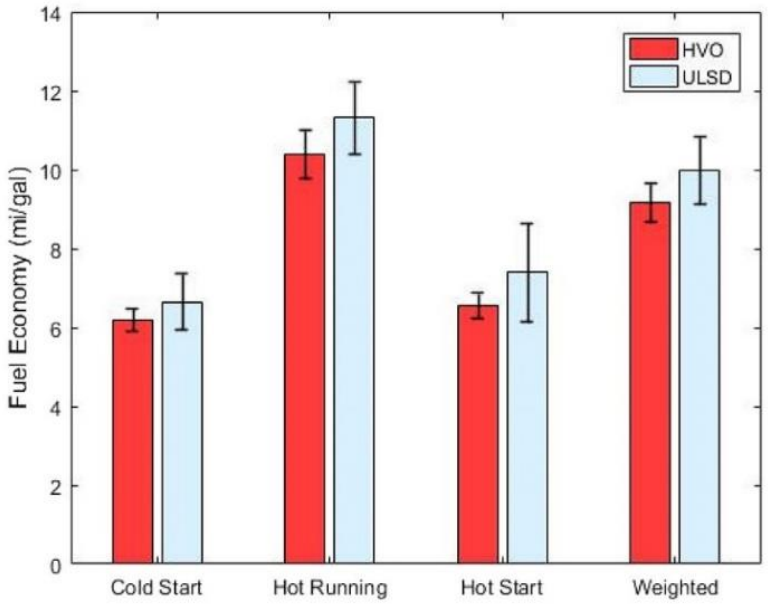

Figure 2-7: Carbon balance fuel economy over the LA-92

2.4.4 Particulate Emissions

Soot mass or black carbon emissions are shown in Figure 2-8. The ULSD resulted in a marginally statistically significant difference in the weighted engine-out soot mass emissions compared to HVO. The reduction in weighted engine-out soot mass emissions for the HVO was 27.6% (marginally statistically significant p=0.057). No significant fuel effects were observed for soot mass emissions during the cold-start and hot-start phases, except for the hot-running phase where HVO led to lower soot mass emissions than ULSD. For the hot-running phase, HVO showed a statistically significant reduction in soot mass emissions of 30.7% (p=0.044).

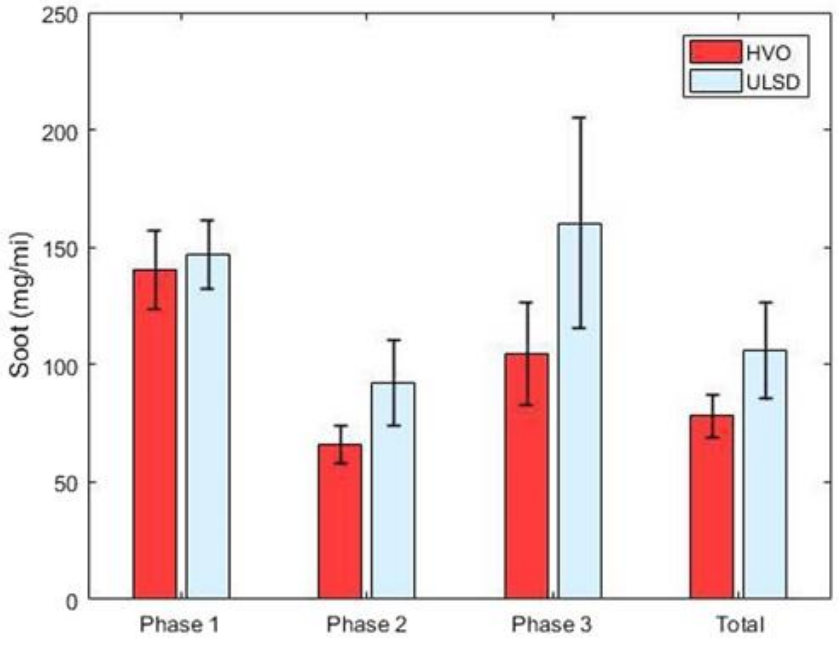

Figure 2-8: Soot mass emissions over the LA-92

Similar to the soot mass emissions, engine-out PM mass emissions showed large reductions with the HVO compared to the ULSD for the weighted LA-92, the cold-start, and hot-running phases (Figure 2-9) that were statistically significant. The statistically significant reductions in PM mass emissions for the HVO were on the order of 31.5% (p=0.008), and 33.7% (p=0.004), respectively, for the weighted LA-92 and the hot-running phase. For the cold-start, the reduction in PM mass for HVO relative to ULSD was 30.1% (p=0.055) at a marginally statistically significant level.

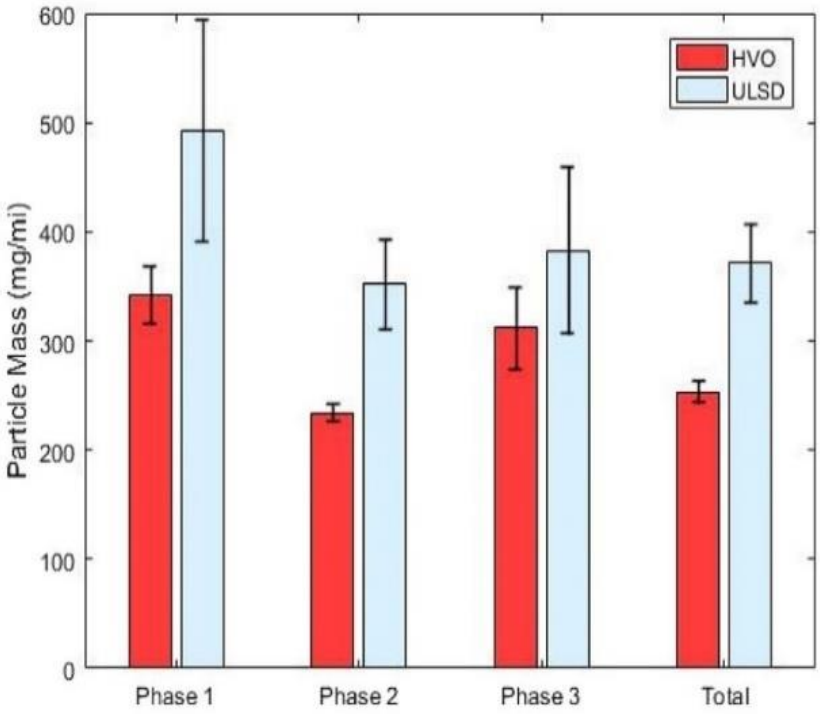

Figure 2-9: PM mass emissions over the LA-92

Engine-out solid particle number emissions followed the same pattern as PM mass emissions and showed statistically significant reductions for the HVO compared to ULSD. As shown in Figure 2-10, these reductions were 31.5% (p=0.005), 30.1% (p=0.055), and 33.7% (p=0.008), respectively, for the weighted LA-92, the cold-start, and hot-running phases. The reductions in solid particle number emissions were either statistically significant or marginally statistically significant.

The results reported here agree with previous studies showing reductions in particulate emissions with HVO relative to petroleum diesel (Singh et al., 2018; Happonen et al., 2012; Singh et al., 2018; Tan et al., 2013; Vo et al., 2018; Prokopowicz et al., 2015). Soot formation during combustion is a complex phenomenon and depends on many parameters such as fuel/air ratio, ignition delay, and fuel composition. The absence of aromatic and

polyaromatic hydrocarbon molecules, as well as sulfur species in the HVO, which are considered as the main precursors of soot formation, were the main contributing factors leading to the reductions in particulate emissions relative to ULSD (Tan et al., 2013; Singh et al., 2015).

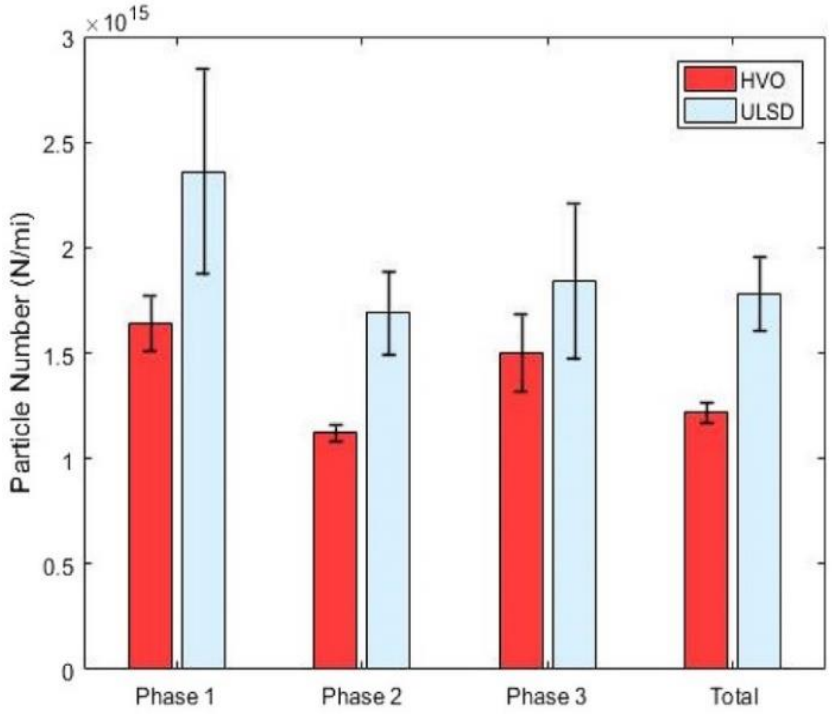

Figure 2-10: Solid particle number emissions over the LA-92

2.4.5 Steady State Emissions Testing

Figure 2-11 (a-b) and Figure 2-12 (a-b) show the engine-out THC and CO emissions, respectively, at different engine loads over the steady-state 30 mph and 50 mph tests. For the engine-out THC emissions, the use of HVO led to reductions relative to ULSD for both steady-state conditions. As previously discussed, the absence of aromatics and the higher

cetane number of HVO resulted in lower THC emissions. Also, due to fuel density differences, less HVO fuel is injected resulting in lower THC emissions.

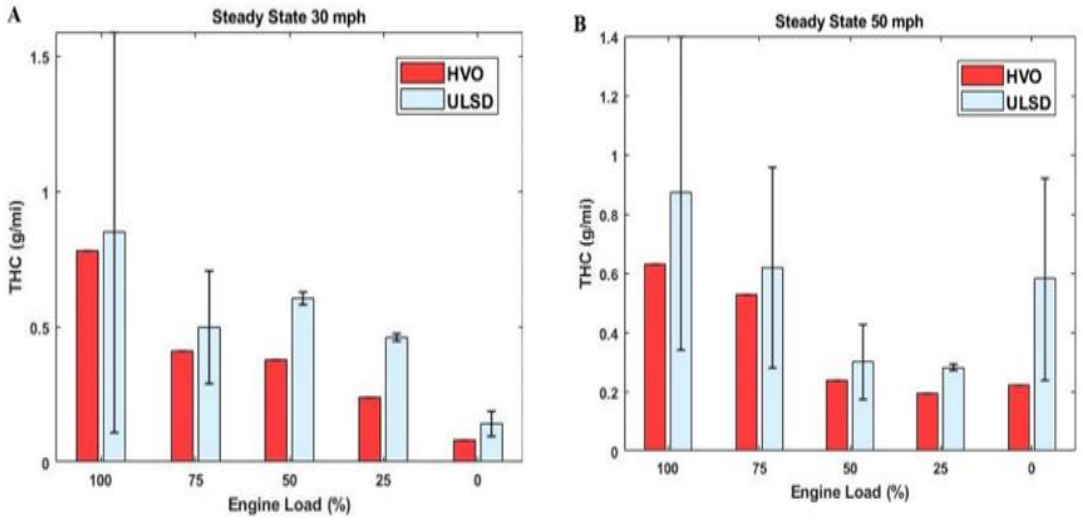

Figure 2-11: (a-b) Engine Out THC emissions over 30mph (a) and 50 mph (b) at different loads

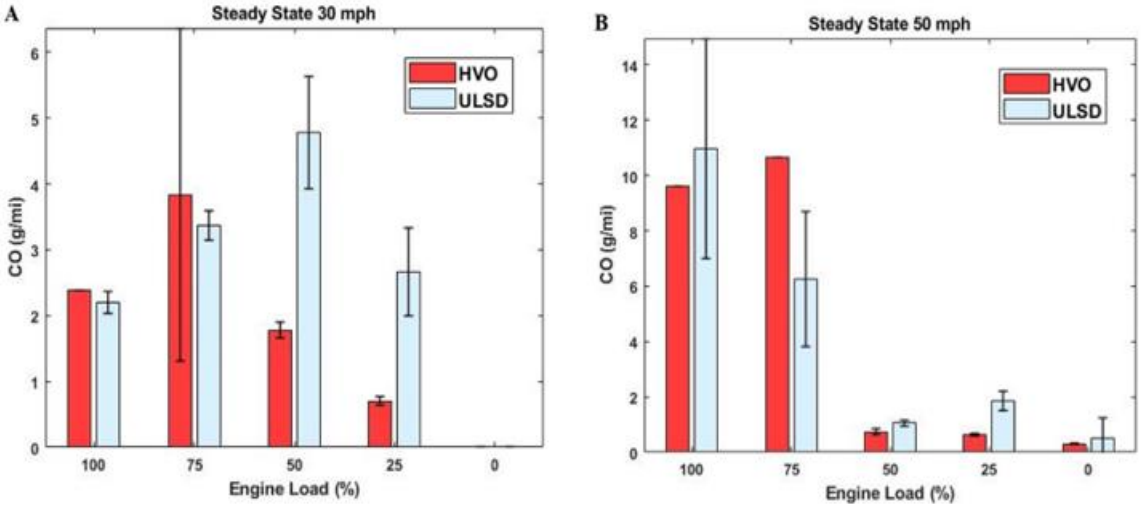

Figure 2-12 (a-b): Engine out CO emissions over 30 mph (a) and 50 mph (b) at different loads

For the engine-out CO emissions, the picture was different with both increases and decreases for HVO. At higher loads (75% and 100%) over 30 mph, the use of HVO resulted in engine-out CO emission increases relative to ULSD, but not at partial and lower load points. At 50 mph conditions, HVO showed higher engine-out CO emissions compared to ULSD only at the 75% load.

Figure 2-13 (a-b) show the engine-out NOx emissions obtained during the steady-state conditions at 30 mph and 50 mph. Engine-out NOx emissions were generally comparable for both test fuels over the two steady-state conditions and the different engine loads, with the exception of the high load (100%) for both 30 mph and 50 mph, where an increase in engine-out NOx was measured for HVO compared to ULSD. Because the engine was not calibrated to account for a high cetane number fuel such as HVO, it is possible that at higher loads the use of HVO resulted in the injection of more fuel at sub-optimal timing. The higher amount of HVO burned along with its higher cetane number compared to ULSD, may increase the maximum temperature and in-cylinder pressure, which may result in higher NOx emissions at higher loads. Previous studies have also shown higher NOx emissions for HVO at higher engine loads (Bohl et al., 2018).

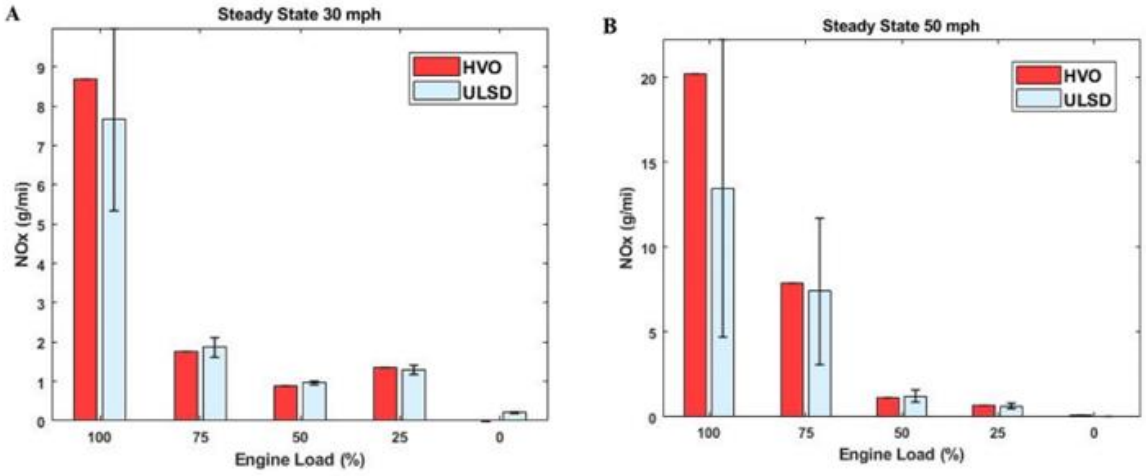

Figure 2-13 (a-b): Engine out NOx emissions over 30mph (a) and 50 mph (b) at different loads

Figure 2-14 (a-b) and Figure 2-15 (a-b) show the engine-out CO_2 emissions and the carbon balance fuel economy, respectively, for the steady-state speeds of 30 mph and 50 mph over different engine loads. For the CO_2 emissions, at low and partial loads, the test fuels did not show any noticeable differences, however, at higher load test points (75% and 100%), a significant trend in increasing CO_2 emissions for HVO was detected at both the 30 mph and 50 mph conditions. Figure 2-14 (a-b) also highlights that at higher load points, both fuels resulted in higher CO_2 values. This is expected and is mainly attributed to the lower fuel economy (higher fuel consumption) at these load points, as shown in Figure 2-15 (a-b). Although fuel economy did not show any statistically significant differences between the test fuels, it is worth noting that HVO led to lower fuel economy than ULSD for the higher load points (75% and 100%) at 30 mph and 50 mph. Overall, the insignificant

differences in fuel economy suggest that modern light-duty diesel vehicles are not calibrated to account for the differences in fuel properties when operated with HVO.

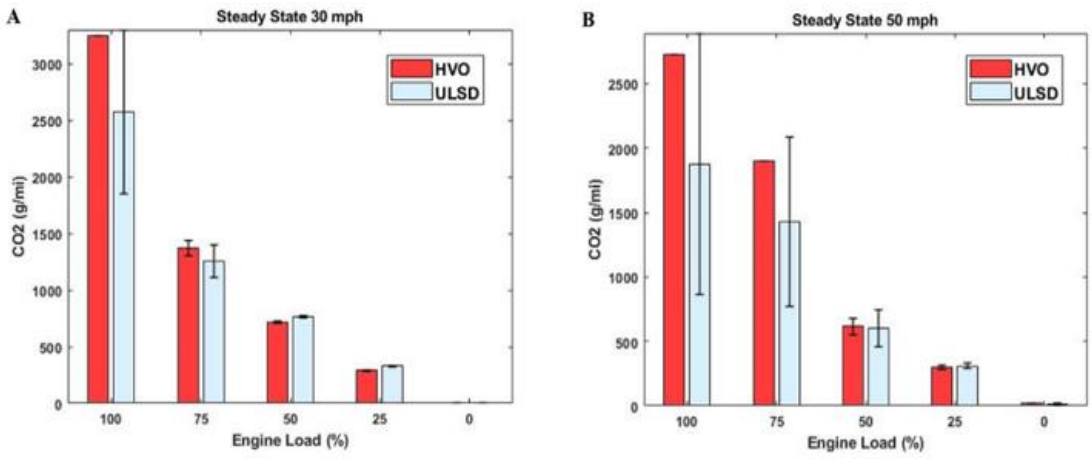

Figure 2-14 (a-b): Engine out CO_2 emissions over 30 mph (a) and 50 mph (b) at different loads

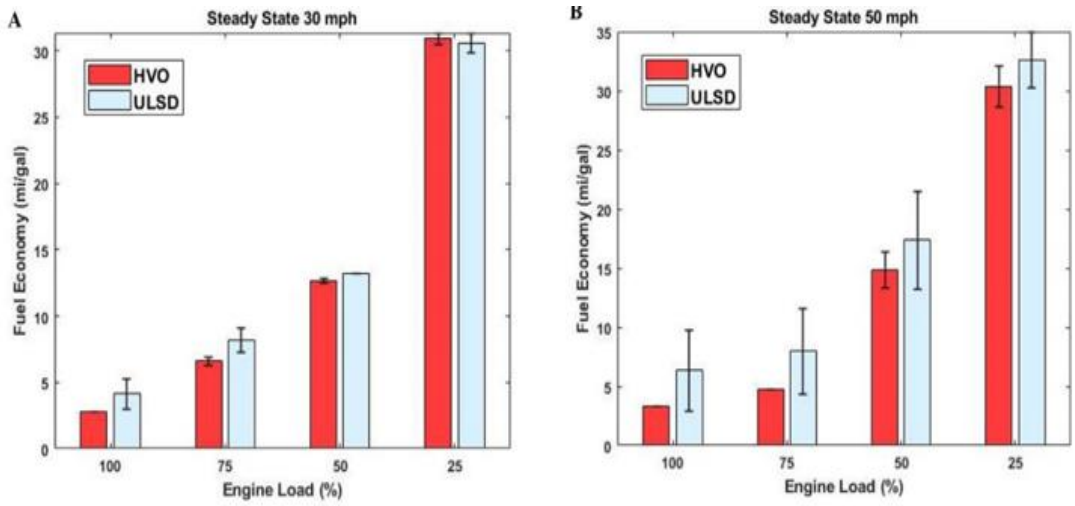

Figure 2-15 (a-b): Carbon Balance fuel economy over 30 mph (a) and 50 mph (b) at different loads

Figure 2-16 (a-b) shows the engine-out soot mass emissions for the different load points and steady-state speeds. It is evident that engine-out soot mass emissions increased for both fuels with increasing engine load. At higher engine loads, more fuel is injected into the combustion chamber, making the combustion directionally more fuel-rich and promoting the formation of soot emissions. The results reported here also show that soot mass emissions were lower for HVO than ULSD at lower and partial load points for the 50 mph conditions, but not at the higher loads (75% and 100%). At 30 mph conditions, HVO showed significantly higher soot mass emissions than ULSD only for the 100% load, but not for the other load points. Dimitriadis et al. (2018) also reported an increase in soot emissions at higher engine loads when they tested a passenger car on HVO fuel. Previous studies have also reported higher particulate emissions with HVO compared to petroleum diesel (Omari et al., 2017; Napolitano et al., 2015; Shukla et al., 2018). They attributed this phenomenon to the higher cetane number of HVO, which may result in reduced premixed combustion and thus more diffusive combustion and higher soot formation, outweighing the benefits of the characteristic of the HVO being aromatic-free compared to diesel fuel. The increased fuel sprayed into the combustion chamber, as shown by the CO_2 emissions, could create more fuel-rich regions in the combustion chamber as well.

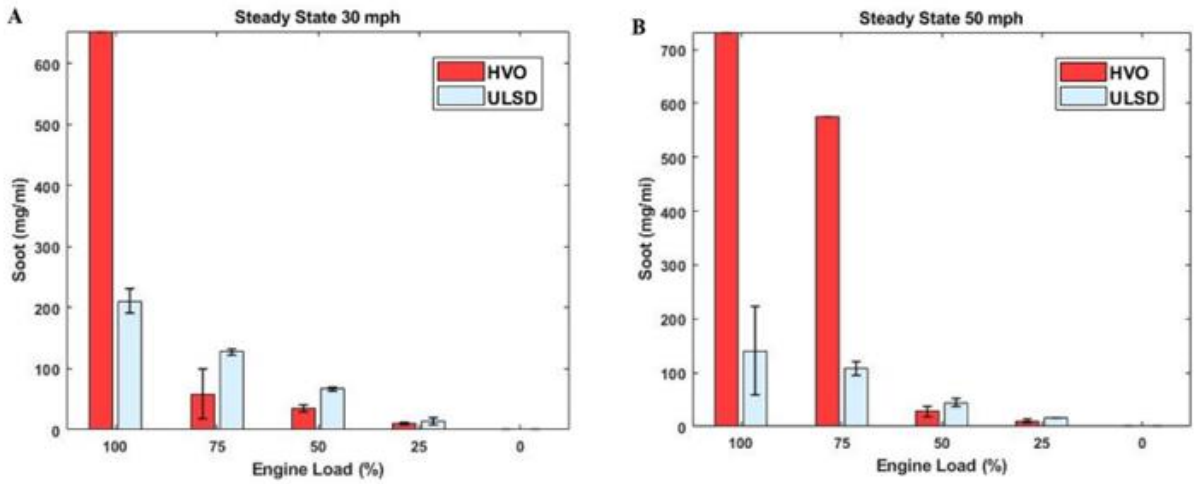

Figure 2-16 (a-b): Engine out soot emissions over 30 mph (a) and 50 mph (b) at different loads

2.4.6 Combustion Analysis

Combustion analysis was performed for the steady state cycles. Figures 2-17(a-e) and 2-18(a-e) show the in-cylinder pressure for the 30mph and 50mph steady state cycles, respectively. 0% load represents engine idling conditions. For the 30-mph steady state runs, ULSD has higher in cylinder pressures peaks after top dead center (ATDC) for all load conditions. This is expected due to the lower volumetric energy content of HVO. This trend continues for the 50-mph steady state runs, with the exception of the 25% and 75% loads. Overall, the peak pressures are very similar for both of the fuels over all steady state runs, indicating a similar work output from both fuels. The 50mph 100% load shows a different pressure rise before TDC for HVO fuel, which could be indicative of issues with the pressure-sensor at the high load conditions.

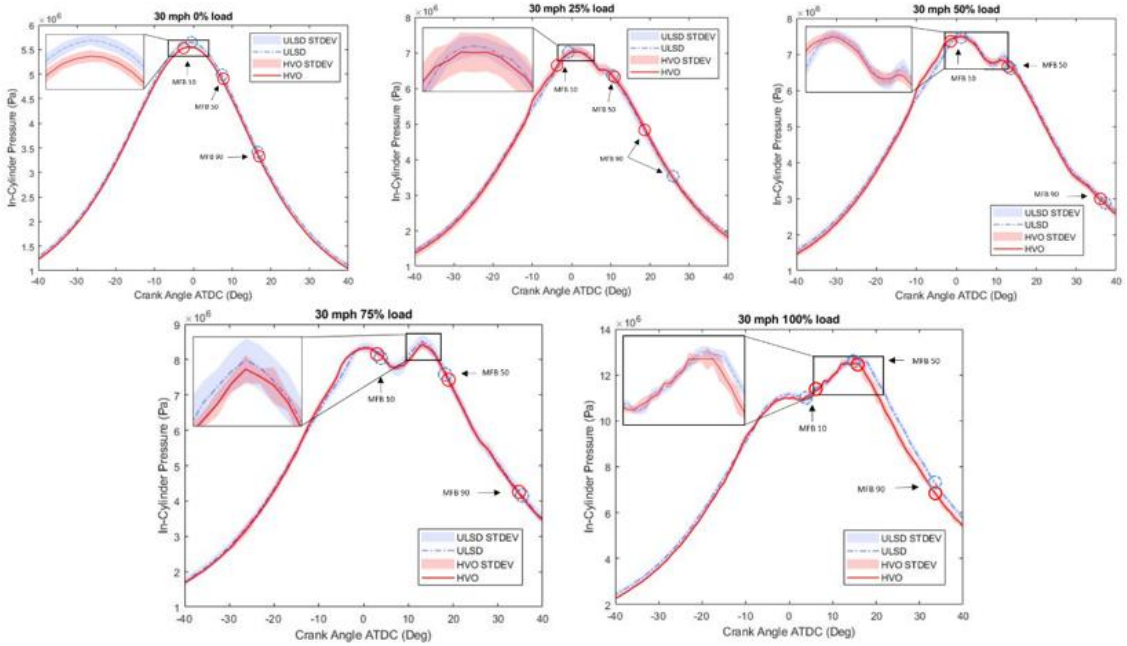

Figure 2-17 (a-e): In-Cylinder Pressure for 30 mph Steady State run at different loads

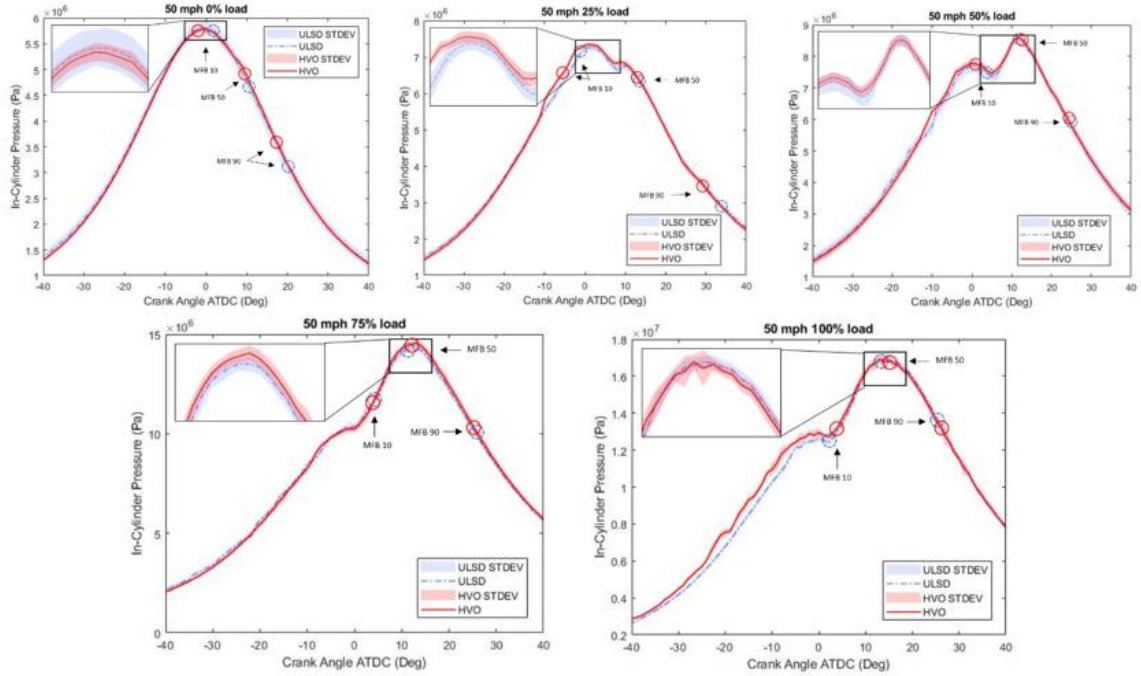

Figure 2-18 (a-e): In cylinder Pressure for 50mph Steady State runs at different loads

The heat release rate is shown in Figures 2-19 and 2-20. Heat release rate is defined as the rate at which the chemical energy of the fuel is released during the combustion process. Interestingly at lower loads the HVO shows a double pilot injection, most likely due a portion of the early injected fuel being ignited prior to a second injection. Ideally, due to shorter ignition delay the HVO fuel needs more retarded injection timing. The LML Duramax 6.6L engine is calibrated to use double pilot injection when necessary to reduce noise and vibration. When single pilot injection is used, NOx, CO, and soot emissions are increased. The longer ignition delay between the pilot injection and main injection for the HVO fuel can lead to more engine cooling prior to the premixed combustion phase, which has been shown to release a lot of heat rapidly and can cause more engine damage as well as increased emissions. The use of pilot injection raises the internal gas temperature so that the cetane number does not affect the main combustion phase. This explains why the NOx emissions are not reduced significantly on this engine but have shown significant reductions in other engines with alternative control strategies.

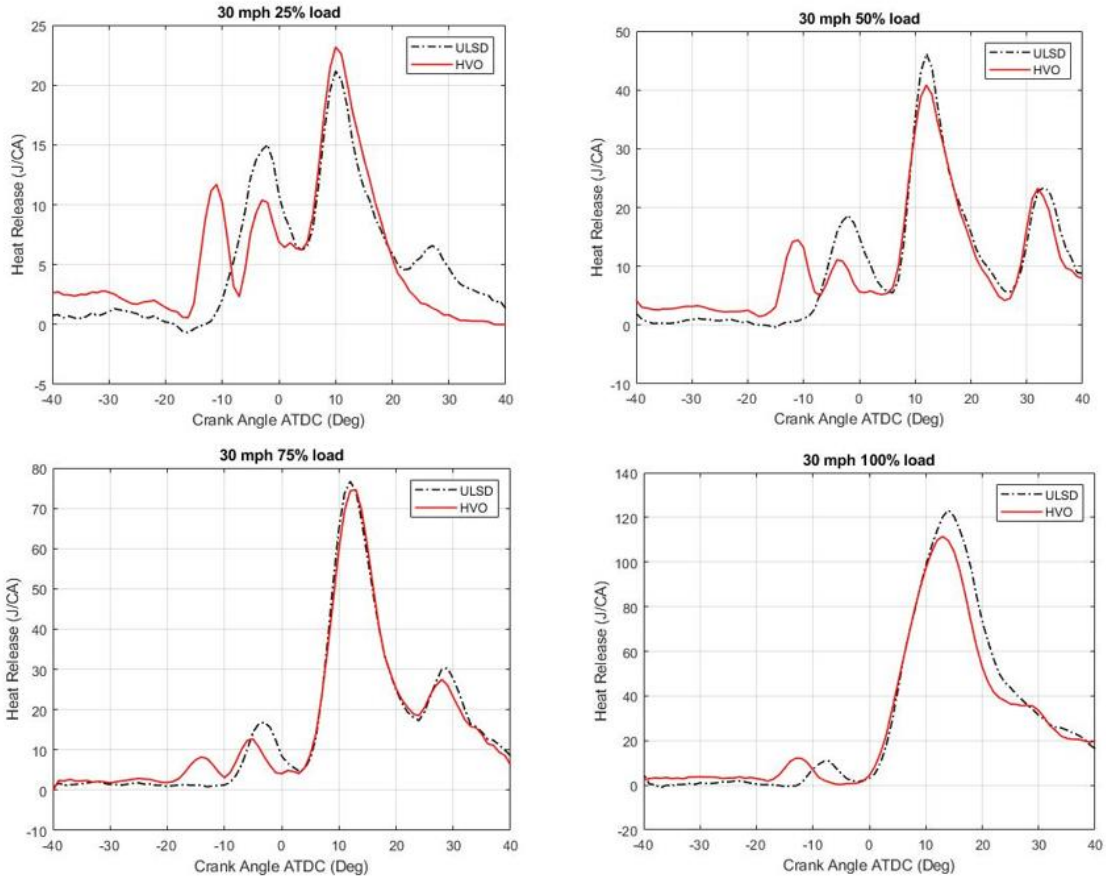

Figure 2-19 (a-d): Heat Release Rates for 30 mph steady state runs at different loads

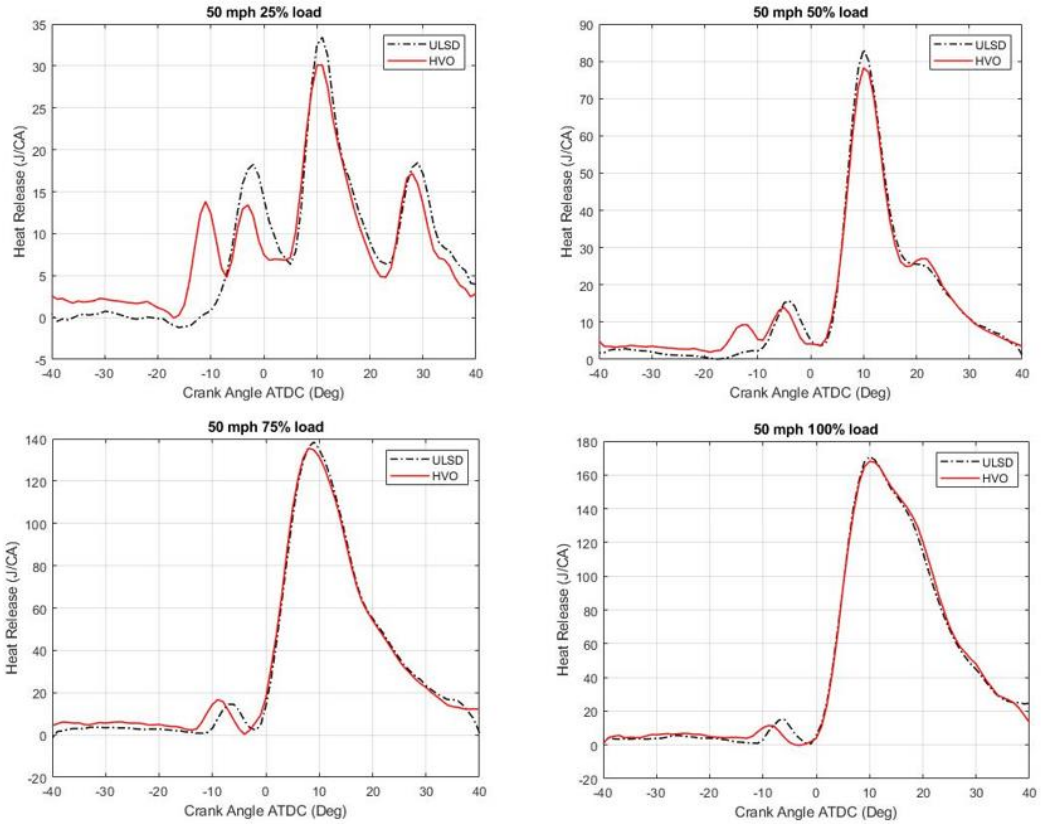

Figure 2-20 (a-d): Heat Release Rate from steady state runs at 50 mph at different loads

2.5 Conclusions

Engine-out emissions testing was conducted on a 2012 model year light-duty truck equipped with common rail diesel engine and operated on ULSD and neat HVO fuels over the LA-92 cycle and on steady-state conditions. The experimental results showed reductions in engine-out THC and CO emissions with HVO over the LA-92 cycle at a statistically significant level. Engine-out hot-running and weighted NOx emissions also showed statistically significant reductions with HVO compared to ULSD. CO_2 emissions and carbon balance fuel economy did not show any significant differences between the test

fuels. The small differences in fuel economy suggest that modern light-duty diesel vehicles are not calibrated to account for the differences in fuel properties when operated with neat HVO. Engine-out PM mass, soot mass, and solid particle number emissions showed large, statistically significant reductions with HVO fuel compared to ULSD, which can be attributed to the absence of sulfur and aromatic soot precursors in the HVO.

For the steady-state conditions, THC emissions were lower with the use of HVO, while CO emissions showed mixed results. Engine-out NOx emissions did not show big differences between the test fuels for the low and partial points; but at 100% load, the use of HVO resulted in noticeable NOx increases compared to ULSD.

In general, the chemical composition of HVO appeared relevant in respect to gaseous and particulate engine-out emissions over transient testing (i.e., LA-92 cycle), but not always for the stead-state conditions. These phenomena can be explained by the fact that the engine was equipped with a common rail system in which the physical properties of fuels had little influence on injection timing, and also the fluidity of HVO is close to petroleum diesel resulting in little differences in injection properties.

2.6 References

Aatola, H., Larmi, M., Sarjovaara, T., and Mikkonen, S., "Hydrotreated Vegetable Oil (HVO) as a Renewable Diesel Fuel: Trade-off between NOx, Particulate Emission, and Fuel Consumption of a Heavy Duty Engine," SAE Technical Paper 2008-01-2500, 2008, doi:https://doi.org/10.4271/200801-2500.

Bhardwaj, O., Kolbeck, A.F., Kkoerfer, T., and Honkanen, M., "Potential of Hydrogenated Vegetable Oil (HVO) in Future High Efficiency Combustion System," *SAE Int. J. Fuels Lubr.* 6(1):157-169, 2013, doi:10.4271/2013-01-1677.

Bohl, T., Smallbone, A., Tian, G., and Roskilly, A.P., "Particulate Number and NOx Trade-Off Comparisons between HVO and Mineral Diesel in HD Applications," *Fuel* 215:90-101, 2018.

Dimitriadis, A., Natsios, I., Dimaratos, A., Katsaounis, D. et al., "Evaluation of a Hydrotreated Vegetable Oil (HVO) and Effects on Emissions of a Passenger Car Diesel Engine," *Front. Mech. Eng* 4, 2018, doi:10.3389/ fmech.2018.00007.

Durbin, T.D., Pisano, J.T., Younglove, T., Sauer, C.G. et al., "The Effect of Fuel Sulfur on NH_3 and Other Emissions from 2000-2001 Model Year Vehicles," *Atmospheric Environment* 38:2699-2708, 2014.

Erkkilä, K., Nylund, N., Hulkkonen, T., Tilli, A. et al.,

"Emission Performance of Paraffinic HVO Diesel Fuel in Heavy Duty Vehicles," SAE Technical Paper 2011-01-1966, 2011, doi:https://doi.org/10.4271/2011-01-1966.

Gomez, A., Soriano, J.A., and Armas, O., "Evaluation of

Sooting Tendency of Different Oxygenated and Paraffinic Fuels Blended with Diesel Fuel," *Fuel* 184:536-543, 2016.

Happonen, M., Heikkila, J., Murtonen, T., Lehto, K. et al., "Reductions in Particulate and NOx Emissions by Diesel Engine Parameter Adjustments with HVO Fuel," *Environ. Sci. Technol.* 46:6198-6204, 2012.

Hartikka, T., Kuronen, M., and Kiiski, U., "Technical Performance of HVO (Hydrotreated Vegetable Oil) in Diesel Engines," SAE Technical Paper 2012-01-1585, 2012, doi:https://doi.org/10.4271/2012-01-1585.

Heikkila, J., Happonen, M., Murtonen, T., Lehto, K. et al., "Study of Miller Timing on Exhaust Emissions of a Hydrotreated Vegetable Oil (HVO)-Fueled Diesel Engine," *Journal of the Air & Waste Management Association* 62:13051312, 2012.

Hoekman, S.K., Broch, A., Robbins, C., and Ceniceros, E., "Investigation of Biodiesel Chemistry, Carbon Footprint and Regional Fuel Quality, CRC Project No. AVFL-17a, Final Report, 2011.

Kuronen, M., Mikkonen, S., Aakko, P., and Murtonen, T.,

"Hydrotreated Vegetable Oil as Fuel for Heavy Duty Diesel Engines," SAE Technical Paper 2007-01-4031, 2007, doi:https://doi.org/10.4271/2007-01-4031.

Kousoulidou, M., Dimaratos, A., Karvountzis-Kontakiotis,

A., Samaras, Z., "Combustion and Emissions of a CommonRail Diesel Engine Fueled with HWCO," *J. Energy Eng.* 140: A4013001(9), 2014.

Lehto, K., Elonheimo, A., Hakkinen, K., Sarjovaara, T., and Larmi, M., "Emission Reduction Using Hydrotreated Vegetable Oil (HVO) with Miller Timing and EGR in Diesel Combustion," SAE Technical Paper 2011-01-1955, 2011, doi:https://doi.org/10.4271/2011-01-1955.

Millo, F., Mallamo, F., Vlachos, T., Ciaravino, C. et al., "Experimental Investigation of the Effects on Performance and Emissions of an Automotive Euro 5 Diesel Engine Fueled with B30 from RME and HVO," SAE Technical Paper 2013-01-1679, 2013, doi:https://doi.org/10.4271/2013-01-1679.

Murtonen, T., Aakko-Saksa, P., Kuronen, M., Mikkonen, S., and Lehtoranta, K., "Emissions with Heavy-Duty Diesel Engines and Vehicles Using FAME, HVO, and GTL Fuels with and without DOC+POC aftertreatment," SAE Technical Paper 2009-01-2693, 2009, doi:https://doi.org/10.4271/200901-2693.

Na, K., Biswas, S., Robertson, W., Sahay, K. et al., "Impact of Biodiesel and Renewable Diesel on Emissions of Regulated Pollutants and Greenhouse Gases on a 2000 Heavy Duty Diesel Truck," *Atmospheric Environment* 107:307-314, 2015.

Napolitano, P., Beatrice, C., Guido, C., Del Giacomo, N. et al., "Hydrocracked Fossil Oil and Hydrotreated Vegetable Oil (HVO) Effects on Combustion and Emissions

Performance of 'torque-controlled' Diesel Engines," SAE Technical Paper 2015-01-2497, 2015, doi:https://doi. org/10.4271/2015-01-2497.

Napolitano, P., Giodo, C., Beatrice, C., and Pellegrini, L., "Impact of Hydrocracked Diesel Fuel and Hydrotreated Vegetable Oil Blends on the Fuel Consumption of Automotive Diesel Engines," *Fuel* 222:718-732, 2018.

No, S.Y., "Application of Hydrotreated Vegetable Oil from Triglyceride Based Biomass to CI Engines - A Review," *Fuel* 115:88-96, 2014.

Omari, A., Pischinger, S., Bhardwaj, O.P., Holderbaum, B. et al., "Improving Engine Efficiency and Emission Reduction Potential of HVO by Fuel-Specific Engine Calibration in

Modern Passenger Car Diesel Applications," SAE Technical Paper 2017-01-2295, 2017, doi:https://doi.org/10.4271/201701-2295.

Painter, L. and Rutherford, J., "Statistical Design and Analysis Methods for the Auto/Oil Air Quality Research Program," SAE Technical Paper 920319, 1992, doi:https://doi. org/10.4271/920319.

Pellegrini, L., Beatrice, C., and Di Blasio, G., "Investigation of the Effect of Compression Ratio on the Combustion Behavior and Emission Performance of HVO Blended Diesel Fuels in a Single-Cylinder Light-Duty Diesel Engine," SAE Technical Paper 2015-01-0898, 2015, doi:https://doi. org/10.4271/2015-01-0898.

Pflaum, H., Hofmann, P., Geringer, B., and Weissel, W.,

"Potential of Hydrogenated Vegetable Oil (HVO) in a Modern Diesel Engine," SAE Technical Paper 2010-32-0081, 2010, doi:https://doi.org/10.4271/2010-32-0081.

Prokopowicz, A., Zaciera, M., Sobczak, A. et al., "The Effects of Neat Biodiesel and Biodiesel and HVO Blends in Diesel Fuel on Exhaust Emissions from a Light Duty Vehicle with a Diesel Engine," *Environ. Sci. Technol.* 49:7473-7482, 2015.

Rantanen, L., Linnaila, R., Aakko, P., and Harju, T., "NExBTL - Biodiesel Fuel of the Second Generation," SAE Technical Paper 2005-01-3771, 2005, doi:https://doi. org/10.4271/2005-01-3771.

Shukla, P.C., Shamun, S., Gren, L., Malmborg, V. et al., "Investigation of Particle Number Emission Characteristics in a Heavy-Duty Compression Ignition Engine Fueled with Hydrotreated Vegetable Oil (HVO)," SAE Technical Paper 2018-01-0909, 2018, doi:https://doi.org/10.4271/2018-01-0909.

Singer, A., Schroder, O., Pabst, C., Munack, A. et al., "Aging Studies of Biodiesl and HVO and Their Testing as Neat Fuel and Blends for Exhaust Emissions in Heavy-Duty Engines and Passenger Cars," *Fuel* 153:595-603, 2015.

Singh, D., Subramanian, K.A., and Singal, S.K., "Emissions and Fuel Consumption Characteristics of a Heavy Duty Diesel Engine Fueled with Hydroprocessed Renewable Diesel and Biodiesel," *Fuel* 155:440-446, 2015.

Singh, D., Subramanian, K.A., and Garg, M.O., "Comprehensive Review of Combustion, Performance and Emissions Characteristics of a Compression Ignition Engine Fueled with Hydroprocessed Renewable Diesel," *Renewable and Sustainable Energy Reviews* 81:2947-2954, 2018.

Singh, D., Subramanian, K.A., Bal, R. et al., "Combustion and Emission Characteristics of a Light Duty Diesel Engine Fueled with Hydro-Processed Renewable Diesel," *Energy* 154:498-507, 2018.

Tan, C., Xu, H., Shuai, S.-J., Ghafourian, A. et al., "Investigation on Transient Emissions of a Turbocharged Diesel Engine Fueled by HVO Blends," SAE Technical Paper 2013-01-1307, 2013, doi:https://doi.org/10.4271/2013-01-1307.

Vo, C., Charoenphonphanich, C., Karin, P., Susumu, S., and Hidenori, K., "Effects of Variable O2 Concentrations and Injection Pressures on the Combustion and Emissions Characteristics of the Petro-Diesel and Hydrotreated Vegetable Oil-Based Fuels under the Simulated Diesel Engine Condition," *Journal of the Energy Institute* 91:10711084, 2018.

Wu, Y., Ferns, J., Li, H., and Andrews, G., "Investigation of Combustion and Emission Performance of Hydrogenated Vegetable Oil (HVO) Diesel," SAE Technical Paper 2017-012400, 2017, doi:https://doi.org/10.4271/2017-01-2400.

3. Physical and Chemical Characteristics of Gaseous and Particulate Emissions from HVO and Biodiesel Blend from Heavy-Duty On-Road and Off-Road Engines

3.1 Abstract

Renewable diesel and renewable diesel/biodiesel blends are among newer fuel types that can help achieve reduced nitrogen oxide (NOx) and particulate matter (PM) emissions from diesel engines. The objective of this study was to characterize the regulated and unregulated emissions from renewable diesel and biodiesel fuel blends in two heavy-duty diesel engines. This testing compared the emissions from different fuels for a new technology on-road diesel engine with diesel oxidation catalyst (DOC), diesel particle filter (DPF), and selective catalytic reduction (SCR) emissions aftertreatment and a legacy off-road diesel engine with no aftertreatment systems. Emissions testing was conducted on an engine dynamometer over a ramped modal steady state cycle and transient certification cycle. Testing was conducted utilizing a California Air Resources Board ultra-low sulfur diesel (ULSD), neat renewable diesel (R100) and two renewable diesel biodiesel blends. Toxic emissions measurements were made to quantify the inorganic speciation of PM, carbonyl compounds (aldehydes and ketones), volatile organic compounds (VOCs), and polycyclic aromatic hydrocarbons (PAHs) and their nitrated derivatives (nitro-PAHs). Additional carcinogenic potency and ozone forming potential of PAHs and all VOCs was performed. Results suggest that Renewable diesel has the potential to reduce NOx

emissions for both engines and cycles compared to CARB ULSD. Increases in NOx emissions were seen for the renewable diesel-biodiesel blends compared to R100 fuel but have the potential to remain NOx neutral in off-road engines with no aftertreatment system at low enough biodiesel blend levels. In general, toxic emissions decreased with increasing biodiesel content.

3.2 Introduction

Global demand for biofuels has increased significantly in recent years due to the potential benefits in emissions reductions and decreased reliance on petroleum derived fuels. The California Air Resources Board (CARB) has committed to adopt a low emission diesel (LED) measure as part of the state strategy for the California State Implementation Plan (SIP) to reduce oxides of nitrogen (NOx) and particulate matter (PM) emissions from on-road and off-road vehicles and equipment (CARB, 2017). This measure is expected to recognize emission reductions from fuels that can reduce NOx and/or PM. Renewable diesel (RD) and renewable diesel/biodiesel blends are among the fuels that can help achieve the goals of the LED measure and contribute to the diesel emissions reduction targets for California.

Fatty acid methyl esters (FAME), commonly known as biodiesel, is the most widely used biofuel used for diesel engines (EIA 2020). Biodiesel is produced through the transesterification reaction from edible or non-edible vegetable oils, animal fats, and waste cooking oils. In this process, triglycerides are reacting in the presence of an alkaline catalyst (usually sodium or potassium methoxide) to form esters and glycerol.

Transesterification is a three-step process in which triglycerides form diglycerides, diglycerides form monoglycerides, and from monoglycerides glycerol is produced (Marchetti et al., 2007; Ma and Hanna, 1999). Biodiesel is an oxygenated fuel (about 11%), free of sulfur and aromatic compounds, readily biodegradable, and non-toxic. It possesses superior lubricating properties than petroleum diesel and is characterized by its relatively higher cetane number (Knothe and Steidley, 2005; Giakoumis EG, Sarakatsanis CK., 2019). Biodiesel's cetane number largely depends on the number of double bonds in the ester backbone, which indicates the degree of unsaturation of the fuel (Knothe et al., 1998). Fewer double bonds and a highly saturated fuel will be characterized by a high cetane number. Biodiesel is also known for its poor oxidation stability, which largely depends on the decree of unsaturation (number of double bonds) in the ester molecule (McCormick et al., 2007).

Many studies have investigated the influence of biodiesel on engine performance, combustion, and emissions (Knothe et al., 2005; Mueller et al., 2009; Lapureta et al., 2007; Ozener et al., 2012; Qi et al., 2010). Owing to its higher oxygen content, biodiesel can provide several benefits over typical petroleum diesel such as decreased PM, THC, and CO emissions (Knothe et al., 2005; Waynick, 2005; Ozener er al., 2012). However, biodiesel does have many drawbacks as evidenced by several chassis and engine dynamometer studies in biodiesel concluding that NOx formation is increased with the use of biodiesel fuels (Szybist et al., 2007; Xue et al., 2011; Basha et al., 2009). Mueller et al. (2009) showed that biodiesel NOx increases can be attributed to a number of different factors that include a shorter, more advanced combustion event, longer residence times, and higher

peak temperatures, for which air fuel ratios closer to stoichiometry are a key factor. In addition to NOx increases, biodiesel faces storage stability issues and is susceptible to oxidation and fuel degradation (Waynick, 2005).

These issues have led to the need to find another alternative fuel source for diesel engines that addresses the issues put forth by biodiesel. Hydrogenated vegetable oil (HVO), also known as renewable diesel, is a second-generation biofuel used in compression engines and is gaining popularity due to its improved cold temperature performance, increased storage stability, and NOx benefits when compared to biodiesel, as well as PM benefits when compared to ultra-low sulfur diesel (ULSD) (Singh et al., 2018; Ogunkoya et al., 2015). Similar to biodiesel, HVO is derived from vegetable oils, animal fats, waste cooking oils, and forest/biomass residues. HVO is produced through a process called hydrotreating, in which the feedstock is mixed with hydrogen and introduced to a catalyst at high temperatures and pressures. During this process, the fatty acids are saturated, triglycerides are broken down, and hydrogen atoms replace the oxygen atoms in the triglyceride molecules to form paraffinic hydrocarbons that are molecularly akin to diesel fuel without any ester functional group. HVO properties, including high cetane number, narrow distillation curve, high heating value can provide many benefits compared to biodiesel (Erkkila et al., 2011; Gomez et al., 2016; Rantanen et al., 2005; Singh et al., 2018). The high cetane number of HVO can lead to shorter ignition delays and reduced engine out emissions. Other researchers have shown THC, CO, NOx, and PM emissions benefits of HVO when compared to ULSD (Aatola et al., 2008; Na et al., 2015; Hajbabaei et al., 2012). Sugiyama et al. (2011) found that the benefits of the shorter ignition delay may not be as

pronounced for HVO in engines configured with pilot injection. However, this study also showed smoke and HC benefits even when pilot injection is utilized due to the aromatic free nature of the fuel. Bohl et al. (2018) also reported no reductions in NOx emissions with HVO, but reductions in particle number emissions. This was attributed to better fuel-air mixing, absence of aromatics, and low boiling range components of HVO compared to diesel fuel. Karavalakis et al. (2016a) also found some operational differences in using an HVO fuel in modern heavy-duty vehicles that lead to some emissions increases for HVO that were outside the impacts that might be expected based on typical combustion chemistry.

Although there are many studies characterizing combustion performance and emissions of HVO and biodiesel, there is a lack of literature on the emissions characterization of HVO-biodiesel fuel blends. This is particularly true for blends in higher cetane diesel fuels, such as CARB ULSD, which is the focus of CARB's LED regulatory effort. There is also limited information available on the impacts of renewable diesel and renewable diesel blends in new technology diesel engines (NTDEs) that are equipped with diesel particular filters (DPFs) and selective catalytic reduction (SCR) or in off-road engines, where the benefits of renewable diesel fuel might be more long lasting due to their less stringent emissions standards over time. The characterization of toxic pollutants from these fuel blends is also limited and needs to be expanded. The purpose of this study is to further evaluate emissions and performance effects resulting for the use of renewable diesel and renewable diesel/biodiesel blends relative to CARB diesel in off-road legacy diesel engines and in new technology on-road diesel engines. Four fuels were utilized in this study including,

neat CARB ULSD, neat renewable diesel (R100), and two renewable diesel-biodiesel blends of 65% renewable diesel and 35% biodiesel (R65/B35) and 50% renewable diesel and 50% biodiesel (R50/B50). In addition to characterizing regulated emissions, sampling for toxic emissions was performed.

3.3 Experimental

3.3.1 Test Engine and Aftertreatment

Testing was conducted on two heavy-duty diesel engines. This included one legacy heavy-duty off-road diesel engine with no DPF or SCR and one NTDE heavy-duty on-road diesel engine equipped with a DOC, a DPF, and a SCR aftertreatment system. Information on the engines and aftertreatment systems is provided in Table 3-1. Both engines were monitored prior to testing to ensure conformability with the emissions standards.

Table 3-1: Vehicle Technical Specs

Category	Off-road legacy	On-road NTDE
Model year	2009	2019
Manufacturer	John Deere	Cummins
Engine Family	9JDXL6.8105	KCEXH0912XAW
Engine Type	In-line 4-cylinder, 4-stroke	In-line 6-cylinder, 4-stroke
Displacement	4.5L	14.9L
Power Rating	115hp	500 hp
Fuel Type	Diesel	Diesel
Induction	Turbocharged	Turbocharged
Emissions Control	None	EGR, DOC, DPF, SCR
Emission Standards	2004	2010

3.3.2 Test Fuels

Four different test fuels were utilized, including a CARB Reference Diesel (CARB ULSD) that was the base fuel for comparisons, a neat renewable diesel (R100), and two renewable diesel and biodiesel blends. The renewable diesel/biodiesel fuels were blended at CE-CERT and included a blend with 65% Renewable Diesel and 35% Biodiesel (R65/B35) and 50% Renewable Diesel and 50% Biodiesel (R50/B50). As a baseline fuel, the CARB reference fuel used in this study met the reference fuel specifications in Table A.9 of the ADF regulation and did not contain any renewable diesel or biodiesel. The reference CARB ULSD was obtained from a single batch in a volume sufficient for the full test program to minimize variations in fuel properties over the course of the study. Fuel

specifications are presented in Table 3-2. The fuel properties show that R100 and the biodiesel blends demonstrated very low or below the detection limits of the method aromatic and polyaromatic hydrocarbons. Cetane number, an ignition quality property, was significantly higher for the paraffinic R100 compared to CARB ULSD.

Table 3-2. Fuel Analysis Results and Specifications

Property	ASTM Test Method	Units	CARB ULSD	R100	R65/B35	R50/B50
Sulfur	D5453	ppm	<0.5	<0.5	1.34	1.60
Aromatics	D5186	Vol. %	9.9	1.2	-	-
Polycyclic aromatic hydrocarbons	D5186	Wt. %	1.2	0.2	-	-
Nitrogen content	D4629	ppm	4.9	<1.0	4.8	6.8
Cetane Number	D613	unitless	48.2	79.8	67.7	67.7
API Gravity	D287	unitless	38.0	49.1	41.5	38.4
Density	D287	g/ml	0.8344	0.7831	0.8179	0.8328
Carbon weight fraction	D5291	wt%	86.30	84.96	82.28	81.13
Kinematic Viscosity, 40°C	D 445	mm^2/s	2.54	3.031	3.510	3.716
Flash Point	D93	°F	189	146	164	175
Distillation Temp, atmospheric, IBP	D86-IBP	°F	395.5	285.8	315.5	332.1
Distillation Temp, atmospheric, T10	D86-T10	°F	435.7	487.7	528.3	546.5
Distillation Temp, atmospheric, T50	D86-T50	°F	486.5	552.3	580.6	597.8
Distillation Temp, atmospheric, T90	D86-T90	°F	559.3	566.9	630.0	639.4
Distillation Temp, atmospheric, TEP	D86-EP	°F	601.6	586.9	654.0	659.6

*API gravity for certificate of analysis used ASTM Method D4052.

3.3.3 Test Cycles and Procedures

Testing was conducted in CE-CERT's heavy-duty engine dynamometer test laboratory. A 600 horsepower (hp) GE DC electric engine dynamometer that was obtained from the EPA's National Vehicle and Fuel Emissions Laboratory in Ann Arbor, MI, was used for the testing. The system is fully complaint according to the Code of Federal Regulations (CFR).

Testing was conducted at least nine times with each fuel over a non-road transient cycle (NRTC) and a steady state (D2) cycle for the Off-Road Legacy engine and a Federal Test Protocol (FTP) and a Ramped Modal Cycle (RMC) for the NTDE. Table 3-3 shows the full test matrix utilized for both engines.

Table 3-3: Full Test Matrix for All Engines and Cycles

Engine Type	Duty Cycle	Day 1	Day 2	Day 3	Day 4	Day 5	Day 6	Day 7
Off-Road Legacy	NRTC	CCC B1B1B1 B2B2B2	B3B3B3 CCC B1B1B1	B2B2B2 B3B3B3 CCC	B1B1B1 CCC B3B3B3	CCC B2B2B2 CCC	-	-
	D2	CCC B1B1B1 B2B2B2	B3B3B3 CCC B1B1B1	B2B2B2 B3B3B3 CCC	B1B1B1 CCC B3B3B3	CCC B2B2B2 CCC	-	-
On-Road NTDE	FTP	CCC B1B1B1	B2B2B2 CCC	B1B1B1 B3B3B3	CCC B2B2B2	B3B3B3 CCC	B2B2B2 B1B1B1	CCC B3B3B3
	RMC	CCC B1B1B1	B2B2B2 CCC	B1B1B1 B3B3B3	CCC B2B2B2	B3B3B3 CCC	B2B2B2 B1B1B1	CCC B3B3B3

C = Reference CARB ULSD
B1 = R100/R99
B2 = R65/B35
B3 = R50/B50

3.3.4 Emissions Test

The engine dynamometer was used in conjunction with CE-CERT's Mobile Emissions Lab (MEL) for the emissions measurements. MEL is designed with a full dilution tunnel and CFR complaint analytical instrumentation. For all tests, standard emissions measurements of total hydrocarbons (THC), carbon monoxide (CO), NO_x, carbon dioxide (CO_2), PM, black carbon (BC), total and solid particle number (PN), and particle size distributions (PSD), were measured. CO and CO_2 emissions were measured with a 602P nondispersive infrared (NDIR) analyzer from California Analytical Instruments (CAI). THC, NMHC, and CH_4 emissions were measured with 600HFID flame ionization detector (FID) from CAI. NO_x emissions were measured with 600HPLC chemiluminescence analyzer from CAI. Fuel consumption was derived from the CO_2, CO, and THC emissions by the carbon balance, using measured densities and carbon weight fractions of the fuels. PSDs and total particle number (TPN) measurements were taken from the CVS using a TSI 3090 Engine Exhaust Particle Sizer (EEPS) and TSI 3722 Condensation Particle Counter (CPC), respectively. BC and solid particle number (SPN) were measured using an AVL MSS and AVL Advanced Particle Counter (APC).

The mass concentrations of PM2.5 were obtained by analysis of particulates collected on 47mm diameter 2μm pore Teflo filters (Whatman brand). The filters were measured for net gains using a UMX2 ultra precision microbalance with buoyancy correction in accordance with the weighing procedure guidelines of the Code of Federal Regulations (CFR). Two tunnel blanks before and after the campaign were run to correct the data

represented here. Tunnel blanks were collected over the same duration at the NRTC cycle. These and other tunnel blanks were also used to correct the toxic samples.

Elemental carbon (EC), organic carbon (OC), metals, carbonyls, volatile organic compounds (VOCs), polycyclic aromatic hydrocarbons (PAHs), and nitrated polycyclic aromatic hydrocarbons (nitro-PAHs) were measured in addition to the regulated gaseous and PM emissions for a select number of tests. Table 3-4 describes the cycles in which the emission measurements were made.

A Thermal/Optical Carbon Aerosol Analyzer (Sunset Laboratory, Forest Grove, OR) was used to quantify elemental and organic carbon (EC/OC) emissions using NIOSH (National Institute of Occupational Safety and Health) Method 5040. EC/OC samples were collected on QAT Tissuquartz quartz-fiber filters (Pall-Gelman, Ann Arbor, MI, USA) that were pre-cleaned firing for 5 hours at 600 °C to remove carbonaceous contaminants. Filters were kept frozen after testing and sent to Chester LabNet (Tigard, OR) for analysis.

Exhaust PM2.5 samples collected on 47mm Teflon filters were sent to Chester LabNet for analysis using X-Ray fluorescence (XRF) method, according to EPA IO-3.3, to quantify trace elements and metals. Carbonyls were collected on 2,4-dinitrophenylhydrazine cartridges (DNPH) from the secondary dilution unit. Carbonyl analysis was performed according to EPA Method T0-11 to determine the emission rates of formaldehyde, acetaldehyde, as well as other aldehydes and ketones. Exhaust from the CVS was collected in SUMMA® canisters for analysis of volatile organic compounds, including monoaromatic hydrocarbon species. EPA Method T0-15 was used to provide

concentrations for 69 VOCs that are included in the 189 hazard air pollutants (HAPs) listed in title III of the Clean Air Amendments of 1990. Analysis of the hydrocarbon species was conducted using a Gas Chromatography/Mass Spectrometry/Flame Ionization Detector (GC/MS/FID) analytical system. Carbonyl and monoaromatic VOC analysis was performed by Atmospheric Analysis and Consulting (AAC) (Ventura, CA).

Particle-phase and vapor-phase PAH and nitrated PAH analysis was performed by Desert Research Institute (DRI) (Reno, NV). Particulate-phase PAH samples were collected on Teflon-impregnated glass fiber (TIGF) filters (100 mm). Semi-volatile organic compounds (SVOC) were collected using an Amberlite XAD-4 polyaromatic absorbent resin (Aldrich Chemical Company, Inc.). The PAH samples were cumulative samples over the full LA92 cycle. The SVOCs were extracted separately for the semi-volatile and particle-PAHs with high-purity, high performance liquid chromatography (HPLC)-grade dichloromethane. The accelerated solvent extraction (ASE) method was used for extraction, where the media was put in an cell for 15 min at 1500 psi and 80 °C. Deuterated internal standards that were added prior to extraction for both the XAD and filters included: naphthalene-d_8, acenaphthylene-d_8, phenanthrene-d_{10}, anthracene-d_{10}, chrysene-d_{12}, pyrene-d_{10}, benz[a]anthracene-d_{12}, benzo[a]pyrene-d_{12}, benzo[e]pyrene-d_{12}, benzo[k]fluoranthene-d_{12}, benzo[g,h,i]perylene-d_{12}, and coronene-d_{12}. Extracts were vacuum concentrated at 35-45 °C by rotary evaporation to ~1 mL, and filtered with a disposable 0.2 μm PTFE filter (Whatman Pura disc TM 25TF). The filtrate volume, including the flask rinse with solvent, was ~4 mL, to which ~500 μl of hexane was added. This mixture was then reduced to ~250

μL using a gentle stream of ultra-high purity (UHP) nitrogen (with a Chrompack CP-Gas-Clean moisture filter).

Electron impact (EI) gas chromatography-mass spectrometry (GC-MS) by selective ion monitoring (SIM) using a CP-8400 autosampler equipped Varian 4000 GC-MS with a 30-m 5% phenylmethylsilicone fused-silica capillary column (DB-5MS+DG, J&W Scientific, Folsom CA) was used to analyze the XAD extracts. Filter-based PAHs were analyzed with a Scion 456 GC interfaced with a Scion TQ triple quadrupole MS/MS and equipped with CP-8400 autosampler with the same capillary column described above. For each compound quantified, a 6-level calibration a mid-level check was done at least once every ten samples.

Statistical analysis was performed using a simple two-sample t-test assuming equal variances with a two-tailed distribution in order to evaluate the emissions differences between fuels. T-test results with a P-value less than 0.05, giving a 95% confidence interval, were considered statistically significant for this study.

Table 3-4: Toxics Emissions Measurements for On-Road Cummins Engine and Off-Road John Deere Engine

Fuel	Number of Tests for Each Cycle	
	FTP/NRTC	SET/D2
CARB ULSD	2	2
R100	2	2
R65/B35	2	-
R50/B50	2	2

3.4 Results

3.4.1 NOx Emissions

Average NOx emissions in g/bhp-hr are presented in Figure 3-1. Note that the John Deere engine results are divided by a factor of 10 to show the results for both engines on the same graph. The error bars for the graphs represent on standard deviation of the average for each test sequence.

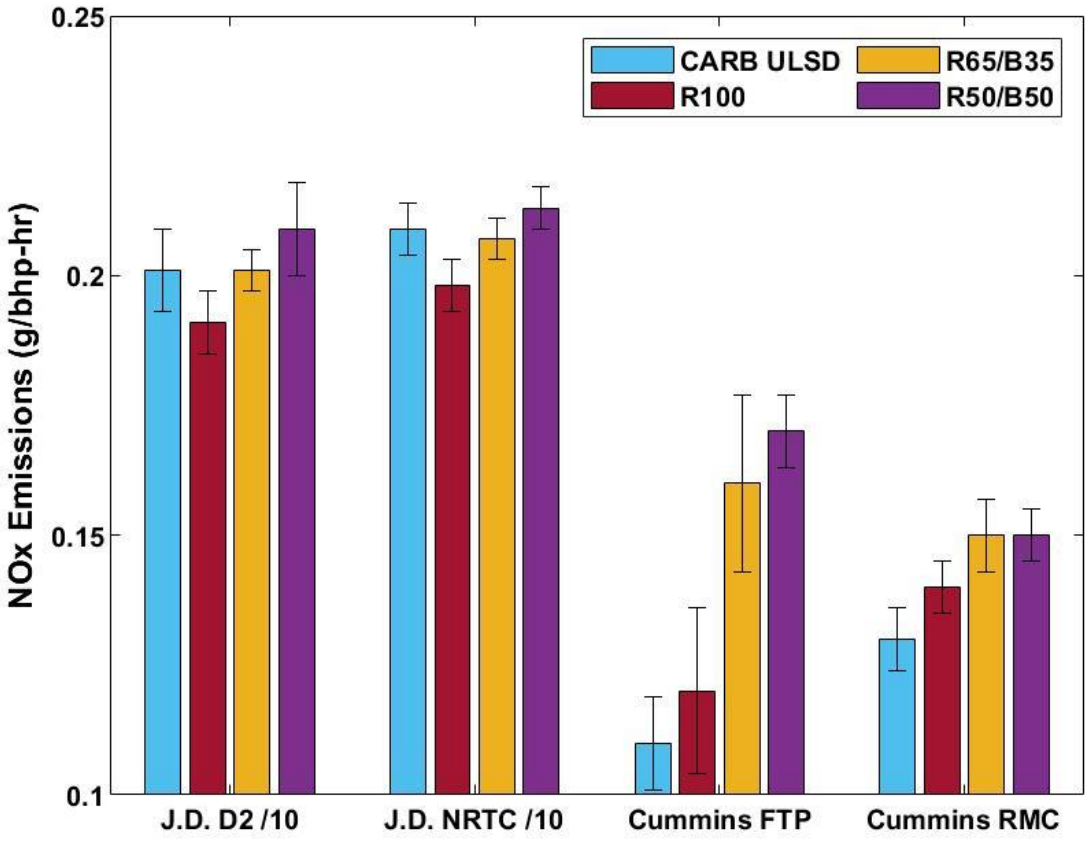

Figure 3-1: Averaged NOx emissions for all fuel/cycle combinations and both engines

The off-road legacy John Deere engine showed statistically significant reductions in NOx emissions for the R100 compared to the CARB ULSD of 4.9% and 5.3% over the D2 and NRTC cycles, respectively. The biodiesel-renewable diesel fuel blends showed increases in NOx emissions when compared to the R100 fuel. The R65/B35 blend showed NOx emissions similar to those of the CARB ULSD and did not show any statistically significant differences. However, the R50/B50 blend did show statistically significant increases in NOx emissions of 4.2% and 1.8%, respectively, over the D2 and NRTC cycles.

For the on-road Cummins engine, NOx emission levels were lower than those of the John Deere engine due to the SCR technology, as well as the use of exhaust gas recirculation (EGR). The latter helps prevent in-cylinder NOx formation by lowering the combustion temperature. SCR technology converts NOx into elemental hydrogen and water over a catalyst. R100 did not show any statistically significances with the CARB ULSD for the Cummins engine. Increases in NOx emissions were seen, however, when the renewable diesel was mixed with higher levels of biodiesel. These differences were statistically significant and ranged from 14.2% to 49.61%, respectively, for the RMC and FTP cycles depending on the biodiesel blend level. For both cycles, the higher biodiesel blend (R50/B50) resulted in higher NOx emissions. Previous studies have also reported NOx emission increases from SCR-equipped vehicles with biodiesel fuels (Karavalakis et al., 2017; Borillo et al., 2015; Kawano et al., 2010). NOx emissions were also measured using the data from the NOx sensors equipped on the Cummins engine before and after the SCR. Sensor data is not as reliable as laboratory grade instruments, but it does provide insight into the reduction efficiency of the SCR and the fuel effect on NOx emissions from the

engine out combustion. Figure 3-2 shows the sensor NOx emissions for the Cummins engine over the RMC cycle. Engine out NOx sensor data shows that there are increases in engine out NOx levels for the biodiesel blends, which is the main factor contributing to the higher tailpipe emissions for the renewable diesel/biodiesel blends. The SCR had a NOx reduction efficiency of 95% for all fuels suggesting the SCR will not be affected by the differences in NOx emissions between the different fuels. Note that the FTP cycle NOx sensor data is not available as it is a hot-start cycle and the NOx sensor did not reach its operation temperature until 280 seconds into the cycle.

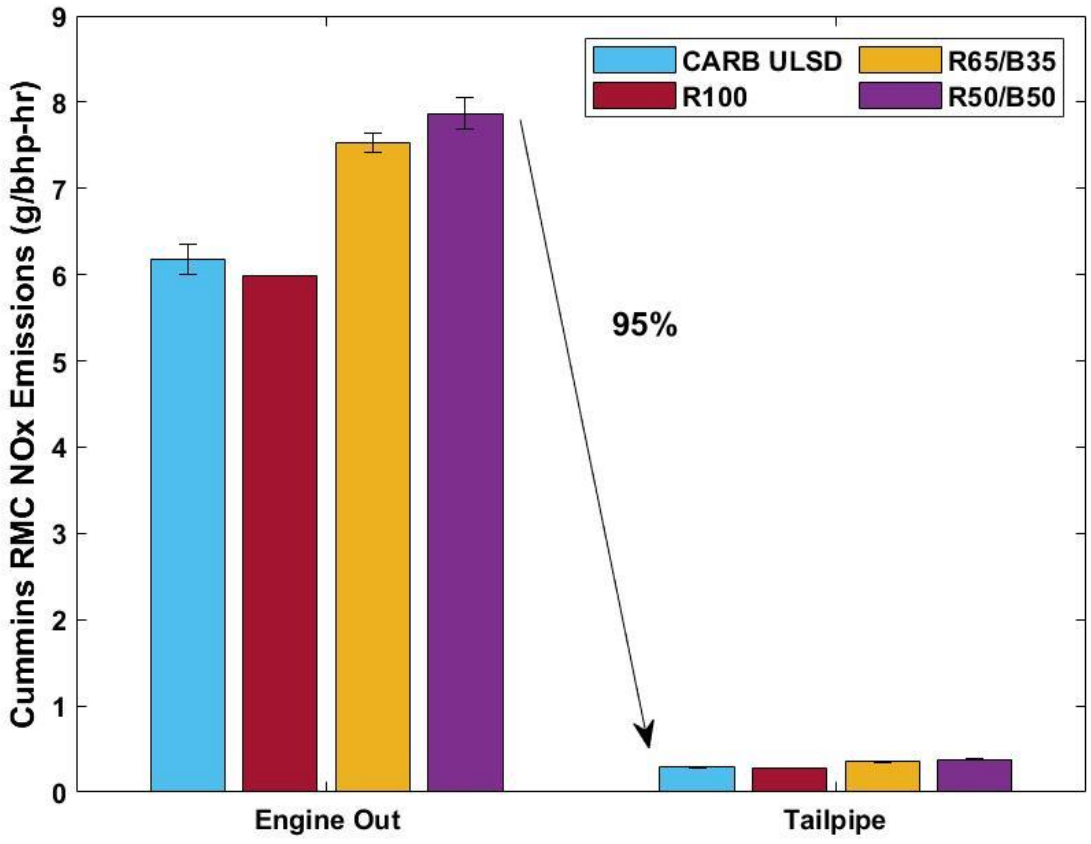

Figure 3-2: Average sensor-based NOx emissions for the Cummins RMC cycle

Differences in NOx emissions between renewable diesel and petroleum diesel are due to the different composition of these fuels. Renewable diesel contains mostly straight chain hydrocarbons in the C11-C14 range. Petroleum diesel contains more aromatic compounds and longer alkane chains. The reductions in NOx emissions with pure renewable diesel (R100) can be ascribed to the absence of aromatic hydrocarbon in the fuel. Aromatics have higher adiabatic flame temperature and lower H/C ratio, therefore producing higher combustion temperature and more thermal NOx formation (Happonen et al., 2012; Heikkila et al., 2012; Karavalakis et al., 2016a; Suarez-Bertoa et al., 2019).

The elevated NOx emissions for the biodiesel blended fuels are likely due to the oxygen content in the methyl ester, which led to an air-fuel ratio closer to stoichiometry than for the CARB ULSD or neat R100, which contributes to higher in-cylinder combustion temperatures and longer residence times at high temperatures (Mueller et al., 2009). The results reported here are consistent with previous studies reporting higher NOx emissions with biodiesel fuels compared to petroleum diesel (Hajbabaei et al., 2012, 2014; Karavalakis et al., 2016; Mueller et al., 2009; Na et al., 2015; Eckerle et al., 2008; Borillo et al., 2015; Kousoulidou et al., 2010; Karavalakis et al., 2017).

3.4.2 CO and THC Emissions

Average CO and THC emissions are presented in Figure 3-3 and Figure 3-4, respectively. CO and THC emissions are products of incomplete combustion in compression ignition engines. CO emissions depend mainly on the air-fuel ratio, with higher CO concentrations in the exhaust as air-fuel ratio decreases (Giakoumis et al., 2012). THC emissions are

formed during the ignition delay period due to either very low air-fuel ratios or under-mixing of fuel that prevents ignition.

For the John Deere engine, all biofuel blends showed CO and THC emissions decreases over both test cycles. THC emissions showed the same trends as CO emissions, with the R50/B50 blend showing the largest reductions. CO emissions showed decreases ranging from 13.7% - 21.9%, 25.6% - 27.9%, and 31.6% - 31.9% for the R100, R65/B35, and R50/B50, respectively, over both test cycles. THC emissions showed decreases ranging from 34.7% - 45.5%, 49.4% - 58.1%, 66.0% - 70.7% for the R100, R65/B35, and R50/B50, respectively, when compared to CARB ULSD. Reductions in THC and CO emissions with the biofuel blends were mainly attributed to the higher oxygen content in the ester moiety that favors more complete combustion. For the R100 fuel, the higher cetane number compared to CARB ULSD may have contributed to the advanced injection and thus lower engine-out CO and THC emissions.

The on-road Cummins engine produced significantly lower CO and THC emissions compared to the John Deere engine. This is due to the presence of the DOC, which effectively oxidizes CO and THC to CO_2 and H_2O. As such, there was no fuel effect seen on the CO and THC emissions. THC emissions were near background levels for each test.

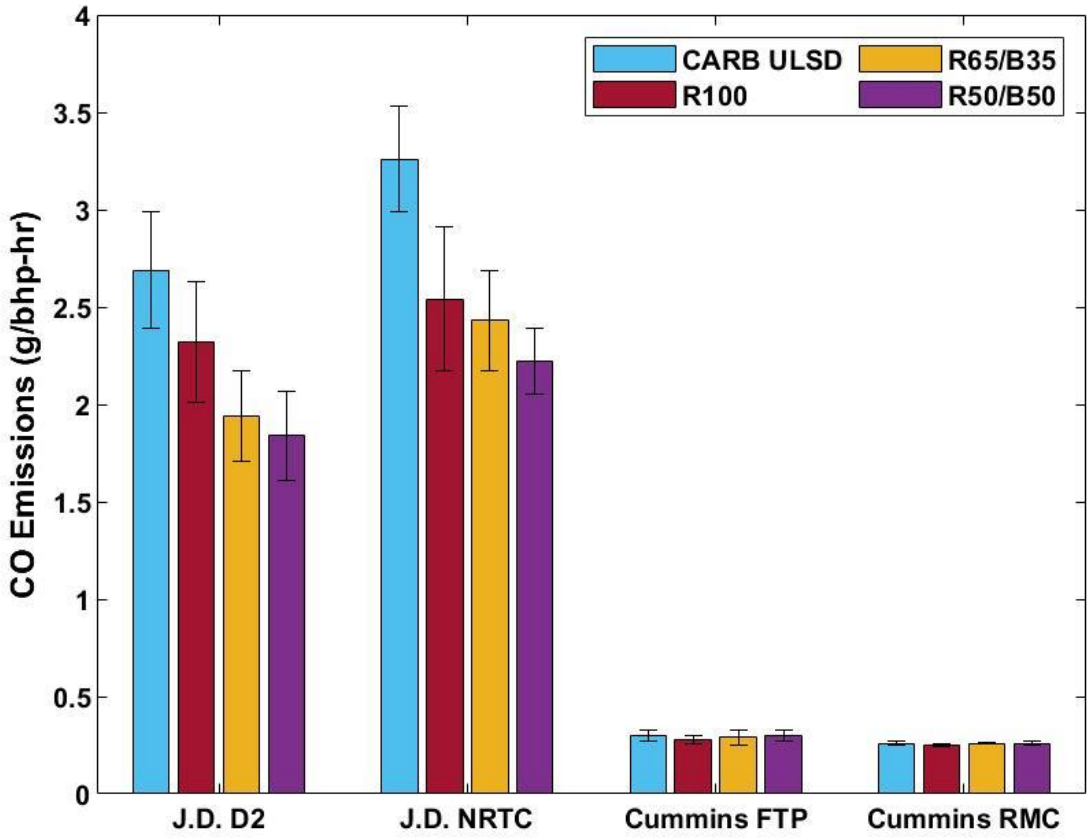

Figure 3-3: Averages CO emissions for all fuel/test cycle combinations and both engines

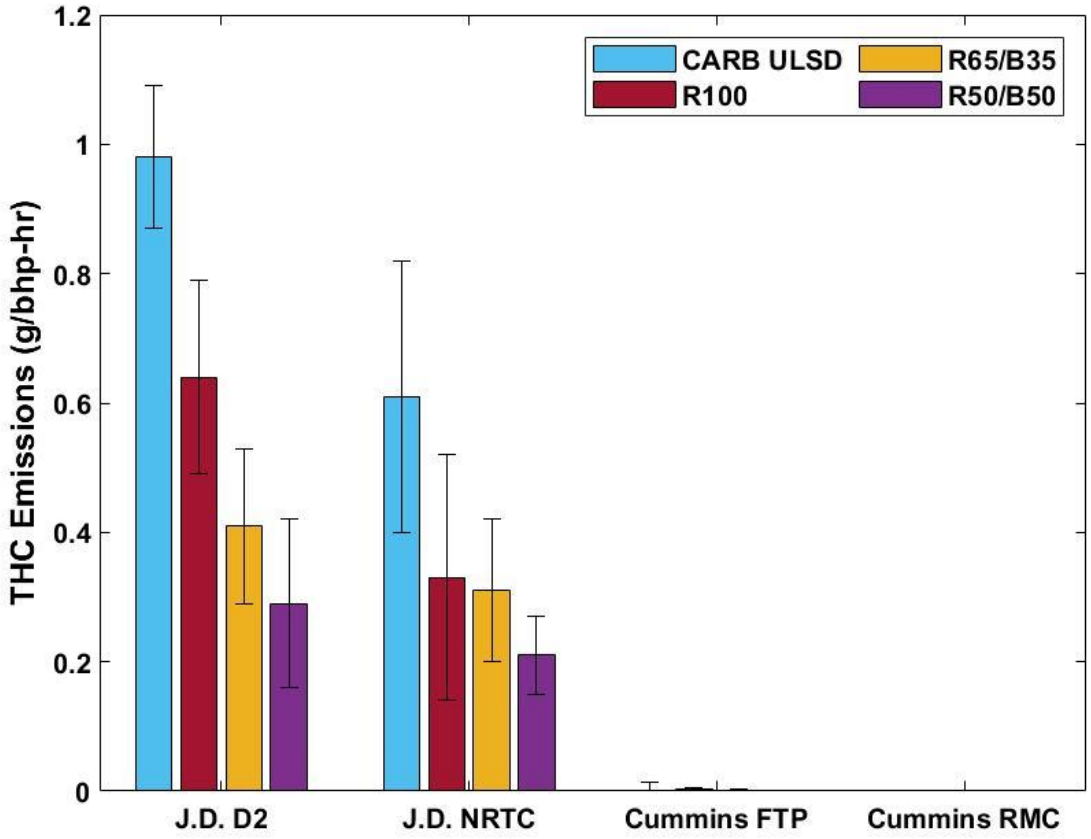

Figure 3-4: Averaged THC emissions for all fuel/test cycle combinations and both engines

3.4.3 CO_2 Emissions

CO_2 emissions are shown in Figure 3-5 and calculated brake specific fuel consumption (BSFC) is shown in Figure 3-6. CO_2 emissions showed decreases for the neat R100 and for both biodiesel and renewable diesel blends. Previous studies have reported lower CO_2 emissions with renewable diesel fuels and were attributed to the lower C/H ratios for these fuels relative to petroleum diesel (Karavalakis et al., 2016b; Suarez-Bertoa et al., 2019). Previous studies of biodiesel, on the other hand, have typically shown higher CO_2 emissions relative to typical diesel fuels, which has been attributed to a higher carbon

content per unit of energy in the fuel for biodiesel (U.S. EPA, 2002). For this study, the renewable diesel/biodiesel blends show higher emissions than the neat R100 fuels, which can be attributed to the higher carbon content per unit energy for the biodiesel fuels, but the renewable diesel/biodiesel blends still have lower CO_2 emissions than the CARB ULSD, which suggest the lower C/H ratios for R100 fuel is a more important factor in this comparison.

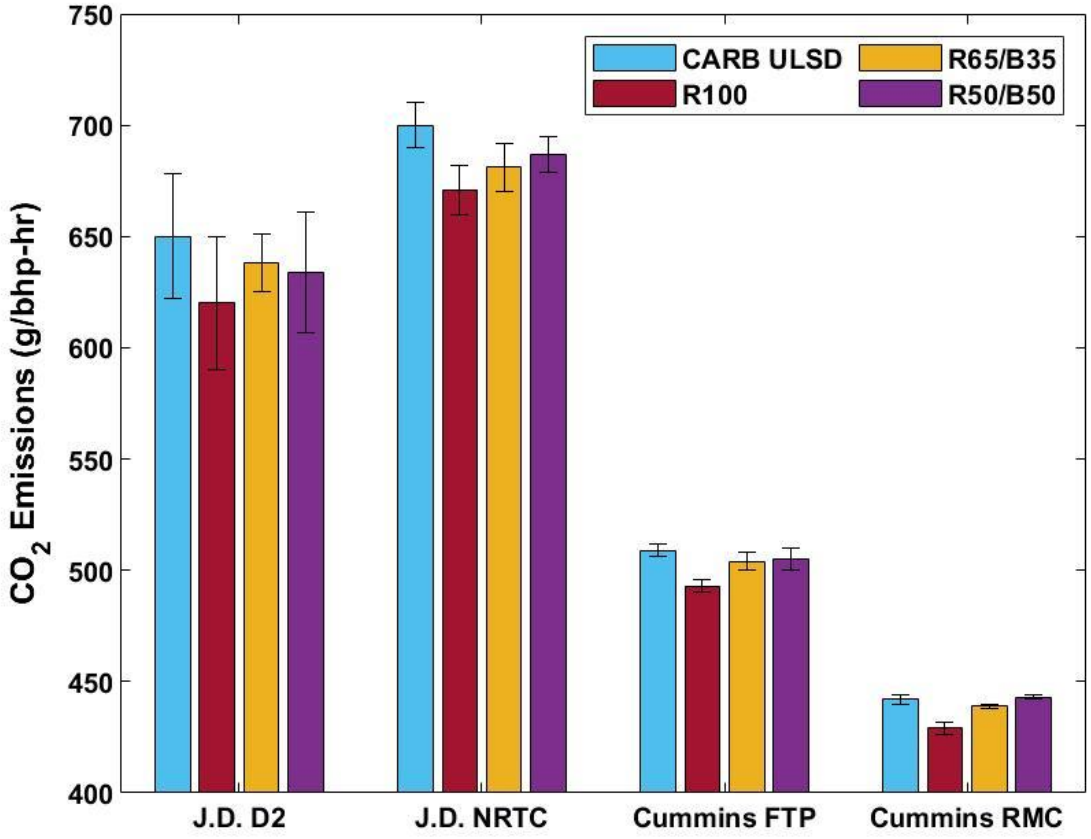

Figure 3-5: Averaged CO_2 emissions for all fuel/test cycle combinations and both engines

The R100 and the renewable diesel/biodiesel blends both showed higher BSFC than the CARB ULSD. The higher fuel consumption for the renewable diesel can be attributed to the lower density and energy content of the renewable diesel (Hajbabaei et al., 2013; Karavalakis et al., 2016a; Rothe et al., 2005). Biodiesel also has a lower energy content, due to the oxygen in the fuel (Graboski and McCormick, 1998; Hoekman et al., 2012; U.S. EPA, 2002), which leads to higher fuel consumption, with the blends for the renewable/biodiesel blends generally showing slightly greater BSFC compared to the R100.

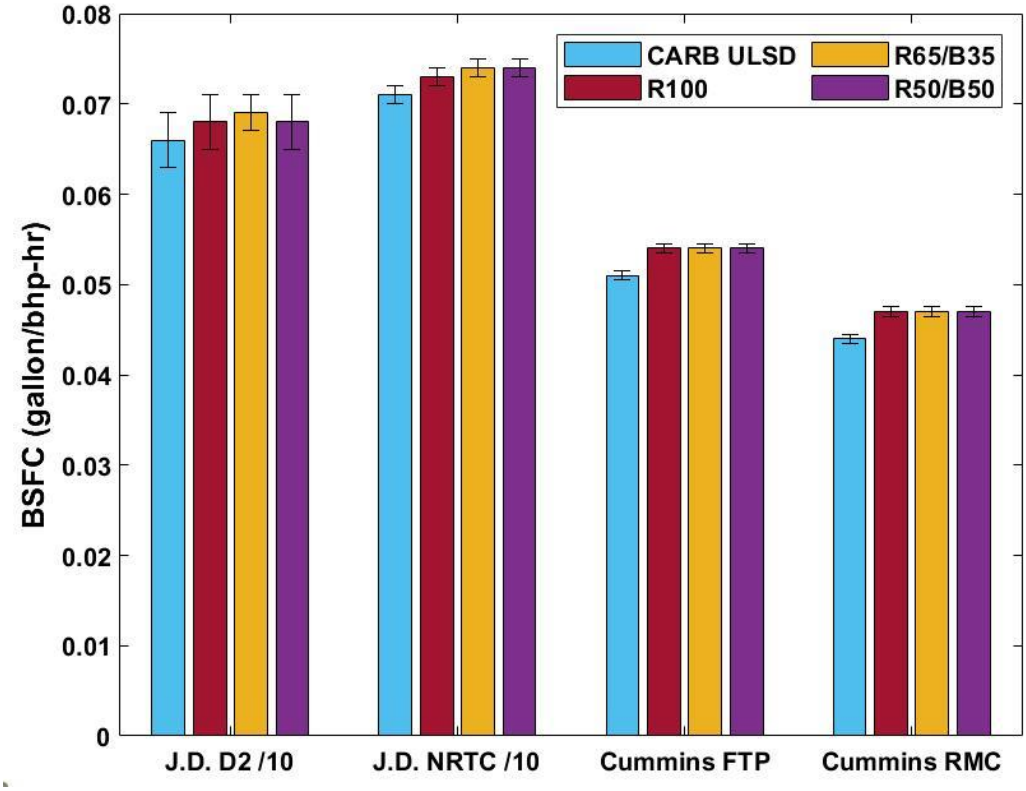

Figure 3-6: Averaged Brake Specific Fuel Consumption for all fuel/test cycle combinations and both engines

3.4.4 Carbonyl Emissions

Carbonyls are a group of organic compounds including aldehydes and ketones, which can be produced from incomplete combustion of petroleum and biomass-derived fuels. Short-term exposure to formaldehyde, acetaldehyde, and acrolein is known to cause adverse side effects that include irritation of the eyes, skin, and membranes of the upper respiratory tract. Carbonyl compounds have also been shown to be major contributors in the formation of photochemical ozone, peroxyacyl nitrates (PAN), and secondary organic aerosol through their atmospheric oxidation and interaction with NOx. Carbonyl emissions for all fuel/cycle combinations are shown in Figure 3-7 and Figure 3-8 for the Cummins and John Deere engines, respectively. The carbonyl emissions were reduced by a factor of 42 when comparing the Cummins engine to the John Deere engine.

For the off-road John Deere engine, no statistically significant differences were seen between R100 and R65/B35 fuels compared to CARB ULSD for either the NRTC or D2 cycles. Formaldehyde and acetaldehyde were the dominant aldehydes in the exhaust for all fuels, followed by acrolein, acetone, MEK/butyraldehyde, propionaldehyde, and valeraldehyde. Previous studies have also shown the predominance of formaldehyde and acetaldehyde emissions from biodiesel exhaust, primarily formed in the combustion process from fuel fragments produced in the initial fuel pyrolysis (Karavalakis et al., 2017; Magara-Gomez et al., 2012; Fontaras et al., 2009; Fontaras et al., 2010; Ratcliff et al., 2010; Nelson et al., 2008). Heavier aldehydes were also detected in the exhaust, but in lower levels. The R50/B50 blend showed significant decreases in formaldehyde, acetaldehyde, and acrolein emissions, as well as decreases in heavier carbonyl emissions for both the D2

and NRCT cycles. For the NRTC cycle, formaldehyde, acetaldehyde, and acrolein emissions decreased with increasing biodiesel concentration in the fuel. Formaldehyde emissions reductions ranged from 10.7% to 50.7% while acetaldehyde and acrolein emissions reductions ranged from 7.0% to 55.4% and 19.8% to 44.6%, respectively. Overall, the biodiesel blends showed total carbonyl emissions reductions ranging from 34% to 52% for the NRTC and D2 cycles when compared to CARB ULSD. Neat renewable diesel showed an increase in total carbonyl emissions of 35% and a reduction of 8% for the FTP and RMC cycles, respectively.

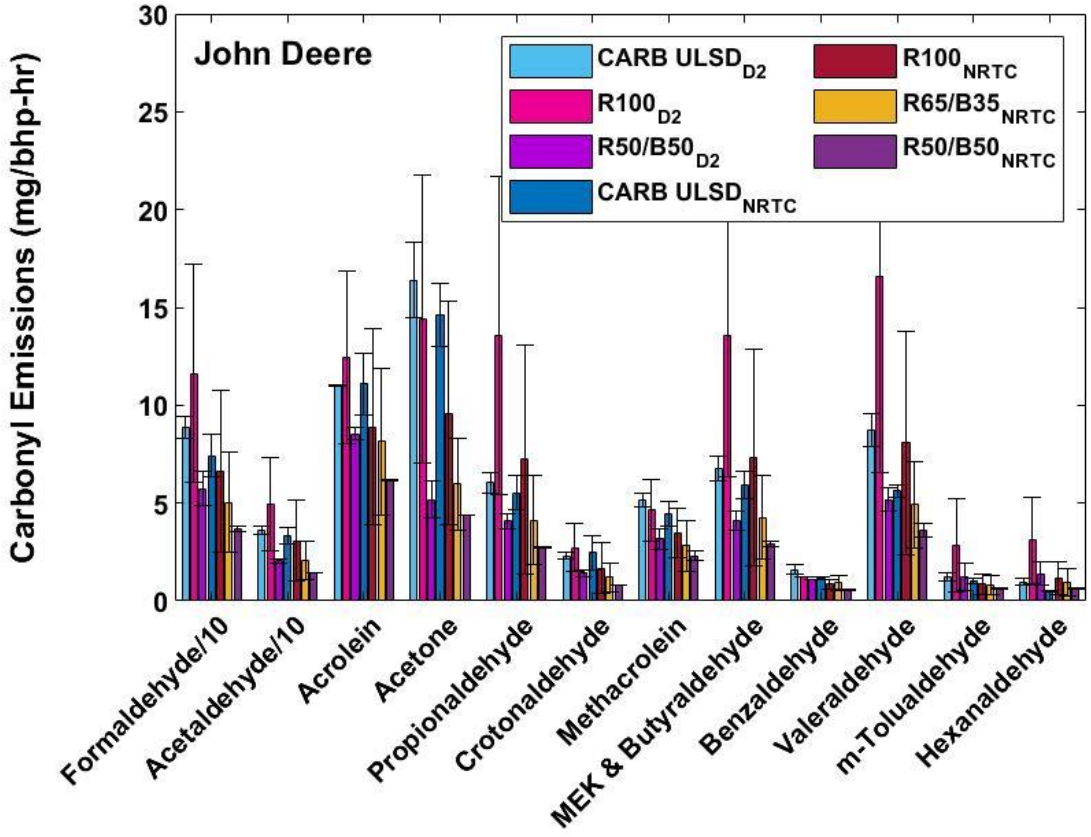

Figure 3-7: Carbonyl Speciation for John Deere Engine

The on-road Cummins engine showed much lower carbonyl emissions across all fuels, as a result of the DOC that effectively oxidized these pollutants. In contrast to the John Deere engine, acetone was the dominant ketone in the exhaust, followed by formaldehyde and acetaldehyde. Higher molecular weight aldehydes and ketones, such as aromatic aldehydes and heavier saturated aliphatic aldehydes were detected in lower concentrations. Overall, more carbonyl emissions were produced during FTP cycle than the steady-state test cycle due to the more aggressive operating characteristics and the more frequent hot-start events of this test cycle. The renewable diesel and biodiesel blends showed reductions in carbonyl emissions during the FTP cycle, with these reductions being more pronounced as biodiesel concentration increased in the fuel. The emissions reductions ranged from 31.5% to 53.8% for acetone, 6.3% to 39.4% for formaldehyde, and 14.2% to 39.9% for acetaldehyde, respectively. Previous studies of heavy-duty diesel vehicles operated with biodiesel blends have demonstrated reductions in carbonyl emissions with biodiesel (Karavalakis et al., 2017; Cahill and Okamoto, 2012). These reductions can be attributed to the decomposition of esters via decarboxylation, which could decrease the probability of forming oxygenated combustion intermediates compared to petroleum diesel combustion (Lapuerta et al., 2008; Karavalakis et al., 2017). Total carbonyl emissions were reduced for R100 and biodiesel blends ranging from 26% to 44% over the FTP cycle when compared to CARB ULSD. Carbonyl reductions over the RMC cycle were much lower at 4% and 2% for the R100 and R50/B50 blend, respectively.

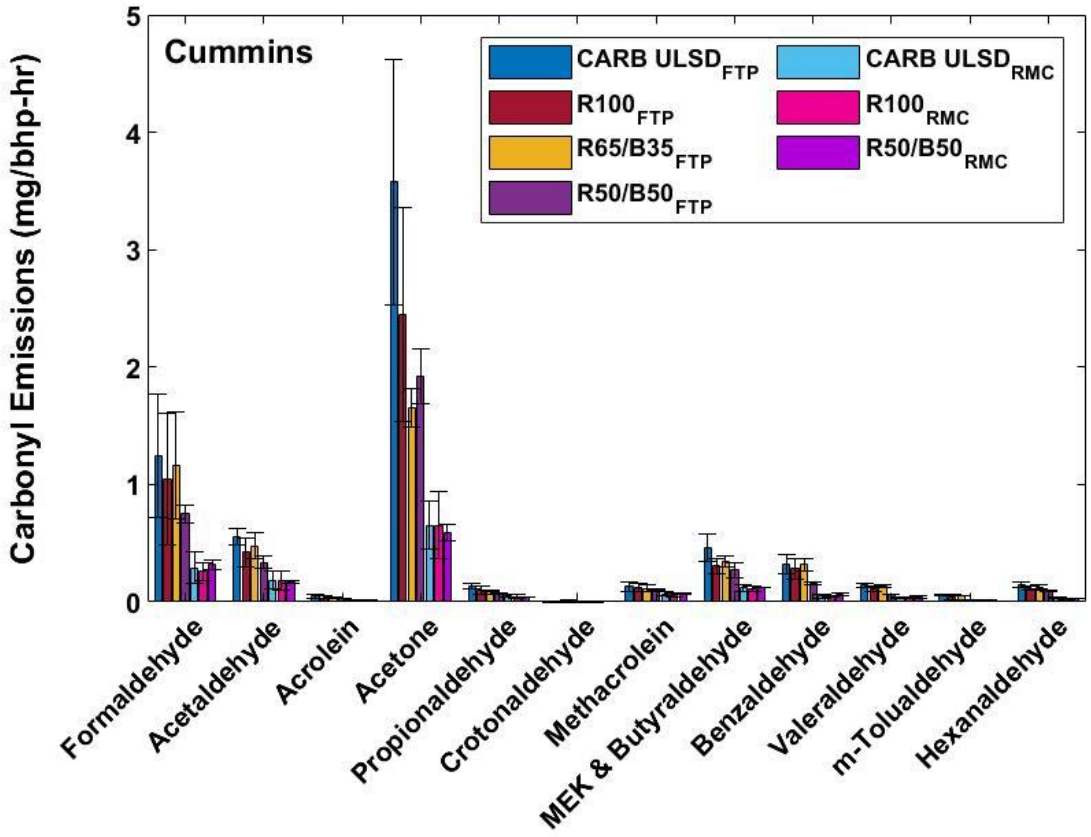

Figure 3-8: Carbonyl Speciation for Cummins Engine

3.4.5 VOC Speciation

Many of the VOCs from the analysis of all fuels from both cycles showed concentrations that were below the sample reporting limit (SRL). In general, diesel engines produce lower VOC emissions than gasoline engines, including monoaromatic VOCs such as benzene, toluene, ethylbenzene, m/p- and o-xylenes (collectively known as BTEX). Although VOC emissions are not pollutants of increased interest in diesel engines equipped with advanced aftertreatment controls, their emissions are known to contribute to the formation of secondary organic aerosol (Robinson et al., 2007). Figures 3-9 and 3-10 shows the

emissions rates of the VOCs above the SRL for all fuel/cycle combinations for the Cummins and John Deere engines, respectively. For the John Deere engine, propene levels are typically highest for every fuel for both cycles. Propene emissions reduction ranged from 55%to 61% for when utilizing renewable diesel and the biodiesel blends when compared to CARB ULSD. For both cycles on the John Deere engine, the low aromatic biofuel blends led to lower VOC emissions with the exception of the R65/B35 fuel over the NRTC cycle.

For the on-road Cummins engine, the VOC emissions concentrations, including the BTEX species, were substantially lower than those obtained for the John Deere engine, with the majority of the VOC species being below SRL. This phenomenon was a result of the DOC which effectively oxidized these pollutants. Only ethane and propane were above the SRL for every fuel, with ethylene and toluene also measurable for a number of fuels. Increasing renewable diesel and biodiesel concentration in the fuel showed reductions in both ethane and propane concentrations.

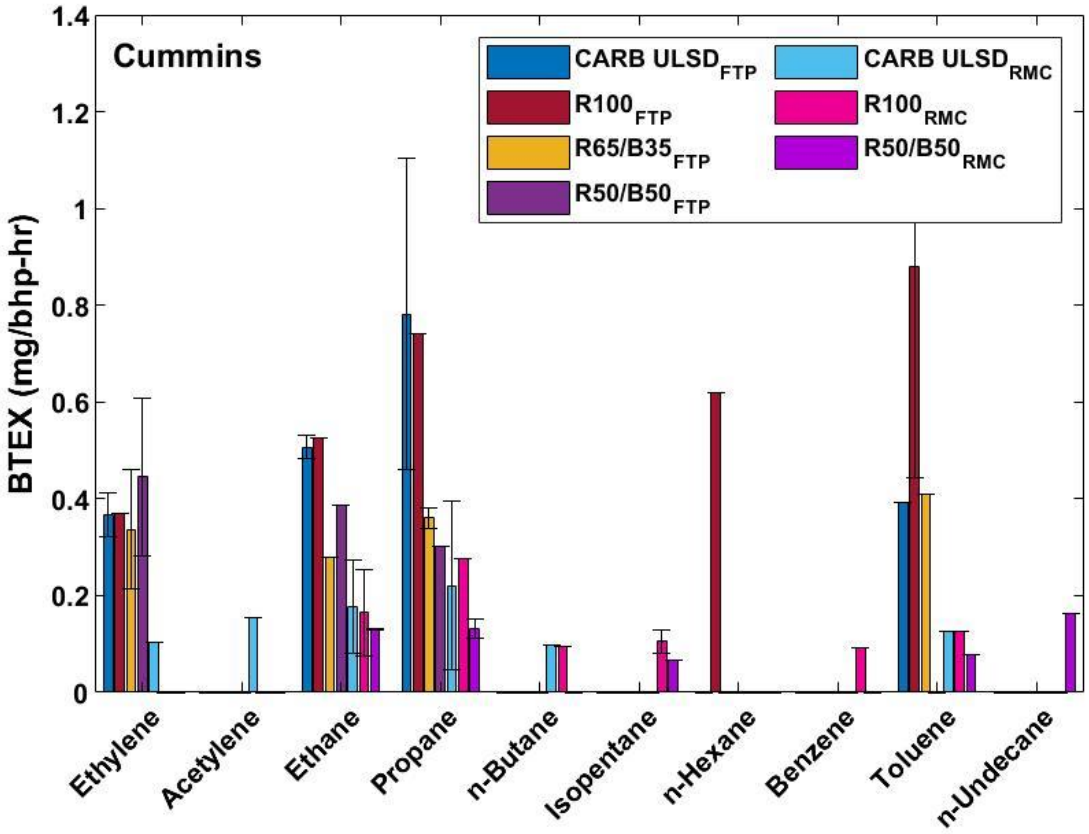

Figure 3-9: VOC Emissions Speciation for Cummins Engine

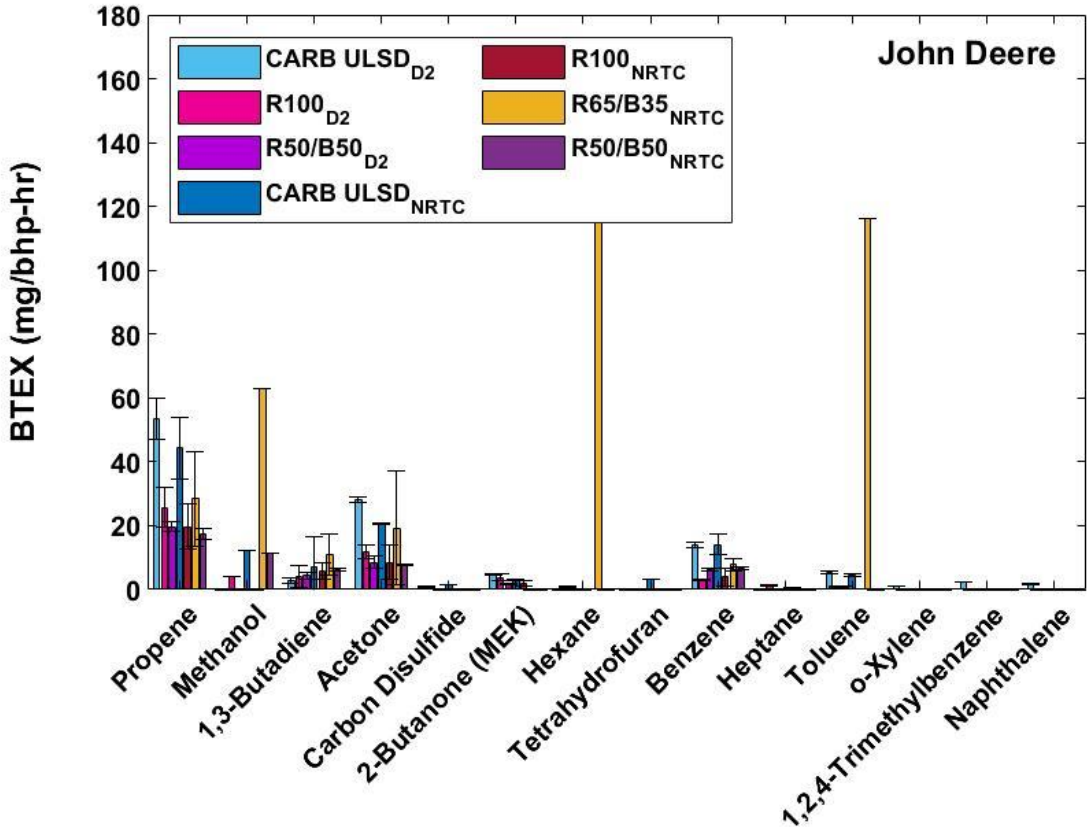

Figure 3-10: VOC Emissions Speciation John Deere Engine

3.4.6 PM Emissions and PM Composition

Averaged PM mass emissions in mg/bhp-hr are presented in Figure 3-11, with the total PM composition presented in Figure 3-12. PM mass emissions were found in significantly higher levels for the off-road John Deere engine than the on-road, DPF-equipped Cummins engine. Fuel effect was particularly noticeable for the John Deere engine, with lower PM mass emissions for the biofuel blends for both test cycles. PM mass emissions reductions have been shown in previous studies with biodiesel and renewable diesel fuels (Hajbabaei et al., 2013; Kousoulidou et al., 2010; Karavalakis et al., 2017; Karavalakis et al., 2016b; Westphal et al., 2013). The reductions in PM mass for R100 were 26.7% and 38.0%,

respectively, for the D2 and NRTC cycles, at statistically significant levels. The largest reductions in PM mass emissions were seen for the biodiesel blends with renewable diesel and trended higher with more biodiesel in the fuel blend. For the D2 test cycle, the statistically significant PM mass reductions were 50.8% and 58.4%, respectively for R65/B35 and R50/B50 blends. For the NRTC, the statistically significant PM mass reductions were 53.4% and 62.6%, respectively for R65/B35 and R50/B50 blends. The large reductions in PM mass emissions with biodiesel blends was a consequence of the oxygen in the methyl ester molecule, which reduced locally fuel-rich zones and limited soot nucleation early in the formation process (Fontaras et al., 2009; Lapuerta et al., 2008; Giakoumis et al., 2012). A different study proposed that the higher oxygen availability will allow more of the carbon to be oxidized to CO, thereby removing it from soot-precursor reactions (Flynn et al., 1999). For the R100 fuel, the PM mass reductions were due to the absence of sulfur and aromatic compounds that act as soot precursors (Heikkila et al., 2012; Prokopowicz et al., 2015). For the on-road Cummins engine, PM mass emissions showed relatively large test-to-test variability mainly due to the very low PM mass levels for this engine. Fuel effect on PM mass emissions was almost absent, although the higher biodiesel blend trended lower in PM mass emissions over both test cycles compared to the other fuels. Overall, the application of the DPF efficiently trapped engine-out soot emissions and masked any potential fuel effects on PM emissions. This finding suggest that biofuel blends likely will not provide significant additional PM emissions benefits in current technology on-road heavy-duty diesel engines.

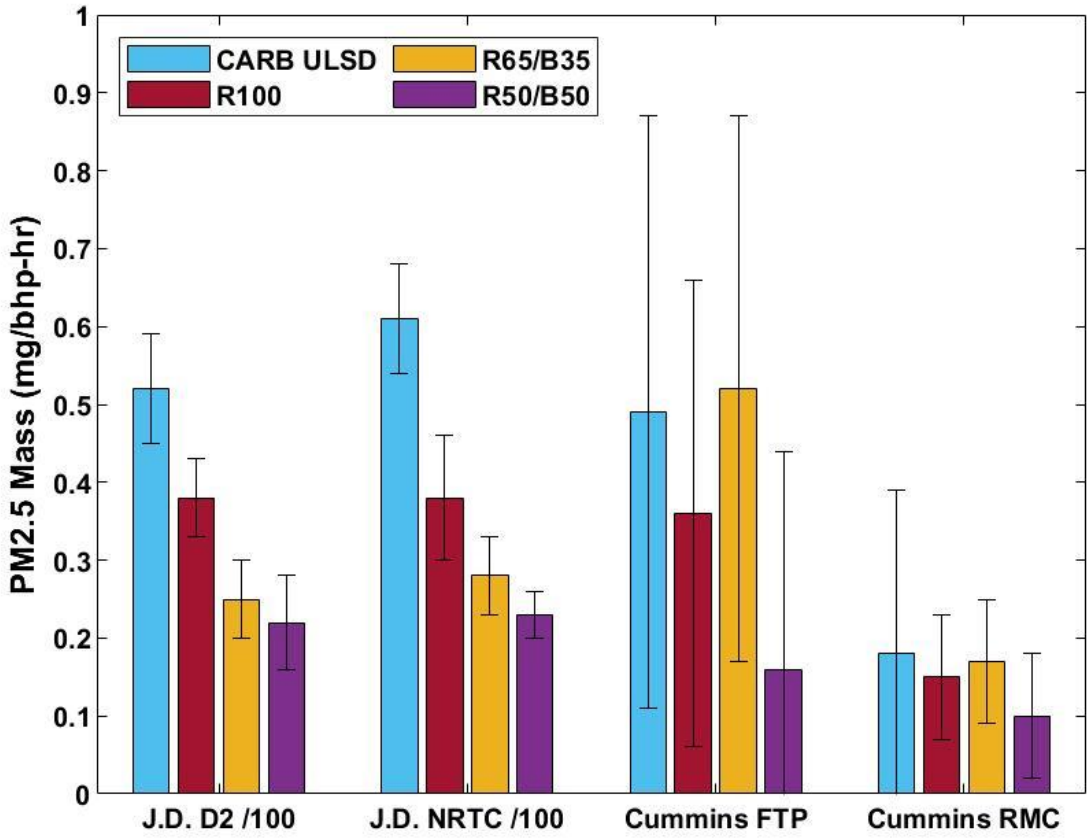

Figure 3-11: Average PM mass emissions for all fuel/test cycle combinations and both engines

Figure 3-12 (a-d) show the PM composition of all fuels/cycle combinations for both engines. For the John Deere engine, OC emissions were comparable between the CARB ULSD and renewable diesel and renewable diesel-biodiesel blends within the experimental variability, with the exception of the R50/B50 fuel over the NRTC cycle, which showed statistically significant reductions at a 95% confidence level. Elemental carbon emissions seemed to decrease much more for the biofuel blends when compared to CARB ULSD. R100 showed reductions in EC emissions ranging from 14%-28% over the D2 and NRTC cycles, respectively, when compared to CARB ULSD. Both biodiesel blends showed

statistically significant decreases over both test cycles. The R65/B35 and R50/B50 blends showed decreases ranging from 58% to 68% compared to CARB ULSD for both cycles. The higher biodiesel concentration in the fuel led to reduced EC emissions. This is due to the fuel-bound oxygen, which aided to more efficient combustion, and subsequently a reduction in PM soot emissions. The presence of oxygen reduces excessively fuel rich zones during combustion, primarily in the core region of the fuel spray, effectively limiting soot nucleation. The absence of any aromatics and sulfur compounds in the fuel, which are generally considered to be soot precursors, led to reduced soot formation as well. These observations also agree with the particle size distribution discussed later, which showed a decrease in accumulation mode particles that are commonly attributed to soot particles.

The on-road Cummins engine showed much lower concentrations of both EC and OC emissions due to the DPF and DOC aftertreatment systems, which significantly reduced the organic material in PM, as well as soot particles. Organic carbon dominated the total PM composition with over 92% for every fuel and cycle. The OC emissions for the different fuels were all comparable within the experimental variability. The EC fraction showed decreases for all biodiesel blends with the EC fraction accounting for only 0.8% to 1.5% of the total PM mass for both cycles. Renewable diesel showed an increase of 28% and a decrease of 35% for the FTP and RMC cycles, respectively, when compared to CARB ULSD.

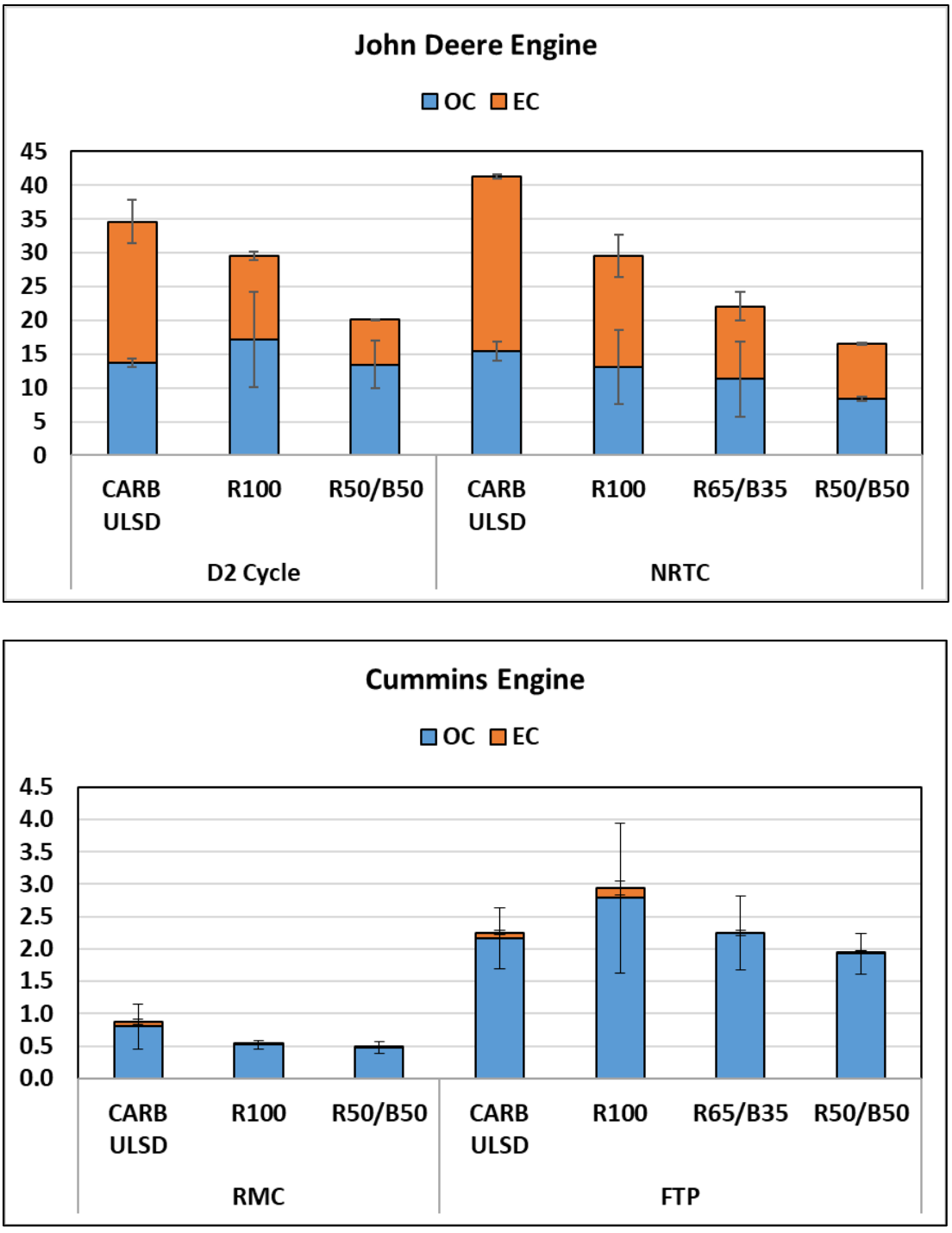

Figure 3-12: Averaged EC/OC emissions for all fuel/test cycle combinations and both engines

3.4.7 Total and Solid Particle Number Emissions

Total and solid particle number emissions in #/bhp-hr for each engine, fuel, and cycle are shown in Figure 3-13. Note that the John Deere total and solid particle number emissions are divided by a factor of 1000 in order to effectively show both engines on the same figure. Solid particle number represent measurements of solid particle above 23 nm in diameter, according to the European Union solid particle number emissions regulations.

For both engines, the biofuel blends generally showed a reduction in both total and solid particle number emissions, with the exception of total particle number for R100 fuel over the D2 cycle that also showed a relatively large variability as indicated by the wide error bars. Total and solid particle number emissions for both engines were seen in lower levels for the higher biodiesel blends relative to R100 and CARB ULSD. This is consistent with the PM mass trends for the John Deere engine, and some of the trends for the on-road Cummins engine. This was a result of the higher oxygen content in the fuel, which led to the better oxidation of soot particles, as well as to the reduced soot formation from the C=O bond.

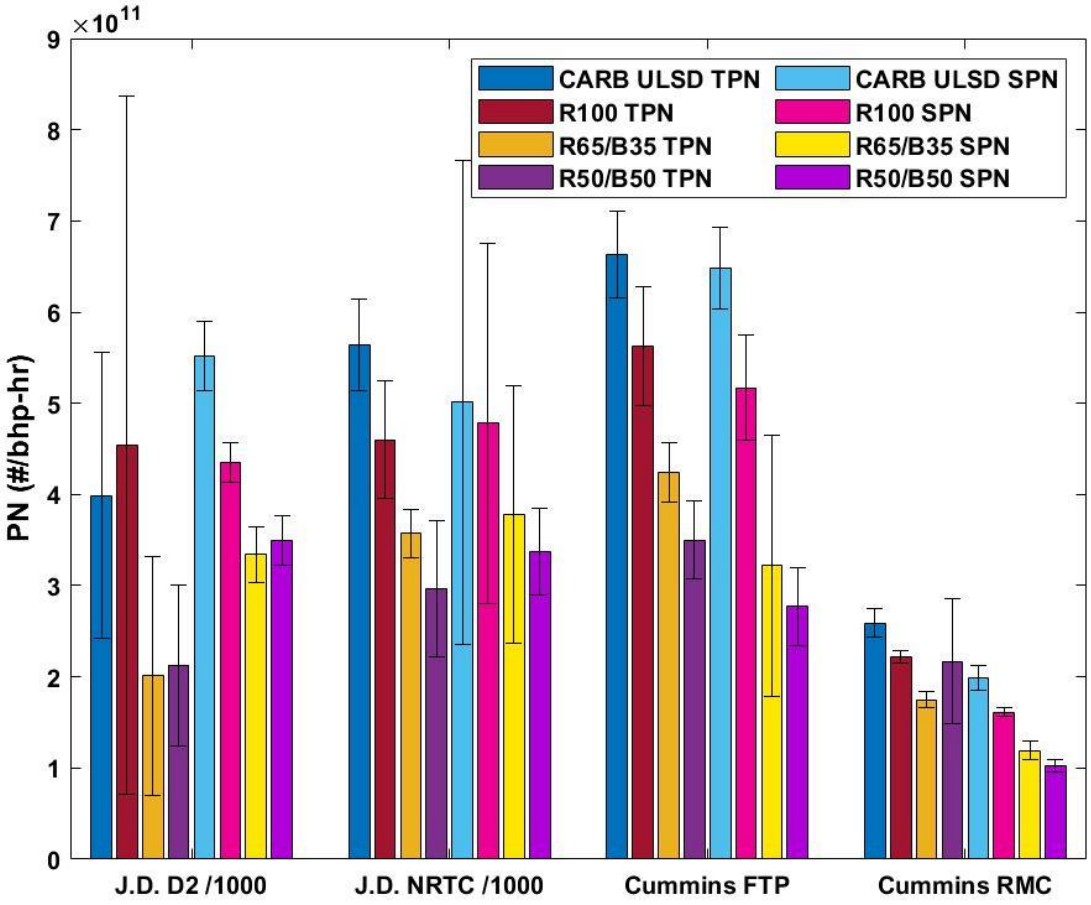

Figure 3-13: Total and solid (>23 nm) particle number emissions for all fuel/test cycle combinations and both engines

3.4.8 Particle Size Distributions

Figure 3-14 and Figure 3-15 show the particle size distributions (PSD) of all fuels/test cycle combinations in normal scale and log scale for the John Deere and Cummins engine, respectively. Diesel-generated combustion particles are typically divided in three modes including, nucleation mode (10-100 nm), accumulation mode (100-1000 nm), and coarse mode (1000-10000 nm). The nucleation mode typically consists of organic volatile compounds and can contain ash and soot particles. Most soot particles agglomerate,

however, and are usually found in the accumulation mode. Coarse mode particles are typically from larger soot particles breaking off of the exhaust walls.

For the John Deere engine, the biofuel blends over the D2 test cycle showed statistically significant decreases from 80 nm to 254 nm, 52 nm to 166 nm, and 39 nm to 299 nm, for R100, R65/B35, and R50/B50, respectively, when compared to CARB ULSD. Larger particle sizes, in the accumulation mode range, are reduced for R100, R65/B35, and R50/B50. This is expected as the lack of aromatic hydrocarbons and sulfur compounds in the biofuel blends led to lower accumulation mode particles, which consist mainly of soot agglomerates (Fontaras et al., 2009; Heikkila et al., 2012). Nucleation mode particles peaked at around 30 nm for all test fuels. The nucleation mode particle count decreased with an increase in biodiesel in the fuel due to the oxygen content leading to higher combustion efficiency and causing carbonaceous particles to change from fine to ultrafine size particles. The elevated population of nucleation mode particles with the biodiesel blends was also a consequence of the increased surface area available for subsequent adsorption and condensation of volatile hydrocarbons within the exhaust, promoting the nucleation of particles. It is interesting to note that the R100 fuel showed higher concentrations of accumulation and nucleation mode particles than the biodiesel blends, despite the lack of sulfur and aromatics in R100. This finding indicates that the fuel-bound oxygen was the key property for soot suppression in diesel combustion (Young et al., 2012; Tan et al., 2014).

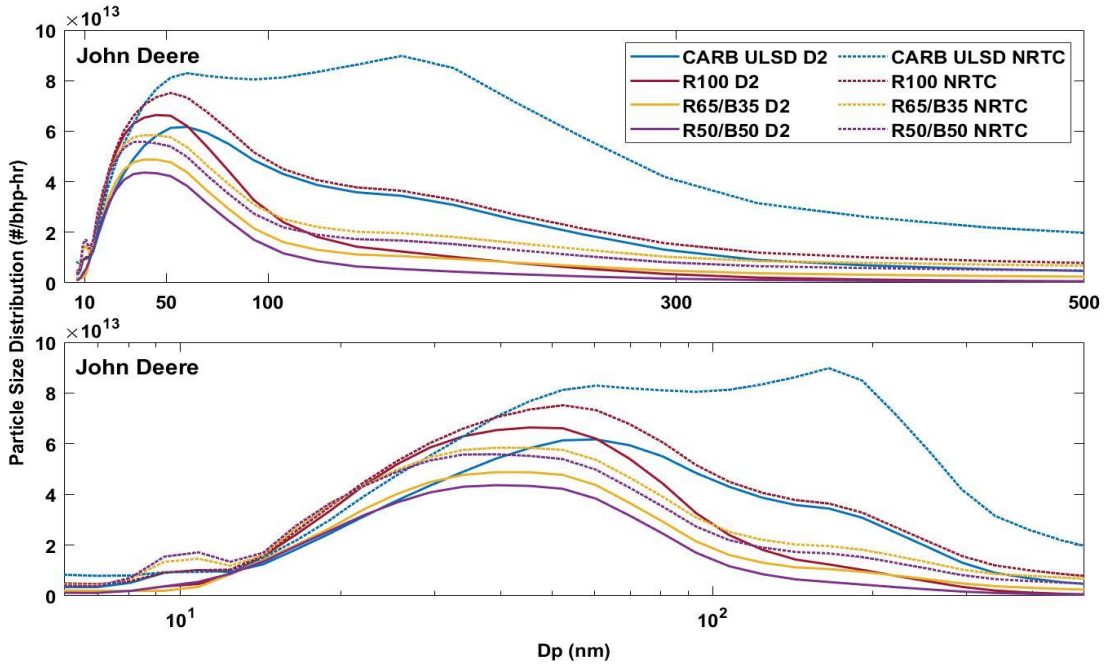

Figure 3-14: Average particle size distributions for all fuel/test cycle combinations in normal scale and log scale for the John Deere engine

The on-road Cummins engine generally only showed particle sizes less than 100 nm, suggesting the DPF effectively reduced the accumulation and coarse particles. Figure 1-14 was shortened to only show particle size range from 0 to 200 nm in order to show emission differences between fuels. Nucleation mode particles were about an order of magnitude lower than those measured for the John Deere engine. The lower nucleation mode particles for the Cummins engines were not only a consequence of the DPF system, but also a consequence of the DOC that was capable of oxidizing the semi-volatile materials contributing to the formation of nucleation mode particles. Surprisingly, the R65/B35 fuel showed the highest emissions for the FTP cycle, but also showed large measurement variability as indicated by the wide error bars. Overall, the use of biofuel blends resulted in lower populations of nucleation mode particles than CARB ULSD.

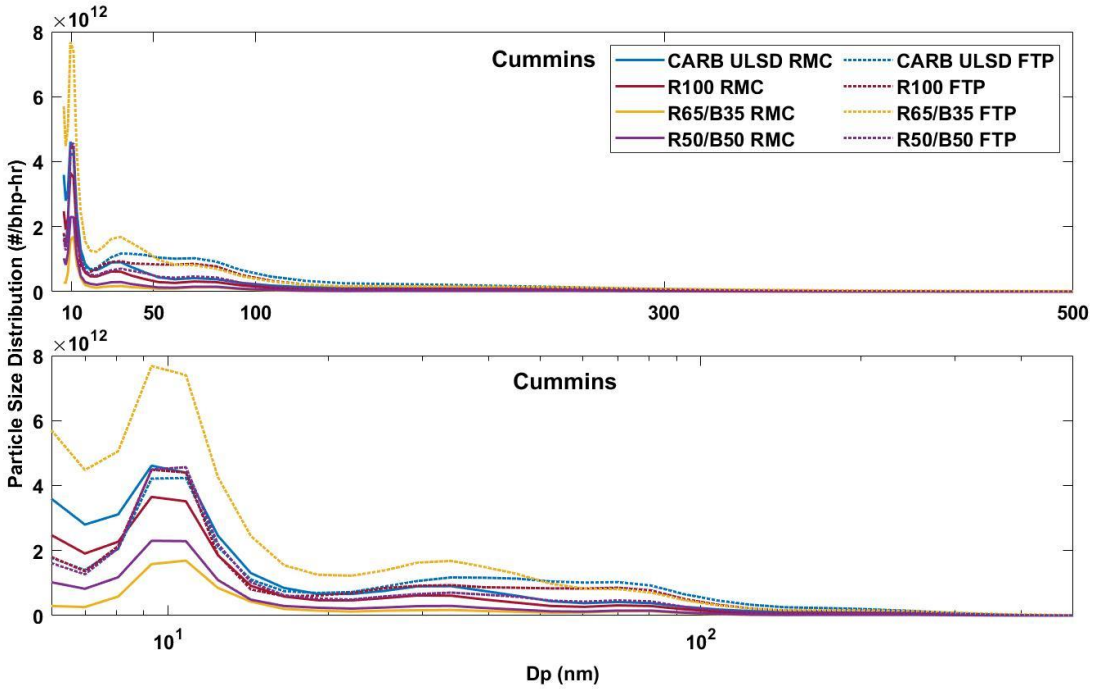

Figure 3-15: Average particle size distributions for all fuel/test cycle combinations in normal scale and log scale for the Cummins engine

3.4.9 Inorganic composition of PM

Figure 3-16 and Figure 3-17 show the trace element and metal emissions of all fuel/cycle combinations for the John Deere and Cummins engines, respectively. Many of the trace element and metal species were below the uncertainty level of that metal and were not included in the analysis. Trace elements and metals that were above the uncertainty level include sodium (Na), silicon (Si), phosphorus (P), sulfur (S), chlorine (Cl), calcium (Ca), iron (Fe), cooper (Cu), and zinc (Zn). Although differences are not statistically significant at a 95% confidence level, metals and elements in PM emissions showed some interesting trends for both engines. For the off-road John Deere engine, the dominant metal species found in PM emissions were Fe, Ca, Cu, and Zn, whereas the dominant non-metallic

elements were Na, S, Si, P, and Cl. Iron and S can be sourced from both the fuel and lubricant oil. Metals and elements such as Fe, Cu, and Si can be sourced from engine wear due to abrasion from piston rings, cylinder liners, and valves. Metals and elements such as Na, Ca and Zn could be originated from the lubricant oil since these compounds exist in lubricant oil additive package. For example, Zn exists in the lubricant oil in the form of zinc dialkyl dithiophospate (ZDDP) as an anti-wear additive compound (Ferreira da Silva et al., 2010). The use of biofuel blends resulted in reductions in PM-bound metal and element emissions compared to CARB ULSD. Similar findings have been reported elsewhere (Tsai et al., 2019). For the on-road Cummins engine, metals and elements were seen in significantly lower concentrations than those of the uncontrolled John Deere engine, indicating high removal efficiencies of these pollutants with the DPF system.

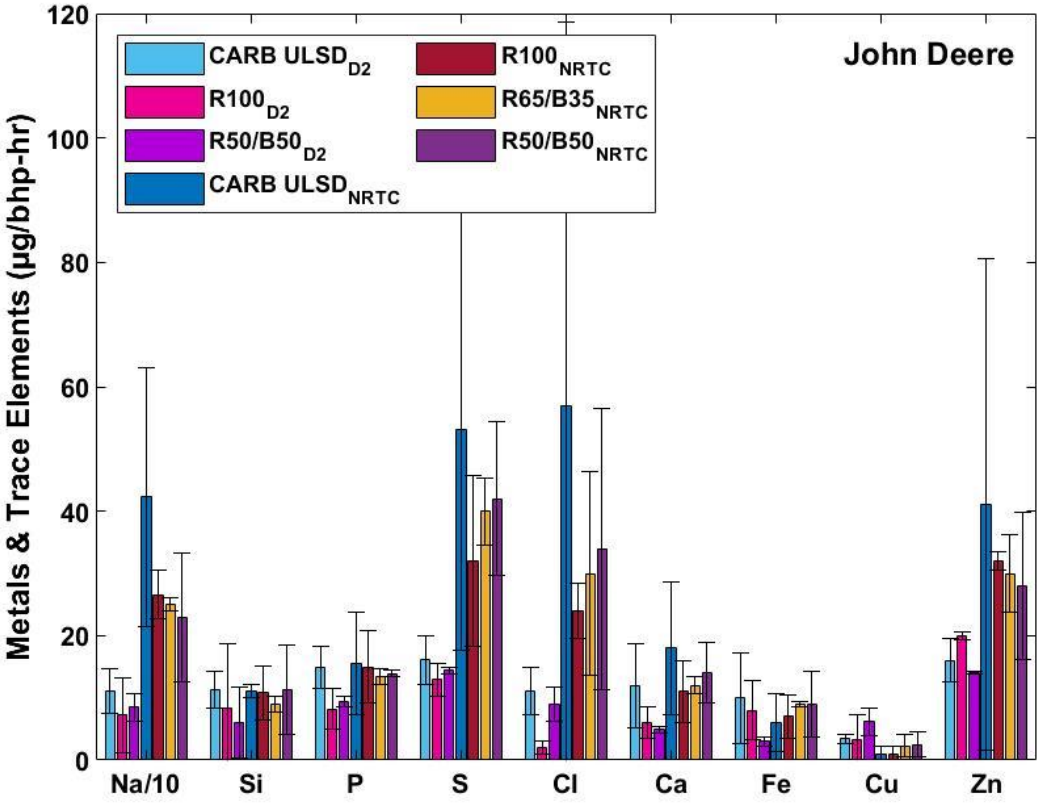

Figure 3-16: Average trace elements and metals emissions for all fuel/test cycle combinations for the John Deere engine

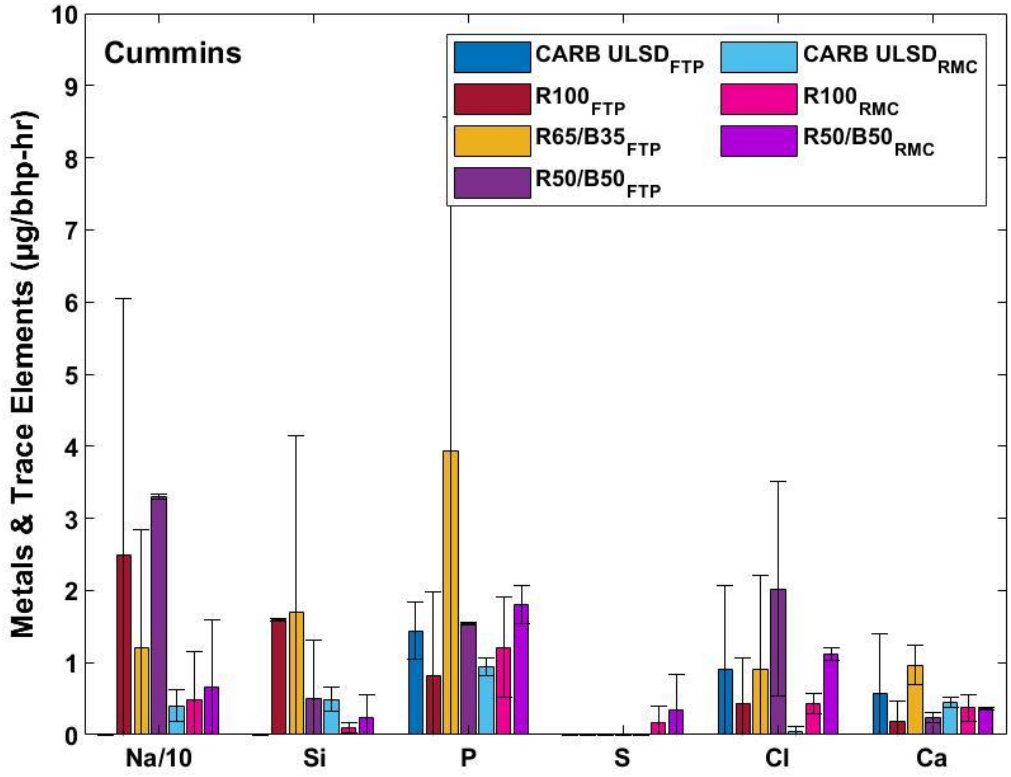

Figure 3-17: Average trace elements and metals emissions for all fuel/test cycle combinations for the Cummins engine

3.4.10 PAH Emissions

PAHs are generated by combustion processes of carbon-based fuels due to incomplete combustion or pyrosynthesis of low molecular weight aromatic hydrocarbons via a complex series of reactions. PAH formation has three different pathways: 1. PAH fragments in the fuel can survive the combustion process retaining the original carbon skeleton. 2. Pyrosynthesis during combustion of lower molecular weight aromatic compounds, where PAHs isolated from exhaust gases can be produced by the recombination of fragments of previous partially destroyed compounds to form new PAHs.

3. Pyrolysis of lubricant oils and unburnt fuel (Ravindra et al., 2008; Richter and Howard, 2000; Samburova et al., 2017).

PAHS are known for their high toxicity and mutagenic and carcinogenic effects on humans (IARC, 2010). PAHs known for their carcinogenic and teratogenic properties are benzo[a]anthracene and chrysene ($C_{18}H_{12}$); benzo[b]fluoranthene, benzo[j]fluoranthene, benzo[k]fluoranthene, and benzo[a]pyrene ($C_{20}H_{12}$); indeno[1,2,3-cd]pyrene ($C_{22}H_{12}$); and dibenzo[a,h]anthracene ($C_{20}H_{14}$). Benzo[a]pyrene is being classified as Group 1, carcinogenic to humans, by the International Agency for Research on Cancer (IARC), while dibenzo[a,l]pyrene and dibenzo[a,h]pyrene are considered as probably carcinogenic to humans (Group 2A) and possible carcinogenic to humans (Group 2B), respectively. Beside parent PAHs, some derivatives, like nitrated PAHs (nitro-PAHs) and oxygenated PAHs (oxy-PAHs) are also of growing concern since it is generally considered that these derivatives are more toxic than the parent PAHs (Andreou and Rapsomanikis, 2009; Durant et al., 1996; Walgraeve et al., 2010; Ravindra et al., 2008).

Figure 3-18 (a-b) and Figure 3-19 (a-b) show the sum of phenyl PAH, methyl- and ethyl-substituted PAH, oxygenated PAH, non-substituted PAH, and total PAH emissions of all fuel/cycle combinations for both engines in the particle-phase and vapor-phase, respectively. On average the total particle-phase and gas-phase PAHs were reduced by a factor of 32 and 12, respectively, when comparing the Cummins on-road engine to the John Deere engine. The presence of a DOC and DPF in the aftertreatment system was able to oxidize and trap most of the PAHs being released into the atmosphere. Low-molecular

weight PAHs (containing 3-5 aromatic rings) were the most prominent PAHs emitted. The results reported here agree with previous studies that have also reported the dominance of light PAHs in diesel engines (Ratcliff et al., 2010; Khalek et al., 2011; Karavalakis et al., 2017).

In general, both engines showed decreases in total vapor-phase and particle-phase PAH emissions with renewable diesel fuel and increasing biodiesel content in the blends, with some exceptions. This can be attributed to the renewable diesel and biodiesel fuels being aromatic free (Karavalakis 2010). Oxygenated PAH perinaphthenone showed the highest concentrations of any particle-phase PAH for the John Deere engine when utilizing CARB ULSD. As such, oxygenated PAHs showed the highest concentration of PAH species for the John Deere engine utilizing CARB ULSD. For the vapor-phase PAHs the majority of total PAHs were the 16 EPA-priority PAHs (naphthalene, acenaphthylene, acenaphthene, fluorene, phenanthrene, anthracene, fluoranthene, pyrene, benzo[a]anthracene, chrysene, benzo[b]fluoranthene, benzo [k]fluoranthene, benzo[a]pyrene, benzp[g,h,i]perylene, indeno[1,2,3-c,d]pyrene, and dibenz[a,h]anthracene) followed by methyl- ethyl-substituted PAHs for all fuel/cycle combinations on the John Deere engine. Low molecular weight PAH compounds general exist in the vapor-phase, while heavy PAHs with five rings or more are absorbed onto PM due to the lower vapor pressure associated with larger PAH compounds (Odabasi et al., 1999).

For the Cummins engine, particle-phase PAHs were dominated by the 16 EPA priority compounds, methyl- and ethyl-substituted, and phenyl-type PAHs. Vapor-phase PAHs, on

the other hand, were dominated by a majority of phenyl type PAHs, such as biphenyl, 2-methylbiphenyl, 3-methylbiphenyl, 4-methylbiphenyl, followed by the 16 EPA priority PAHs, and methyl- and ethyl- substituted PAHs. For all fuel/test cycle combinations, the dominate PAHs in the exhaust were light molecular weight 2-aromatic ring PAHs.

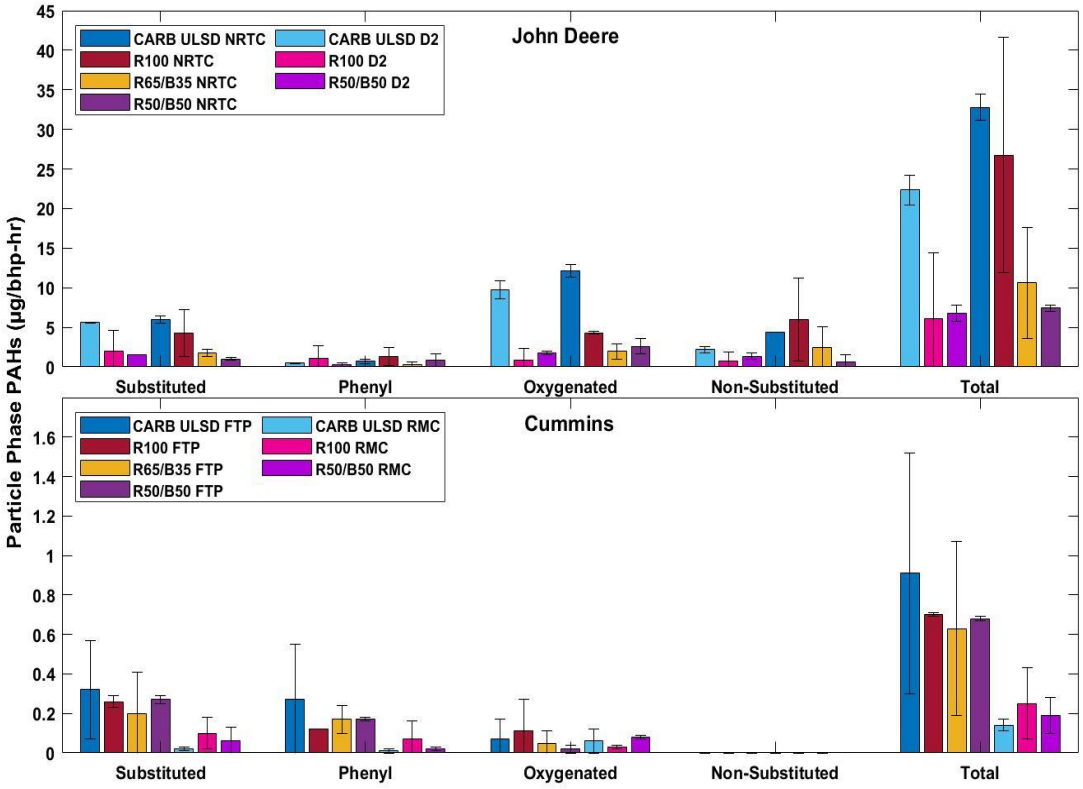

Figure 3-18 (a-b): Total, substituted, phenyl, oxygenated, and non-substituted particle-phase PAH emissions for all fuel/cycle combinations for both engines

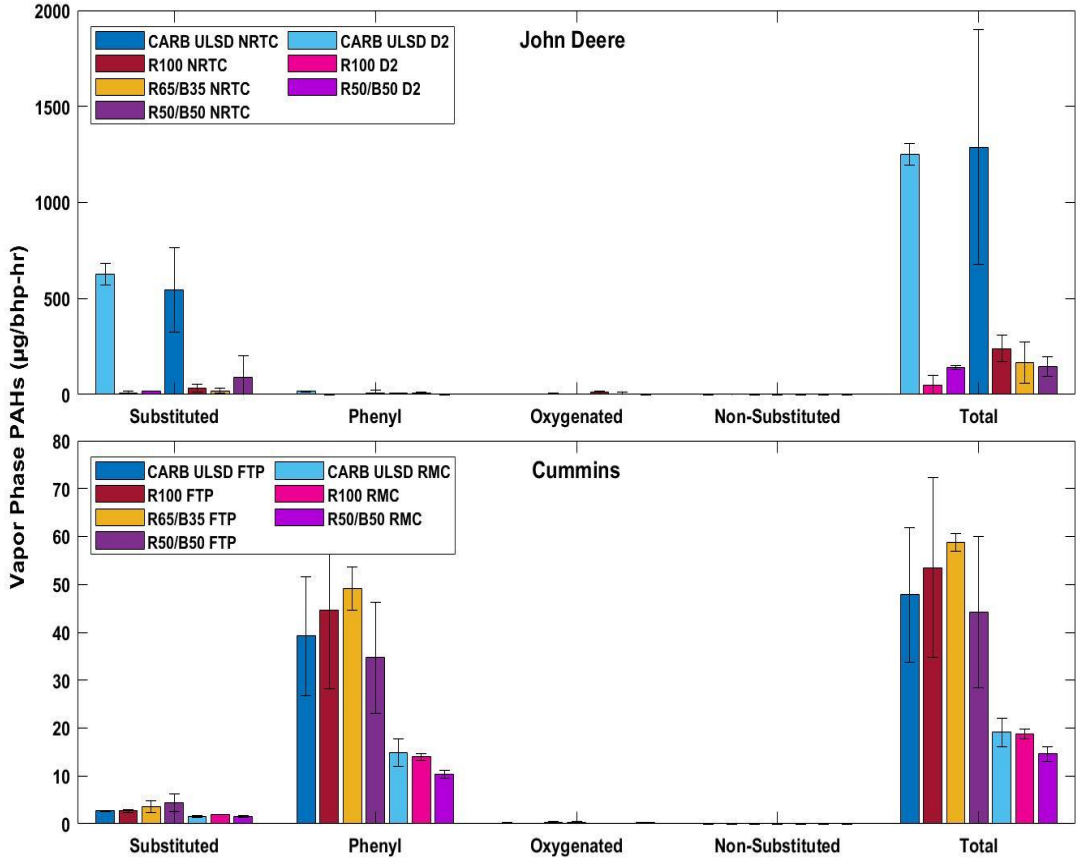

Figure 3-19 (a-b): Total, substituted, phenyl, oxygenated, and non-substituted vapor-phase PAH emissions for all fuel/cycle combinations for both engines

Figures 3-20 (a-b) and 3-21 (a-b) show the individual EPA priority PAH species for the particle- and vapor-phases, respectively, for each fuel/cycle combination and both engines. In general, the presence of a DPF and DOC in the Cummins engine aftertreatment greatly reduced the concentration of both lighter and heavier PAH emissions. In general, the particle-phase and vapor-phase EPA priority PAHs were reduced by a factor of 34 and 64, respectively, relative to the John Deere.

For the John Deere engine, reductions up to 75% for the particle-phase were seen with the R100, R65/B35, and R50/B50 blends when compared to ULSD and 95% for the gas-phase. The higher reduction efficiencies for the gas-phase PAHs can be attributed to the large reductions in naphthalene. Fluoranthene and phenanthrene were the dominant particle-phase PAHs from the John Deere engine for all fuel/cycle combinations. The dominance of lighter PAHs in the exhaust suggests that these compounds were formed from incomplete combustion in the fuel (Lea-Langton et al., 2008; Ravindra et al., 2008). The decreasing PAH emissions with increasing biodiesel was due to the oxygen content in the ester molecule, which led to better combustion in the cylinder for biodiesel blends. In addition, the absence of aromatic compounds in both biodiesel and renewable diesel contributed to the reduction in PAH emissions relative to CARB ULSD. Previous studies have also reported reductions in PAH emissions with biodiesel and renewable diesel fuels (Li et al., 2018; Karavalakis et al., 2017; Borillo et al., 2018; Heikkila et al., 2012; Ratcliff et al., 2010; Westphal et al., 2013). Since heavier PAH compounds were found at lesser amounts than lighter PAHs, the formation of these species might be due to pyrosynthesis of lower molecular weight aromatics compounds to larger PAHs (Lim McKenzie et al., 2007). Karavalakis et al. (2010) also showed low-molecular weight PAHs were the most prominent compound emitted from a diesel engine operating on ULSD, biodiesel, and ULSD-biodiesel blends.

For the Cummins engine, EPA priority PAH emissions generally declined with renewable diesel and renewable diesel biodiesel blends when compared to CARB ULSD. These reductions were not as pronounced as with the John Deere engine due to the DOC and DPF

aftertreatment oxidizing PAHs. Acenaphthene was the most dominate particle phase-PAH followed by fluoranthene. For the vapor-phase, 2-3 ring aromatic compounds were the dominate species in the exhaust.

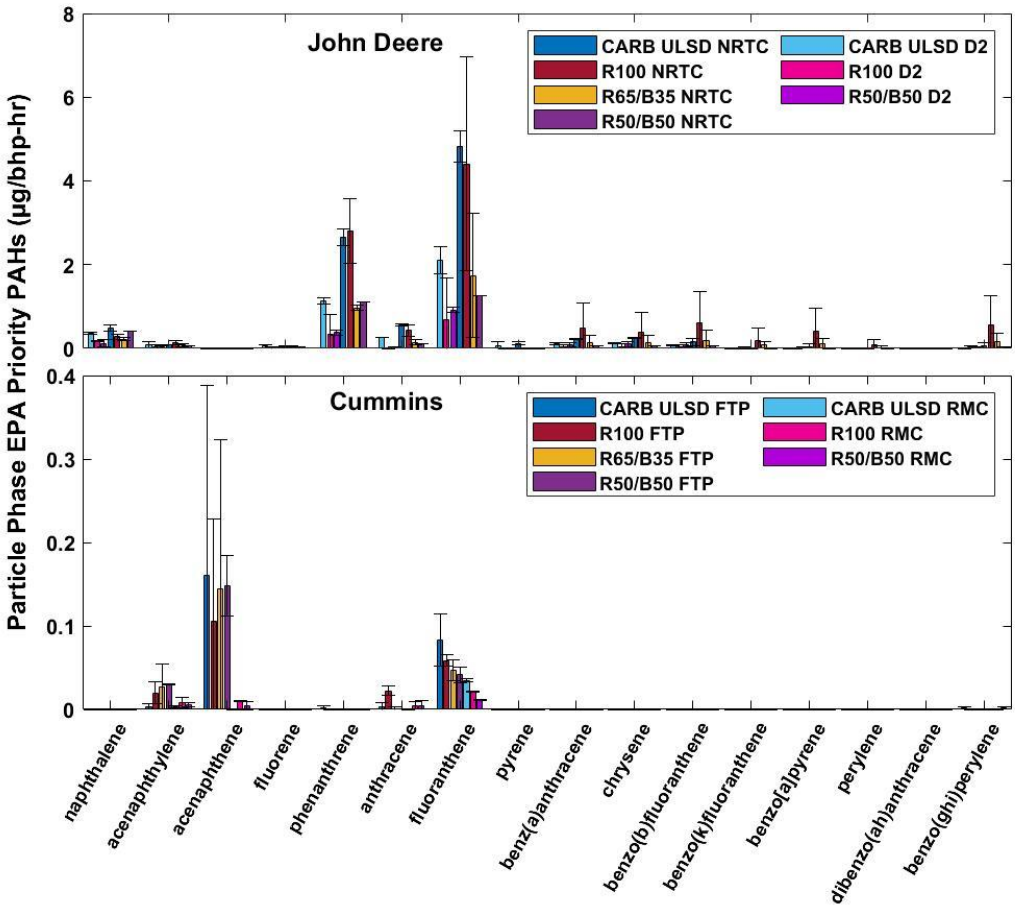

Figure 3-20 (a-b): Average Particle-Phase EPA Priority PAHs for all fuel/cycle combinations for both engines

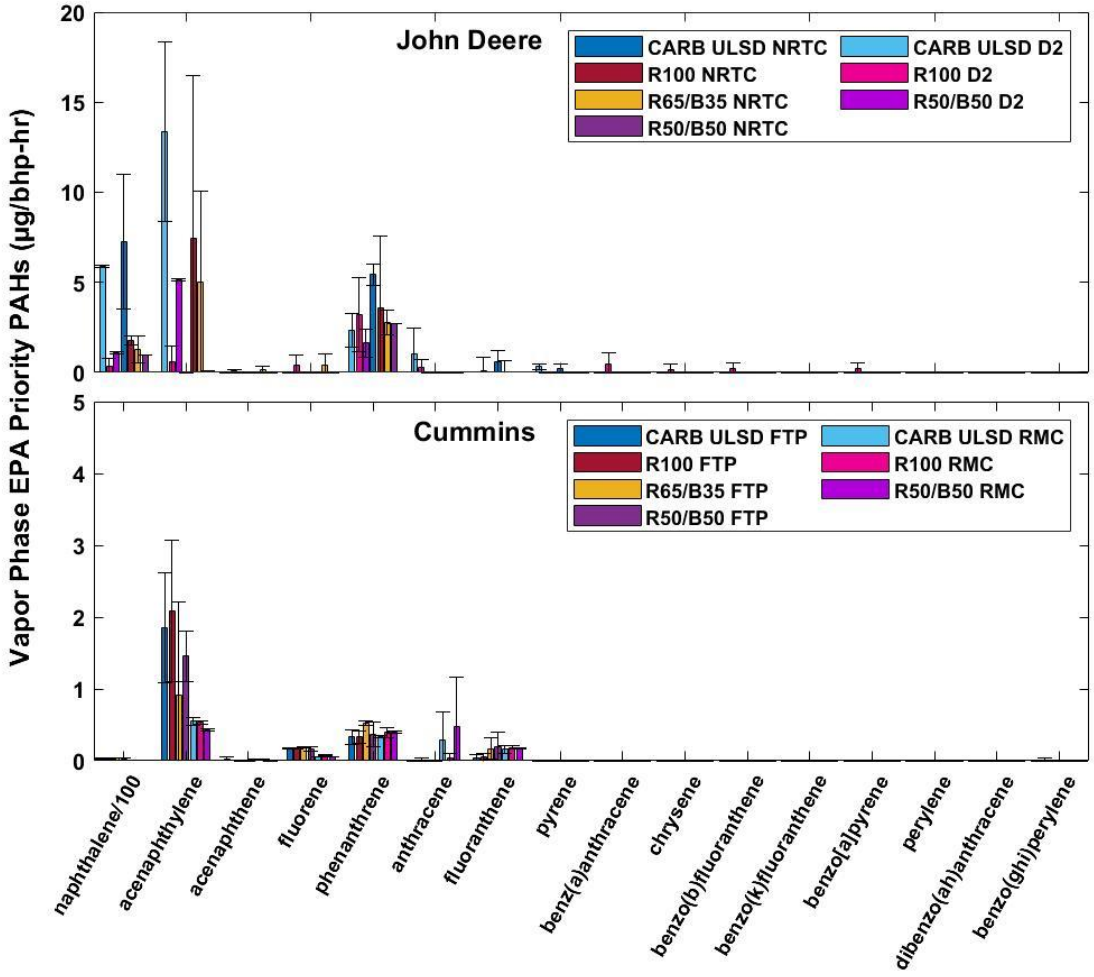

Figure 3-21 (a-b): Average vapor-phase EPA Priority PAHs for all fuel/cycle combinations for both engines

3.4.11 Nitro-PAH Emissions

As of this writing, the nitro-PAH analysis for the Cummins engine has not been completed. As such, this section will focus on the nitro-PAH emissions from the John Deere engine. Figure 3-22 (a-b) provides the average vapor-phase and particle-phase nitro-PAH emissions from the John Deere engine for all fuel/cycle combinations. Nitro-PAHs are derivatives of PAHs that contain at least one nitro-functional group on the aromatic ring

(Dimashki et al., 2000). Nitro-PAHs can be formed by the reaction of PAHs with hydroxyl and nitrate radicals in the presence of NOx or through nitration during combustion processes (Miet er al., 2009).

Results of nitro-PAH emissions were found to be significantly lower than those of their parent PAHs, consistent with previous studies (Karavalakis et al., 2010; Li et al., 2018; Khalek et al., 2011). Only 5 particle-phase nitro-PAHs of 35 nitro-PAHs measured were detected in the exhaust. For the vapor-phase nitro-PAHs, 8 of 35 nitro-PAHs measured were detected in the exhaust. For the vapor-phase only 2-ring aromatic compounds, such as 1-nitronapthalene, showed quantifiable results for nearly all fuel types. The dominant species in the particle-phase were 3-4 ring aromatic compounds, such as 3-nitrophenanthrene and 2-nitrofluoranthene. For 3-nitrophenanthrene, emissions increased with renewable diesel and increasing biodiesel content for each cycle. Emissions of 2-nitrofluoranthene showed mixed results, with R100 and R50/B50 fuels showing lower emissions than CARB ULSD over the NRTC cycle, while R65/B35 showed increases.

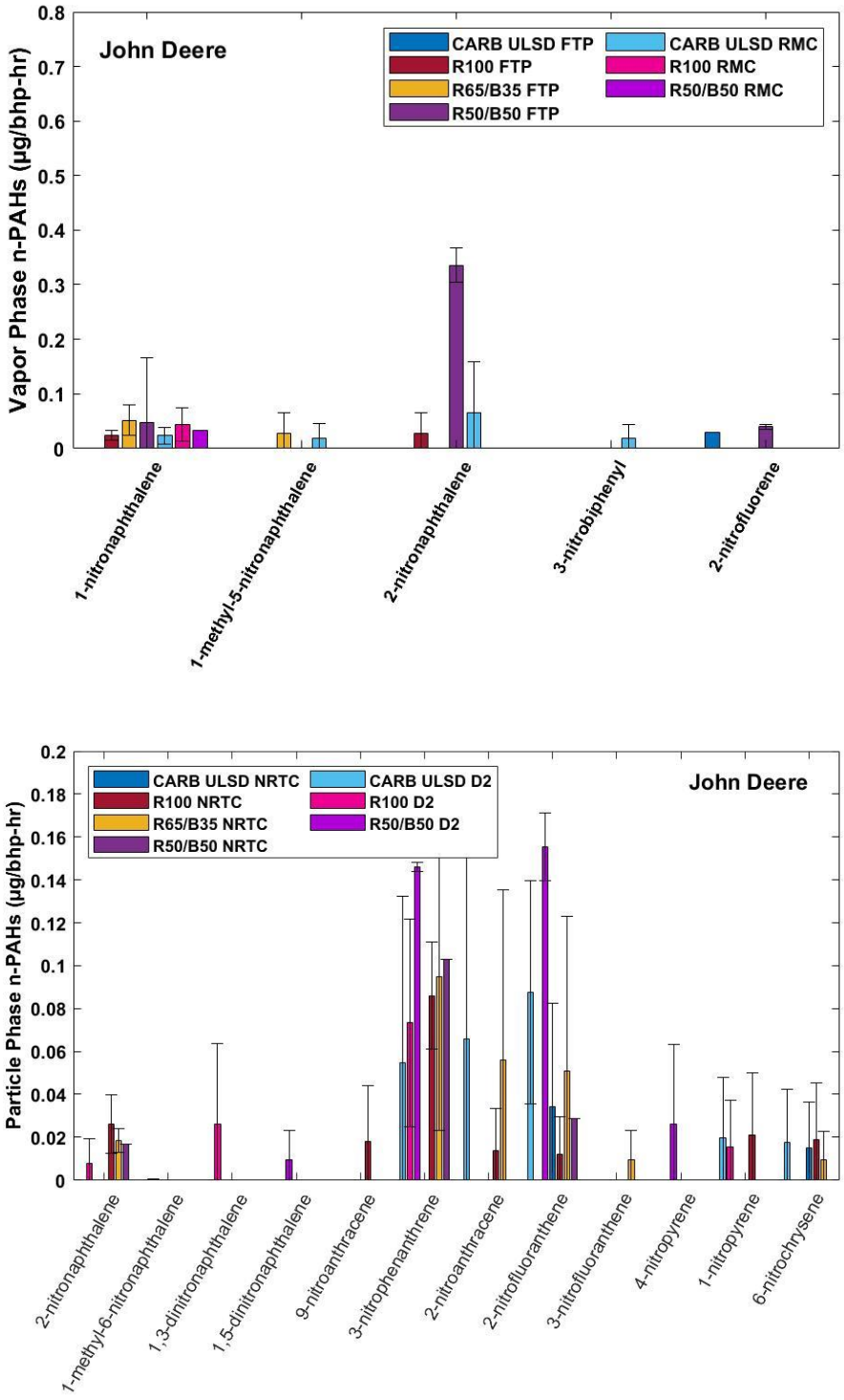

Figure 3-22 (a-b): Average vapor-phase and particle-phase N-PAHs for all fuel/cycle combinations for the John Deere engine

3.4.12 Carcinogenic potency of PAH emissions

The carcinogenic and genotoxic potency of vapor-phase and particle-phase PAH emissions was calculated using toxicity equivalency factors (TEFs) as proposed by Nisbet and LaGoy (1992). The cancer risk potential of the PAH emissions was calculated by multiplying individual PAH compounds by their TEF value and summing the total. TEF values were not available for all PAH compounds in this study so the TEF of 2-methylnapthalene (0.001) was used for compounds with similar chemical structures. This concept allowed for a more complete understanding of the overall carcinogenic potency of the PAH emissions from all fuel/cycle combinations used in this study.

Figure 3-23 shows the calculated carcinogenic potency of the PAH emissions for all fuel/cycle combinations for both engines. On average the on-road Cummins engine showed a 20 times reduction in carcinogenic potential when compared to the John Deere engine. This can be attributed to the much lower PAH emissions seen in the Cummins engine due to the DOC/DPF aftertreatment system, which effectively oxidized the semivolatile PAH compounds and trapped the PM-bound PAHs. In general, the vapor-phase PAHs played a larger role compared to particle-phase PAHs when calculating the total carcinogenic potential. Vapor-phase PAHs accounted for 65% and 99% of the total carcinogenic potential for the John Deere and Cummins engine, respectively. The John Deere engine clearly shows significant reductions in the carcinogenic potential with renewable diesel and higher biodiesel blending contents. The Cummins engine, on the other hand, did not show large fuel differences, as the DOC and DPF effectively masked the fuel effects of the renewable diesel and biodiesel blends.

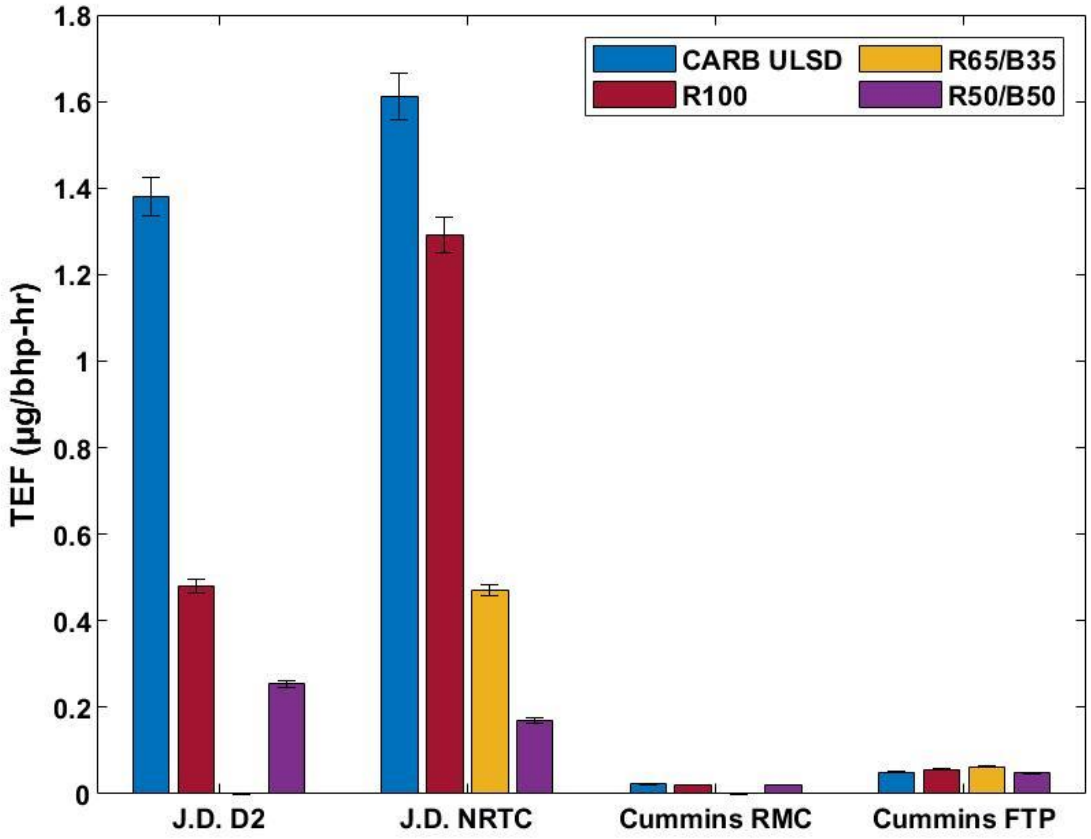

Figure 3-23: Carcinogenic potency of PAH emissions for all fuel/cycle combinations for both engines

3.4.13 Ozone Forming Potential (OFP)

Ground level ozone is one of six criteria pollutants and has been regulated in national ambient air quality standards (NAAQS) since 1971 to protect public health. In 2015 the ambient ozone standard was restricted to an 8-hour average of less than 0.07 ppm to be in attainment (EPA 2021). Ozone is considered a secondary pollutant that is formed through complex reactions involving sunlight, NOx, and VOCs in the atmosphere (Finlayson-Pitts and Pitts, 2012). Ozone formation is a non-linear reaction meaning ambient concentrations of ozone are usually not proportional to precursor emissions (Venecek et al., 2018).

Different VOC compounds have different incremental reactivities, meaning the amount of ozone formed per molecule will be different based on the chemical structures of the compounds. For this project, the ozone forming potential (OFP) of VOC emissions from the Cummins and John Deere engines were calculated using the carbonyl (aldehydes and ketones), monoaromatic VOCs (i.e., BTEX) and 1,3-butadiene, and PAH compounds presented earlier. The maximum incremental reactivity (MIR) scale used by CARB to calculate ozone impacts of VOC emissions was utilized for this study and is based off the work of Carter (2010).

The ozone forming potential (OFP) of all fuel/cycle combinations for both engines is shown in Figure 3-24. In general, the Cummins engine showed OFP fractions over 100 times lower compared to the John Deere engine. A large reason for the reductions can be attributed to the large reductions in VOCs and monoaromatic species (i.e., BTEX), and carbonyl concentrations. Specifically, propene, 1,3-butadiene, formaldehyde, and acetaldehyde, which have MIR values of 11.7, 12.6, 9.4, and 6.5, respectively, were reduced significantly in the Cummins exhaust largely due to the DOC system effectively oxidizing these hydrocarbon species. In general, renewable diesel and renewable diesel-biodiesel fuel blends showed slight reductions in OFP when compared to CARB ULSD. This can be attributed to the absence of aromatics in the fuel, as well as more complete combustion leading to a reduction of carbonyl and BTEX formation.

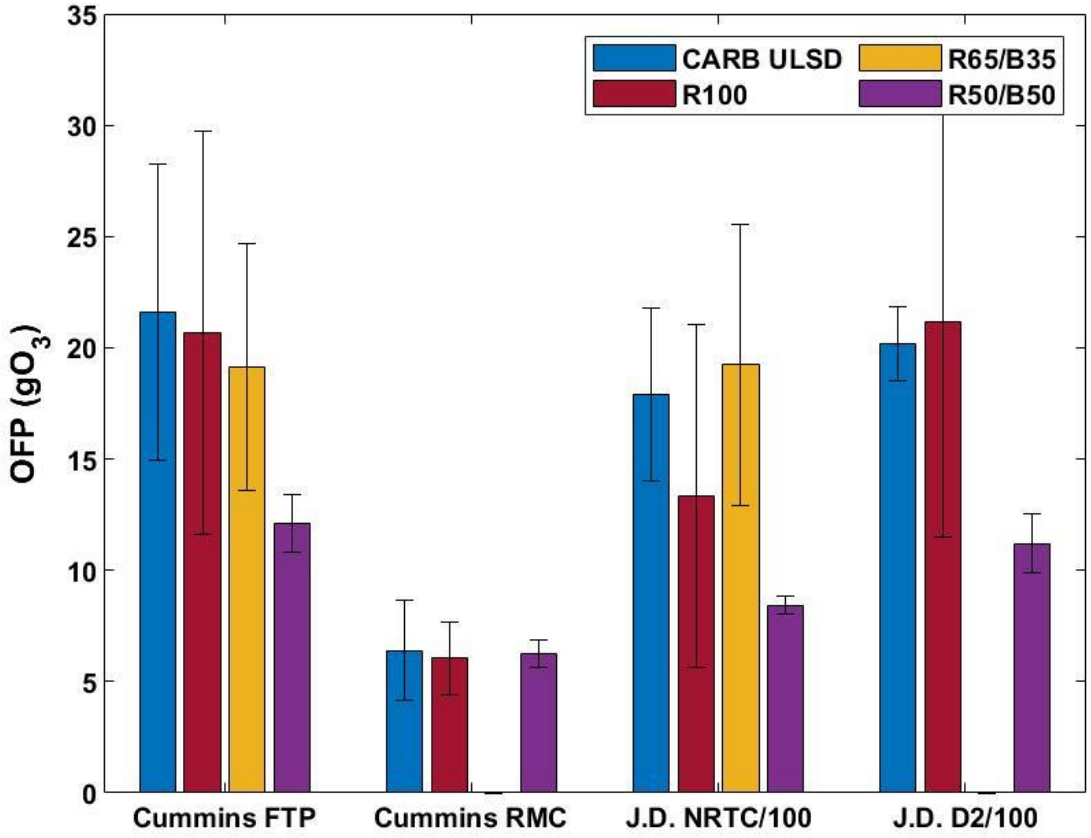

Figure 3-24: Average OFP for all fuel/cycle combinations for both engines

3.5 Conclusions

This study characterized the gaseous and particulate emissions of ULSD, renewable diesel and two renewable diesel biodiesel fuel blends. Testing was conducted on a new technology on-road heavy duty engine and legacy off-road heavy-duty engine. Results showed NOx emissions benefits when utilizing renewable diesel but showed increases in NOx emissions with increasing biodiesel content for both engines. CO and THC emissions showed significant reductions with renewable diesel and increasing biodiesel content for the John Deere engine but showed no noticeable changes for the Cummins engine due to

the presence of the DOC, which efficiently oxidized the THC and CO emissions. The increase in combustion efficiency for renewable diesel and renewable diesel-biodiesel fuel blends led to reductions in carbonyls and BTEX emissions for both engines. The absence of aromatics in the fuel, oxygen content in the biodiesel, and better combustion properties led to reduced formation of PAHs, PM mass, and total and solid particle number emissions for pure renewable diesel and the renewable diesel-biodiesel fuel blends. Overall, renewable diesel and renewable diesel-biodiesel fuel blends have the potential to significantly reduce pollutant formation from diesel engines, so long as renewable diesel and biodiesel are blended in such a manner that NOx emissions do not increase.

3.6 References

Aatola, Hannu, et al. "Hydrotreated Vegetable Oil (HVO) as a Renewable Diesel Fuel: Trade-off between NOx, Particulate Emission, and Fuel Consumption of a Heavy Duty Engine." *SAE International Journal of Engines*, vol. 1, no. 1, 2008, pp. 1251–1262., doi:10.4271/2008-01-2500.

Andreou G., Rapsomanikis S. "Polycyclic aromatic hydrocarbons and their oxygenated derivatives in the urban atmosphere of Athens." J Hazard Mater. 2009, 172, 363-73.

Basha, Syed Ameer, et al. "A Review on Biodiesel Production, Combustion, Emissions and Performance." *Renewable and Sustainable Energy Reviews*, vol. 13, no. 6-7, 2009, pp. 1628–1634., doi:10.1016/j.rser.2008.09.031.

Bohl, T., et al. "Particulate Number and NOx Trade-Off Comparisons between HVO and Mineral Diesel in HD Applications," *Fuel* 215:90-101, 2018.

Borillo GC, et al. "Effectiveness of selective catalytic reduction systems on reducing gaseous emissions from an engine using diesel and biodiesel blends." Environ Sci Technol 2015;49:3246-3251.

Cahill TM, Okamoto RA. "Emissions of acrolein and other aldehydes from biodiesel-fueled heavy-duty vehicles." Environ Sci Technol 2012; 46:8382-8388.

CARB. 2017. Revised Proposed 2016 State Strategy for the State Implementation Plan. https://www.arb.ca.gov/planning/sip/2016sip/rev2016statesip.pdf. March, 2017.

Carter, William P.L. “Development of the SAPRC-07 Chemical Mechanism.” *Atmospheric Environment*, vol. 44, no. 40, 2010, pp. 5324–5335., doi:10.1016/j.atmosenv.2010.01.026.

Dimashki, M. “Measurements of Nitro-PAH in the Atmospheres of Two Cities.” *Atmospheric Environment*, vol. 34, no. 15, 2000, pp. 2459–2469., doi:10.1016/s1352-2310(99)00417-3.

Durant et al. Human cell mutagenicity of oxygenated, nitrated and unsubstituted polycyclic aromatic hydrocarbons associated with urban aerosols. Mutat Res. 1996, 371, 123-57.

Eckerle WA, et al. “Effects of methyl ester biodiesel blends on NOx emissions.” SAE Technical Paper 2008; 2008-01-0078.

Erkkilä, K., et al., “Emission Performance of Paraffinic HVO Diesel Fuel in Heavy Duty Vehicles,” SAE Technical Paper 2011-01-1966, 2011, doi:https://doi.org/10.4271/2011-01-1966.

Ferreira da Silva, M., et al., “Characterization of metal and trace element contents of particulate matter (PM10) emitted by vehicles running on Brazilian fuels-hydrated ethanol and gasoline with 22% of anhydrous ethanol.” Journal of Toxicology and Environmental Health, Part A, 2010, 73, 901-909.

Finlayson-Pitts, B.J., and J.N. Pitts. “Atmospheric Chemistry of Tropospheric Ozone Formation: Scientific and Regulatory Implications.” *Air & Waste*, vol. 43, no. 8, 1993, pp. 1091–1100., doi:10.1080/1073161x.1993.10467187.

Flyn P.F., et al. “Diesel combustion: An integrated view combining laser diagnostics, chemical kinetics, and empirical validation.” SAE Technical Paper 1999, 1999-01-0509.

Fontaras G, et al., “Effects of biodiesel on passenger car fuel consumption, regulated and non-regulateed pollutant emissions over legislated and real-world driving cycles.” Fuel 2009; 88:1608-1617.

Fontaras G., et al., “Effects of low concentration biodiesel blend application on modern passenger cars. Part 2: Impact on carbonyl compound emissions”. Environmental Pollution 158, 2010, 2496-2503.

Giakoumis EG et al., “Exhaust emissions of diesel engines operating under transient conditions with biodiesel fuel blends.” Progress in Energy and Combustion Science 2012; 38: 691-715.

Giakoumis EG, Sarakatsanis CK. “A comparative assessment of biodiesel cetane number predictive correlations based on fatty acid composition.” Energies 2019, 12, 422.

Gomez, A., et al., “Evaluation of Sooting Tendency of Different Oxygenated and Paraffinic Fuels Blended with Diesel Fuel,” *Fuel* 184: 536-543, 2016.

Graboski MS, McCormick RL. Combustion of Fat and Vegetable Oil Derived Fuels in Diesel Engines. Progress in Energy and Combustion Science. 1998; 24(2):125-64.

Hajbabaei, Maryam, et al. “Evaluation of the Impacts of Biodiesel and Second Generation Biofuels on NOx Emissions for CARB Diesel Fuels.” *Environmental Science & Technology*, vol. 46, no. 16, 2012, pp. 9163–9173., doi:10.1021/es300739r.

Hajbabaei, M., Johnson, K.C., Okamoto, R., and Durbin, T.D., 2013, Evaluation of the Impacts of Biofuels on Emissions for a California Certified Diesel Fuel from Heavy-Duty Engines, Society of Automotive Engineers, SAE Technical Paper No. 2013-01-1138, doi:10.4271/2013-01-1138 saefuel.saejournals.org.

Hajbabaei M, et al. Impacts of biodiesel feedstock and additives on criteria emissions from a heavy-duty engine. Fuel Processing Technology 2014; 126:402-414.

Happonen, M., Heikkila, J., Murtonen, T., Lehto, K., Sarjovaara, T., et al., “Reductions in particulate and NOx emissions by diesel engine parameter adjustments with HVO fuel,” Environ. Sci. Technol. 46, 6198-6204, 2012.

Heikkila J., Happonen M., Murtonen T., Lehto K., Sarjovaara T., Larmi M., Keskinen J., et al. “Study of Miller timing on exhaust emissions of a hydrotreated vegetable oil (HVO)-fueled diesel engine,” Journal of the Air & Waste Management Association 62, 1305-1312, 2012.

Hoekman, S.K., Broch, A., Robbins, C., Ceniceros, E., Natarajan, M., 2012, Review of biodiesel composition, properties, and specifications, Renewable and Sustainable Energy Reviews 16, 143– 169.

Karavalakis G, et al. “Emissions and fuel economy evaluation from two current technology heavy-duty trucks operated on HVO and FAME blends.” SAE Int J Fuels Lubr 2016a, 9, 177-190.

Karavalakis, G. et al. “The Impact of Soy-Based Biodiesel on PAH, Nitro-PAH and Oxy-PAH Emissions from a Passenger Car Operated over Regulated and Nonregulated Driving Cycles.” *Fuel*, vol. 89, no. 12, 2010, pp. 3876–3883., doi:10.1016/j.fuel.2010.07.002.

Karavalakis G., et al., “Application of low-level biodiesel blends on heavy-duty (diesel) engines: Feedstock implications on NOx and particulate emissions.” Fuel 2016b;151:259-268.

Karavalakis G, et al., “Impact of biodiesel on regulated and unregulated emissions, and redox and proinflammatory properties of PM emitted from heavy-duty vehicles.” Science of the Total Environment 2017, 584-585, 1230-1238.

Kawano D, et al., “Exhaust emission characteristics of commercial vehicles fuelled with biodiesel.” SAE Technical Paper 2010; 2010-01-2276.

Khalek et al. “Regulated and unregulated emissions from highway heavy-duty diesel engines complying with U.S. Environmental Protection Agency 2007 emissions standards.” J Air Waste Manag Assoc. 2011, 61, 427-42.

Kousoulidou M, et al. “Biodiesel blend effects on common-rail diesel combustion and emissions.” Fuel 2010; 89:3442-3449.

Knothe, Gerhard, et al. “Exhaust Emissions of Biodiesel, Petrodiesel, Neat Methyl Esters, and Alkanes in a New Technology Engine†.” *Energy & Fuels*, vol. 20, no. 1, 2006, pp. 403–408., doi:10.1021/ef0502711.

Knothe G., et al. “Precombustion of fatty acids and esters of biodiesel. A Possible Explanation for differing cetane numbers.” J Am Oil Chem Soc 1998, 75, 1007-1013.

Knothe G., Steidley K.R. “Lubricity of components of biodiesel and petrodiesel. The origin of biodiesel lubricity” Energy and Fuels 205, 19, 1192-1200.

Lapuerta, M, et al. “Effect of Biodiesel Fuels on Diesel Engine Emissions.” *Progress in Energy and Combustion Science*, vol. 34, no. 2, 2008, pp. 198–223., doi:10.1016/j.pecs.2007.07.001.

Lea-Langton A, et al. “Comparison of particulate PAH emissions for diesel,biodiesel and cooking oil using a heavy duty DI diesel engine” SAE Technical Paper Series; 2008. 2008-01-1811.

Li, X., Zheng, Y., Guan, C. *et al.* Effect of biodiesel on PAH, OPAH, and NPAH emissions from a direct injection diesel engine. *Environ Sci Pollut Res* 2018, **25,** 34131–34138

Lim McKenzie CH, et al. “Influence of fuel composition on polycyclic aromatic hydrocarbon emissions from a fleet of in-service passenger cars” Atmos Environ 2007;41:150–60

Ma F., Hanna M.A. “Biodiesel production: a review.” Bioresource Technology 1999, 70, 1-15.

Magara-Gomez KT, et al. “Sensitivity of hazardous air pollutant emissions to the combustion of blends of petroleum diesel and biodiesel fuel.” Atmospheric Environment 2012;50:307-313.

Marchetti J.M., et al., “Possible methods for biodiesel production.” Renewable and Sustainable Energy Reviews 2007, 11, 1300-1311.

McCormick R.L., et al., “Several factors affecting the stability of biodiesel in standard accelerated tests.” Fuel Processing Technology 2007, 88, 651-657.

Miet, K., et al. “Heterogeneous reactivity of pyrene and 1-nitropyrene with NO2: kinetics, product yields and mechanism”. Atmospheric Environment 43, 837–843. 2009.

Mueller, Charles J., et al. “An Experimental Investigation of the Origin of Increased NOx Emissions When Fueling a Heavy-Duty Compression-Ignition Engine with Soy Biodiesel.” *SAE International Journal of Fuels and Lubricants*, vol. 2, no. 1, 2009, pp. 789–816., doi:10.4271/2009-01-1792.

Na, Kwangsam, et al. “Impact of Biodiesel and Renewable Diesel on Emissions of Regulated Pollutants and Greenhouse Gases on a 2000 Heavy Duty Diesel Truck.” *Atmospheric Environment*, vol. 107, 2015, pp. 307–314., doi:10.1016/j.atmosenv.2015.02.054.

Nelson PF, et al. “Effects of vehicle type and fuel quality on real world toxic emissions from diesel engines.” Atmospheric Environment 2008, 42, 5291-5303

Nisbet, I.C.T., LaGoy, P.K. Toxic equivalency factors (TEF)s) for polycyclic aromatic hydrocarbons (PAHs). Regul. Toxicol. Pharm. 1992, 16, 290-30

Odabasi, Mustafa, et al. “Polycyclic Aromatic Hydrocarbons (PAHs) in Chicago Air.” *Science of The Total Environment*, vol. 227, no. 1, 1999, pp. 57–67., doi:10.1016/s0048-9697(99)00004

Ogunkoya, Dolanimi, et al. “Investigation of the Effects of Renewable Diesel Fuels on Engine Performance, Combustion, and Emissions.” *Fuel*, vol. 140, 2015, pp. 541–554., doi:10.1016/j.fuel.2014.09.061.

Özener, Orkun, et al. “Effects of Soybean Biodiesel on a DI Diesel Engine Performance, Emission and Combustion Characteristics.” *Fuel*, vol. 115, 2014, pp. 875–883., doi:10.1016/j.fuel.2012.10.081.

Prokopowicz A, et al. “The effects of neat biodiesel and biodiesel and HVO blends in diesel fuel on exhaust emissions from a light duty vehicle with a diesel engine.” Environ Sci Technol 2015;49:7473-7482.

Qi, D.H., et al. “Experimental Studies on the Combustion Characteristics and Performance of a Direct Injection Engine Fueled with Biodiesel/Diesel Blends.” *Energy Conversion and Management*, vol. 51, no. 12, 2010, pp. 2985–2992., doi:10.1016/j.enconman.2010.06.042.

Ratcliff MA, et al. “Diesel particle filter and fuel effects on heavy-duty diesel engine emissions.” Environ Sci Technol 2010;44:8343-8349.

Rantanen, L, et al. “NExBTL - Biodiesel Fuel of the Second Generation,” SAE Technical Paper 2005-01-3771, 2005, doi:https://doi. org/10.4271/2005-01-3771.

Ravindra K, et al. ”Atmospheric polycyclic aromatic hydrocarbons:source attribution, emission factors and regulation.” Atmos Environ 2008;42:2895–921.

Richter H. Howard J.B. “Formation of Polycyclic Aromatic Hydrocarbons and Their Growth to Soot - a Review of Chemical Reaction Pathways.” Prog. Energy Combust. Sci. 2000, 26, 565−608.

Robinson, A. L, et al. “Rethinking Organic Aerosols: Semivolatile Emissions and Photochemical Aging.” *Science* **2007**, *315*, 1259–1262.

Rothe D, Lorenz J, Lammermann R, Jacobi E, Rantanen L, Linnaila R., New BTL Diesel Reduces Effectively Emissions of a Modern Heavy-Duty Engine. In: Kolloquium “Fuels” der Technischen Akademie, Esslingen (TAE). 2005.

Samburova et al. “Do 16 polycyclic aromatic hydrocarbons represent PAH air toxicity?” Toxic 2017, 5, 17.

Singh, Devendra, et al. “Comprehensive Review of Combustion, Performance and Emissions Characteristics of a Compression Ignition Engine Fueled with Hydroprocessed Renewable Diesel.” *Renewable and Sustainable Energy Reviews*, vol. 81, 2018, pp. 2947–2954., doi:10.1016/j.rser.2017.06.104.

Suarez-Bertoa R, et al. “Impact of HVO blends on modern diesel passenger cars emissions during real world operation.” Fuel 2019, 235, 1427-1435.

Sugiyama, Kouseki, et al. “Effects of Hydrotreated Vegetable Oil (HVO) as Renewable Diesel Fuel on Combustion and Exhaust Emissions in Diesel Engine.” *SAE International Journal of Fuels and Lubricants*, vol. 5, no. 1, 2011, pp. 205–217., doi:10.4271/2011-01-1954.

Szybist, James P., et al. “Biodiesel Combustion, Emissions and Emission Control.” *Fuel Processing Technology*, vol. 88, no. 7, 2007, pp. 679–691., doi:10.1016/j.fuproc.2006.12.008.

Tan Pi-Q, et al. “Particle number emissions from a light-duty diesel engine with biodiesel fuels under transient-state operating conditions.” Applied Energy 2014, 113, 22-31.

“Timeline of Ozone National Ambient Air Quality Standards (NAAQS).” *EPA*, Environmental Protection Agency, 21 Jan. 2021, www.epa.gov/ground-level-ozone-pollution/timeline-ozone-national-ambient-air-quality-standards-naaqs.

Tsai, Jen-Hsiung, et al. “Emissions of PM2.5-Bound Polycyclic Aromatic Hydrocarbons and Metals from a Diesel Generator Fueled with Biodiesel Converted from Used Cooking Oil.” *Aerosol and Air Quality Research*, vol. 19, no. 7, 2019, pp. 1555–1565., doi:10.4209/aaqr.2019.04.0204.

U.S Environmental Protection Agency. A Comprehensive Analysis of Biodiesel Impacts on Exhaust Emissions. EPA Draft Final Report; 2002.

"U.S. Energy Information Administration - EIA - Independent Statistics and Analysis." *Use of Biomass-Based Diesel Fuel - U.S. Energy Information Administration (EIA)*, 2020, www.eia.gov/energyexplained/biofuels/use-of-biodiesel.php.

Walgraeve et al. Oxygenated polycyclic aromatic hydrocarbons in atmospheric particulate matter: Molecular characterization and occurrence. Atmospheric Environment 2010, 44, 1831–1846.

Waynick, J. "Characterization of Biodiesel Oxidation and Oxidation Products." *SwRI Report*, 2005, doi:10.2172/909194.

Westphal GA, et al. "Combustion of hydrotreated vegetable oil and jatropha methyl ester in a heavy duty engine: emissions and bacterial mutagenicity." Environ Sci Technol 2013;47:6038-6046.

Xue, Jinlin, et al. "Effect of Biodiesel on Engine Performances and Emissions." *Renewable and Sustainable Energy Reviews*, vol. 15, no. 2, 2011, pp. 1098–1116., doi:10.1016/j.rser.2010.11.016.

Young LH, et al. "Effects of biodiesel, engine load and diesel particulate filter on nonvolatile particle number size distributions in heavy-duty diesel engine exhaust." Journal of Hazardous Materials 2012;199-200:282-289.

4. On-Road Gaseous and Particulate Emissions from GDI Vehicles with and Without Gasoline Particulate Filters (GPFs) Using Portable Emissions Measurement Systems (PEMS)

4.1 Abstract

This study assessed the on-road gaseous and particulate emissions from three current technology gasoline direct injection (GDI) vehicles using portable emissions measurement systems (PEMS). Two vehicles were also retrofitted with catalyzed gasoline particulate filters (GPFs). All vehicles were exercised over four routes with different topological and environmental characteristics, representing urban, rural, highway, and high-altitude driving conditions. The results showed strong reductions in particulate mass (PM), soot mass, and particle number emissions with the use of GPFs. Particle emissions were found to be highest during urban and high-altitude driving compared to highway driving. The reduction efficiency of the GPFs ranged from 44% to 99% for overall soot mass emissions. Similar efficiencies were found for particle number and PM mass emissions. In most cases, nitrogen oxide (NOx) emissions showed improvements with the catalyzed GPFs in the underfloor position with the additional catalytic volume. No significant differences were seen in carbon dioxide (CO_2) and carbon monoxide (CO) emissions with the vehicles equipped with GPFs.

4.2 Introduction

Road transport is a major source of nitrogen oxides (NOx) and particulate matter (PM), impacting air quality throughout the world. Elevated concentrations of mobile source emissions are responsible for adverse health impacts, including respiratory and cardiovascular diseases, or even premature mortality (Kampa and Castanas, 2008; Bates et al., 2015). Mobile source emissions have been significantly changed over the years as a result of stricter vehicle emission standards and efforts to reduce greenhouse gas (GHG) emissions. In the United States (US), Corporate Average Fuel Economy (CAFE) standards are pushing automotive manufacturers to meet fuel economy levels for passenger cars. Similarly, carbon dioxide (CO_2) emissions from newly registered cars in the European Union (EU) must decrease to about 95 g per kilometer by 2021.

The share of gasoline direct injection (GDI) engines has grown rapidly in both the US and the EU. GDI technology enables both an increase in specific power and a better fuel economy (with simultaneous reduction in CO_2 emissions), compared to traditional port fuel injection (PFI) engines (Alkidas, 2007). However, GDI engines are known to produce higher PM mass, black carbon, and particle number emissions than PFI engines and modern technology diesel engines equipped with diesel particulate filters (DPFs) (Karavalakis et al., 2015; Saliba et al., 2017; Zinola et al., 2016). PM formation in GDI engines is due to partially evaporated liquid fuel leading to fuel rich regions in the combustion chamber that promote the generation of PM (Karlsson and Heywood, 2001; Piock et al., 2011). Studies have shown that most GDI PM emissions are formed during the cold-start phase and during

highly transient operations (Chen et al., 2017; Koczak et al., 2016). The dynamic market penetration of GDI engines along with their elevated PM emissions create a growing public health concern in terms of PM exposures in urban areas.

Concerns about the real-world performance of vehicles and the lack of real-world operation represented of chassis dynamometer tests are now being addressed with test protocols capable of characterizing real-world vehicle emissions. Portable emissions measurement systems (PEMS) have been widely used to measure vehicle gaseous and particulate emissions under real-world conditions (Weiss et al., 2011; Gallus et al., 2016; Kwon et al., 2017; Yang et al., 2018a). PEMS have been proved to be an important tool for emission inventories because they enable testing under a wide variety of driving conditions, including road gradients, altitude and environmental conditions variations, and strong accelerations (Zhang et al., 2019; Bishop et al., 2019; O'Driscoll et al., 2018). In the US, PEMS measurements are required for in-use compliance testing of heavy-duty diesel vehicles, while the EU has implemented PEMS-based type-approval testing for light-duty vehicles starting from the Euro 6 standards. Overall, previous work has shown that there are substantial differences in emissions measured on-road using PEMS compared to laboratory testing (May et al., 2014; Chossière et al., 2018; Fontaras et al., 2017; Andersson et al., 2014). A number of studies have been conducted on different types of vehicles using PEMS, including heavy-duty trucks (Mendoza-Villafuerte et al., 2017; Johnson et al., 2009) and light-duty diesel and gasoline cars (Valverde et al., 2019; Khan and Frey, 2018), and off-road equipment (Cao et al., 2016; Cao et al., 2018). Gallus et al. (2017) found CO_2 and nitrogen oxides (NOx) emissions were strongly correlated with driving parameters,

showing increases with road grade. Wang et al. (2018) reported increases in carbon monoxide (CO), NOx, and particle number emissions at elevated altitude. Other PEMS studies have shown that real-world NOx and particulate emissions are affected by fuel type, after-treatment control, and engine power (Quiros et al., 2016; Huang et al., 2013; Demuynck et al., 2017).

The introduction of more challenging test procedures, such as realdriving emissions (RDE) for type approval in the EU, as well as stricter emission standards, such as the California LEV III PM mass limit of 1 mg/mile beginning in 2025 and the Euro 6a particle number limit of 6×10^{11} particles/km, make the reductions in target pollutants more difficult to be met with engine improvements alone. While stricter solid particle number regulations in the EU may have led to the introduction of gasoline particulate filters (GPFs) in the passenger car fleet there, at the time it is not expected that GPFs will be widely adopted in the US. Several studies have reported that the use of GPFs resulted in dramatic reductions in PM mass, number, and black carbon emissions from GDI vehicles (Yang et al., 2018b; Araji and Stokes, 2019). A recent study even showed that the use of catalyzed GPFs can reduce secondary organic aerosol formation (Roth et al., 2019). In addition, studies have shown reductions in particulate emissions and improved conversion efficiencies for CO and NOx emissions with the use of catalyzed GPFs under real-world conditions with minimal impact on CO_2 emissions (Schoenhaber et al., 2017; Yoshioka et al., 2019). Demuynck et al. (2017) investigated the deployment of GPFs on GDI vehicles using PEMS and found significant reductions in particle number emissions under RDE conditions. A

similar study also showed reductions in particle number emissions with the use of GPFs, without any detectable increase in CO_2 emissions (Ogata et al., 2017).

The primary objective of this study was to improve our understanding of the particulate emissions from three current technology GDI light-duty vehicles under different driving conditions mimicking urban, rural, and highway driving patterns, and included changes in altitude, road grade, and environmental conditions. Emissions testing were conducted on two vehicles in the stock configuration as well as after replacing the OEM underfloor three-way catalyst (TWC) with a catalyzed GPF. The catalyst formulation on the GPF was typical of an underfloor catalyst on vehicles of the same class, however, no attempt was made to exactly match the GPF catalyst formulation with that on the stock underfloor converter. Furthermore, the mileage accumulated on the GPF was not matched with the mileage of the TWC that it replaced. Therefore, the gaseous emissions are provided as observations for the purpose of relative comparison and are not intended to draw absolute conclusions. The results of this study will be useful in understanding real-world emissions from GDI vehicles and their contribution to air pollution in the Los Angeles Basin and other urban areas.

4.3 Experimental

4.3.1 Vehicles and GPFs

Three 2017 and 2018 model year GDI vehicles, referred to as GDI1, GDI2, and GDI3, were tested on-road for gaseous and particulate emissions. Detailed descriptions of the test vehicles are shown in Table 4-1. GDI1 and GDI3 were equipped with naturally aspirated

engines and wall-guided fuel injection systems, whereas GDI2 was equipped with a turbocharged engine and a centrally-mounted fuel injection system. All vehicles were operated with overall stoichiometric air-fuel ratios and certified to meet the Federal Tier 3 emission standards. Testing on all vehicles was performed on typical California E10 fuel.

Table 4-1: Technical specifications of the test vehicles

	GDI1	**GDI2**	**GDI3**
Vehicle Model Year	2017	2017	2018
Cylinder Number	4, inline	4, inline	V6
Displacement	2.0 L	1.5 L	3.6 L
Horsepower	155 at 6000 rpm	181 at 6300 rpm	305 at 6800 rpm
Torque	150 ft-lb at 4000 rpm	185 lb-ft at 4320 rpm	264 ft-lb at 5200 rpm
Compression Ratio	13.0:1	10.0:1	11.5:1
Air Intake	Naturally Aspirated	Turbocharged	Naturally Aspirated
Fuel Delivery	Wall-guided	Centrally-mounted	Wall-guided
Emission Standards	USEPA: T3B30, CA SULEV 30 PZEV	USEPA: T3B30, CA SULEV 30 PZEV	USEPA: T3 LDV, CA SULEV 30

For GDI1 and GDI2, testing was also conducted with a catalyzed GPF installed in the place of the underfloor TWC. The original close-coupled catalysts were retained in their stock location. The GPFs were sized based on the engine displacement of each vehicle and they were catalyzed with precious metal loadings typical of underfloor catalysts at the same certification levels of the two vehicles. Both GPFs were 4.66 in. in diameter and 4.5 in. in length, with an 8-mil cell wall thickness and a cell density of 300 cells per square inch (cpsi). More details on the GPFs are provided in Yang et al. (2018b). Briefly, both GPFs followed a de-greening process, which included on-road highway driving of the vehicles for about 500 miles. Both GPFs were wall-flow type. Considering the low level of PM emissions for GDI vehicles compared to heavy-duty diesel vehicles, it is assumed the GPF fill state may not have changed significantly during the test period.

PEMS Installation

The PEMS units employed in this work to measure gaseous and particulate emissions were compliant with federal test methods (CFR 1065) for on-road testing and installed following manufacturers recommendations. PEMS installation included the use of a generator for power, backup lithium batteries, and a power inverter. The PEMS units were placed inside the vehicles (backseats and trunk), while the generator was attached to a hitch at the back of each vehicle. Prior the on-road testing, a calibration procedure including leak checks and zero-span calibration was performed.

For GDI1, the AVL 493 M.O.V.E gas PEMS and the AVL 494 PM PEMS systems were used. The AVL 493 PEMS system measures NOx (NO and NO_2) using non-dispersive

ultraviolet radiation (NDUV), CO and CO_2 using non-dispersive infrared radiation (NDIR), and THC using flame ionization detection (FID). The AVL 494 PM PEMS system includes a dilution sampling system and a real-time AVL 483 micro soot sensor (MSS), in conjunction with AVL's integrated gravimetric PM filter module. For GDI2 and GDI3, the Sensors Semtech-DS unit was employed for the measurement of NOx, CO, CO_2, and THC emissions and the AVL 494 PM PEMS system. Solid particle number emissions according to the European Particle Measurement Programme (PMP) were measured for GDI1 and GDI3 vehicles with the use of AVL's M.O.V.E PN PEMS iS, which uses diffusion charger technology. For GDI2, particle number emissions were measured with the NTK NCEM mini-PEMS unit. This system measures PM mass and particle number emissions using a sensor based on the Pegassor PPS-M technology, where particles are charged in a corona discharge, such that the total measured charge is proportional to the particle active surface area. The NTK NCEM measures total particle number including solid and volatile particles and does not comply with the PMP protocol that excludes volatile particles and solid particles b23 nm. More details on the NTK NCEM systems are given elsewhere (Yang et al., 2018a). GDI1 and GDI 3 used a Sensors Inc. 2.5-in. exhaust flow meter (EFM) system, whereas GDI2 used a Sensors Inc. 2-in. EFM to provide integrated mass emissions as well as second by second emissions data. The EFM systems were equipped with an averaging pitot tube and thermocouples to obtain the exhaust mass flow. Both systems were designed to have wide dynamic range to measure exhaust flows so that the vehicle exhaust can be measured over the full range. Both EFM systems were calibrated following procedures according to CFR40 Part 1065.307.

4.3.2 Test Routes

On-road testing was performed in triplicate for each vehicle on four routes with different topological and environmental characteristics. Topological maps of each test route are shown in Figure 4-1 (a-d). The test routes were designed to represent urban, rural, and highway driving conditions and included changes in altitude and ambient climatic conditions. The first route, referred to as Downtown Los Angeles (LA), primarily consisted of urban driving in the downtown area of LA and had a total distance of 16 miles. This route was characterized by dense traffic, frequent start and stop conditions, and an average speed of 15.7 miles/h. The route was created from the same route used to develop the LA Route Four (LA4) as part of the original certification Federal Test Procedure (FTP). The second route, referred to as Highway, started from LA and headed east to Ontario. This route utilized Interstate-10 (I-10), which is one of Southern California's major freeways. This route mainly consisted of high-speed driving with some congestion coming out of LA. The route covered 43 miles and had an average speed of 48.3 miles/h. The third route, referred to as Mountain (Mt) Baldy, consisted of mountainous roads with uphill/downhill driving, steep road grades, and medium to higher speeds during operation. The route started and ended at sea level, while on elevation change of 1524 m to the top of the mountain. It also consisted of some urban/rural driving on the historic route 66 and highway driving at high speeds. The average speed for this 44.2-mile route was 25.1 miles/h. The last and fourth route, referred to as Downtown San Diego (SD), started and ended in downtown San Diego on sea level roads near the harbor. This 13.1-mile route consisted of mainly urban driving with some highway portions in the Interstate-5. It was also characterized by high

humidity with moderate temperatures. The total elevation change for the route was around 60 m. The Downtown LA and Downtown SD routes were similar in that both consisted of largely urban driving with some highway driving, but the Downtown SD route had more elevation changes and a lower average speed of 13.1 miles/h.

All PEMS emissions tests were conducted in the same sequence. For a single testing day, tests started with the Downtown LA route, followed by the Highway route, and ended with the Mt. Baldy route. The Downtown SD route was tested on a separate day. Testing on all routes was performed when the engine and TWC were fully warmed up. Cold-start emissions were obtained at the beginning of each test day prior to the vehicle's arrival on the testing site.

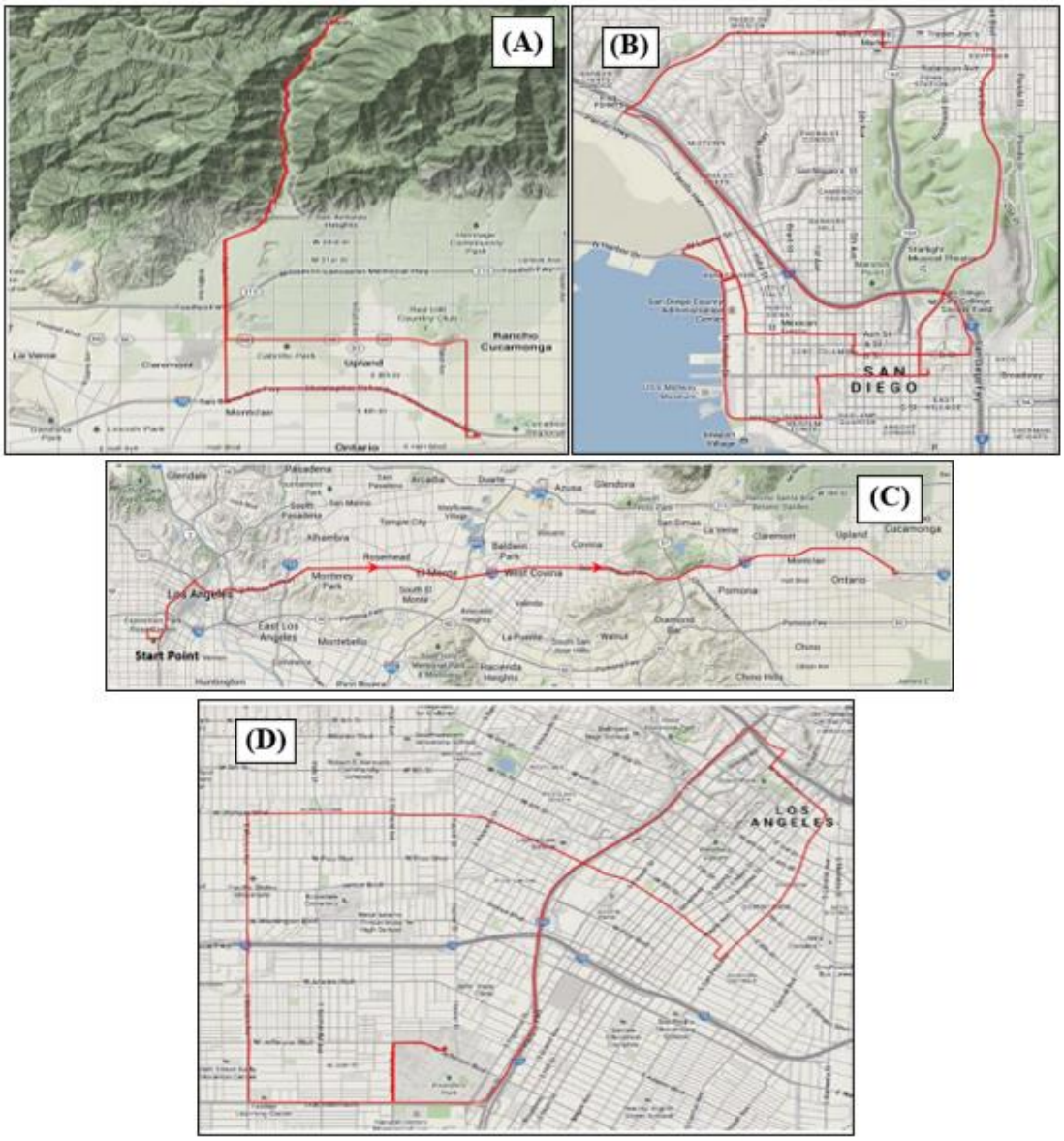

Figure 4-1 (a-d): Test Route topographical map for Mt Baldy (a), Downtown SD (b), Highway (c), and Downtown LA (d).

4.4 Results and Discussion

4.4.1 Particulate Emissions

Fig. 4-2 (a–b) show the soot mass or black carbon emissions and gravimetric PM mass, respectively. For all vehicles on all test routes, PM mass emissions were below the Tier 3 PM mass standard of 3 mg/mile. Consistent with previous studies, the use of catalyzed GPFs resulted in important reductions in PM mass and black carbon emissions (Yang et al., 2018b; Chan et al., 2014). The decreases in PM emissions with the GPFs ranged from 12%–49% for GDI1 and 60%–96% for GDI2. Similar filtration efficiencies were also observed for the soot mass emissions, ranged from 44%–66% for GDI1 and 93%–99% for GDI2. Our results showed some higher GPF filtration efficiencies for the urban test routes compared to the Highway route, which agrees with the results of Yoshioka et al. (2019). The quasi steady-state operation of the engine over the Highway route may have led to more fuel cut-off and oxygen-rich phases, which prevented the formation of a soot layer in the filter channels due to passive regeneration. This was most likely the reason for the lower filtration efficiency of GDI1 due to the lower engine-out PM levels compared to GDI2.

The higher compression ratio Atkinson engine equipped GDI1 generally showed lower PM mass and soot mass emissions over all test routes compared to GDI2 and GDI3, with the exception of the Mt. Baldy route where the differences in PM mass emissions were indistinguishable between the three vehicles. Yang et al. (2018b) attributed these phenomena to the earlier fuel injection and the subsequent formation of a homogeneous air-fuel mixture because of more time for mixture preparation. In addition, the higher in-

cylinder temperature may have led to better oxidation of soot particles and hydrocarbon gases inside the combustion chamber, which will result in lower engine-out PM mass and soot.

Overall, PM mass and soot emission rates were higher for the urban routes (i.e., Downtown LA and Downtown SD) compared to the Highway route. Both urban routes included increased transient and aggressive driving with frequent stop-and-go events, which lead to greater particulate emissions. The large number of stop-and-go events for the urban test routes compared to highway driving caused increased PM mass and soot mass emissions per mile. Compared to the Highway route, Mt. Baldy showed elevated PM mass and soot emission rates. A recent study suggested that the lower oxygen concentration at higher altitudes may help to enhance the formation of PM emissions (Wang et al., 2018). For the Mt. Baldy route, uphill driving showed higher soot mass emissions and lower PM and soot percentage reductions for the GPF retrofitted vehicles compared to downhill driving. The positive road grade for uphill driving is linked to higher load and acceleration events on the engine, which caused higher soot mass emissions and generally lower PM mass and soot percentage reductions for the GPFs. It should be noted that the Downtown SD route generally showed trends of higher PM emissions than the downtown LA route. The climatic conditions between these two routes likely influenced PM emissions, with generally lower ambient temperatures and high humidity in the San Diego area due to the very close proximity to the sea. This contributed to more PM formation by the combination of PM and moisture coming from the ambient air as well as being generated by exhaust gas condensation (Kwon et al., 2017).

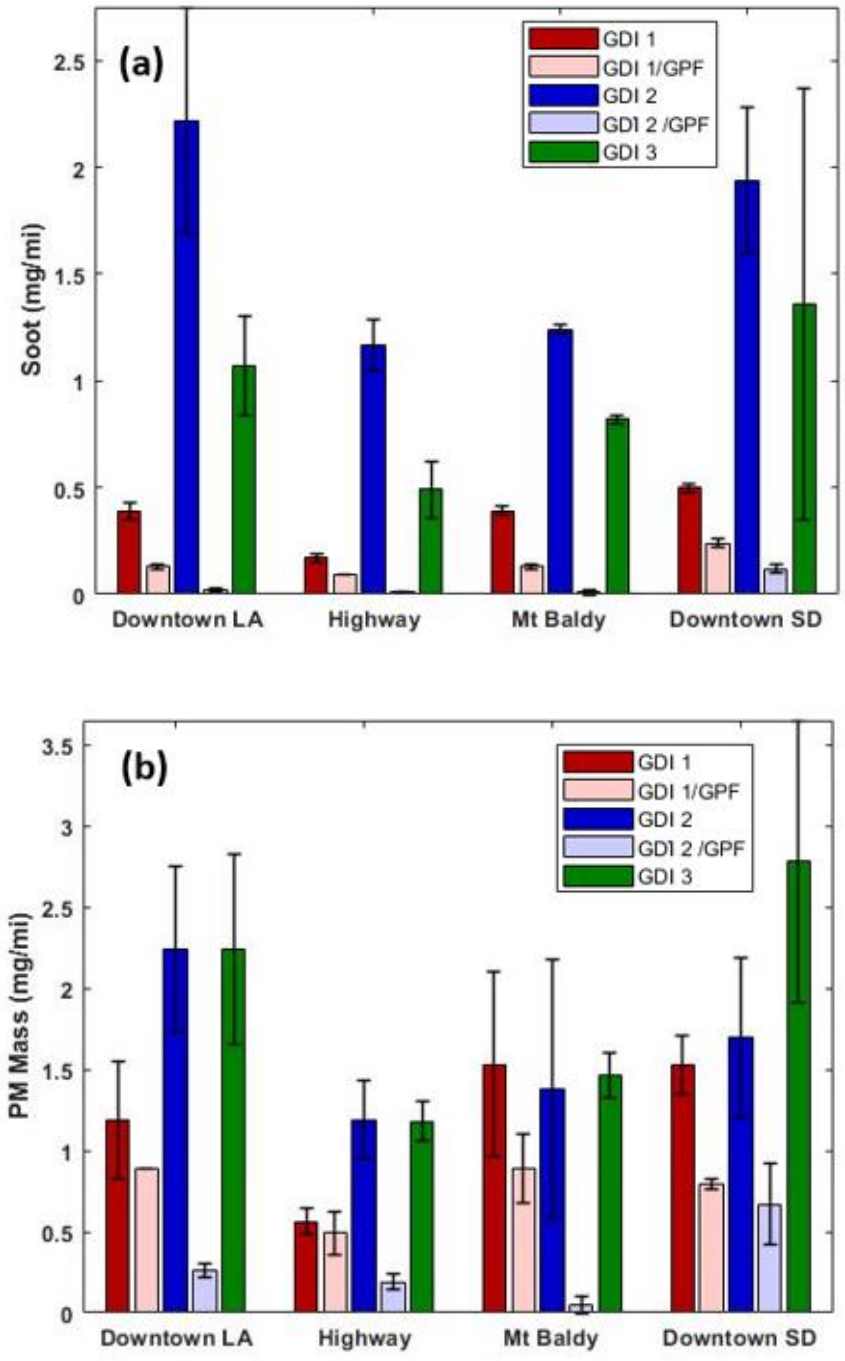

Figure 4-2 (a-b): Soot mass and gravimetric PM mass emissions for the test vehicles over the different routes

Soot mass and PN emissions were affected by vehicle speed and load for every test route. For the Downtown LA, Downtown SD, and Highway routes, the highest soot mass and particle number emissions were seen for the during speeds bins between 0–20 miles/h, and positive acceleration conditions from a stop. These findings are graphically depicted in Fig. 4-3 (a–d) for the solid particle number emissions for GDI1, while soot mass emissions are shown in Figure 4-4 (a-d). Urban driving includes a large amount of idling, congestion, and start/ stop traffic conditions. This is an important finding from a PM exposure perspective since these driving conditions usually occur in densely populated urban centers. Under deceleration conditions or relatively high speeds, soot mass and particle number emissions were lower, suggesting that free flow driving at higher speeds in urban centers will not contribute to high concentrations of particulate emissions. For the Highway route, soot mass and particle number emissions showed elevated concentrations at low and intermediate speed bins and during acceleration events, suggesting that the bulk of these emissions were spikes formed during acceleration events as opposed to steady-state high speed driving. For the Mt. Baldy route, the intermediate speed bins and high accelerations produced higher soot mass and particle number emissions. GDI1 showed a 65% reduction in soot mass emissions with the GPF for the 0–10 miles/h speed bin that gradually decreased towards higher speed bins, with the lowest soot mass reduction with the GPF of 36% for the 50–60 miles/h speed bin. GDI2 showed strong soot mass reductions with the GPF (N99%) for all speed bins. Overall, soot mass and particle number emissions increased with engine loading for all test routes and vehicles. The soot mass reductions for both GPF-retrofitted vehicles tended to be higher at the highest load bins.

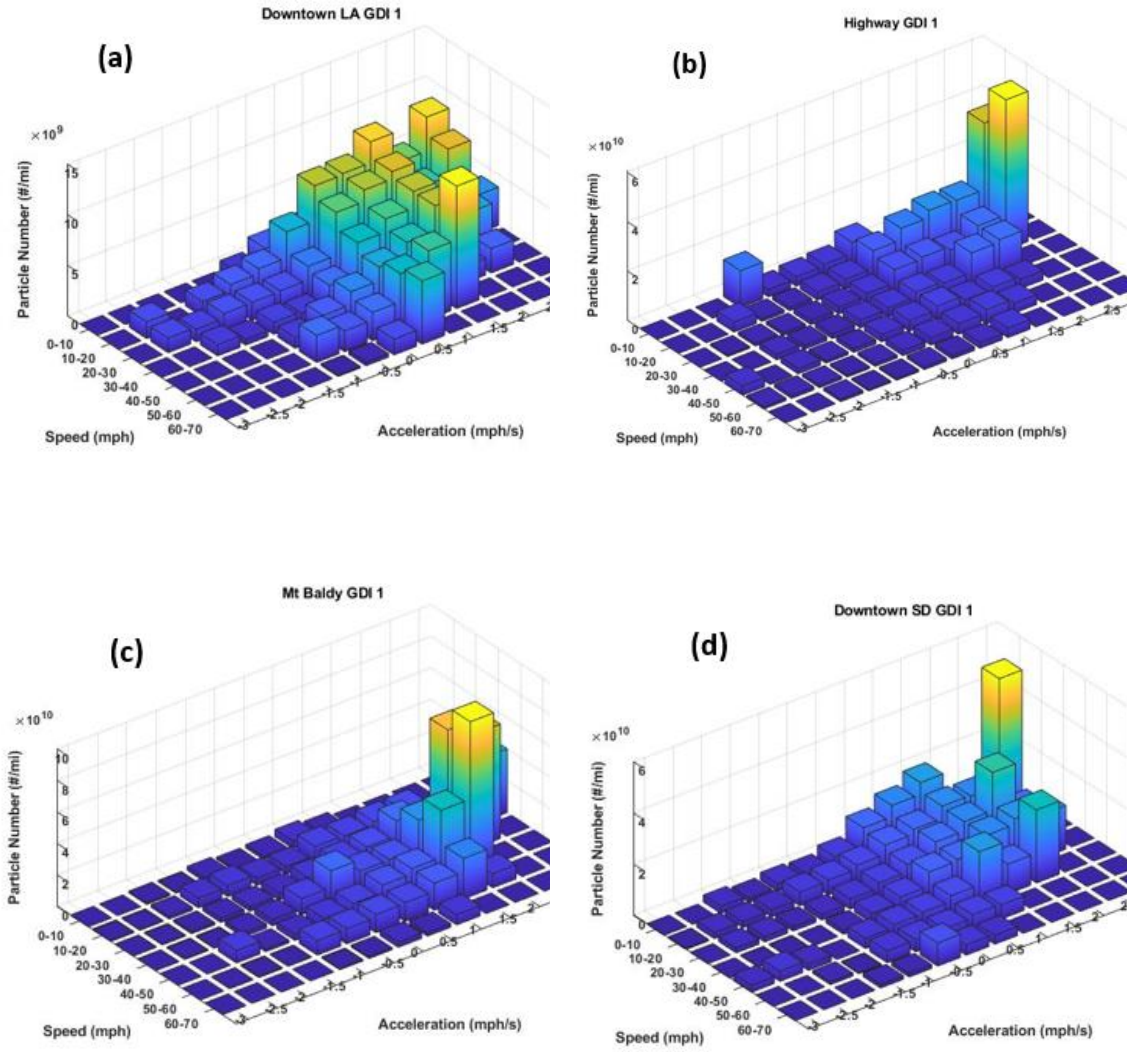

Figure 4-3 (a-d): Solid particle number emissions for GDI1 as a function of vehicle speed and acceleration over the Downtown LA (a), Highway (B), Mt Baldy (c), and Downtown SD (d) test routes

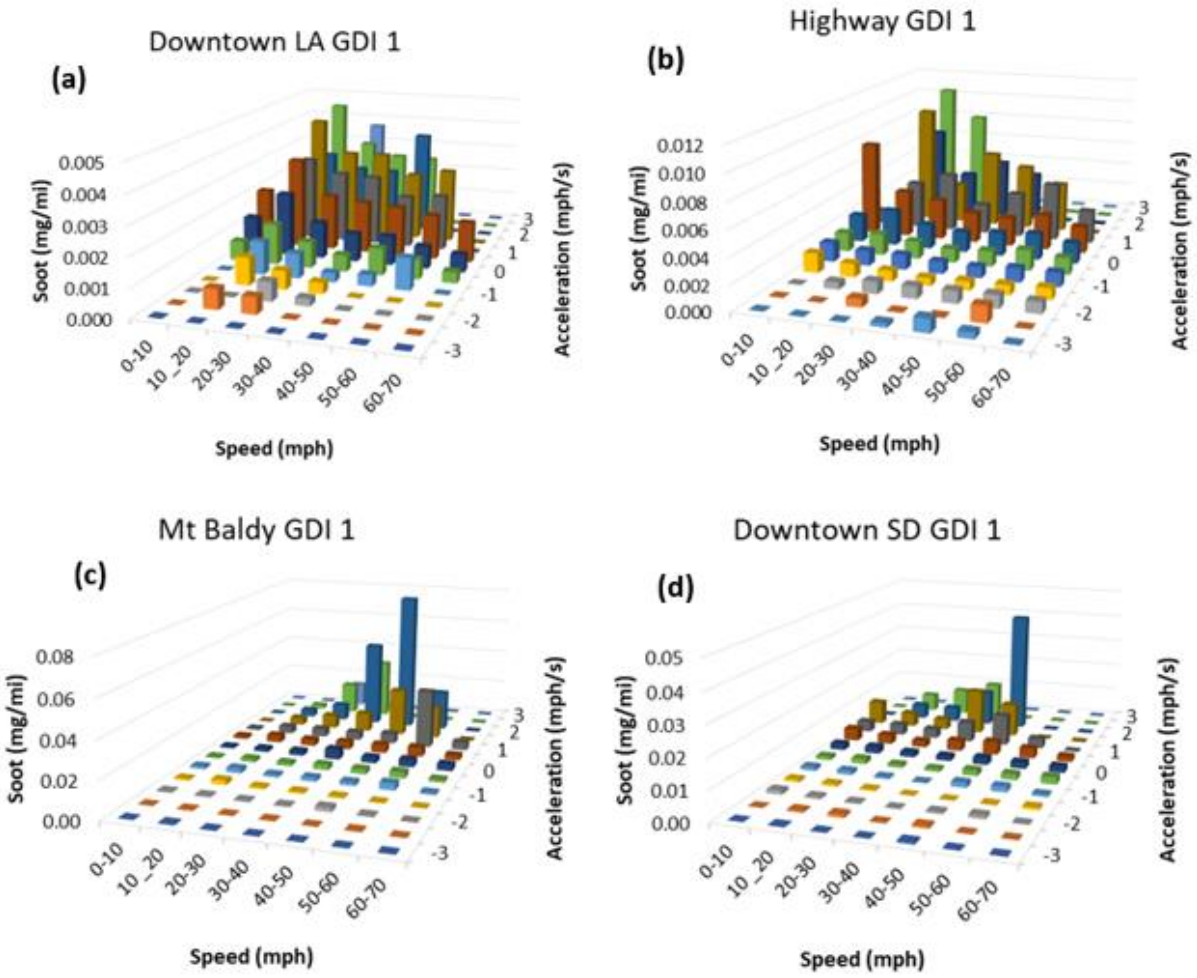

Figure 4-4 (a-d): Soot mass emissions for GDI1 as a function of vehicle speed and acceleration over the Downtown LA (a), Highway (B), Mt Baldy (c), and Downtown SD (d) test routes

Particle number emissions are shown in Fig. 4-5. Similar to PM mass and soot mass emissions, particle number emissions exhibited strong, statistically significant decreases with the use of catalyzed GPFs for GDI1 and GDI2 over all test routes. It is worth noting that all vehicles with and without GPFs were below the Euro 6c limit for solid particle number emissions at 6×10^{11} #/km, with the only exception of GDI2 on the Mt. Baldy route. For the Mt. Baldy route, the GPF performance was calculated for the entire trip,

which included uphill and downhill driving. For the uphill driving, GDI2 showed an almost negligible particle number reduction (~6%), whereas the particle number reduction for the downhill driving was about 93%. The large discrepancies in the particle number emissions reductions of GDI2 will be discussed later in more detail.

Particle number emissions were seen at higher levels for the urban test routes compared to the Highway route. It is reasonable to assume that the enriched combustion that occurred during frequent stop-and go events in congested situations resulted in elevated particle number emissions for the urban test routes. The relatively lower particle number emissions for the Highway route could likely be due to the high engine load and high speed, which increased the in-cylinder temperature and improved the mixing of fuel with air, leading to lower particle number emissions. The Downtown SD route also showed some increases in particle number emissions compared to the Downtown LA route, which can be ascribed to some of the unique topological characteristics of the Downtown SD route, such as uphill/downhill driving and a portion of highway driving.

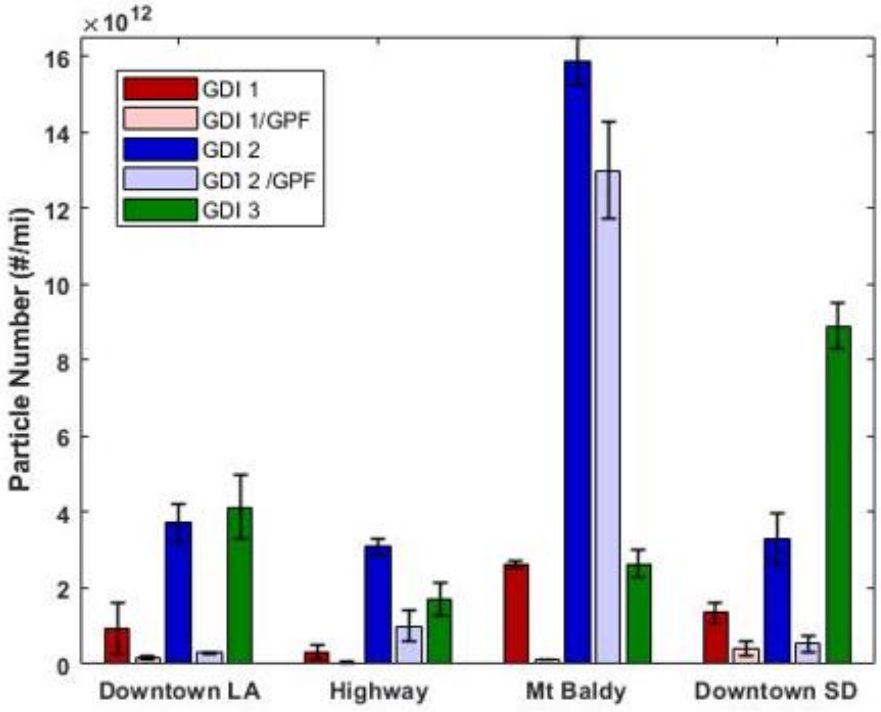

Figure 4-5:Particle number emissions for the test vehicles over the different routes

It is interesting to note the significantly higher particle number emissions for GDI2 over the Mt. Baldy route compared to the other vehicles. The vast majority of particles were produced during the uphill segment of the Mt. Baldy route followed by the urban segment. As mentioned earlier, particle number measurements for GDI2 were made with the NTK NCEM unit, which uses diffusion charging principle and infers particle number emissions assuming a lognormal particle size distribution with a specific geometric mean diameter, whereas the AVL M.O.V.E PN PEMS iS unit was used for GDI1 and GDI3 to measure solid particle number. It was hypothesized that the higher engine loading when driving over the mountainous roads caused the elevated formation of small volatile or solid particles in the raw exhaust, which agrees with findings from a recent study that showed gasoline

vehicles could produce significant concentrations of solid particles below 23 nm (Giechaskiel et al., 2018). Similar phenomena were also observed in an earlier study by Zheng et al. (2014). They reported that aggressive uphill driving led to significant increase in particle emissions above 23 nm for a heavy-duty diesel vehicle with DPF. Since the particle number sensor was direct type to the exhaust and did not have a volatile particle remover (VPR) to remove semi-volatile components from the aerosol stream, it counted both volatile and solid particles. For the mountainous route, the phenomena of condensation and nucleation of volatile raw exhaust gas components in the size range below 23 nm downstream of the GPF, were much more prevalent than for the urban and highway test routes for this vehicle, especially during the uphill segment of Mt. Baldy. Therefore, we propose testing on GDI2 did not exactly show a volatile artifact during measurement, but instead a design weakness or oversensitivity of the particle number sensor, which could be resolved by changing the trap voltage in the diffusion charger to include the cut-off of particles below 23 nm. In addition, the poor PM and soot percentage reduction for GDI2 over Mt. Baldy does not suggest poor performance of the catalyzed GPF beyond its function to trap solid soot particles, but it does show the tendency of a catalyzed GPF to store semi-volatile particles in the wash coat and release them as secondary nucleated particles under certain types of driving conditions.

4.4.2 Gaseous Emissions

NOx emissions for all vehicles and test routes are shown in Fig. 4-6. NOx emissions in grams per mile ranged from 0.003–0.066 for the Downtown LA route, 0.007–0.035 for the Highway route, 0.013–0.027 for the Mt. Baldy route, and 0.011–0.085 for the Downtown

SD route. GDI1 showed 3–4 times higher NOx emissions for all test routes compared to the certification standard for this engine, while GDI2 testing only exceeded the NOx emissions standard over the Highway route. Higher real-world NOx emissions were also seen for GDI3 compared to the certification standard for this engine for all test routes except the Downtown LA route. These are important findings considering that adverse health effects of NO_2 and NOx emissions will affect urban air pollution by participating in the ground level ozone formation. It should be noted that the Los Angeles Basin faces significant air quality issues due to smog concentrations and is currently under EPA's (Environmental Protection Agency) nonattainment designation for ozone.

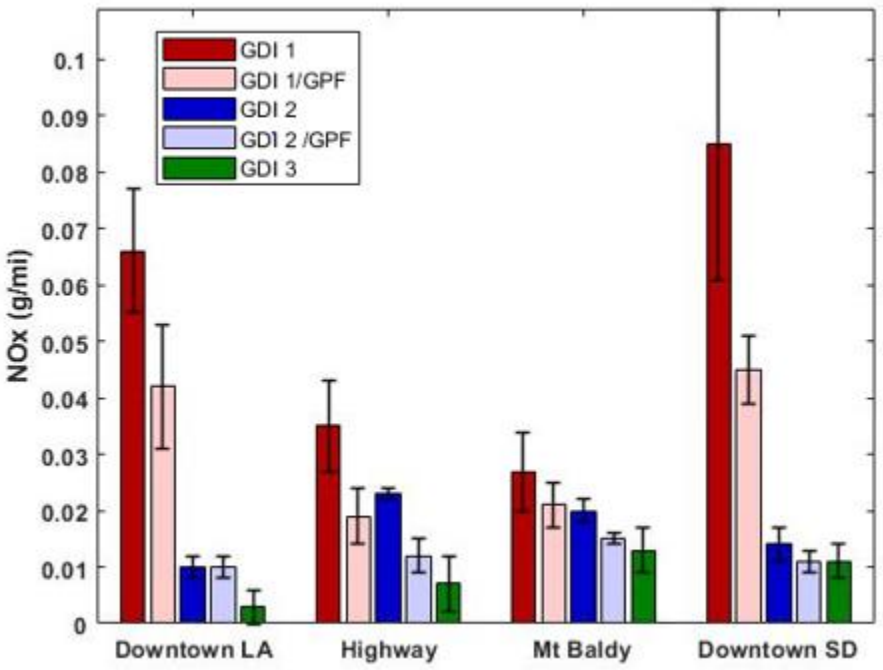

Figure 4-6: **NOx emissions for the test vehicles over the different routes**

Results showed a strong dependency between NOx emissions, the different test routes, and the test vehicles, with both urban routes having higher NOx emission levels for GDI1 and lower NOx emission levels for GDI2 and GDI3, respectively, compared to the Highway and Mt. Baldy routes. Overall, GDI1 showed higher NOx emissions than the other vehicles, which was likely due to the relatively higher compression ratio for this vehicle causing increases in the in-cylinder combustion temperature that favored thermal NOx production. Although the primary function of the catalyzed GPF was to eliminate particulate emissions, the additional catalytic surface enhanced the conversion of NOx emissions for both GDI1 and GDI2, provided statistically significant NOx reductions for some test routes. Previous studies have also reported NOx reductions from GDI vehicles with catalyzed GPFs (Yang et al., 2018b; Xia et al., 2017). A different study, however, did not show any further NOx reductions when they tested a GDI vehicle with and without a catalyzed GPF on-road (Demuynck et al., 2017). For GDI2 and GDI3, NOx emissions were higher during uphill driving, while urban and highway driving NOx emissions were higher for all vehicles compared to downhill driving. The relatively high NOx emissions for GDI1 over the urban segment and low NOx emissions over the uphill segment could be attributed to the engine combustion strategies associated with this vehicle's driving behavior over different driving conditions (i.e., road grade, start/stop). Our results agree with previous studies that have also shown higher NOx emissions with uphill driving (Gallus et al., 2017; Prati et al., 2015). It was also evident that for the uphill segment of the Mt. Baldy route, lambda (λ) values were closer to stoichiometric and above (lean engine operation), resulting in

elevated NOx emissions for all test vehicles. A recent study also reported a strong linkage between real-world NOx emissions and lean engine operation (Suarez-Bertoa et al., 2019).

Comparing the two urban routes, all vehicles showed higher NOx emissions over the Downtown SD route. There may be many contributing factors that could have led to more NOx on the Downtown SD route, including driving conditions and regional variations in temperature and humidity in the area of testing. The increased humidity in the inlet air and its subsequent higher moisture content would have been expected to reduce NOx emissions due to the reduced peak in-cylinder temperature. It appeared that climatic conditions had no effect on NOx emissions, but rather the higher NOx levels for the Downtown SD route were due to the higher engine load during uphill/downhill and highway driving for this route compared to the flat road driving in the Downtown LA route.

CO emissions are shown in Fig. 4-7. Note that CO emissions were reduced by a factor of 20 for the Mt. Baldy route in Fig. 4-7 to show comparisons with the other routes. CO emissions were found to be above the certification standards for GDI1 on the Mt. Baldy and Downtown SD routes, GDI2 for the Highway route, and GDI3 for all test routes except Mt. Baldy. Unlike NOx, CO emissions did not show reductions with the catalyzed GPFs over real-world conditions, which contradicts a previous study that showed CO reductions with GPFs over the LA92 cycle (Yang et al., 2018b). CO emissions were found to be higher for the more dynamic Downtown SD route compared to the Downtown LA route, due to more transition engine operating conditions and higher loads that favor rich air-fuel mixtures. Similarly, Demuynck et al. (2017) and Suarez-Bertoa et al. (2019) reported

higher real-world CO emissions over more dynamic routes. Results reported here indicate the effects from rich engine operation during uphill/downhill and high-speed driving conditions for the Downtown SD route compared to the flat road Downtown LA route. The Highway route generally showed higher CO emissions compared to both urban routes. For some vehicles, CO emissions were higher over the mountainous roads than the Highway route. Although CO emissions were expected to increase with high altitude and lower atmospheric pressure conditions, this was not the case for some of the vehicles, suggesting that emissions strategies affecting conversion rates in the TWC may have played a role during mountainous driving. However, looking at the uphill segment of the Mt. Baldy route, it is evident that CO emissions were higher compared to the downhill segment. The uphill segment represents typical engine operation with low air-fuel ratios during acceleration events, which favor CO emissions formation.

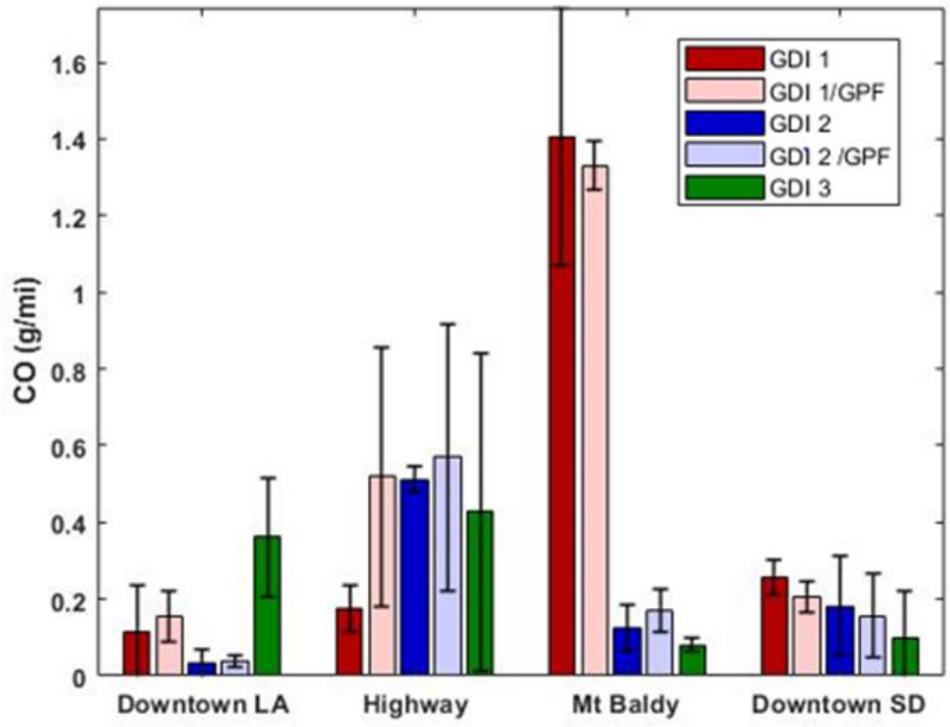

Figure 4-7: **CO emissions for the test vehicles over the different routes; Note the CO emissions for the Mt Baldy route are divided by a factor of 20 for all test vehicles**

CO_2 emission rates increased with engine displacement (i.e., GDI3), indicating important CO_2 savings for smaller downsized engines. The use of catalyzed GPFs did not show any appreciable CO_2 emission penalties for GDI1 and GDI2. Overall, CO_2 emissions showed an increasing trend for both urban routes, with the Downtown SD route showing higher CO_2 emissions due to higher engine loads for uphill driving relative to flat road driving. For the uphill segment of the Mt. Baldy route, CO_2 emissions were on average 80%–92% higher than during the downhill segment of this route. Similar findings have been reported by Chong et al. (2018), where they showed that higher engine loadings will increase CO_2 emissions due to higher fuel consumption. Wyatt et al. (2013) attributed the higher uphill

CO_2 emissions to the increased power demand required to maintain speed or acceleration of the vehicle to overcome the effect of gravity acting as a breaking force that increases with road grade. In addition, the GPF retrofitted vehicles showed higher CO_2 emissions than the original configuration for the uphill segment, with CO_2 increases ranging from 0.9% to 7.8% for GDI1 and GD2, respectively. CO_2 reductions for the downhill segment ranged from 11.7% to 17.2% for GDI1 and GDI2, respectively.

4.4.3 Cold-Start Emissions

For the purpose of this analysis, the cold-start increment was defined as the first 5 min after initial start of the engine or until the coolant temperature had reached 70 °C for the first time. Figure 4-8 (a–b) shows the real-time soot mass and particle number emissions evolution for the cold-start period. Both soot mass and particle number populations were significantly higher during the first 50 s of the cold-start period, whereas gradual reductions in both pollutants were seen due to the warm-up of the TWC, engine, and exhaust surfaces. It is noteworthy that the use of GPFs resulted in large reductions of both soot mass and particle number emissions, indicating their beneficial role at the remediation of these pollutants. All vehicles showed different heat-up rates in achieving the coolant warm-up temperature value of 70 °C, with GDI1 and GDI3 reaching full warm-up temperature at 386 s and 266 s, respectively. GDI1 showed the higher particle number and soot mass emissions during the first 50 s and had the lowest coolant temperature and longer heat-up period, followed by GDI3 and GDI2. PM formation during cold-start operation for GDI engines is particularly sensitive, since the injected fuel lands on the cold piston surfaces resulting in the formation of liquid fuel films that fail to completely evaporate, causing

diffusive combustion and the formation of soot particles (Chen et al., 2017; Koczak et al., 2016; Yang et al., 2019). Figure 4-9 (a–d) present the soot mass, particle number, NOx, and CO emissions for all vehicles on the Downtown LA route with and without cold-start emissions, respectively. For most cases, the inclusion of the cold-start did not show significant differences in soot mass and particle number emissions, with the exception of GDI1. The limited differences between tests could be due to the total distance covered in the test route compared to the short distance and duration of the cold-start period. In addition, the transient and dynamic operation significantly contributes to soot mass and particle number emissions. In agreement with previous studies, CO emissions were significantly affected by the inclusion of cold-start, showing the low conversion efficiency for the TWC when it is below its light-off temperature, while NOx emissions showed lower sensitivity for cold-starts (Merkisz et al., 2019; Khan and Frey, 2018).

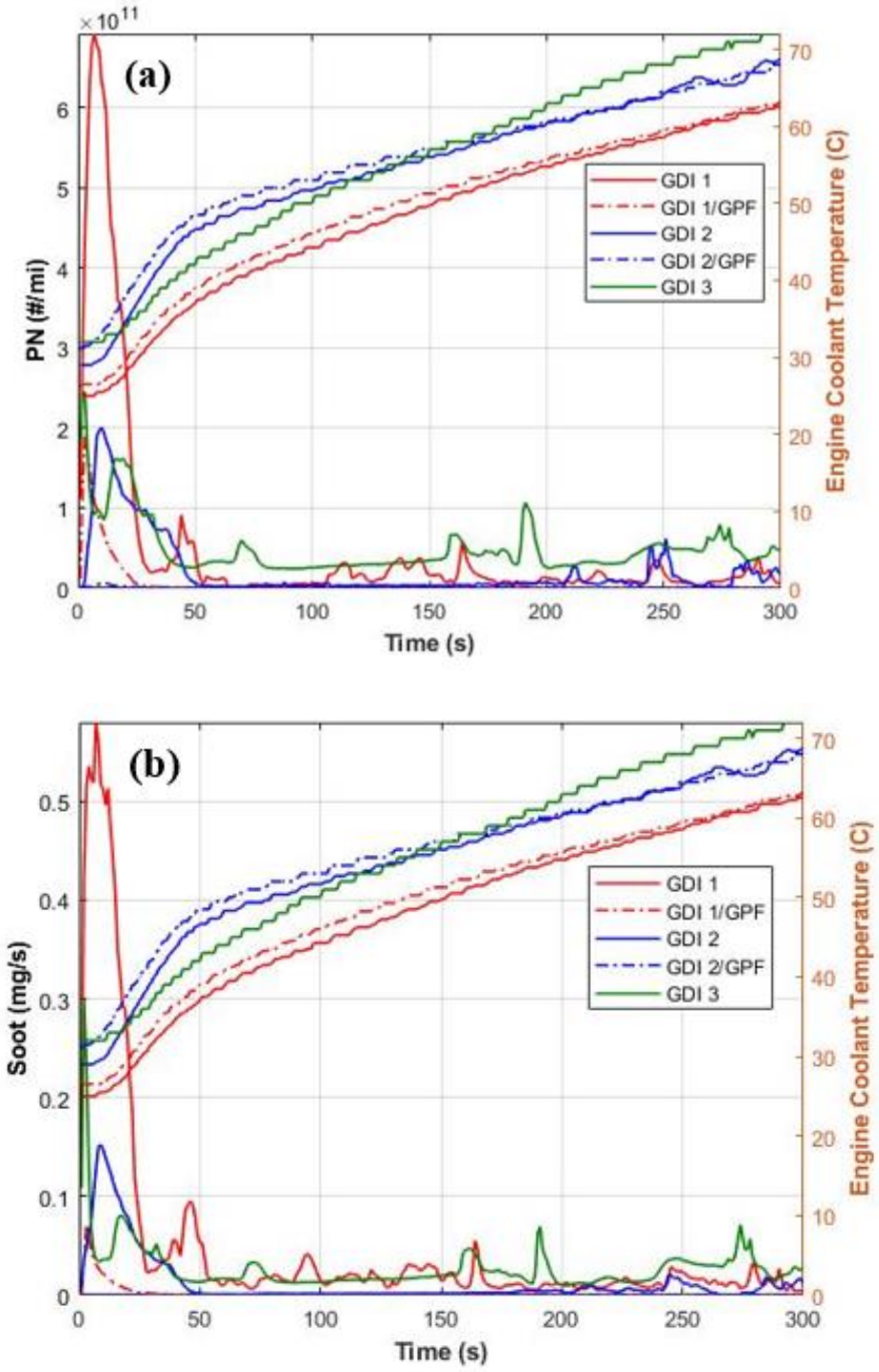

Figure 4-8 (a-b): Real-time traces of particle number (a) and soot mass (b) emissions with coolant temperature for all vehicles during cold-start operation

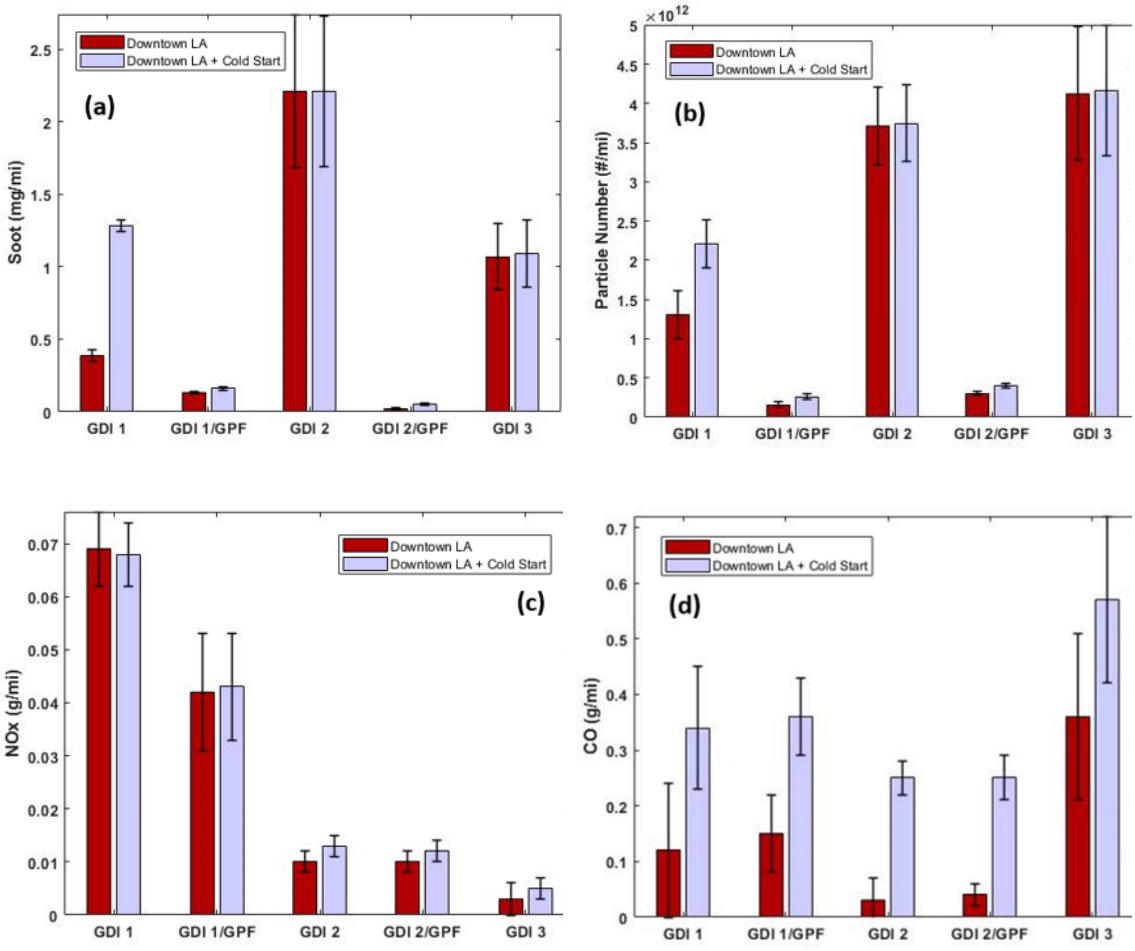

Figure 4-9 (a-d): Emissions of soot mass (a), particle number (b), NOx (c), and CO (d) over the Downtown LA route with and without the inclusion of the cold-start

4.4.4 Hot Spot Analysis

An emissions hotspot analysis was performed to find areas with high risk for vehicle pollutant exposure on each route and to find the causes of increasing pollutant formation. For this analysis, all pollutants, GPS data, and ECM data was averaged together over the triplicated routes to create an average run for each vehicle/cycle combination. A MATLAB code was created to access the averaged data and create a scatter plot with latitude and

longitude as the x-y coordinates, while the pollutant or ECM data was plotted as the z coordinate. The figures were then overlaid on topological map and matched to the route sequence that was driven.

Figure 4-10 (a-d) shows the hotspot analysis of soot mass, acceleration, NOx, and CO_2 for GDI1 over the Downtown LA cycle. CO_2 and soot mass hotspots correlate very well with the acceleration hotspots. This is likely due to increased fuel spray in the combustion chamber leading to more fuel rich zones during combustion. The heavy-traffic nature and abundance of streetlights in downtown LA created a lot of stop and go driving patterns as evidenced by the acceleration plot. This in turn lead elevated soot and CO_2 emissions during the cycle, especially in congested areas where many people are exposed. NOx emissions also correlated well with acceleration, however the large NOx emission events occurred during high-speed freeway driving and accelerating to high speeds during the freeway on-ramp.

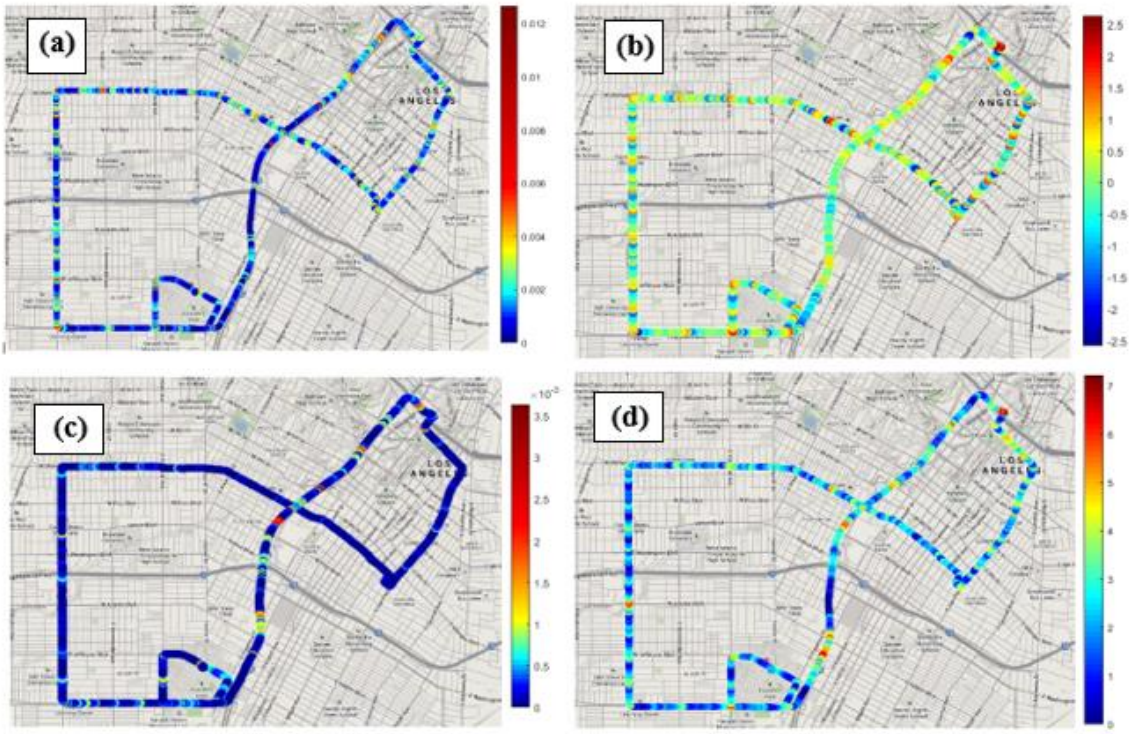

Figure 4-10 (a-d): Real world soot mass (a), acceleration (b), NOx (c), and CO_2 (d) hotspots for GDI1 over the Downtown LA cycle

4.5 Conclusions

A reduction in real-world emissions from GDI vehicles is essential for air quality and health in populated areas and megacities. This study investigated on-road gaseous and particle emissions from three current technology GDI vehicles using PEMS. Two vehicles were also retrofitted with catalyzed GPFs to evaluate whether this technology is able to reduce on-road ultrafine particles and black carbon emissions and ultimately improve air quality. Testing was conducted on four test routes in the greater LA Basin and San Diego representing urban, rural, highway, and high-altitude driving patterns. Results revealed significant reductions in soot mass and solid particle number emissions with the catalyzed GPFs. Mountainous driving showed elevated PM emissions compared to driving without

elevation change. The highest PM emissions were seen for the urban routes where public exposure is highest. For all test routes, the highest soot mass and particle number emissions were recorded for the low and intermediate speed bin and high acceleration events. The spread in NOx emissions was lower with the catalyzed GPFs due to the additional catalytic volume compared to the original configuration, suggesting additional NOx reductions in real-driving conditions. Unlike NOx, CO emissions did not show any benefits with the GPFs. Emissions of CO_2 were found to be a function of engine size and were greater for the urban routes, as well as for the uphill segment. The use of GPFs did not show a statistically significant penalty in CO_2 emissions and fuel economy during real-world operation.

4.6 References

Alkidas AC. Combustion advancements in gasoline engines. Energy Conversion and Management 2007;48:2751-2761.

Andersson J, May J, Favre C, Bosteels D, de Vries S, Heaney M, Keenan M, Mansell J. On-road and chassis dynamometer evaluations of emissions from two Euro 6 diesel vehicles. SAE Technical Paper 2014, 2014-01-2826.

Araji F, Stokes J. Evaluation of emissions from light duty trucks with and without the use of a gasoline particulate filter. SAE Technical Paper 2019, 2019-01-0971.

Bates JT, Weber RJ, Abrams J, Verma V, Fang T, Klein M, Tolbert PE. Reactive oxygen species generation linked to sources of atmospheric particulate matter and cardiorespiratory effects. Environ. Sci. Technol. 2015;49:13605-13612.

Bishop JDK, Molden N, Boies AM. Using portable emissions measurement systems (PEMS) to derive more accurate estimates of fuel use and nitrogen oxides emissions from modern Euro 6 passenger cars under real-world driving conditions. Applied Energy 2019;242:942-973.

Cao T, Durbin TD, Russell RL, Cocker III DR, Scora G, Maldonado H, Johnson KC. Evaluations of in-use emission factors from off-road construction equipment. Atmospheric Environment 2016; 147:234-245.

Cao T, Russell RL, Durbin TD, Cocker III, DR, Burnette A, Calavita J, Maldonado H, Johnson KC. Characterization of the emissions impacts of hybrid excavators with a portable emissions measurement system (PEMS)-based methodology. Science of the Total Environment 2018; 635:112-119.

Chan TW, Meloche E, Kubsh J, Brezny R. Black carbon emissions in gasoline exhaust and a reduction alternative with a gasoline particulate filter. Environ. Sci. Technol. 2014;48:6027-6034.

Chen L, Liang Z, Zhang X, Shuai S. Characterizing particulate matter emissions from GDI and PFI vehicles under transient and cold start conditions. Fuel 2017;189:131-140.

Demuynck J, Favre C, Bosteels D, Hamje H, Andersson J. Real-world emissions measurements of a gasoli e direct injection vehicle without and with a gasoline particulate filter. SAE Technical Paper 2017, 2017-01-0985.

Fontaras G, Zacharof NG, Ciuffo B. Fuel consumption and CO_2 emissions from passenger cars in Europe – Laboratory versus real-world emissions. Progress in Energy and Combustion Science 2017;60:97-131.

Gallus J, Kirchner U, Vogt R, Benter T. Impact of driving style and road grade on gaseous exhaust emissions of passenger vehicles measured by a Portable Emission Measurement System (PEMS). Transportation Research Part D 2017;52:215-226.

Gallus J, Kirchner U, Vogt R, Borensen C, Benter T. On-road particle number measurements using a portable emission measurement system (PEMS). Atmospheric Environment 2016;124:37-45.

Giechaskiel B, Lähde T, Suarez-Bertoa R, Clairotte M, Grigoratos T, Zardini A, Perujo A, Martini G. Particle number measurements in the European legislation and future JRC activities Combust. Engine. 2018;174:3-16.

Guillaume P. Chossière, Robert Malina, Florian Allroggen, Sebastian D. Eastham, Raymond L. Speth, Steven R.H. Barrett. Country- and manufacturer-level attribution of air quality impacts due to excess NOx emissions from diesel passenger vehicles in Europe. *Atmospheric Environment*, 2018; 189: 89.

Huang C, Lou D, Hu Z, Feng Q, Chen Y, Chen C, Tan P, Yao D. a PEMS study of the emissions of gaseous pollutants and ultrafine particles from gasoline- and diesel-fueled vehicles. Atmospheric Environment 2013;77:703-710.

Kampa M, Castanas E. Human health effects of air pollution. Environmental Pollution 2008;15:362-367.

Karavalakis G, Short D, Vu D, Russell R, Hajbabaei M, Asa-Awuku A, Durbin TD. Evaluating the effects of aromatics content in gasoline on gaseous and particulate matter emissions from SI-PFI and SI-DI vehicles. Environ. Sci. Technol. 2015;49:7021-7031.

Karlsson RB, Heywood JB. Piston fuel film observations in an optical access GDI engine. SAE Technical Paper 2001; 2001-01-2022.

Khan T, Frey HC. Comparison of real-world and certification emission rates for light duty gasoline vehicles. Science of the Total Environment 2018;622-623:790-800.

Koczak J, Boehman A, Brusstar M. Particulate emissions in GDI vehicle transients: An examination of FTP, HWFET, and US06 measurements. SAE Technical Paper 2016; 2016-01-0992.

Kwon S, Park Y, Park J, Kim J, Choi KH, Cha JS. Characteristics of on-road NOx emissions from Euro 6 light-duty diesel vehicles using a portable emissions measurement system. Science of the Total Environment 2017;576:70-77.

May J, Bosteels D, Favre C. An assessment of emissions from light-duty vehicles using PEMS and chassis dynamometer testing. SAE Technical Paper 2014, 2014-01-1581.

Mendoza-Villafuerte P, Suarez-Bertoa R, Giechaskiel B, Riccobono F, Bulgheroni C, Astorga C, Perujo A. NOx, NH3, N2O, and PN real driving emissions from a Euro VI heavy-duty vehicle. Impact of regulatory on-road test conditions on emissions. Science of the Total Environment 2017;609:546-555.D, Cocker DR, Miller WJ, Bishnu DK, Maldonado H, Moynahan N, Ensfield C, Laroo CA. On-road comparison of a portable emission measurement system with a mobile laboratory for a heavy-duty diesel vehicle. Atmospheric Environment 2009;43:2877-2883.

Merkisz J, Bielaczyc P, Pielecha J, Woodburn J. RDE testing of passenger cars: The effect of the cold start on the emissions results. SAE Technical Paper 2019; 2019-01-0747.

O'Driscoll R, Stettler MEJ, Molden N, Oxley T, ApSimon HM. Real world CO_2 and NOx emissions from 149 Euro 5 and 6 diesel, gasoline, and hybrid passenger cars. Science of the Total Environment 2018;621:282-290.

Ogata T, Makino M, Aoki T, Shimoda T, Kato K, Nakatani T, Nagata K, Vogt CD, Ito Y, Their D. Particle number emission reduction for GDI engines with gasoline particulate filters. SAE Technical Paper 2017, 2017-01-2378.

Piock W, Hoffmann G, Berndorfer A, Salemi P, Fusshoeller B. Strategies towards meeting future particulate matter emission requirements in homogeneous gasoline direct injection engines. SAE Int. J. Engines 2011;4:1455-1468.

Prati M, Meccariello G, Della Ragione L, Costagliola M. Real driving emissions of a light-duty vehicle in Naples. Influence of road grade. SAE Technical Paper 2015; 2015-01-2509.

Quiros DC, Thiruvengadam A, Pradhan S, Besch M, Thiruvengadam P, Demirgok B, Carder D, Oshinuga A, Huai T, Hu S. Real-world emissions from modern heavy-duty diesel, natural gas, and hybrid diesel trucks operating along major California freight corridors. Emission Control Science and Technology 2016;2:156-172.

Roth P, Yang J, Fofie E, Cocker III, DR, Durbin TD, Brezny R, Geller M, Asa-Awuku A, Karavalakis G. Catalyzed gasoline particulate filters reduce secondary organic aerosol production from gasoline direct injection vehicles. Environ. Sci. Technol. 2019;53:3037-3047.

Saliba G, Saleh R, Zhao Y, Presto AA, Lamber AT, Frodin B, Sardar S, Maldonado H, Maddox C, May AA, Drozd GT, Goldstein AH, Russell LM, Hagen F, Robinson AL. Comparison of gasoline direct-injection (GDI) and port fuel injection (PFI) vehicle emissions: Emission Certification standards, cold-start, secondary organic aerosol formation potential, and potential climate impacts. Environ. Sci. Technol. 2017;51:6542-6552.

Schoenhaber J, Kuehn N, Bradler B, Richter JM, Bauer S, Lenzen B, Beidl C. Impact of European real-driving-emission legislation on exhaust gas aftertreatment systems of turbocharged direct injected gasoline vehicles. SAE Technical Paper 2017, 2017-01-0924.

Suarez-Bertoa R, Valverde V, Clairotte M, Pavlovic J, Giechaskiel B, Franco V, Kregar Z, Astorga C. On-road emissions of passenger cars beyond the boundary conditions of the real-driving emissions test. Environmental Research 2019;176:108572.

Valverde V, Mora BA, Clairotte M, Pavlovic J, Suarez-Bertoa R, Giechaskiel B, Astorga-LLorens C, Fontaras G. Emission factors derived from 13 Euro 6b light-duty vehicles based on laboratory and on-road measurements. Atmosphere 2019;10:243.

Wang H, Ge Y, Hao L, Xu X, Tan J, Li J, Wu L, Yang J, Yang D, Peng J, Yang J, Yang R. The real driving emission characteristics of light duty diesel vehicle at various altitudes. Atmospheric Environment 2018; 191:126-131.

Weiss M, Bonnel P, Hummel R, Provenza A, Manfredi U. On-road emissions of light-duty vehicles in Europe. Environ. Sci. Technol. 2011;45:8575-8581.

Wyatt DW, Li H, Tate J. Examining the influence of road grade on vehicle specific power (VSP) and carbon dioxide (CO_2) emission over a real-world driving cycle. SAE Technical Paper 2013; 2013-01-1518.

Xia W, Zheng Y, He X, Yang D, Shao H, Remias J, Roos J. Wang, Y. Catalyzed gasoline particulate filter (GPF) performance: effect of driving cycle, fuel, catalyst coating. SAE Technical Paper 2017; 2017-01-2366.

Yang J, Durbin TD, Jiang Y, Tange T, Karavalakis G, Cocker III DR, Johnson KC. A comparison of a mini-PEMS and a 1065 compliant PEMS for on-road gaseous and

particulate emissions from a light duty diesel truck. Science of the Total Environment 2018a;640-641:364-376.

Yang J, Roth P, Durbin TD, Johnson KC, Cocker III DR, Asa-Awuku A, Brezny R, Geller M, Karavalakis G. Gasoline particulate filters as an effective tool to reduce particulate and PAH emissions from GDI vehicles: A case study with two GDI vehicles. Environ. Sci. Technol. 2018b;52:3275-3284.

Yang J, Roth P, Ruehl CR, Shafer MM, Antkiewicz DS, Durbin TD, Cocker D, Asa-Awuku A, Karavalakis G. Physical, chemical, and toxicological characteristics of particulate emissions from current technology gasoline direct injection vehicles. Science of the Total Environment 2019;650:1182-1194.

Yoshioka F, Kato K, Aoki T, Makino M, Waters D, Jahnke H, Striebel F. Performance of next generation gasoline particulate filter materials under RDE conditions. SAE Technical Paper 2019, 2019-01-0980.

Zhang L, Hu X, Qiu R, Lin J. Comparison of real-world emissions of LDGVs of different vehicle emission standards on both mountainous and level roads in China. Transportation Research Part D 2019;69:24-39.

Zheng Z, Durbin TD, Xue J, Johnson KC, Li Y, Hu S, Huai T, Ayala A, Kittelson DB, Jung HS. Comparison of particle mass and solid particle number (SPN) emissions from a heavy-duty diesel vehicle under on-road driving conditions and a standard testing cycle. Environ. Sci. Technol. 2014;48:1779-1786.

Zinola S, Raux S, Leblanc M. Persistent particle number emissions sources at the tailpipe of combustion engines. SAE Technical Paper 2016; 2016-01-22

5. Real-World NOx Emissions from Heavy-Duty Diesel, Natural Gas, and Diesel Hybrid Electric Vehicles of Different Vocations on California Roadways

5.1 Abstract

This study assessed the real-world nitrogen oxide (NOx) emissions from 50 heavy-duty vehicles of different vocations and engine technologies using portable emissions measurement systems (PEMS). In-use emissions testing was performed on school and transit buses, refuse haulers, goods movement vehicles, and delivery vehicles while were driven over their normal operating routes in the South Coast Basin. Engine technologies included diesel engines with and without selective catalytic reduction (SCR) systems, compressed natural gas (CNG) engines and liquified petroleum gas (LPG) engines, and SCR-equipped diesel hybrid electric vehicles. For most vehicles, the in-use NOx emissions were higher than the certification standards for the engine. Diesel vehicles generally showed higher brake-specific NOx emissions compared to the CNG vehicles. NOx emissions were strongly dependent on the SCR temperature, with SCR temperatures below 200 °C resulting in elevate brake-specific NOx. The 0.02 g/bhp-hr certified CNG vehicles showed the largest reductions in NOx emissions. The diesel hybrid electric vehicles showed important distance-specific NOx benefits compared to the conventional diesel vehicles, but higher emissions compared to the CNG and LPG vehicles. Overall, average NOx reductions were 75%, 94%, 65%, 79%, respectively, for the 0.2 CNG, 0.02 CNG,

diesel hybrid electric, and LPG vehicles compared to diesel vehicles, indicating that the widespread implementation of advanced technology and alternative fuel vehicles could provide important NOx reductions and a path for meeting air quality targets in California and elsewhere.

5.2 Introduction

On-road heavy-duty diesel engines are major contributors to ambient nitrogen oxide (NOx) emissions (Anenberg et al., 2017; Stohl et al., 2015). Despite the strict Environmental Protection Agency (EPA) and California Air Resources Board (CARB) 2010 emission standards for heavy-duty engines that forced a 90% reduction of NOx emissions from the previous emission standards, in California on-road heavy-duty vehicles are still responsible for more than 30% of overall NOx emissions (CARB, 2020). NOx ($NO+NO_2$) emissions are important precursors for tropospheric ozone formation through photochemical reactions involving volatile organic compounds (Monks et al., 2015). Both pollutants are critical for meeting the requirements of the National Ambient Air Quality Standards (NAAQS), especially in the South Coast Air Basin (SCAB) and the San Joaquin Valley. Meeting the NAAQS requirements in 2023 and 2031 in SCAB, for example, will still require further reductions of 70% and 80%, respectively, in overall NOx emissions from current levels (CARB, 2020).

In a response to the stricter emission standards for heavy-duty vehicles, engine and aftertreatment manufacturers introduced selective catalytic reduction (SCR) technology for reducing tailpipe NOx for 2010 and newer vehicles. SCR technology uses an aqueous urea

solution, which hydrolyzes to ammonia (NH_3), leading to the conversion of NOx into nitrogen and water over a catalyst (Piumetti et al., 2015; Guan et al., 2014). NOx conversion is highly dependent on the catalyst temperature and therefore greatly sensitive to the operating conditions of the engine, as well as on catalyst material and urea dosing strategy. It has been demonstrated that at low load and low speed urban driving conditions tailpipe NOx emissions are usually increased due to the reduced conversion efficiency of the SCR catalyst (Jiang et al., 2018; Sowman et al., 2018; Zhang et al., 2014). Thiruvengadam et al. (2015) showed elevated NOx emissions at exhaust temperatures below 250 °C when they tested heavy-duty diesel trucks equipped with SCR over the local and near-dock drayage driving cycles in a chassis dynamometer. Misra et al. (2013) also found elevated NOx emissions during driving conditions where SCR temperature was below its light-off operating range and during cold-starts.

An additional effort to lower NOx emissions from on-road heavy-duty vehicles in the transportation sector is the widespread use of natural gas powered engines and in particular the development of ultra-low NOx natural gas engines, capable of achieving 0.02 g/bhp-hr of NOx emissions (Zhu et al., 2020; Li et al., 2019). Stoichiometric natural gas engines are equipped with three-way catalysts (TWC) that control NOx, carbon monoxide (CO), and total hydrocarbon (THC) emissions. Previous studies have demonstrated NOx emissions reductions with stoichiometric natural gas engines compared to SCR-equipped diesel engines (Yoon et al., 2013; Quiros et al., 2016; Thiruvengadam et al., 2015). A recent study has shown dramatic reductions in NOx emissions from two ultra-low NOx natural gas heavy-duty vehicles when operated on different test cycles, concluding that the use of these

engines in captive fleets and goods movement vehicles will contribute to the alleviation of ground-level smog formation (Zhu et al., 2020).

Controlling NOx emissions from heavy-duty vehicles remains a significant challenge, especially during real-world driving conditions. Heavy-duty engines are certified under controlled laboratory conditions over an engine dynamometer and using the Federal Test Procedure (FTP) cycle and the Supplemental Emissions Test (SET). Heavy-duty vehicles should also meet the in-use not-to-exceed (NTE) standard that controls NOx emissions under real-world, high-speed cruise operation (as specified in CFR Title 40 Parts 86 and 1065). Several studies have shown that NOx emissions measured from heavy-duty vehicles can significantly differ in real-world conditions compared to laboratory certification testing (Misra et al., 2017; Anenberg et al., 2017; Quiros et al., 2016; Dixit et al., 2017; Wu et al., 2012). Conditions such as urban driving, stop-and-go traffic, excessive idling, and low load/low speed operation can all affect SCR efficiency and tailpipe NOx (Yoon et al., 2017; Grigoratos et al., 2019; Mendoza-Villafuerte et al., 2017; Kotz et al., 2016).

For the current study, in-use NOx emissions were measured from 50 heavy-duty vehicles of different vocations, engine type, and aftertreatment controls using portable emissions measurement systems (PEMS). This study is part of a larger and more comprehensive testing campaign executed in SCAB that included about 200 in-use heavy-duty vehicles tested for emissions under in-use conditions and on a chassis dynamometer, and monitored for activity. The goal was to better characterize and understand in-use NOx emissions that will affect efforts to meet future ambient ozone goals in SCAB and elsewhere, to identify

technology benefits/shortfalls for a range in vehicles technologies in different vocations, and to provide information that can be used to guide future research and development initiatives, to develop future regulations and to improve emissions inventory estimates. The full study represents one of the largest studies of in-use emission rates of heavy-duty vehicles to date and is being used as a key basis for the development of the next generation CARB's Emission Factor (EMFAC) model. Results are discussed as a function of engine technology, vocation, aftertreatment control, and emissions certification level.

5.3 Experimental

5.3.1 Test vehicles

Table 5-1 describes the allocation of test vehicles by vocation and vehicle technology. All test vehicles were equipped with model year 2009 and later engines, except for one earlier model year 2000 engine, and were of different vocations, including transit buses, school buses, refuse haulers, delivery trucks, and goods movement trucks. Vehicle selection was based on three criteria that included (a) a representative mix of technologies to best estimate the entire population in SCAB, (b) testing advanced technology vehicles that will likely become a more significant fraction in the future, and (c) providing at least two vehicles for each category when possible. Six different manufacturers and 20 different engine models were included for in-use testing. The technology types that were tested included two diesel engines without SCR certified to a 2.3 g/bhp-hr NOx emissions limit, 14 diesel engines with SCR technology certified to a 0.20 g/bhp-hr NOx emissions limit, two diesel hybrid electric engines certified to a 0.20 g/bhp-hr NOx emissions limit, 19 compressed natural

gas (CNG) engines certified to a 0.20 g/bhp-hr NOx emissions limit, 10 CNG engines certified to a 0.02 g/bhp-hr ultra-low NOx emissions limit, two liquified petroleum gas (LPG) engines certified to a 0.20 g/bhp-hr NOx emissions limit, and one LPG engine certified to a 0.02 g/bhp-hr ultra-low NOx emissions limit.

Table 5-1: Allocation of test vehicles

Vocation	Transit	School Bus	Refuse	Delivery	Goods Movement
Number of PEMS Vehicles	6	7	7	10	20
CNG 0.20g	3	4	5	2	4
CNG 0.02g	3	0	2	0	6
Diesel 0.20g	0	1	0	4	9
Diesel (No SCR)	0	1	0	0	1
Diesel-Electric Hybrid	0	0	0	2	0
Propane (0.2g)	0	1	0	1	0
Propane (0.02g)	0	0	0	1	0

5.3.2 Emissions testing

A gaseous PEMS unit (Semtech DS, Sensors Inc., Saline, MI) was used throughout the test campaign for all 50 vehicles. While the emission of carbon monoxide (CO), total hydrocarbons (THC), carbon dioxide (CO_2), and NOx were measured, the focus of this study is the presentation of in-use NOx emissions. The Semtech DS unit is equipped with a non-dispersive infrared (NDIR) analyzer for CO and CO_2 measurements, a non-dispersive ultraviolet (NDUV) analyzer for NO and NO_2 measurements, and a hot flame ionization detector (HFID) for THC measurements. This unit is recognized by the US EPA as being capable of meeting accuracy requirements for in-use regulatory testing

requirements. A Sensors, Inc. exhaust flow meter (EFM) compatible with the PEMS unit was used to provide integrated mass emissions and second by second emissions data. The EFM system was equipped with an averaging pitot tube and thermocouples to obtain the exhaust mass flow. The EFM system was calibrated following procedures according to CFR40 Part 1065.307. Each vehicle was equipped with a CAN communication system for acquiring engine output data under working conditions from the ECU. A GPS and weather station were equipped with the PEMS unit to monitor driving conditions and weather conditions, which included velocity, altitude, location, ambient temperature, atmospheric pressure, and humidity.

Testing on each vehicle was conducted over a typical day during in-use operation for the fleet that the vehicle was recruited from. The test routes corresponded to the normal routine of each vehicle's vocation in SCAB and varied in length from 15 to 141 miles. Depending on the vocation, daily trips while measuring in-use emission were 1.5-14 h long. Before testing each vehicle and at the end of each testing day, the PEMS unit was zeroed and spanned to check for drift.

5.4 Results and Discussion

5.4.1 NOx emissions rates

Figure 5-1 (a-c) show NOx emissions on a g/bhp-hr and a g/mile basis, as well as exhaust and/or SCR temperature for each vehicle vocation and engine technology in box and whisker plots showing the average emissions, the 25^{th} and 75^{th} quartile values, and the maximum and minimum values. Note that SCR temperature was available for the diesel

vehicles, but three-way catalyst temperatures were not available for the CNG vehicles, hence, these were plotted based on exhaust temperature measured by the PEMS. Table 5-2 lists the brake-specific, distance-specific, grams per gallon of fuel used, and total daily NOx emissions for each individual vehicle. For the school bus, goods movement, and delivery vehicle categories, the diesel vehicles generally showed higher emissions that those of the other applications. The diesel vehicles without SCR typically showed higher NOx emissions than those for the 0.2 SCR-equipped diesel vehicles, although some of the goods movement and delivery 0.2 diesel vehicles showed relatively high emission rates as well, as denoted by the relatively large emission ranges in Figure 5-1 and in Table 5-2. Both the 0.2 diesel goods movement and delivery vehicles were considerably higher than the 0.2 g/bhp-hr certification standard. The 0.2 diesel school bus was an exception in that its NOx emissions were 3 to 5 times lower than those for the CNG and LPG school buses. NOx emissions for the CNG vehicles averaged below 0.4 g/bhp-hr for all technology categories, with the 0.02 CNG vehicles averaging 0.05 to 0.06 g/bhp-hr. The average 0.2 CNG emissions comparable across the different vocations, ranging from 0.14 to 0.37 g/bhp-hr, with the school buses and goods movement vehicles showing slightly higher NOx emissions and the delivery vehicles showing slightly low NOx emissions compared to the other vocations. It is important to note the significant benefits in brake-specific and grams per mile NOx emissions and NOx emissions on a grams per day basis for the CNG vehicles compared to diesel vehicles. For the goods movement vehicles, the reductions in brake-specific NOx emissions were 63% and 94% on average for the 0.2 g/bhp-hr and 0.02 g/bhp-gr certified CNG engines, respectively. Similar findings were seen for the delivery trucks.

The LPG school bus showed slightly higher emissions than the CNG school buses, while the newer model LPG delivery vehicles showed lower emissions than the corresponding CNG delivery vehicles, with a 0.02 g certified LPG vehicle having emissions comparable to its certification levels.

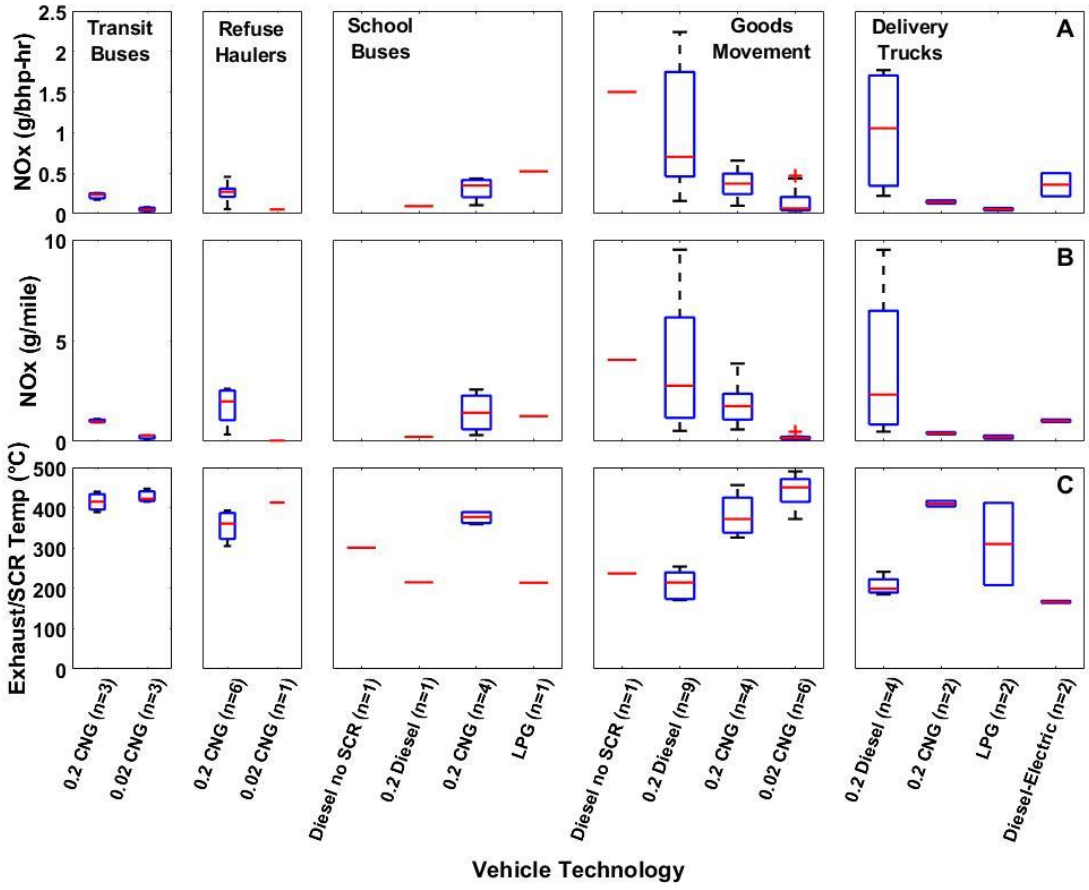

Figure 5-1 (a-b): Box and whisker plots of average brake-specific NOx emissions (top panel-A), average grams per mile NOx emissions (middle panel-B), and exhaust/SCR temperatures for each vocation and technology (bottom panel-C)

Table 5-2: Brake-specific, distance-specific, and total NOx emissions for each individual test vehicle

Vehicle ID	Vocation	Technology	NOx (g/bhp-hr)	NOx (g/mile)	NOx (g/day)	NOx (g/gallon)
18018	School Bus	Diesel (No SCR)	5.39	17.16	635.0	86.00
18089	School Bus	0.2 Diesel	0.09	0.22	8.9	1.23
18002	School Bus	0.2 NG	0.43	2.57	52.8	8.54
18004	School Bus	0.2 NG	0.11	0.31	13.9	2.05
18005	School Bus	0.2 NG	0.39	1.96	63.4	5.73
18090	School Bus	0.2 NG	0.30	0.88	55.5	4.91
18020	School Bus	LPG	0.52	1.25	18.8	4.77
18080	Transit Bus	0.2 NG	0.17	0.94	68.8	1.54
18017	Transit Bus	0.2 NG	0.26	1.11	60.0	3.71
18112	Transit Bus	0.2 NG	0.24	0.98	45.6	3.72
18113	Transit Bus	0.02 NG	0.03	0.09	4.3	0.37
18114	Transit Bus	0.02 NG	0.08	0.30	14.3	0.98
18081	Transit Bus	0.02 NG	0.05	0.29	18.6	0.58
18024	Refuse	0.2 NG	0.29	2.32	160.2	3.58
18016	Refuse	0.2 NG	0.46	2.52	215.8	6.25
18013	Refuse	0.2 NG	0.31	2.61	132.2	3.79
18014	Refuse	0.2 NG	0.26	1.64	80.5	3.31
18023	Refuse	0.2 NG	0.06	0.34	36.7	0.74
18015	Refuse	0.2 NG	0.21	1.05	138.8	2.53
18025	Refuse	0.02 NG	0.05	0.39	19.4	0.36
18071	Goods Movement	Diesel (No SCR)	1.50	4.04	621.9	18.07
18034	Goods Movement	0.2 Diesel	0.16	0.52	41.4	4.17
18035	Goods Movement	0.2 Diesel	0.25	0.88	158.4	4.88
18036	Goods Movement	0.2 Diesel	0.86	2.76	518.3	8.88
18072	Goods Movement	0.2 Diesel	0.53	1.26	242.8	6.62
18074	Goods Movement	0.2 Diesel	0.59	1.41	380.0	7.76
18078	Goods Movement	0.2 Diesel	2.51	8.24	914.0	37.59
18079	Goods Movement	0.2 Diesel	2.09	5.45	711.6	31.31
18048	Goods Movement	0.2 Diesel	2.24	9.51	1551.2	25.25
18049	Goods Movement	0.2 Diesel	0.70	3.14	820.8	10.65
18104	Goods Movement	0.2 NG	0.29	1.24	75.7	3.07
18094	Goods Movement	0.2 NG	0.44	1.75	256.9	5.24
18103	Goods Movement	0.2 NG	0.65	3.86	185.6	7.46
18045	Goods Movement	0.2 NG	0.10	0.59	33.8	1.39
18043	Goods Movement	0.02 NG	0.04	0.17	12.3	0.68
18044	Goods Movement	0.02 NG	0.13	0.46	21.9	1.64
18082	Goods Movement	0.02 NG	0.03	0.09	25.9	0.43
18083	Goods Movement	0.02 NG	0.04	0.09	13.8	0.44
18084	Goods Movement	0.02 NG	0.07	0.16	16.6	0.75
18095	Goods Movement	0.02 NG	0.05	0.24	22.5	0.51
18051	Delivery Vehicle	0.2 Diesel	1.77	9.50	71.2	14.57
18093	Delivery Vehicle	0.2 Diesel	1.64	3.45	140.0	15.28
18110	Delivery Vehicle	0.2 Diesel	0.22	0.48	25.6	3.47
18070	Delivery Vehicle	0.2 Diesel	0.47	1.19	107.6	8.37
18105	Delivery Vehicle	0.2 NG	0.12	0.35	66.2	1.29
18062	Delivery Vehicle	0.2 NG	0.16	0.46	207.8	2.29
18056	Delivery Vehicle	Hybrid	0.50	1.08	81.1	5.50
19001	Delivery Vehicle	Hybrid	0.22	0.96	41.0	3.25
19002	Delivery Vehicle	0.02 LPG	0.04	0.13	8.8	0.78
18097	Delivery Vehicle	LPG	0.07	0.29	22.8	1.77

On average, brake-specific NOx emissions exhibited large reductions between different certification standards for the same technology type (Figure 5-2). For the transit buses, average NOx emissions were 0.22 g/bhp-hr for the 0.2 g/bhp-hr NOx emissions certified CNG engines and 0.05 g/bhp-hr for the 0.02 g/bhp-hr ultra-low NOx emissions certified CNG engines, resulting in a 76% reduction in NOx emissions for the newer standards. For the CNG-powered refuse haulers, there was an 80% reduction in NOx emissions between the 0.2 g/bhp-hr certified engines and the 0.02 g/bhp-hr certified engines. It should be noted that while the CNG vehicles showed significant reductions relative to the diesel vehicles and between different certification levels, the CNG vehicle emission levels were also greater than to 0.2 and 0.02 g/bhp-hr certification limits as well.

For the refuse haulers, a more in-depth analysis of in-use NOx emissions for each of their unique operational segments can reveal interesting findings (Table 5-3). All refuse haulers utilized arterial driving to reach the neighborhood (arterial), followed by collection of the refuse (curbside pickup), and a mix of highway/arterial (highway) driving to the landfill facility to dispose of the collected refuse. The average speeds were 11.5 miles/hr, 3.7 miles/hr, and 33.3 miles/hr for the arterial, pickup, and highway segments, respectively. The average distance-specific NOx emissions for all 7 refuse haulers were 0.94 g/mile, 2.13 g/mile, and 0.59 g/mile for the arterial, pickup, and highway segments, respectively. Previous studies have also reported lower in-use NOx emissions under more steady-state, high speed conditions as a result of fewer transient accelerations and the shorter residence time of the fuel in the cylinder at high temperatures and the overall shorter combustion process, which inhibits the formation of thermal NOx (Misra et al., 2017; Grigoratos et al.,

2019; Grigoratos et al., 2016). The much higher NOx emissions during the curbside pickup operation, including the arm lift and compaction process, were likely attributed to the low speed stop-and-go accelerating conditions. Similar findings have been also reported elsewhere (Karavalakis et al., 2013; Grigoratos et al., 2016).

For the diesel-powered goods movement vehicles, the decrease in NOx emissions between no SCR and SCR-equipped engines was small (33%) and was attributed to the significantly higher in-use NOx emissions for three of the SCR-equipped vehicles, which showed 2-4 times higher NOx emissions than the other SCR-equipped vehicles. For the CNG-powered goods movement vehicles, there was a clearer reduction of 83.4% between the 0.2 g/bhp-hr certified engines (average NOx of 0.37 g/bhp-hr) and the 0.02 g/bhp-hr certified engines (average NOx of 0.061 g/bhp-hr). For the delivery trucks category, there was a more diverse population of engine platforms, including diesel engines, CNG engines certified to 0.2 g/bhp-gr NOx emissions standard, diesel hybrid electrics, and LPG engines certified to both 0.2 g/bhp-hr and 0.02 g/bhp-hr NOx emissions standards. All engine platforms for the delivery trucks showed higher in-use NOx emissions compared to their equivalent certification standards. Average brake-specific NOx emissions for the diesel delivery vehicles (1.02 g/bhp-hr) were similar to those of the diesel goods movement vehicles (1.00 g/bhp-hr), but the mass of NOx emissions per day were about 6 times lower on average when compared goods movement vehicles (522 g/day for goods movement vs. 86 g/day for delivery trucks). This was attributed to the shorter routes and the less time spent on the road for the delivery trucks compared to the goods movement trucks. NOx emissions for

the CNG and LPG delivery vehicles were 86% and 95% lower than those for the diesel delivery vehicles.

The diesel hybrid electric delivery vehicles showed lower emissions than the conventional diesel delivery trucks, but not as low as the LPG and CNG delivery vehicles. For the diesel hybrid electric delivery vehicles, the most appropriate comparisons are on a grams per mile basis, since the g/bhp-hr values do not consider the energy supplied by the battery. On that basis, the diesel hybrid electric vehicles displayed a 72% reduction compared to the conventional SCR-equipped diesel vehicles (3.65 g/mile vs. 1.020 g/mile), while the CNG (0.40 g/mile) and LPG (0.20 g/mile) delivery vehicles were 61% and 79% lower than those of the diesel hybrid electric vehicles. The results reported here show important benefits when using these advanced powertrains compared to traditional SCR-equipped diesel vehicles, but not in comparison to the 0.2 g/bhp-hr NOx emissions certified CNG engines and the LPG engines certified to either the 0.2 g/bhp-hr or the 0.02 g/bhp-hr standards. Although different vocations, it is worth mentioning that the greater average distance-specific NOx emissions benefits were achieved with the 0.02 g/bhp-hr ultra-low NOx certified CNG engines for the goods movement vehicles compared to the diesel hybrid electric vehicles (0.20 g/mile vs. 1.02 g/mile). While this study employed only two diesel hybrid electric vehicles, the results suggest that a widespread use of more 0.02 g/bhp-hr ultra-low NOx certified CNG engines will likely provide larger NOx emissions reductions from heavy-duty vehicles and help California meet the strict ambient ozone limits.

The emission rates from this study can be compared to the results from other studies and inputs being used in emissions inventory models. The results of this study do show that in-use emissions rates are often above the applicable emissions standards, which agrees with previous in-use studies on heavy-duty vehicles (Misra et al., 2017; Yoon et al., 2017; Quiros et al., 2016). In comparison with other studies of in-use emission rates, the heavy-duty in-use testing (HDIUT) program is probably the most significant data source for diesel vehicles, although the vehicles recruited for the HDIUT program do not necessarily represent a random sample, as vehicles can be rejected for testing for a number of reasons, such as poor maintenance (Badshah et al., 2019). Several studies of various iterations of this data set have shown full trip emissions to be on the order of 0.3 to 0.4 g/bhp-hr (Badshah et al., 2019; Spears et al., 2018). Spears, (2018) analyzed data from the HDIUT program and found average in-use NOx emission rates of 0.37 g/bhp-hr for diesel vehicles with engines certified to the 0.2 g/bhp-hr standard, and higher average NOx emissions of 0.70 g/bhp-hr for 2010 and newer diesel vehicles certified to higher levels with emissions credits. These values are generally lower than the emission rates found in this study, although this study focuses more on local or urban vocational types. On a grams per mile basis, the diesel emission factors can be compared to values from the EMFAC2017 emission inventory model. The base emission factors (unadjusted for speed corrections) for 2010+ diesel vehicles in EMFAC are 1.70 g/mile for diesel buses, 1.17 to 1.32 g/mile for diesel refuse haulers, 1.48 to 4.27 g/mile for medium-heavy duty diesel trucks, and 2.68 to 7.29 g/mile for heavy-heavy duty diesel trucks (CARB, 2018). In use emissions data for CNG vehicles is more limited, although studies by Misra et al. (2017) of two 0.2 g/bhp-hr

CNG refuse haulers and Quiros et al. (2016) of a Class 8 truck with a 0.2 g/bhp-hr certified CNG engine found emission rates that were comparable to the 0.2 g/bhp-hr certification limit. The base emission factors for 0.2 g/bhp-hr CNG vehicles in EMFAC2017 are 0.61 g/mile for buses, 0.88 g/mile for refuse haulers, 1.48 to 4.27 g/mile for medium-heavy duty trucks, and 2.68 to 7.29 g/mile for heavy-heavy duty trucks (CARB, 2018).

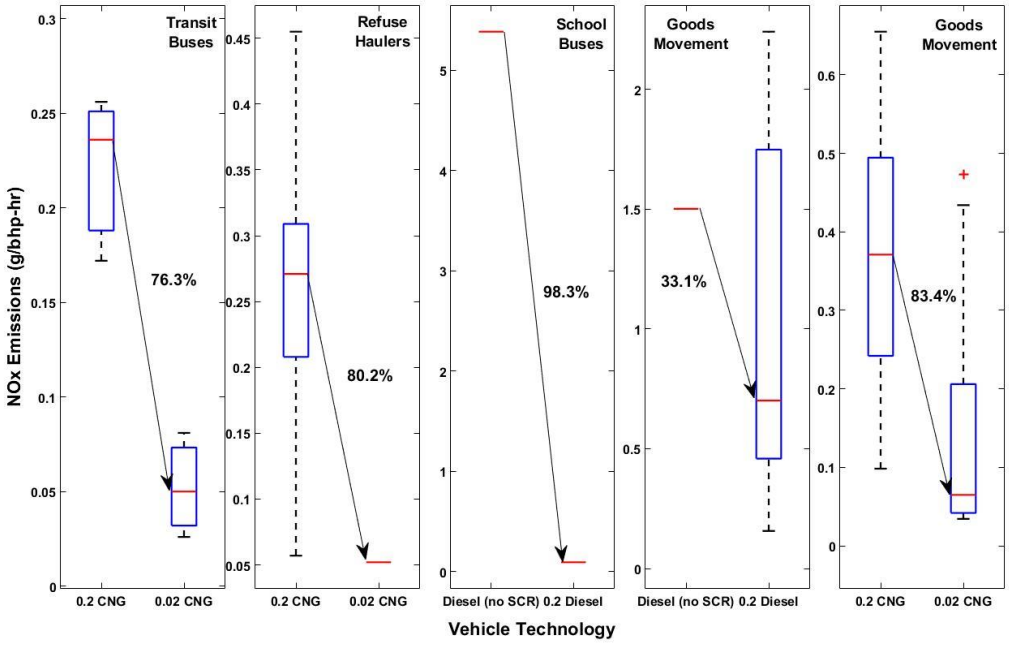

Figure 5-2: Percentage reductions between engines with different emissions certification standards

Table 5-3: **Average NOx emissions in g/mile for each segment of refuse hauler operation**

Engine Technology	Arterial	Highway	Pickup
0.2 CNG	1.74	-	1.56
0.2 CNG	0.62	0.60	2.47
0.2 CNG	0.56	0.51	0.90
0.2 CNG	1.75	1.06	3.38
0.2 CNG	0.35	0.22	0.17
0.2 CNG	1.44	1.02	6.08
0.02 CNG	0.15	0.14	0.35

5.4.2 Effects of duty cycles and aftertreatment temperature on NOx emissions rates

Figure 5-3 shows brake-specific NOx emissions as a function of the percentage of the route spent idling and the percentage of the route spent with exhaust temperatures below 200 ℃. The diesel vehicles exhibited higher percentages of time with their exhaust temperatures being below 200 ℃ when compared to CNG vehicles. This was a consequence of the lower exhaust gas temperatures for lean burn diesel engines compared to stoichiometric spark ignition engines. Compression ignition (diesel) engines run at higher compression ratios and leaner compared to spark ignition engines, resulting to a prolonged expansion stroke (thus more energy extracted) and lower temperatures inside the combustion cylinder by the end of the expansion stroke, as well as to a greater dilution of the exhaust gases with air leading to lower exhaust temperatures. As discussed above, diesel vehicles showed higher in-use NOx emissions compared to CNG vehicles, which is consistent with previous studies (Quiros et al., 2016; Thiruvengadam et al., 2015; Lee et al., 2011). Exceptions were

observed between some of the SCR-equipped diesel goods movement vehicles and the 0.2 g/bhp-hr NOx certified CNG goods movement vehicles, with the later exhibiting higher brake-specific NOx emissions. This was primarily due to the longer duration of the route for these vehicles and the much larger portion of time dedicated at urban driving conditions. It can also be seen that the percentage of time for the emissions aftertreatment system being below 200 ℃ for the CNG-powered vehicles was dramatically lower than those of the diesel vehicles, suggesting that temperature had a rather limited impact on NOx emissions for the stoichiometric engines as opposed to the operating air-fuel ratio of the engine.

For the diesel vehicles, there was an association between elevated brake-specific NOx emissions and higher percentages of time at lower exhaust aftertreatment temperatures, although this finding was not necessarily consistent across all diesel vehicles. For a number of diesel-powered goods movement and delivery trucks, brake-specific NOx emissions were elevated as a result of the low exhaust gas temperatures, which led to SCR system temperatures being below their optimal temperature range of about 250 ℃ and lower NOx conversion efficiencies. However, while the highest emitting goods movement vehicles and delivery vehicles showed similar emissions rates, these goods movement vehicles spent about 3 times more time operating at idle and had a considerably higher fraction of time with the exhaust temperature below 200 ℃ compared to the highest emitting delivery trucks. In general, it is not always straightforward to predict in-use NOx emissions for vehicles of different vocations. This study showed that most of these vehicles had unique characteristics, such as route duration, number of delivery stops with the engine either turned off or idling, and different percentages of time spent during low speed/load urban

or freeway driving conditions. These characteristics, and especially the number of stop-and-go/idling conditions, significantly affected the operational SCR temperatures and in-use NOx emissions. For many vehicles tested, it was found that the engine was turned off at different parts of the route instead of idling, which led to NOx reductions over the entire route. Previous studies have also demonstrated that NOx emissions are strongly correlated with SCR temperature (Bishop et al., 2013; Misra et al., 2013; Boriboonsomsin et al., 2018; Jiang et al., 2018; Zhang et al., 2014). For example, Tan et al. (2018) showed that NOx conversion rates of SCR systems can decrease below 80% when SCR inlet temperature is lower than 200 ℃.

Real-time NOx emissions plots, as shown in Figure 5-4a and 5-4b, show that both the high and low emitting goods movement vehicles show spikes in NOx emissions during the initial accelerations at the beginning of different trips where the SCR temperature was below 200 ℃. For the low emitting vehicles, NOx emissions were generally low during high speed and relatively steady state driving conditions as a result of the optimum SCR temperature being above 250 ℃. However, NOx emissions for the high emitting vehicles were elevated almost throughout the entire route, even though SCR inlet temperature was above 200 ℃-250 ℃ for most of the route (Figure 5-5). There are several contributing factors to explain the elevated NOx emissions with the SCR temperatures being above 200 ℃-250 ℃, including the possible malfunction or deterioration of the SCR system or the urea dosage levels (not measured in this study). It appeared that periods during hard accelerations, stop-and-go hot-start conditions, and dynamic driving caused high NOx emissions, which contributed to the overall high brake-specific NOx emissions during the

entire route. Although exhaust gas temperatures were high enough for the SCR system to effectively reduce NOx emissions, our results showed high NOx emission spikes coinciding even with small accelerations. These findings are consistent with those of Misra et al. (2017), where they showed elevated in-use NOx emissions during accelerations and stop-and-go driving even when exhaust temperatures were sufficiently high for a fully functioning SCR system. A similar picture was seen for the high emitting delivery trucks, where they spent a higher share of time with the engine turned off, leading to excessive NOx emissions from the subsequent hot-start events due to the colder exhaust gas temperatures (Figure 5-6). The results reported here raise concerns about the effectiveness of SCR systems in controlling NOx emissions from diesel vehicles during real-world operation, which will ultimately adversely affect California's targets in reducing ambient ozone levels.

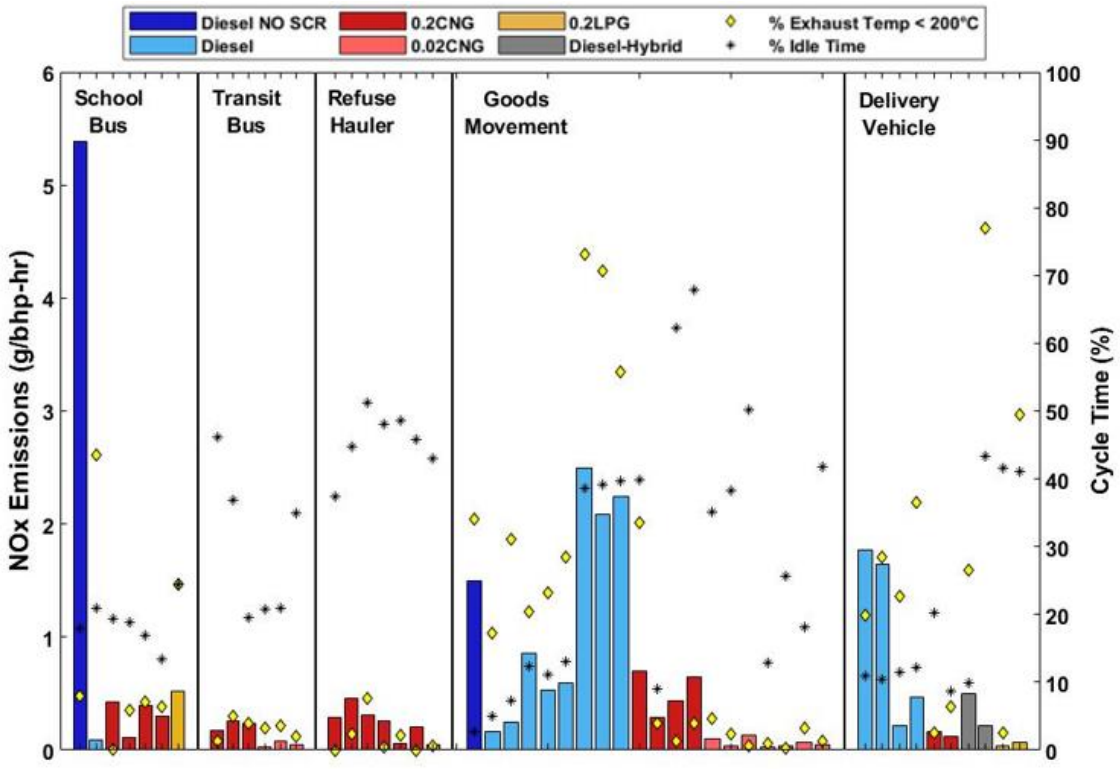

Figure 5-3: Brake-specific NOx emissions, time of idling operation, and time of exhaust temperature below 200 ℃

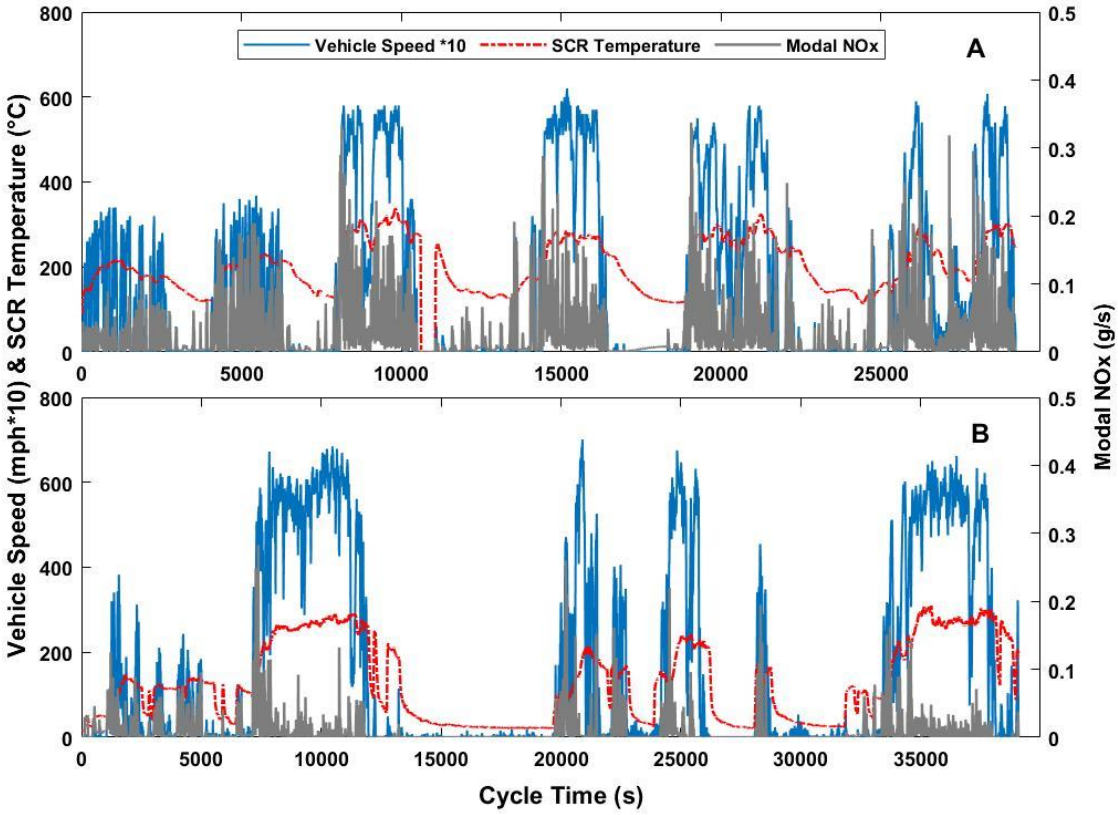

Figure 5-4 (a-b): Real-time accumulated NOx emissions as a function of vehicle speed and SCR temperature for a high emitting goods movement vehicle (top panel-A) and a low emitting goods movement vehicle (bottom panel-B)

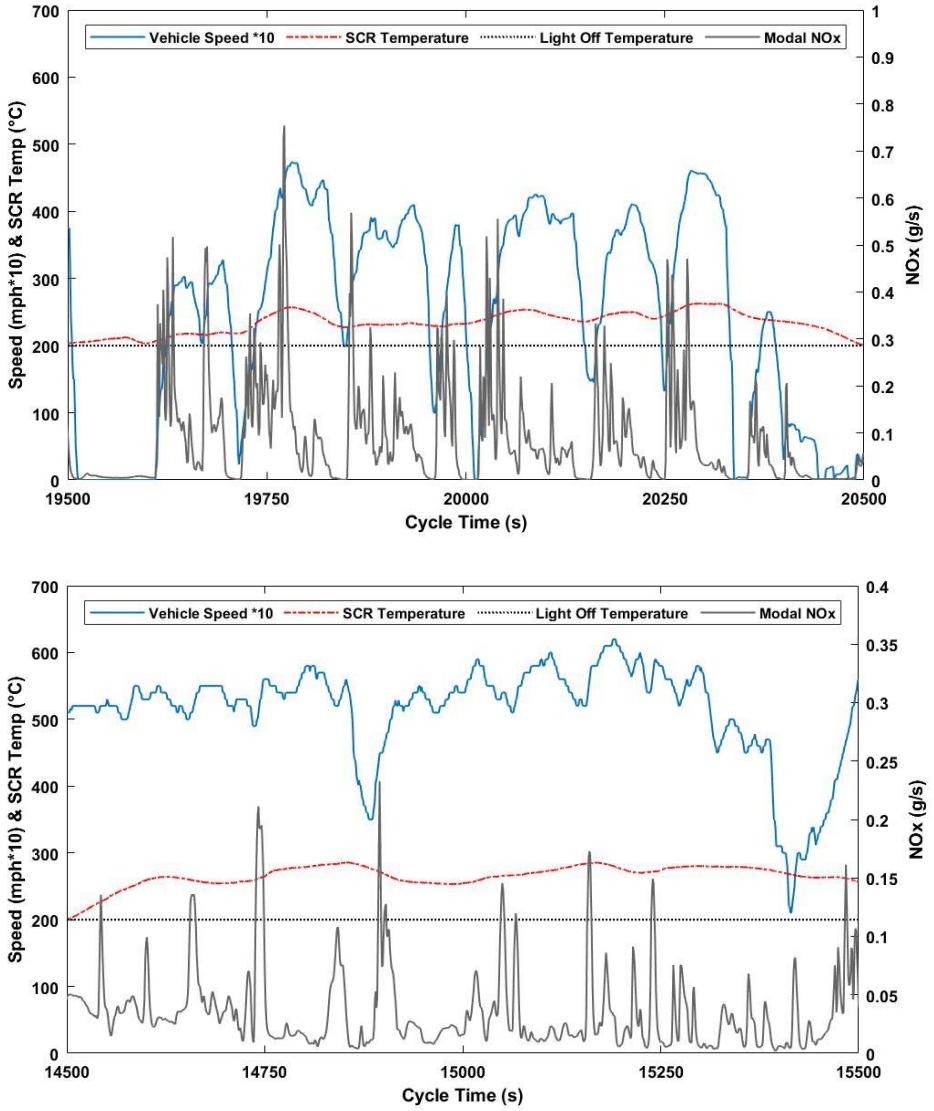

Figure 5-5: Snapshots of real-time modal NOx emissions as a function of vehicle speed and SCR temperature for two high emitting goods movement vehicles

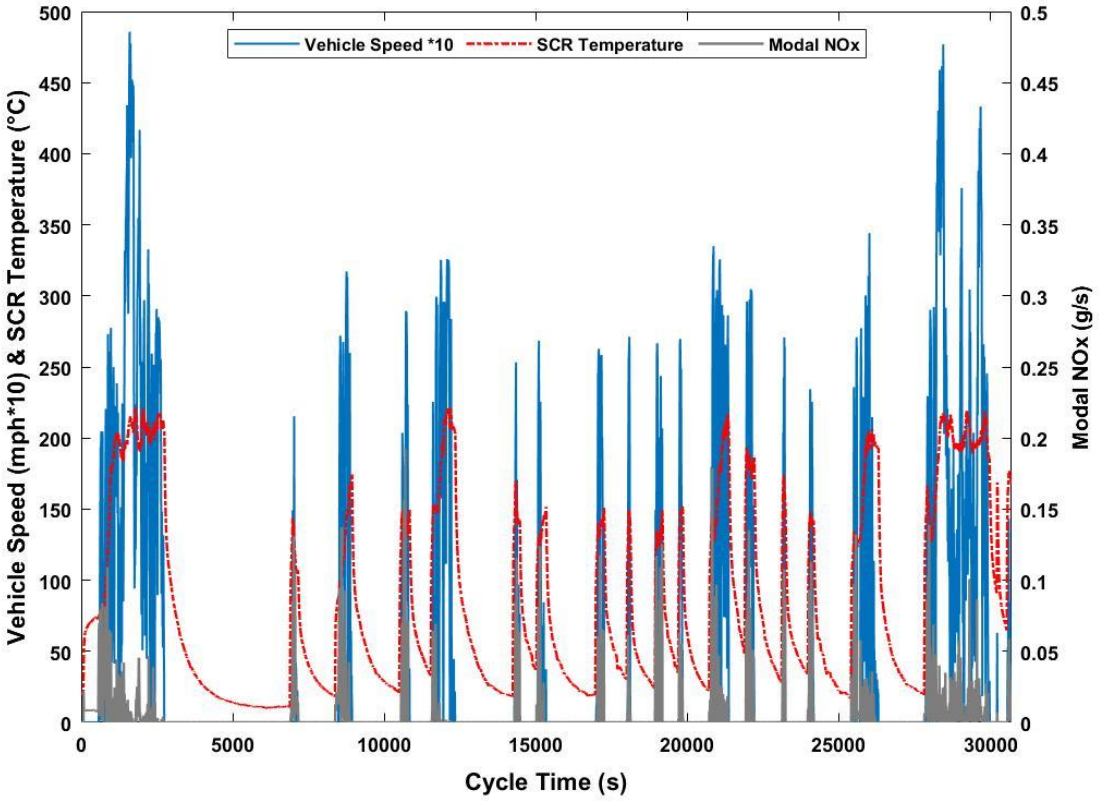

Figure 5-6: Real-time accumulated NOx emissions as a function of vehicle speed and SCR temperature for a high emitting delivery truck

5.4.3 Influence of speed and load on NOx emissions rates

Figure 5-7 (a-e) shows the NOx emissions for each vocation/engine technology as a function of engine load and vehicle speed bins. Engine loads below 25% were considered low loads, between 25%-45% were considered medium loads, and above 45% were considered high loads. Within each load bin, three speed bins were created for low speed (0.25 miles/h, urban), medium speed (25-45 miles/hr, rural), and high speed (>45 miles/hr, highway). School buses dedicated the majority of time during their operation in the lower speed and power bins. For the diesel-powered engine without SCR, a total of 40% of NOx

emissions were generated during high power and medium speed bins, even though only 17% of the route was spent inside these bins. For the SCR-equipped vehicles, 31% of the total NOx emissions were produced during idling conditions, where the SCR efficiency rapidly dropped. For the CNG transit buses, over 25% of total NOx emissions were produced within the high power bin at low speeds, while these vehicles only spent about 17% of the total time inside this bin. The large number of acceleration events and the stop-and-go conditions led to elevated NOx emissions for this bin. Idling operation was also prevalent and accounted for 20%-33% of the total NOx emissions for the CNG transit buses. Refuse haulers showed the largest percentage of their operation during idling conditions compared to all other vocations, representing nearly 50% of the total route. Although nearly half of the refuse haulers routes spent under idling, less than 35% of the total NOx emissions was produced at these conditions. Unlike the SCR-equipped diesel vehicles, the stoichiometric combustion engines maintained higher exhaust temperatures during idling, which kept the TWC above its light-off temperature where it could efficiently control NOx emissions. The hydraulic operation during curbside pick would also provide a greater load on the engine during these idle periods for the refuse haulers compared to other vocations. The lowest NOx emissions for the refuse haulers were seen for the high-speed bins during highway operation, with similar findings also reported in previous studies (Grigoratos et al., 2019; He et al., 2017; Fu et al., 2013).

For the goods movement vehicles, a large amount of their operation was spent either with the engine turned off or at idling conditions usually at warehouses (including storage and distribution centers). NOx emissions were substantially lower for those diesel vehicles

where the engine was shut off as opposed idled at or around the warehouse locations, as a significant portion of NOx emissions can be produced during idling. The delivery vehicles showed a similar picture to the goods movement vehicles, with most of their operation characterized by either prolonged idling conditions or with the engine turned off. Half of the diesel vehicles tested from both vocations showed NOx emission rates higher than 1 g/bhp-hr, because of excessive idling or the engine being turned off and having the SCR system drop below its optimal temperature range. Less of a NOx penalty was seen for the CNG, diesel hybrid electric, and LPG delivery vehicles, where NOx emissions were near the certification limit. The highest NOx emission rates for the delivery vehicles were observed for the high load conditions, with the diesel hybrid electric and CNG vehicles showing higher NOx in the medium and high-speed bins compared to diesel vehicles. It is also interesting to note that NOx emissions were generally higher as a fraction of operation time for all vocations and technologies in the high load bins. Although the SCR temperatures were sufficiently high during high load conditions due to increased urea dosing, the likely increased flow and space velocity of exhaust gases passing through the SCR at high load conditions may have resulted to less residence times for catalytic reaction and lower SCR efficiency (Fu et al., 2013; Koebel et al., 2000).

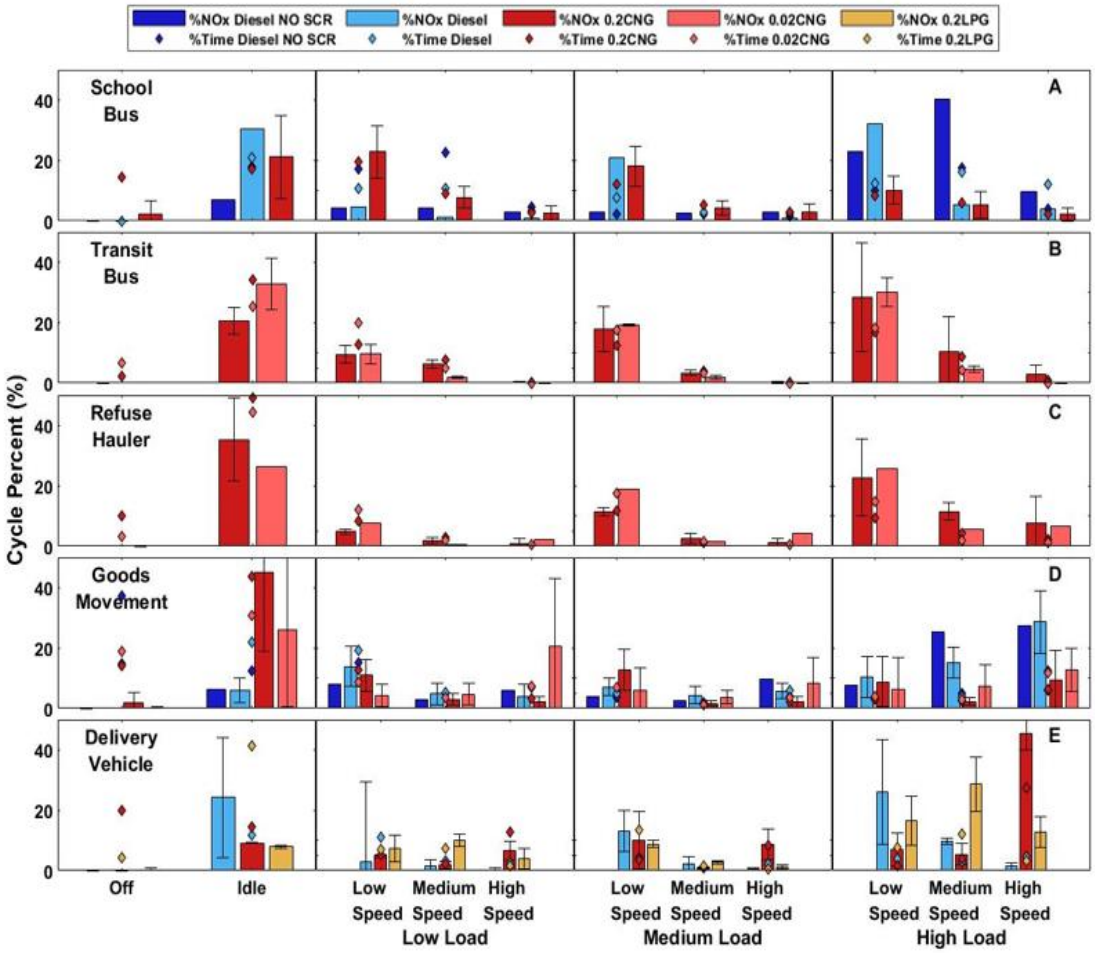

Figure 5-7 (a-e): Average percentage of NOx emissions and time spent at each speed and power bin for the school buses (A), transit buses (B), refuse haulers (C), goods movement (D), and delivery vehicles (E)

5.4.4 NTE analysis

The emissions data for the vehicles were also evaluated to determine emissions during NTE events and the percentage of activity in the NTE events. The requirements for an NTE event include operation in the NTE zone, with the engine load above 30% and SCR operational temperatures ≥250 °C, among other factors, for a period 30 continuous seconds,

as specified in CFR 86.1370-2007. Diesel vehicles with no SCR were not included in the NTE analysis. The operation of 14 out of the 48 vehicles tested did not meet the requirements for an NTE event over the course of the full day's operation. Seven of these vehicles with no NTE events were in the delivery vocation. Of the 34 vehicles tested with valid NTE events, 29 vehicles passed the NTE criteria, which specifies that no more than 10% of NTE event operation can be in excess of the NTE limit. NTE violations were mostly recorded for the diesel vehicles, with 3 out of 8 diesel vehicles and only 2 CNG vehicles out of 26 failing the NTE criteria. The percentage of activity in the NTE zone showed that only 4 vehicles spent more than 10% of their daily activity within valid NTE events. Two of these vehicles were in the delivery vocation and two were in the goods movement vocation. On average across all vehicles tested, only 5.4% of operation was within the NTE thresholds, which accounted for 8.4% of in-use NOx emissions. Our results are consistent with previous studies on heavy-duty diesel and CNG vehicles that have reported small amounts of their overall operation being within the NTE zone (Tan et al., 2019; Kotz et al., 2016; Badshah et al., 2019). For example, Badshah et al. (2019) showed that less than 10% of the total emissions data from in-use compliance testing represented valid NTE event data.

Figure 5-8 compares the average NOx emission rate for the full day of operation with that for the NTE events for all the test vehicles that had NTE events. As shown in Figure 5-8, the goods movement diesel vehicles showed the highest NOx emission rates during valid NTE events. All the other vehicles showed NOx emissions below the 0.2 g/bhp-hr certification limit during valid NTE events. The CNG vehicles certified for 0.02 g

NOx/bhp-hr showed larger reductions, even below the certification limit during valid NTE events. There was a large discrepancy between the total NOx emission rates and the NTE emission rates, with the NTE NOx emissions being much lower than the average emissions generated during the routes. These phenomena were more pronounced for the delivery diesel vehicles, which produced average NOx emission rates of 0.68 g/bhp-hr over the entire route, while showing only 0.01 g/bhp-hr during the NTE events. On average, NOx emissions during NTE events were 72% lower than the emissions generated throughout the entire route across all vocations.

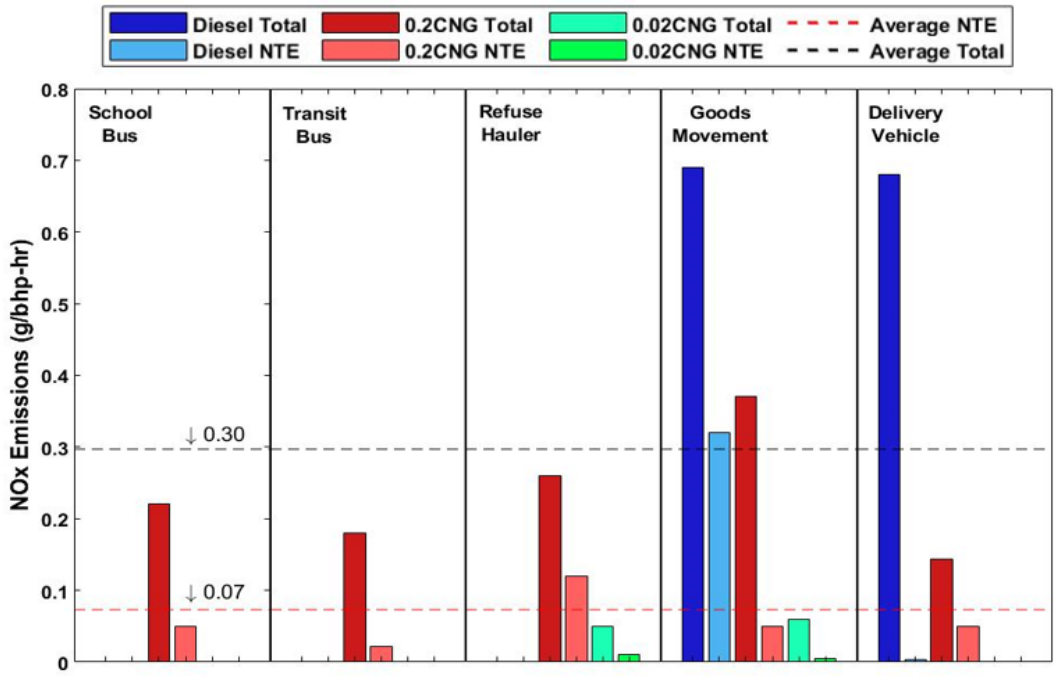

Figure 5-8: Total and valid NTE NOx emissions for all test vehicles with valid NTE events

5.5 Conclusions

In this study, an overview of NOx emissions from a large in-use heavy-duty vehicle emissions study was presented, which included 50 vehicles of different vocations and engine technologies. Emissions testing included school buses, transit buses, refuse haulers, goods movement, and delivery vehicles equipped with diesel engines with and without SCR, CNG and LPG engines, and diesel hybrid electric powertrains. This information will significantly add to the body of literature available on in-use emission rates of different heavy-duty vehicle types and is being used as a basis for the development of the next generation EMFAC model. Our results showed reductions in real-world NOx emissions as the emission standards tightened, but generally higher NOx emissions compared to the FTP certification standards for each engine category. On average, in-use NOx emissions exceeded the FTP certification standards by 80%, 21%, 66%, 44%, and 34%, respectively, for the 0.2 diesel, 0.2 CNG, 0.02 CNG, 0.2 diesel hybrid electric, and 0.14 LPG vehicles. Overall, the certification NOx emissions alone were not an accurate predictor for the real-world NOx emissions, independent of vehicle vocation or engine technology.

The results showed the potential benefits of different advanced technology vehicles, suggesting that a range of technologies could play an important role in meeting air quality targets in California and elsewhere. CNG-powered vehicles showed considerably lower average in-use NOx emissions, with reductions of 75% and 94%, respectively, for 0.2 and 0.02 certified CNG engines compared to their diesel counterparts. Newer LPG vehicles in the delivery vehicle category also showed solid NOx reductions compared to diesel

vehicles, with average brake-specific NOx reductions of about 79%. Diesel hybrid electric vehicles showed distance-specific NOx emissions benefits relative to the conventional SCR-equipped diesel vehicles (70% lower NOx emissions), but higher distance-specific NOx compared to CNG and LPG vehicles.

Our results showed a strong influence of SCR temperature on NOx emissions and a lesser impact of exhaust temperature on NOx emissions for the CNG-powered vehicles. It was demonstrated that for the highest emitting vehicles, NOx emissions remained elevated even during periods when the SCR temperature was above 250 ℃, however. These findings suggest that further improvements in engine management and aftertreatment control should be implemented if future NOx emission reduction targets are to be fully realized. Depending on vehicle operation, including the amount of idling, number of stops, low speed and low load driving conditions, additional efforts in the design of aftertreatment and engine control systems are needed to reduce in-use NOx emissions more effectively under these conditions.

5.6 References

Anenberg, S.C., Miller, J., Minjares, R., Du, L., Henze, D.K., Lacey, F., Malley, C.S., Emberson, L., Franco, V., Klimont, Z., Heyes, C. Impacts and mitigation of excess diesel-related NOx emissions in 11 major vehicle markets. Nature 2017, 545, 467-471.

Badshah, H., Posada, F., Muncrief, R. Current state of NOx emissions from in-use heavy-duty diesel vehicles in the United States. White Paper, November 2019, The International Council on Clean Transportation, https://theicct.org/sites/default/files/publications/NOx_Emissions_In_Use_HDV_US_20191125.pdf

Bishop, G.A., Schuchmann, B.G., Stedman, D.H. Heavy-duty truck emissions in the South Coast Air Basin of California. Environ. Sci. Technol. 2013, 47, 9523-9529.

Boriboonsomsin, K., Durbin, T., Scora, G., Johnson, K., Sandez, D., Vu, A., Jiang, Y., Burnette, A., Yoon, S., Collins, J., Dai, Z., Fulper, C., Kishan, S., Sabisch, M., Jackson, D. Real-world exhaust temperature profiles of on-road heavy-duty diesel vehicles equipped with selective catalytic reduction. Science of the Total Environment 2018, 634, 909-921.

California Air Resources Board, 2018. EMFAC2017 Volume III -Technical Documentation V1.0.2, March. https://www.arb.ca.gov/msei/downloads/emfac2017-volume-iii-technical-documentation.pdf (access 11/13/2018).

California Air Resources Board, 2020, Staff report: Initial Statement of Reasons, for Public Hearing to Consider the Proposed Heavy-Duty Engine and Vehicle Omnibus Regulation and Associated Amendments, June, https://ww3.arb.ca.gov/regact/2020/hdomnibuslownox/isor.pdf.

Dixit, P., Miller, J.W., Cocker III, D.R., Oshinuga, A., Jiang, Y., Durbin, T.D., Johnson, K.C. Differences between emissions measured in urban driving and certification testing of heavy-duty diesel engines. Atmospheric Environment 2017, 166, 276-285.

Fu, M., Ge, Y., Wang, X., Tan, J., Yu, L. and Liang, B. NOx emissions from Euro IV busses with SCR systems associated with urban, suburban and freeway driving patterns. Science of the Total Environment 2013, 452, 222-226.

Grigoratos, T., Fontaras, G., Martini, G., Peletto, C. A study of regulated and green house gas emissions from a prototype heavy-duty compressed natural gas engine under transient and real life conditions. Energy 2016, 103, 340-355.

Grigoratos, T., Fontaras, G., Giechaskiel, B., Zacharof, N. Real world emissions performance of heavy-duty Euro VI diesel vehicles. Atmospheric environment 2019, 201, 348-359.

Guan, B., Zhan, R., Lin, H., Huang, Z. Review of state of the art technologies of selective catalytic reduction of NOx from diesel engine exhaust. Applied Thermal Engineering 2014, 66, 395-414.

He, L., Hu, J., Zhang, S., Wu, Y., Guo, X., Guo, X., Song, J., Zu, L., Zheng, X. and Bao, X. Investigating Real-World Emissions of China's Heavy-Duty Diesel Trucks: Can SCR Effectively Mitigate NOx Emissions for Highway Trucks?. Aerosol Air Qual. Res. 2017, 17, 2585-2594.

Jiang, Y., Yang, J., Cocker III, D., Karavalakis, G., Johnson, K.C., Durbin, T.D. Characterizing emission rates of regulated pollutants from model year 2012+ heavy-duty diesel vehicles equipped with DPF and SCR systems. Science of the Total Environment 2018, 619-620, 765-771.

Karavalakis, G., Hajbabaei, M., Durbin, T.D., Johnson, K.C., Zheng, Z., Miller, W.J. The effect of natural gas composition on the regulated emissions, gaseous toxic pollutants, and ultrafine particle number emissions from a refuse hauler vehicle. Energy 2013, 50, 280-291.

Koebel, M., Elsener, M., Kleemann, M. Urea-SCR: a promising technique to reduce NOx emissions from automotive diesel engines. Catalysis Today 2000, 59, 335-345.

Kotz, A.J., Kittelson, D.B., Northrop, W.F. Lagrangian hotspots of in-use NOx emissions from transit buses. Environ. Sci. Technol. 2016, 50, 5750-5756.

Lee, D.-W., Zietsman, J., Farzaneh, M., Johnson, J. Characterization of On-Road Emissions of Compressed Natural Gas and Diesel Refuse Trucks. Transportation Research Record 2011, 2233, 80-89.

Li, C., Han, Y., Jiang, Y., Yang, J., Karavalakis, G., Durbin, T.D., Johnson, K. Emissions from advanced ultra-low NOx heavy-duty natural gas vehicles. SAE Technical Paper 2019, 2019-01-0751.

Mendoza-Villafuerte, P., Suarez-Bertoa, R., Giechaskiel, B., Roccobono, F., Bulgheroni, C., Astorga, C., Perujo, A. NOx, NH3, N2O and PN real driving emissions from a Euro VI heavy-duty vehicle. Impact of regulatory on-road test conditions on emissions. Science of the Total Environment 2017, 609, 546-555.

Misra, C., Collins, J.F., Herner, J.D., Sax, T., Krishnamurthy, M., Sobieralski, W., Burntizki, M., and Chernich, D. In-Use NOx Emissions from Model Year 2010 and Heavy-Duty Diesel Engines Equipped with Aftertreatment Devices. Environ. Sci. Technol. 2013, 47, 7892−7898.

Misra, C., Ruehl, C., Collins, J., Chernich, D., Herner, J. In-use NOx emissions from diesel and liquefied natural gas refuse trucks equipped with SCR and TWC, respectively. Environ, Sci. Technol. 2017, 51, 6981-6989.

Monks, P.S., Archibald, A.T., Colette, A., Cooper, O., Coyle, M., Derwent, R., Fowler, D., Granier, C., Law, K.S., Mills, G.E., Stevenson, D.S., Tarasova, O., Thouret, V., von Schneidemesser, E., Sommariva, R., Wild, O., Williams, M.L. Tropospheric ozone and its precursors from the urban to the global scale from air quality to short-lived climate forcer. Atmos. Chem. Phys. 2015, 15, 8889-8973.

Piumetti, M., Bensaid, S., Fino, D., Russo, N. Catalysis in diesel engine NOx aftertreatment: a review. Catalysis, Structure & Reactivity 2015, 1, 155-173.

Quiros, D. C., Thiruvengadam, A., Pradhan, S., Besch, M., Thiruvengadam, P., Demirgok, B., Carder, D., Oshinuga, A., Huai, T., Hu, S. Real-World Emissions from Modern Heavy-Duty Diesel, Natural Gas, and Hybrid Diesel Trucks Operating Along Major California Freight Corridors. Emission Control Science and Technology 2016, 2, 156-172.

Sowman, J., Box, S., Wong, A., Grote M., Laila D.S., Gillam, G., Cruden, A.J., Preston, J.M., Fussey, P. In-use emissions testing of diesel-driven buses in Southampton: is selective catalytic reduction as effective as fleet operators thing? IET Intell. Transp. Syst. 2018, 12, 521-526.

Spears, M. Needs and Opportunities for Reducing Real World NOx Emissions from Heavy-Duty On-Highway Engines. Presentation at 28th CRC Real World Emissions Workshop, Garden Grove, CA, March 2018.

Stohl, A., Aamaas, B., Amann, M., Baker, L. H., Bellouin, N., Berntsen, T. K., Boucher, O., Cherian, R., Collins, W., Daskalakis, N., Dusinska, M., Eckhardt, S., Fuglestvedt, J. S., Harju, M., Heyes, C., Hodnebrog, Ø., Hao, J., Im, U., Kanakidou, M., Klimont, Z., Kupiainen, K., Law, K. S., Lund, M. T., Maas, R., MacIntosh, C. R., Myhre, G., Myriokefalitakis, S., Olivié, D., Quaas, J., Quennehen, B., Raut, J.-C., Rumbold, S. T., Samset, B. H., Schulz, M., Seland, Ø., Shine, K. P., Skeie, R. B., Wang, S., Yttri, K. E., Zhu T. Evaluating the climate and air quality impacts of short-lived pollutants. Atmos Chem. Phys. 2015, 15, 10529-10556.

Tan, Y., Henderick, P., Yoon, S., Herner, J., Montes, T., Boriboonsomsin, K., Johnson, K., Scora, G., Sandez, D., Durbin, T.D. On-board sensor-based NOx emissions from heavy-duty diesel vehicles. Environ. Sci. Technol. 2019, 53, 5504-5511.

Wu, Y., Zhang, S.J., Li, M.L., Ge, Y.S., Shu, J.W., Zhou, Y., Xu, Y.Y., Hu, J.N., Liu, H., Fu, L.X., He, K.B., Hao J.M. The challenge to NOx emission control for heavy-duty diesel vehicles in China. Atmos. Chem. Phys. 2012, 12, 9365-9379.

Yoon, S., Collins, J., Thiruvengadam, A., Gautam, M., Herner, J., Ayala, A. Criteria pollutant and greenhouse gas emissions from CNG transit buses equipped with three-way catalysts compared to lean-burn engines and oxidation catalyst technologies. J Air Waste Manag Assoc 2013, 63, 923-933.

Yoon, S., Collins, J.F., Misra, C., Herner, J.D., Carter, M.W., Sax, T.P. In-use emissions from 2010-technology heavy-duty trucks. Transportation Research Record 2017, 2627, 1-8.

Zhang, S., Wu, Y., Hu, J., Huang, R., Zhou, Y., Bao, X., Fu, L., Hao, J. Can Euro V heavy-duty diesel engines, diesel hybrid and alternative fuel technologies mitigate NOx emissions? New evidence from on-road tests of buses in China. Applied Energy 2014, 132, 118-126.

Zhu, H., McCaffery, C., Yang, J., Li, C., Karavalakis, G., Johnson, K.C., Durbin, T.D. Characterizing emission rates of regulated and unregulated pollutants from two ultra-low NOx CNG heavy-duty vehicles. Fuel 2020, 277, 118192.

6. Evaluation of Small Off-Road Diesel Engine Emissions and Aftertreatment Systems

6.1 Abstract

Off-road engines represent one of the largest categories for mobile source emissions in the United States. Emissions standards for small off road diesel engines (SORDEs) have not been updated since 2004 and do not require aftertreatment for NOx below 75 horsepower (hp) or PM below 25 hp. It has been well established that aftertreatment systems can significantly decrease mobile source emissions, and improvements in these technologies could warrant consideration for adopting more stringent standards for the SORDE category.

The objective of this study is to evaluate the efficiency, durability, and cost benefit of implementing regulations that require the use of SCRs and DPFs on off-road engines under 75 hp. This project included a durability demonstration on four engines and verification of the emissions performances of these devices through a series of emissions test, as well as an evaluation of the cost implications of a potential regulation implementing such aftertreatment systems, and an evaluation of the potential benefits of such a regulation on the emissions inventory. Two engines under 25 hp were tested with a DPF and 2 engines between 25 and 75 hp were tested with an SCR.

The results suggest that implementing a DPF can provide 98% PM reductions with no deterioration after 1,000 hours of durability testing. SCR aftertreatment systems provided

reductions ranging from 26-91% largely dependent on the cycle tested and initial engine temperatures with no significant deterioration after the durability testing. With these efficiencies the adoption of new SORDE standards can provide a PM reduction of 3.8% and a NOx reduction of 8.8-13.7% for the total off-road equipment emissions.

6.2 Introduction

Diesel engines are a major contributor to air pollution in urban areas, with particulate matter (PM2.5) and nitrogen oxide (NOx) emissions being the primary concern for environmental and regulatory agencies (Dallman et al., 2010; Anenberg et al., 2017). Epidemiological and clinical studies have shown an association between diesel exhaust and various short-term and chronic health outcomes, including respiratory and cardiovascular diseases, cancer, and increased mortality (Vermeulen et al., 2014; Pope and Dockery, 2006; Pandya et al., 2002). Currently, PM and NOx emissions from on-road diesel engines are controlled with the use of advanced aftertreatment systems such as diesel particulate filters and selective catalytic reduction (SCR), respectively. The reductions in emissions from on-road diesel engines have been dramatic, with more than 90% PM reductions and 75% NOx reductions compared to engines without aftertreatment controls (Biswas et al., 2008; Haugen and Bishop, 2018; Haugen et al., 2018; Preble et al., 2019). In addition to the on-road diesel engines, off-road engines have also been the subject to some tighter emission regulations, although these regulations are less stringent and have not been updated in over a decade (DieselNet, 2017). Off-road engine applications include agricultural and construction equipment, locomotives, marine engines, mining equipment, lawn equipment,

transport refrigeration units (TRUs), and so on. Currently, off-road emissions represent about 24% of the total NOx emissions inventory in the United States (U.S.) (U.S. Environmental Protection Agency [EPA], 2020). In California, off-road equipment represented about 13% of the total mobile source inventory for NOx emissions, with mobiles sources in turn representing approximately 71.3% of the total statewide NOx emissions inventory, based on the emissions inventories for 2017 (California Air Resources Board [CARB], 2019a, 2019b). It is also expected that the proportional share of the inventory will continue to increase relative to that for on-road vehicles, as engines meeting the more stringent on-road regulations become the predominant share of the on-road vehicle fleet.

The existing standard for Tier 4 off-road engines was developed based on a Regulatory Impact Analysis (RIA) conducted in 2004 (U.S. EPA, 2004). Emissions control strategies such as DPF and SCR were implemented into these standards. PM and NOx aftertreatment was not widely implemented at this time, as such, there was considerable uncertainty as to how viable such aftertreatment devices would be for smaller sized engines. Hence, the adopted compliance standards were designed to be met without using aftertreatment controls for NOx emissions below 75 horsepower (hp) or for PM emissions below 25 hp. This left an important gap in the existing emissions regulations, as engines under 25 hp represented 18% of off-road engines sales, while engines from 25 to 75 hp represented 38% of engine sales back in the timeframe of the Tier 4 off-road regulations were developed (U.S. EPA, 2004). Since aftertreatment control devices for diesel vehicles and diesel-powered equipment are considerably more common now, the use of these strategies

for small off-road diesel engines (SORDEs) may be considerably more viable than when the standards were last updated, which could warrant renewed consideration for adopting more stringent exhaust standards for these engines.

The application of DPF and SCR technologies to SORDEs can introduce several challenges. It is important that the aftertreatment systems can be maintained at a sufficiently high temperature to effectively reduce PM and NOx emissions, and to prevent the systems from increasing backpressure. For example, SCR performance largely depends on exhaust temperature to ensure adequate SCR activity and NOx emissions reductions (Guan et al., 2014; Koebel et al., 2000). These conditions are usually achieved under high engine load/speed operation, where exhaust temperatures are high enough for NOx conversion (Jiang et al., 2018; Misra et al., 2013). This could be problematic in applications where the engines are operating under lower loads or idle conditions for long periods of time. Packaging and positioning are also important considerations, as the amount of space available for the engine and aftertreatment system on SORDE equipment can be very constrained, and the positioning of the catalyst can influence overall efficiencies (Blakeman et al., 2001). It is also important to fully understand the extent to which such aftertreatment systems will deteriorate in terms of emissions benefits or create additional engine wear over the course of the engine's useful life. Degradation of the aftertreatment performance can be impacted by different mechanisms, including thermal aging, sintering, and thermal collapse (Praveena et al., 2018). Williams et al. (2013) showed that SCR and DPF performance can be affected by impurities in the fuel deactivating catalytic sites on the wash coat of the SCR and DPF substrate. Sulfur and ash (trace metals) have also been

shown to act as a catalytic inhibitor on aftertreatment systems (Zhao et al, 2009). These mechanisms can lead to decreased efficiencies and an increased operation cost for the fleet when repairs are necessary. While some work to characterize the potential benefits and limitations of aftertreatment for smaller off-road engines (Welch and Durbin, 2004), there are still many uncertainties as to how effective and practical such systems might be in real world applications.

This project was part of a larger study to evaluate the potential effectiveness, feasibility, and cost-effectiveness of implementing regulations on mobile off-road diesel engines with rated powers of less than 75 hp (i.e., 56 kW [kilowatt]) that could be achieved using advanced emission control strategies, such as DPFs and SCR. This project included a comprehensive review of available aftertreatment and other technologies, demonstration of selected aftertreatment technologies on actual engines, verification of the emissions performance of these devices through a series of emissions and durability tests, evaluation of the potential impacts of additional emissions controls on the emissions inventory, and evaluation of the cost implications of the added emissions control strategies. The focus of this thesis chapter is on the durability emissions testing results, and the emissions and cost benefit analysis. The information from this study could provide the background for a future round of more stringent emissions regulations for SORDE's, as these engines remain an important part of the emissions inventory.

6.3 Experimental Section

6.3.1 Test Engines and After Treatment Systems

Testing for this study was conducted on a total of 4 diesel engines under 75 hp. This included two under 25 hp engines that were equipped with DPFs and two 25 to 75 hp engines that were equipped with SCR systems. The engines included a transportation refrigeration unit (TRU), a ride mower, a mini-excavator, and a skid steer engine with the associated aftertreatment. Information on the engines and after treatment systems is provided in Table 6-1. The TRU engine, originally equipped with no aftertreatment, was tested with a DPF that utilized an electric heating element for DPF regenerations. This heating element would heat the intake air effectively raising the temperature of the exhaust to a level where the catalyzed DPF substrate is activated for regeneration. The mini-excavator engine, originally equipped with no aftertreatment system, was tested with a DPF that utilized a diesel fuel injection strategy prior to the diesel oxidation catalyst (DOC) to initiate regenerations. The fuel would be injected upstream of the DOC and the reaction of the diesel fuel across the DOC created heat to raise the exhaust temperature to a high enough level that was sufficient to regenerate PM on the DPF. Both DPF systems were triggered based on back-pressure. The ride mower engine, originally equipped with a DPF/DOC, was tested with an SCR added immediately after the OEM DPF. The skid steer engine, originally equipped with a DOC, was tested with a selective catalytic regenerating technology (SCRT) system that replaced the original DOC. This system effectively functions as a DOC/DPF and SCR allowing for the control of both PM and NOx. The DPF

used NO_2 produced by the DOC to burn the soot collected on the filter at normal operating temperatures.

Table 6-1: Test Engines and After Treatment

System	Transportation Refrigeration Unit	Mini-Excavator	Ride Mower	Skid Steer
Engine power (hp/kW)	20.25/15.10	24.80/18.50	37.4/27.9	49/37
OEM After Treatment	None	None	DPF/DOC	DOC
Added After Treatment	DPF	DPF	SCR	SCRT*

* functions as both a DPF and an SCR

6.3.2 Fuel Properties

The test fuel used was a California No. 2 diesel fuel containing equal portions of retail diesel fuel taken from an Arco, Shell, and Chevron station to provide a diesel fuel that was more representative of the average fuel properties of diesel fuel in California. Selected diesel fuel properties of this blend are listed in Table 6-2

Table 6-2: Fuel Properties of Test Fuel

Analysis	Method	California No. 2 Diesel
Total Aromatics (vol %)	ASTM D5186 - modified	20.1
Total Aromatics (mass %)	ASTM D5186 – modified	20.5
Polycyclic Aromatics (mass %)		2.2
Biodiesel (mass %)		4.0
T10 (deg C)	ASTM D86	216
T50 (deg C)	ASTM D86	272
T90 (deg C)	ASTM D86	335
Sulfur (ppm)	ASTM D5453	7.8
Density (g/ml)	ASTM D4052	0.8348

6.3.3 Engine Dynamometer

Emissions testing was conducted using a 50 hp engine dynamometer from Alternative Motive Power Systems (APMS). The engine dynamometer uses a Baldor/Reliance IDBRPM25504 motor, which provides 50 hp at 1770 rpm at a torque of 150 ft-lbs. The motor can provide constant hp up to 3540 rpm at 75 ft-lbs of torque.

6.3.4 Test Sequence

The engine testing for this work focused on testing that was conducted after the operation of the aftertreatment system for 1,000 hours in the field for the TRU and ride mower engines, the aging of the aftertreatment on the engine dynamometer for an equivalent of 1,000 hours for the mini-excavator engine, or a combination of field operation and engine

dynamometer aging to represent 1,000 hours, as for the skid steer engine. This provided information on how durable the aftertreatment systems were in maintaining the emissions reductions during baseline emissions testing (Yang, 2018) over the period of the demonstration.

6.3.5 Field Demonstration and Catalyst Aging

The mini excavator and skid steer engines were not able to complete the 1,000-hour field demonstration due to the use patterns of these engines not being as high daily compared to the ride mower and TRU engines. Specifically, the mini excavator and skid steer engines accumulated 186 and 233 hours of in use operation, respectively. Additionally, the DPF used for the mini excavator was found to be damaged during the initial post-field demonstration, so post-field emissions data was not available for this DPF.

Since the skid steer engine was not able to achieve the 1,000 hours of accumulation in the field and since post-field data was not available for the mini-excavator DPF, additional aging was conducted on the small engine dynamometer for these engines and aftertreatment systems to achieve a level of deterioration comparable to what would be experienced from the 1,000 hours in the field. For simplicity, the aging protocol used for this study consisted of repeat segments of thermal aging and soot accumulation. While such aging may not be fully representative of real-world aging, which could be subjected to additional poisoning from fuel, oil, or other sources, such as urea oxidation, or ash, sulfur, phosphorous, zinc, or calcium poisoning, it is expected that the contribution of this poisoning would be much smaller than that of thermal aging on deterioration. So, it is

expected that the engine dynamometer aging would provide reasonable estimates of the magnitude of the deterioration that might be seen in the field. The dynamometer aging approach used was based on the Diesel Aftertreatment Accelerated Aging Catalyst (DAAAC) methodology developed by Southwest Research Institute (SwRI) (Bartley, 2012). A two-temperature mode aging profile was developed using in-field temperature data, with a lower temperature that facilitated soot accumulation and a higher temperature that simulated regeneration conditions. The low temperature and high temperature operation modes were cycled in intervals of 30 minutes each. This allowed equal operating time at each mode and provided sufficient time for some soot build up between high-temperature operation periods. Based on the DAAAC methodology, the aging times needed to represent the additional in-use operation for skid steer engine/aftertreatment combination and the full equivalent of 1,000 hours of aging for the mini-excavator engine/aftertreatment combination were calculated to be 27.3 hours at 357°C and 27.2 hours at 447°C, respectively.

6.3.6 Test Cycles

During the engine installation and preparation, the engines were run over an engine map, where the engine was run from the base idle to maximum engine speed while measuring the maximum power and torque at each speed. The engine map created was used to determine the speed and torque test points for the C1 and G2 tests, and the engine rpm and torque values for the associated non-road transient cycle (NRTC) (40 CFR §1039.Appendix II, 2017). The TRU engine was tested in triplicate over the ramped modal G2 test cycle. The G2 test cycle is a 6-mode test cycle and was run as a hot stabilized test,

with the engine warmed up prior to the start of each test. The ride mower, mini-excavator, and skid steer engines were tested in triplicate over a ramped modal C1 test cycle and a cold- and hot-start NRTC. The C1 test is an 8-mode test cycle and was run as a hot stabilized test, with the engine warmed up prior to the start of testing. The NRTC cold-start test was conducted after an overnight engine soak, and the hot-start test was conducted after the cold-start test following a 20-minute soak period.

6.3.7 Emissions Testing

Emissions tests were conducted to evaluate the effectiveness of the aftertreatment systems of PM and NOx performance. The emissions tests were conducted in CE-CERT's Vehicle Emissions Research Laboratory (VERL). The 1,000-hour field and engine dynamometer aging tests were conducted using an AVL AMA SL™ (SlimLine) Exhaust Measurement System for gas-phase pollutants and an AVL 478 Smart Sampler (SPC) for PM sampling. These systems both sample raw exhaust. The AVL AMA gas-emission bench is equipped with a Flame Ionization Detector (FID) for Total Hydrocarbon (THC) emissions, a Chemiluminescence detector (CLD) for NOx measurements, and a Non-Dispersive Infrared (NDIR) detector for CO and CO_2 measurements. Emission measurements were evaluated to determine the reduction efficiency of the aftertreatment by comparing the baseline and degreened aftertreatment testing results (Yang, 2018) to the 1,000-hour aged tests.

6.4 Results and Discussion

This section presents the results for the emissions testing. The graphs in this section show the results for the average of all tests conducted for each engine/aftertreatment system over each specific cycle. Note that for the plots in this section, the NOx emissions are divided by 10 or 2, CO_2 emissions are divided by 2,000 or 1,000, and PM emissions are multiplied by 100 or 10 to allow all pollutants to be represented in the same graph. The error bars represent one standard deviation of the average. Since the NRTC tests were only conducted once for each testing period, these results do not include error bars. It should be noted that although this thesis work focuses on the durability testing results, the results from the initial baseline tests for the engines in their original configurations before adding the aftertreatment and for tests where the aftertreatment systems were installed and initially degreened for 25 hours are also included in the graphs for comparison purposes (Yang, 2018).

6.4.1 TRU Engine Emissions

The regulated gaseous and PM emission results are presented in Figure 6-1 in g/kW-hr units. The primary pollutant of interest in terms of emissions reductions for this DPF are PM mass emissions. The DPF provided a reduction in PM of 98.0% for the degreened test and of 98.5% for the 1,000-hour test. This is comparable to typical PM reduction efficiencies found for DPFs (Rossomando et al., 2020, Shao et al., 2018). The slight improvement in PM reduction efficiency for the 1,000-hour durability test could be due to an increase in soot loading on the filter substrate that could increase the overall PM

reduction efficiency, although it could also be impacted by small changes in the operating condition of the engine. Soot accumulation inside the trap will lead to an increased backpressure which will result in increased fuel consumption (Mokhri et al. 2012; Millo et al., 2015). This phenomenon is shown in Figure 6-2.

Average NOx emissions increased by 9.3% and 19.5% at a statistically significant level for the baseline degreened testing and the 1,000-hour durability testing, respectively, compared to the baseline engine testing results. The increase in NOx emissions can be attributed to the heating of the intake air to raise the exhaust temperature for the DPF regeneration. This in turn increases the in-cylinder temperatures leading to higher thermal NOx emissions formation (Kumar et al., 2013). It should be noted that the increases in NOx emissions could be largely eliminated by placing the heating element in the exhaust prior to the DPF, as opposed to prior to the combustion chamber.

For the TRU engine, the catalyst configuration also included a DOC as an auxiliary catalyst to control THC and CO emissions. THC emissions showed reductions of 91% for the initial degreened and 85% for the 1,000-hour durability testing compared with the baseline engine testing. CO emissions showed reductions of 99.9% for the initial degreened and 99% for the 1,000-hour durability testing compared with the baseline engine testing. Overall, the THC and CO reductions were comparable between the initial degreened and 1,000-hour durability testing, suggesting that there was no significant deterioration of the catalyst configuration (DOC+DPF) over the demonstration period.

CO_2 emission rates increased by 9.5% and 10.6%, respectively, for the 1,000-hour post durability and degreened testing when compared to the baseline tests. Adding a DPF into an exhaust stream will increase the engine backpressure as shown in Figure 1-2. An increase in engine exhaust back pressure leads to an increase in engine work to overcome the manifold pressures. This extra work will result in higher fuel consumption and increased CO_2 emissions (Mikulic et al., 2010). Although the post durability testing showed slightly higher peak backpressures, the CO_2 emissions for the degreened baseline and post durability testing were comparable.

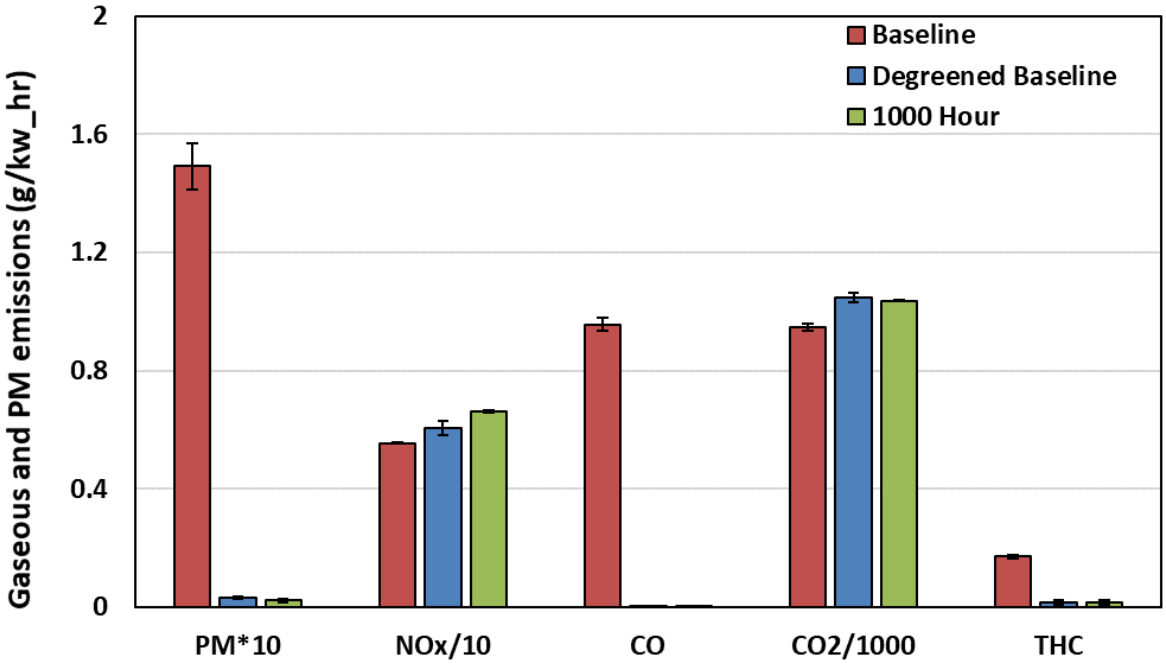

Figure 6-1: Gaseous and PM results for the TRU engine G2 Cycle. Baseline and Degreened Baseline values from Yang (2018) are included for comparison.

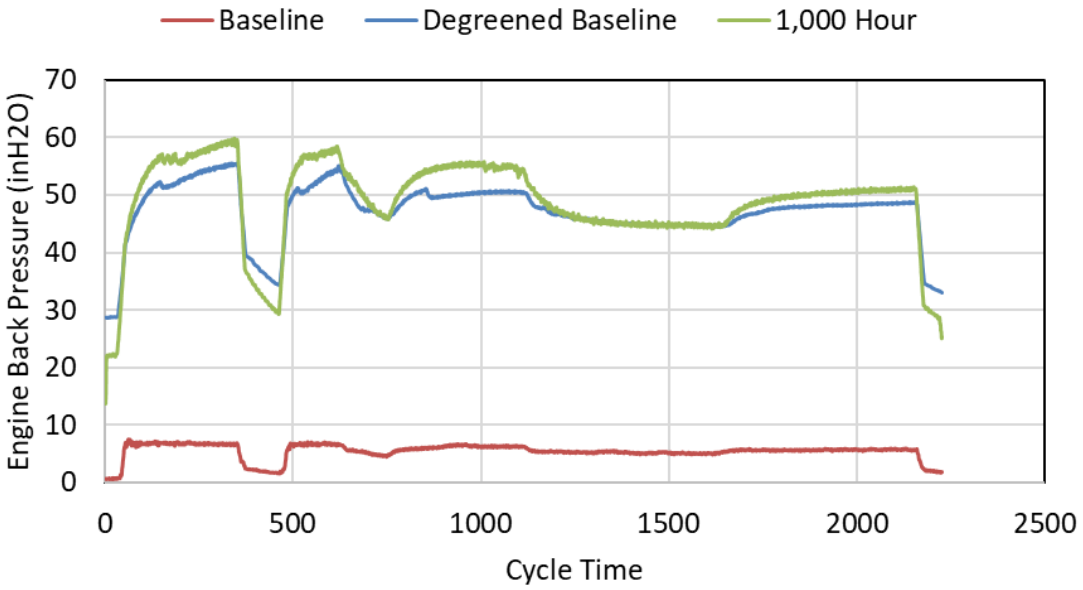

Figure 6-2: Engine Back Pressure

6.4.2 Mini-Excavator Engine Emissions

The regulated gaseous emissions and PM emission results of the mini-excavator engine are presented in g/kW-hr units in Figure 6-3 for the C1 cycle, and in Figure 6-4 for the hot-start and cold-start NRTC cycles. The original DPF was damaged during the in-field demonstration so a second DPF was degreened and then aged on the engine dynamometer for the equivalent of 1,000 hours. The degreened tests for the original and second DPFs are denoted as degreened baseline and degreened baseline 2, respectively, in the figures.

In comparison with the initial baseline engine testing without aftertreatment, the DPF provided a reduction in PM emissions ranging from 98.6% to 99.1%, similar to the previous TRU engine testing. The PM emissions for both degreened tests were seen in low levels, ranging from 0.7 to 1.9 mg/kW-hr. The PM mass reduction efficiency was comparable to

the degreened tests after the 1,000-hour aging demonstration, with efficiencies ranging from 98.5% to 99.0% for all cycles and emissions ranging from 1.2 to 1.9 mg/kW-hr.

The DOC/DPF configuration also provided reductions in THC and CO emissions. For the THC emissions, the reductions were 97.0%, 86.8%, and 80.1%, respectively, for the C1, cold-start NRTC, and hot-start NRTC cycles for the first degreened DPF. Compared to the initial baseline, the second DPF showed lower THC emissions reductions ranging from 70% to 72% for the degreened testing and from 48% to 52% for the 1,000-hour durability testing. For the CO emissions, reductions were from 86.5% to 86.8% for the first degreened DPF, from 90% to 94% for the second degreened DPF, and from 67% to 77% for the second DPF after the 1,000 hours of aging. The less significant reductions seen for the second DPF for THC emissions and the 1,000-hour aging test for CO emissions could be indicative of some deterioration, but it could also be due to some minor differences in engine operation or fuel injection that may have occurred between the different test periods. Figure 6-5 presents a comparison between the CO and THC concentrations for the degreened and post durability tests over the C1 cycle and hot-start NRTC cycle. Initial spikes in CO and THC concentrations for the hot-start NRTC are expected due to the inability for the catalyst to oxidize these pollutants until the DOC reaches light off temperatures. The degreened baseline test shows a much larger initial spike of THC and CO emissions during the start of the cycle, however, concentrations decreased throughout the test, so the integrated emissions over the full cycle were higher for the 1,000-hour test. When comparing the C1 THC results for the degreened tests for the initial DPF with the degreened and 1,000-hour durability tests for the second DPF, it is also worth noting that

the emissions measurements were made with different emissions measurement system. In particular, the degreened tests on the initial DPF were made with a constant volume sampling (CVS) dilution tunnel system, which may not have as much sensitively for the low-level THC measurements as the AVL AMA SL™ that was used for the testing on the second DPF, which samples directly from the raw exhaust.

The average NOx emissions showed reductions ranging from 12.2% to 21.4% for the cold- and hot-start NRTCs for the degreened test on the initial DPF and for the degreened test and the 1,000-hour durability on the second DPF. NOx emissions for the C1 cycle, however, did not show consistent trends between the different tests. Since this DPF utilizes a diesel fuel injection strategy prior to the DOC for DPF regenerations, it is not expected that NOx emissions would change significantly throughout the testing, as opposed to the DPF fitted in the TRU engine where the engine intake air was preheated. Some of the changes in emissions in comparing the different tests could be due to subtle differences in the engine operation that may have occurred between the different test periods.

CO_2 emissions were comparable for all tests, with and without the DPF. CO_2 emission rates for all tests were within 5% of those for the baseline test, except for the cold-start and hot-start NRTC cycles for the 1,000-hour aging test on the second DPF, which were 11%-12% lower than the baseline. This suggests that there is not a significant change in fuel use before and after the 1,000-hour aging demonstration for this DPF.

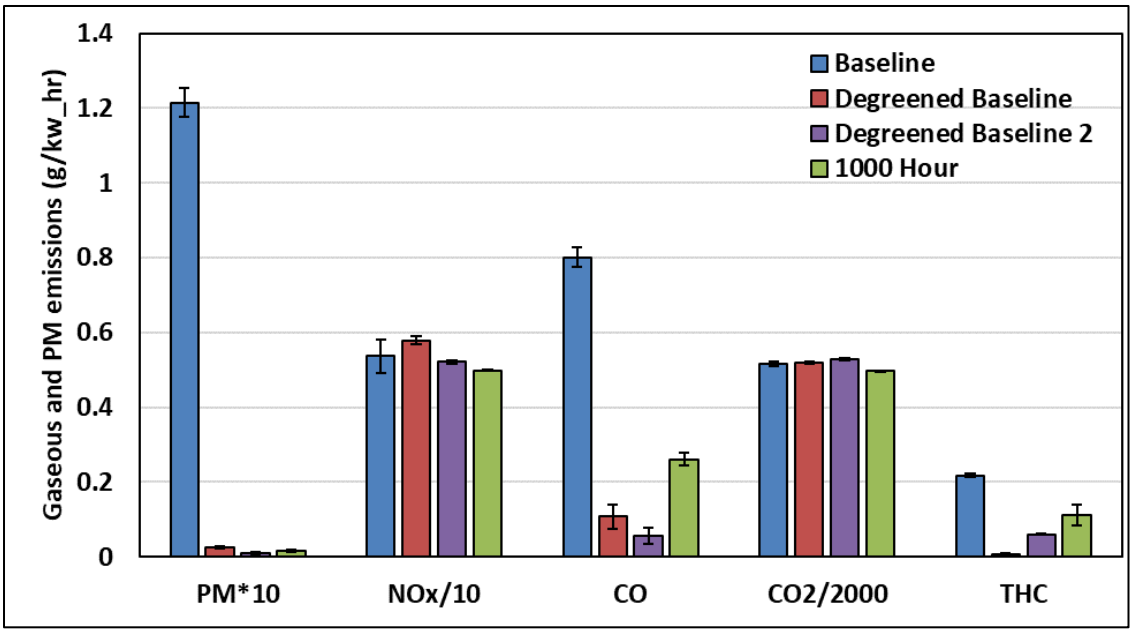

Figure 6-3: Gaseous and PM results for the Mini-Excavator engine C1 cycle. Baseline and Degreened Baseline values from Yang (2018) for comparison.

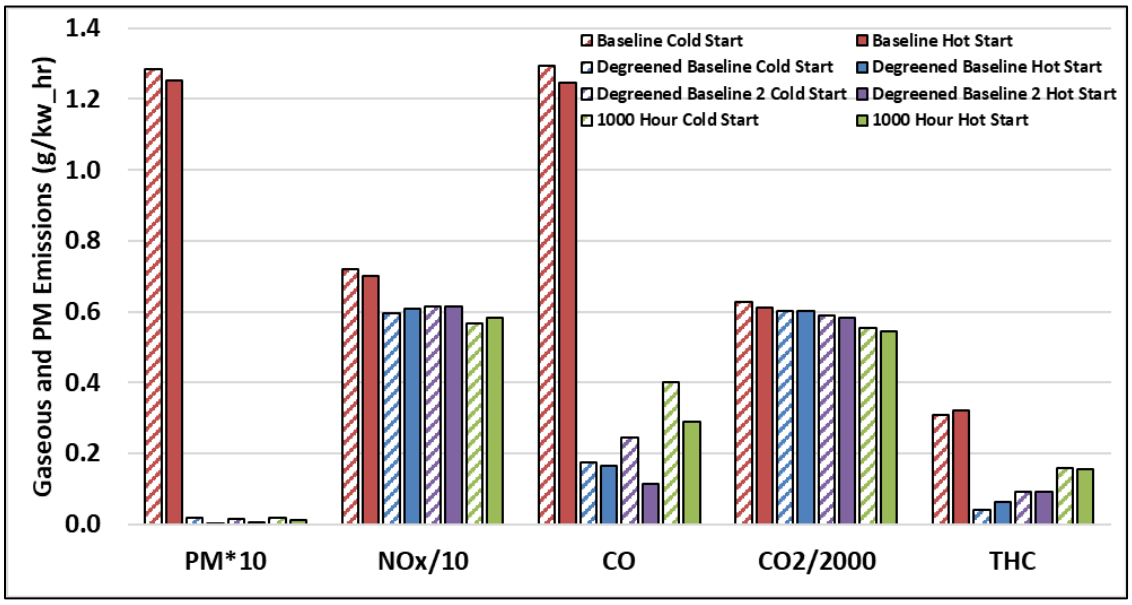

Figure 6-4: Gaseous and PM results for the Mini-Excavator engine NRTC cycle. Baseline and Degreened Baseline values from Yang (2018) for comparison.

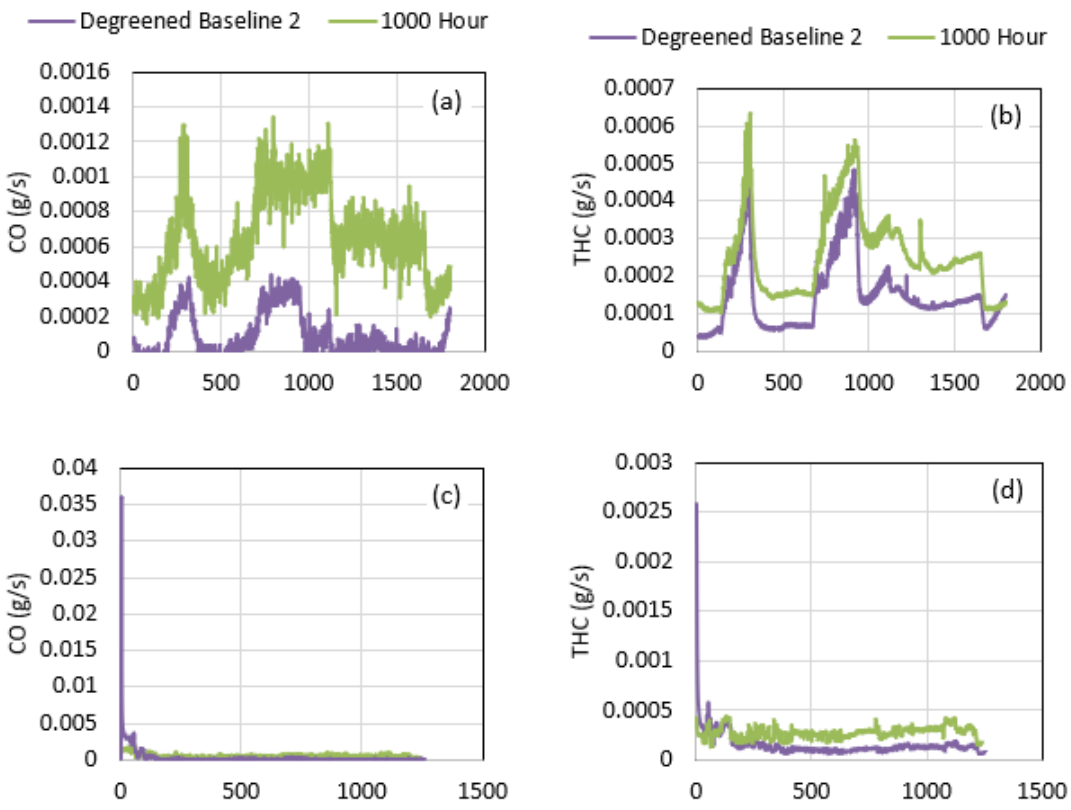

Figure 6-5 (a-d): Real-time CO and THC emissions for C1 cycle (a-b) and hot-start NRTC cycle (c-d)

6.4.3 Ride Mower Engine Emissions

The regulated gaseous and PM emission results of the ride mower engine are presented in g/kW-hr units in Figure 6-6 for the C1 cycle and in Figure 6-7 for the hot-start and cold-start NRTC cycles.

In comparison with the initial baseline testing without aftertreatment, the SCR provided a reduction in NOx ranging from 28.4% to 47.4% for cold-start transient cycles, from 57.0% to 64.9% for the hot-start transient cycles, and from 70.4% to 90.5% for hot-start steady-state cycles. Lower efficiencies during cold-start cycles are expected, due to the SCRs

inability to reduce NOx emissions until the aftertreatment system is warmed up to its light off temperature. SCR systems utilize the injection of urea into the exhaust stream to thermally decompose and convert NOx into nitrogen, oxygen, and water. These chemical reactions are limited by urea decomposition into ammonia and hydrogen isocyanate, which can only occur at temperatures above 152°C and depending on the materials of the catalyst bed (Praveena et al., 2018; Blakeman et al., 2001). As such, the SCR would not provide significant NOx reductions during the cold-start cycle until the exhaust temperature will be adequate for SCR activity. NOx emissions did show greater reduction efficiencies and lower emissions levels for the initial degreened tests compared to the 1,000-hour durability tests for the cold-start NRTC, but greater reductions on the C1 cycle for the initial degreened tests compared to the 1,000-hour durability tests. For the cold start NRTC, the differences were primarily in the first 200 to 300 seconds of the test cycle, as shown in Figure 6-8, when the exhaust temperature was below the typical operating SCR temperature. For the C1 cycle, on the other hand, the higher NOx emissions for the degreened test compared to the 1,000-hour test can be attributed to generally higher emissions throughout the cycle, as illustrated in Figure 6-9. This suggests there could be some operational differences in the engine between the two different test periods for this cycle. At the very least, the high reduction efficiencies of the SCR during C1 cycle after the 1,000-hour field demonstration suggest that there was no significant deterioration of the SCR catalyst.

The average PM emissions were at low levels for both the C1 and NRTC cycles since the engine was originally equipped with an OEM DOC and DPF. PM mass emissions were

within the certification limits for all test sequences. Although there were some PM differences between the different test sequences, these differences were at relatively low levels, which suggests there are not significant differences in the effectiveness of the OEM DPF with or without the SCR attached. THC and CO emissions were also relatively low for the baseline testing due to the presence of a DOC but showed the potential for some additional reductions for the SCR tests. CO emissions for the degreened and 1,000-hour C1 cycle tests showed reductions of 45.0% and 79.5%, respectively, compared to the baseline emissions tests. CO emissions changes for the cold-start and hot-start NRTC cycles were less consistent and showed both increases and decreases. THC emissions showed reductions in the range of 8.1% to 11.6% for some of the degreened and 1,000-hour tests, although these could be within the variability of the testing. The higher THC emissions for the 1,000-hour durability test compared to the initial degreened C1 test was likely a result of the THC emissions being near background levels for the degreened baseline testing, which utilized a CVS for emissions measurements, while the post durability testing utilized a raw emissions bench leading to more accurate readings at lower emission levels.

CO_2 emission rates were stable throughout each test sequence. The emissions rates for the C1 tests were within 5%. CO_2 emission rates for the cold-start and hot-start NRTC tests were within 10%. The CO_2 emissions would be expected to increase slightly due to the additional back-pressure from the SCR, however, based on these results, it is expected the use of this SCR system will not have a significant impact on fuel consumption over extended periods of use.

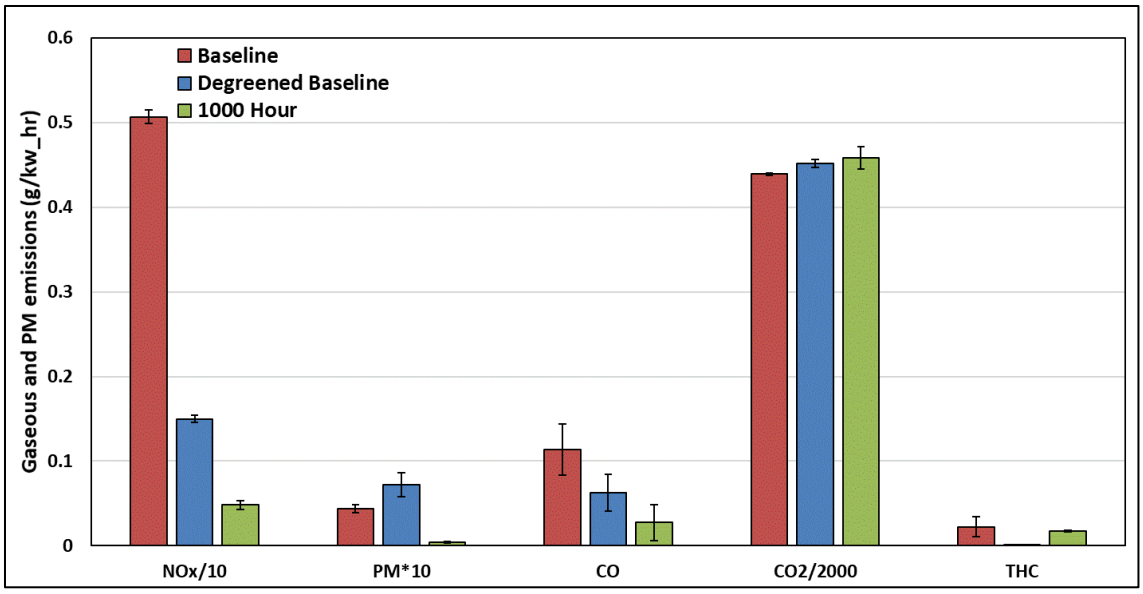

Figure 6-6: Gaseous and PM results for the Ride Mower engine C1 Cycle. Baseline and Degreened Baseline values from Yang (2018) for comparison.

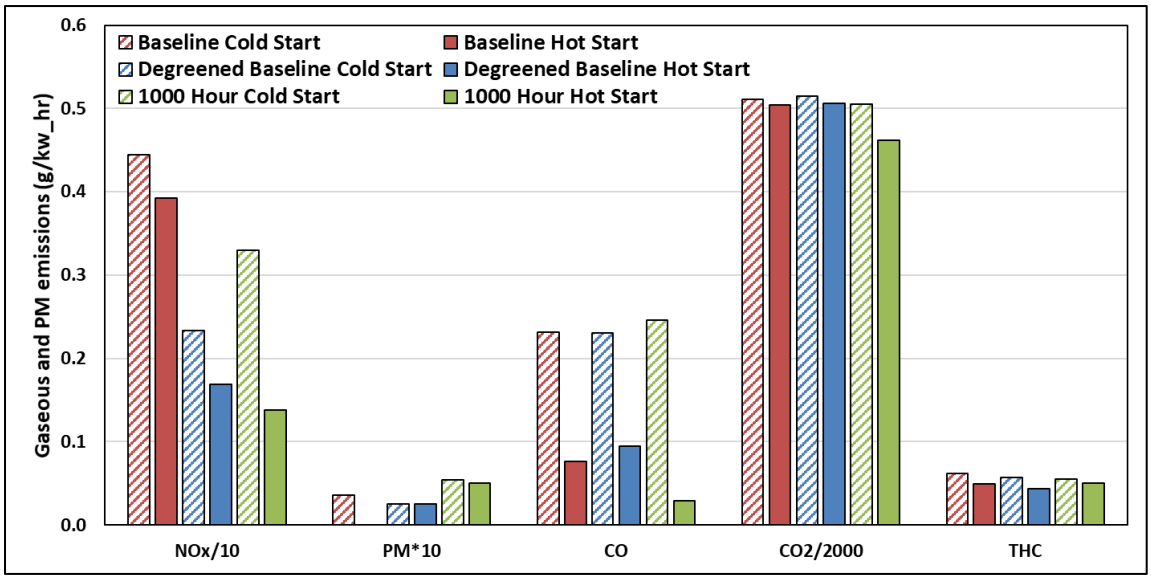

Figure 6-7: Gaseous and PM results for the Ride Mower engine NRTC cycle. Baseline and Degreened Baseline values from Yang (2018) for comparison.

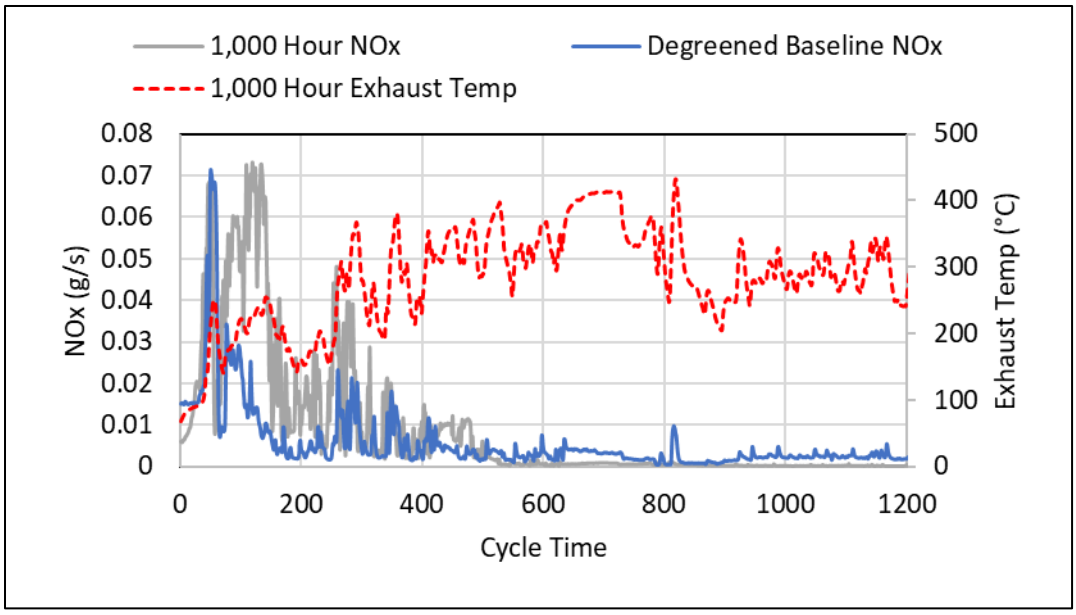

Figure 6-8: Real Time NOx concentrations during cold start NRTC cycle for the ride mower SCR system. Degreened Baseline values from Yang (2018) for comparison. It should be noted that exhaust temperature values were not available for the degreened tests.

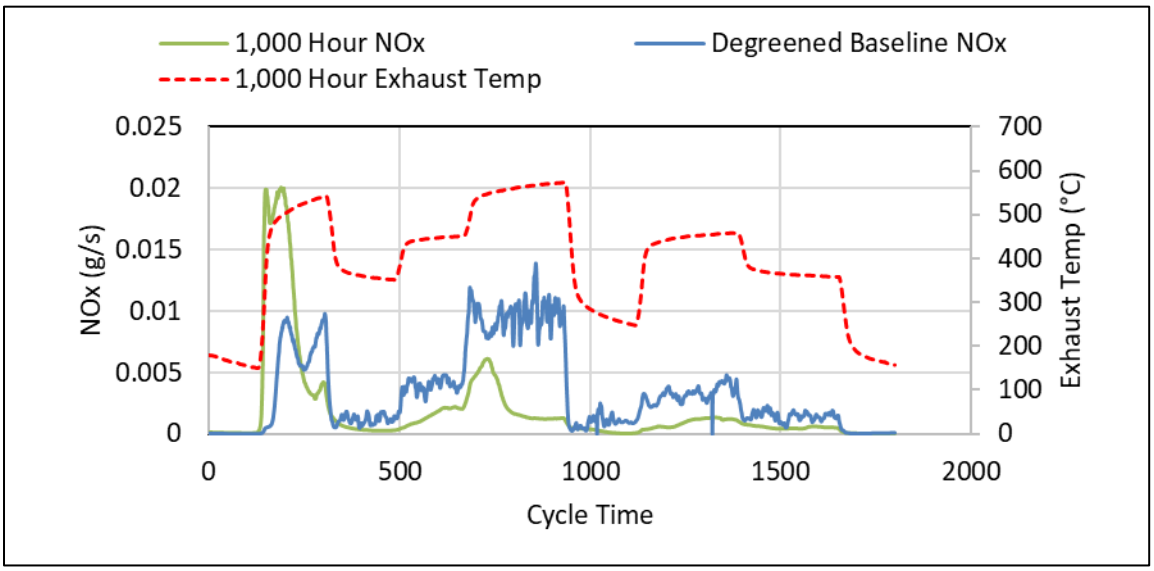

Figure 6-9: Real Time NOx concentrations during C1 cycle for the ride mower SCR system. Degreened Baseline values from Yang (2018) for comparison. It should be noted that exhaust temperature values were not available for the degreened tests.

6.4.4 Skid Steer Engine Emissions

The regulated gaseous emissions and PM emission results of the skid steer engine are presented in Figure 6-10 in g/kW-hr units for the C1 cycle. Figure 6-11 shows the gaseous and PM emission results in g/kW-hr for the hot-start and cold-start NRTC cycles.

In comparison with the initial baseline testing without aftertreatment, the SCRT provided a reduction in NOx emissions ranging from 59.4% for the cold-start transient cycles to 85.3% for the hot-start steady-state cycles. This is similar to the findings from the ride mower engine testing. The NOx emissions reductions for the hot-start and cold-start NRTC cycles were lower due to the SCRT not reaching the dosing temperature threshold of 190°C for the first portion of the cycle. Since the C1 cycle is longer and begins as a hot-running cycle, the dosing temperature was reached faster, as well as this portion being a smaller portion of the entire cycle compared to the NRTC cycles. The NRTC test shows a low SCR conversion efficiency for almost the first half of the cycle due to the SCR not reaching the operating temperature fast enough. Real-time NOx emissions for the 1,000-hour durability testing over the cold-start NRTC and C1 cycles are presented in Figure 6-12 to show this trend. It should be noted that if the engine were calibrated such that the engine-out exhaust temperatures are higher during transient periods, the SCRT could have a better conversion efficiency. It is also important to note that the SCRT dosing control strategy for this SCRT was developed using only feed-forward control for urea dosing, since a full calibration was outside of the scope of this study. Using a storage control strategy, where ammonia is stored on the catalyst based on adsorption and absorption, would help considerably during

transients where the temperatures rise slowly. NOx emissions showed no indication of deterioration between the degreened baseline and 1,000-hour aging test.

The SCRT provided a reduction in PM mass ranging from 87.5% to 92.1% showing similar efficiencies to the DPFs tested earlier in the project. The average PM emissions for the SCRT equipped engine were comparable between the degreened baseline testing and 1,000-hour aging testing. It should be noted that the skid steer engine was certified to a much lower PM emissions level compared to the TRU and mini-excavator engines, and the skid steer was equipped with a DOC and more advanced engine controls. As such, the reductions are not fully representative of the DPF PM reduction efficiency for an uncontrolled engine.

CO emissions showed reductions ranging from 32.7% to 69.7% for the degreened baseline testing cold start and hot start NRTCs. CO reduction efficiency decreased for the transient cycles during the 1,000-hour durability testing, but still showed efficiencies ranging from 20.9% to 29.0%. The SCRT contains a DOC component in front of the DPF and SCR systems which will oxidize both CO and THC into CO_2 andH_2O. These results suggest that the DOC component shows the potential to provide additional reductions, which could be optimized as part of the development process. For the C1 cycle, CO emissions were near the lower detection limits, so no significant changes were found. THC emissions were relatively low, and did not show significant differences between test sequences, apart from the elevated emission results for the degreened test conducted after the field demonstration. The THC emissions for the 1,000-hour test were similar to the emissions for the initial

degreened baseline testing, suggesting that the high THC emissions for the degreened baseline 2 testing was more of an operational issue rather than an aftertreatment issue.

CO_2 emissions did not show any significant changes between tests. It should be noted that the CO_2 emissions might be expected to increase from the increase back-pressure caused by the SCRT, however, given the results it is expected the SCRT will not have a significant impact of fuel consumption over extended periods of use.

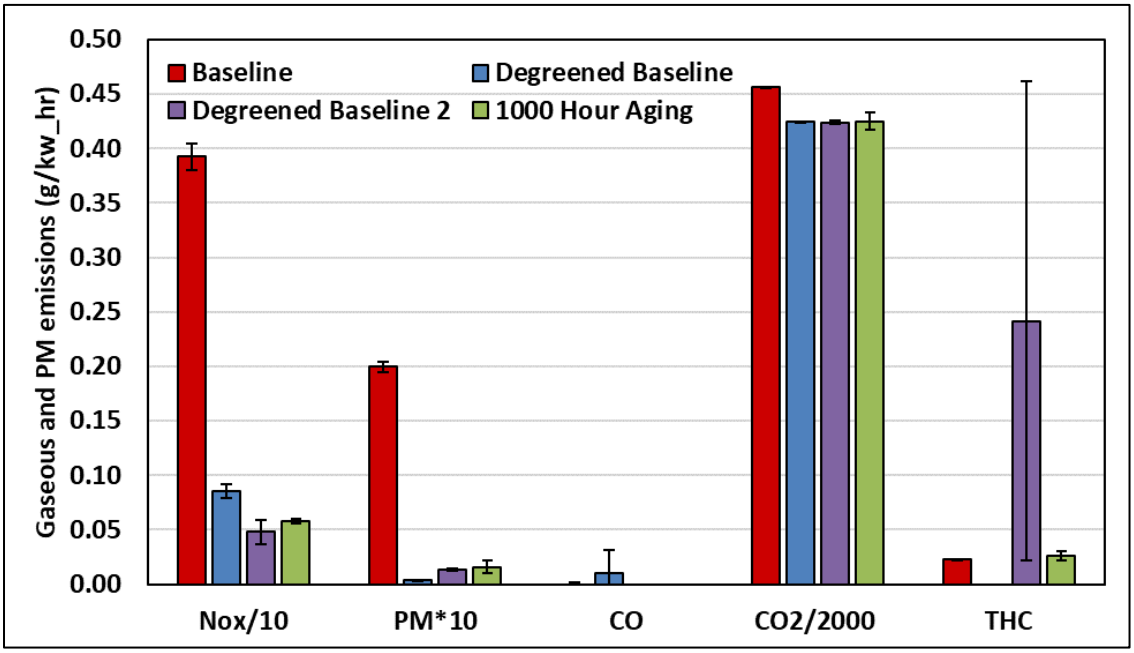

Figure 6-10: Gaseous and PM results for the Skid Steer engine C1 cycle. Baseline and Degreened Baseline values from Yang (2018) for comparison.

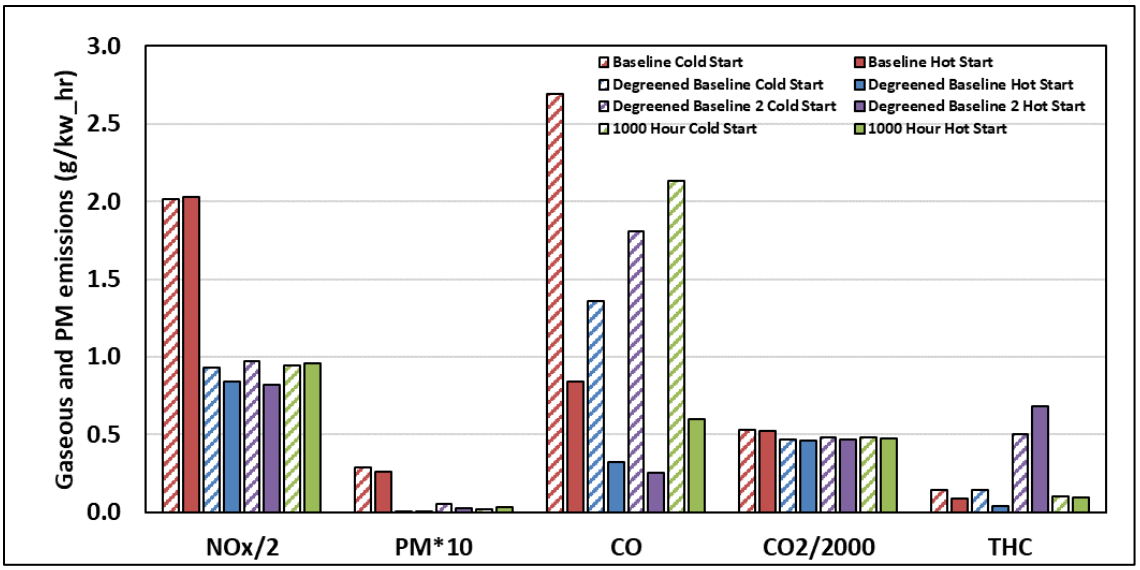

Figure 6-11: Gaseous and PM results for the Skid Steer NRTC. Baseline and Degreened Baseline values from Yang, (2018) for comparison.

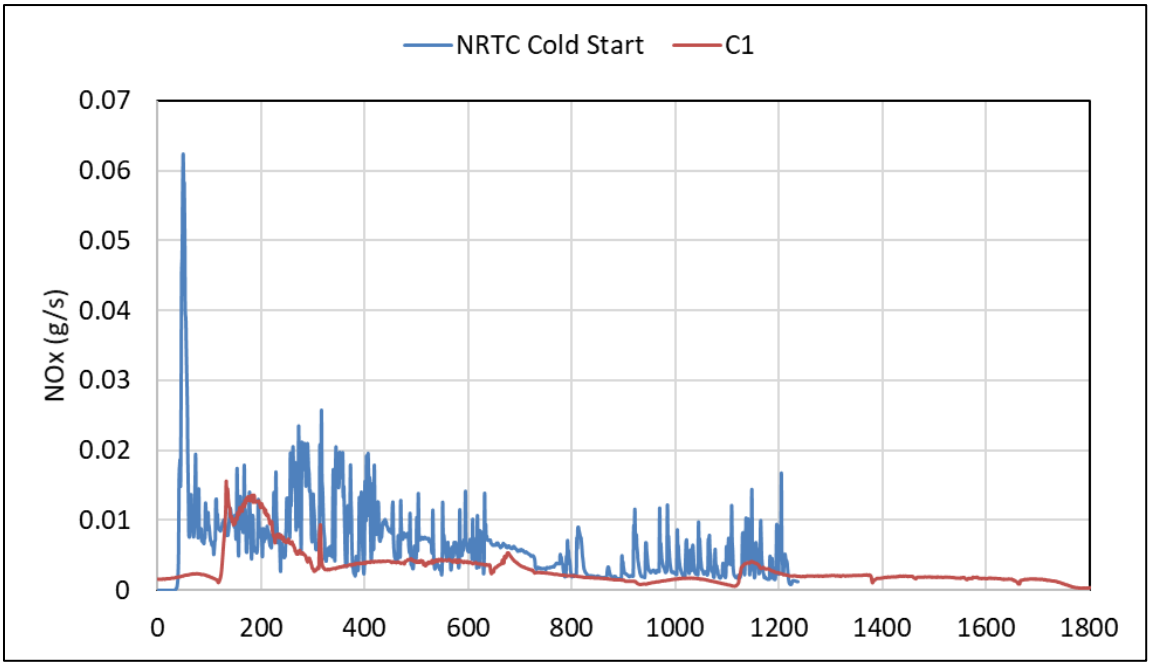

Figure 6-12: Real time NOx emissions for 1,000-Hour cold start NRTC and C1 cycles

6.5 Emissions Inventory and Cost Benefit Analysis

To evaluate the potential effectiveness of the implementation of regulations that would effectively require the use of DPF and SCR aftertreatment systems, an analysis of the emission inventory and cost benefits was conducted. This analysis was based on potential benefits and costs related to regulations that would be implemented in California only, as the initial focus of this study was related to California regulatory development.

6.5.1 Emissions Inventory Benefits

A summary of the baseline emissions inventories and emissions benefits for the under 25 hp (PM) and 25 to 75 hp (NOx) engines is provided in Table 6-3. Baseline emissions inventory data was based off of CARB's online emissions inventory tool (https://www.arb.ca.gov/orion/) for the calendar year 2017 along with information provided by CARB. Estimates of the emission benefits of more stringent emission standards were based on the emissions test results. As such, the DPFs were estimated to reduce PM by 95%, and SCRs were estimated to reduce NOx emissions by 55-85%. Based on these results, it is estimated that NOx reductions in the range from 12.46 to 19.26 tons per day for the 25-75 hp category if the current fleet was fully transitioned to SCR-equipped engines, and PM reductions of 0.372 tons per day for the under 25 hp category if the current fleet was fully transitioned to DPF-equipped engines. Overall, the DPF reductions would represent a reduction in PM of 3.8% for the total off-road equipment emissions inventory and 0.4% of the total mobile sources inventory. The SCR reductions would represent a

reduction in NOx of 8.8-13.7% for the total off-road equipment emissions inventory and of 1.2-1.8% for total mobile sources inventory.

To determine the cumulative benefits of applying SCRs and DPFs, some additional calculations were done. First, the total potential total emissions reductions that could be achieved over a full year were obtained by multiplying the benefits obtained from Table 4-3 by 252 days (the number of working days in a year). It is important to note that only working days were included for the estimate, as much of the equipment in this engine category would be used for industrial work-related tasks. Using this calculation, the emissions reductions of NOx would range from 3139.9 tons/year to 4852.5 tons/year for 25 to 75 hp engines and 93.74 tons per year for PM for under 25 hp engines. While these estimates represent the potential benefits of complete fleet turnover, it is expected that that this would occur over a number of years, with incremental benefits for each year based on the percentage of fleet turn over that occurred for that year. To provide a basis for the cost benefit analysis in section 4.5.2, a 30-year time horizon was utilized for the complete turnover of the fleet to advanced emissions controls. This is consistent with the time frame utilized by the United States Environmental Protection Agency (EPA) in its estimates for the regulatory impact analysis (RIA) for its Tier 4 off-road engine regulations (U.S.EPA, 2004). It was assumed the fleet turnover is equally distributed over the full 30-year period. The amount of PM and NOx reductions for each year are shown in Table 6-4, as well as the cumulative emissions reductions that would be obtained over this 30-year timeframe.

Table 6-3: Small Off-Road Diesel Engine Emission Benefits

Emission Rate (tons/day)	Horsepower range									
	0-10		10-25		25-50			50-75		
	PM		PM		NO_x			NO_x		
Small Off-Road Equipment Category	Current	95% Reduction	Current	95% Reduction	Current	55% Reduction	85% Reduction	Current	55% Reduction	85% Reduction
Totals	**0.019**	**0.0000**	**0.372**	**0.019**	**13.692**	**6.161**	**2.054**	**8.962**	**4.033**	**1.344**
Agricultural Tractors			0.105	0.005	3.416	1.537	0.512	7.998	3.599	1.200
Transport Refrigeration Units	0.001	0.000	0.034	0.000	7.049	3.172	1.057			
Lawn & Garden Tractors*			0.106	0.005						
Welders			0.012	0.001	1.006	0.453	0.151			
Generator Sets			0.026	0.001	0.575	0.259	0.086			
Pumps	0.008	0.000		0.001	0.340	0.153	0.051			
Air Compressors			0.001	0.000	0.224	0.101	0.034			
Other Agricultural Equipment			0.002	0.000						
Crushing/Proc. Equipment*					0.104	0.047	0.016			
Hydro Power Units	0.000	0.000		0.000						
Pressure Washers			0.000	0.000	0.003	0.001	0.000			
Sprayers			0.000	0.000	0.067	0.030	0.010	0.037	0.017	0.006
Signal Boards	0.007	0.000		0.000	0.004	0.002	0.001			
Rollers	0.001	0.000		0.000	0.266	0.120	0.040	0.009	0.004	0.001
Cement and Mortar Mixers	0.001	0.000		0.000						
Plate Compactors	0.000	0.000		0.000						
Other General Industrial/Construction Equipment	0.001	0.000	0.001	0.000	0.327	0.147	0.049	0.172	0.077	0.026
Commercial Turf Equipment										
Skid Steer Loaders			0.015	0.001	0.162	0.073	0.024	0.635	0.286	0.095
Aerial Lifts			0.002	0.000	0.149	0.067	0.022	0.111	0.050	0.017

*These data obtained from Off-Road 2007 (CARB, 2019b)

Table 6-4: Summary of Emissions Reduction

Year	PM Reductions			NO_x Reductions					
	Tons/year			Tons/year					
	(Control efficiency 95%)			(Control efficiency 55%)			(Control efficiency 85%)		
	0-10 hp	10-25 hp	Total	25-50 hp	50-75 hp	Total	25-50 hp	50-75 hp	Total
1	0.16	2.97	3.12	63.26	41.40	104.66	97.76	63.99	161.75
2	0.32	5.93	6.25	126.52	82.81	209.33	195.52	127.98	323.50
3	0.48	8.90	9.37	189.78	124.21	313.99	293.28	191.97	485.25
4	0.64	11.86	12.50	253.04	165.61	418.66	391.04	255.96	647.00
5	0.80	14.83	15.62	316.30	207.02	523.32	488.80	319.96	808.75
6	0.96	17.79	18.75	379.56	248.42	627.98	586.56	383.95	970.50
7	1.12	20.76	21.87	442.82	289.83	732.65	684.31	447.94	1132.25
8	1.28	23.72	25.00	506.08	331.23	837.31	782.07	511.93	1294.00
9	1.44	26.69	28.12	569.34	372.63	941.98	879.83	575.92	1455.75
10	1.60	29.65	31.25	632.60	414.04	1046.64	977.59	639.91	1617.50
11	1.76	32.62	34.37	695.86	455.44	1151.30	1075.35	703.90	1779.25
12	1.92	35.58	37.50	759.12	496.84	1255.97	1173.11	767.89	1941.00
13	2.07	38.55	40.62	822.39	538.25	1360.63	1270.87	831.89	2102.76
14	2.23	41.51	43.75	885.65	579.65	1465.30	1368.63	895.88	2264.51
15	2.39	44.48	46.87	948.91	621.05	1569.96	1466.39	959.87	2426.26
16	2.55	47.44	50.00	1012.17	662.46	1674.62	1564.15	1023.86	2588.01
17	2.71	50.41	53.12	1075.43	703.86	1779.29	1661.91	1087.85	2749.76
18	2.87	53.37	56.25	1138.69	745.26	1883.95	1759.67	1151.84	2911.51
19	3.03	56.34	59.37	1201.95	786.67	1988.62	1857.42	1215.83	3073.26
20	3.19	59.30	62.50	1265.21	828.07	2093.28	1955.18	1279.82	3235.01
21	3.35	62.27	65.62	1328.47	869.48	2197.94	2052.94	1343.82	3396.76
22	3.51	65.23	68.75	1391.73	910.88	2302.61	2150.70	1407.81	3558.51
23	3.67	68.20	71.87	1454.99	952.28	2407.27	2248.46	1471.80	3720.26
24	3.83	71.16	75.00	1518.25	993.69	2511.94	2346.22	1535.79	3882.01
25	3.99	74.13	78.12	1581.51	1035.09	2616.60	2443.98	1599.78	4043.76
26	4.15	77.10	81.24	1644.77	1076.49	2721.26	2541.74	1663.77	4205.51
27	4.31	80.06	84.37	1708.03	1117.90	2825.93	2639.50	1727.76	4367.26
28	4.47	83.03	87.49	1771.29	1159.30	2930.59	2737.26	1791.75	4529.01
29	4.63	85.99	90.62	1834.55	1200.70	3035.26	2835.02	1855.74	4690.76
30	4.79	88.96	93.74	1897.81	1242.11	3139.92	2932.78	1919.74	4852.51
Total	74.2	1378.8	1453.0	29416.0	19252.6	48668.7	45458.0	29755.9	75213.9

6.5.2 Cost Benefit Analysis

An evaluation of the cost/benefits of applying aftertreatment control strategies to SORDEs was also done in this study. For this task, the methodology utilized by the EPA as part of its 2004 rulemaking effort was utilized. This preliminary cost/benefit analysis was done based on estimates of the incremental cost of aftertreatment technologies utilized for the emissions improvements and estimates of their overall emissions benefits, as discussed in section 6.5.1. The cost per ton off emission reduction of the newer standards was based on the net present value for all costs incurred and all emission reductions generated over a 30-year time window following implementation of the rule. The incremental costs of the DOCs, DPFs, and SCRs were based on a study conducted by the International Council for Clean Transportation (ICCT) to evaluate what the costs of such systems would be for 1.5 to 3 liter engines, which are typical of the engine sizes found in European automobiles, but are also representative of the size engines that are utilized for 0 to 75 hp off-road applications. For engines displacement sizes ranging from 1.5-3 liters, long term cost estimates ranged from $62-$116 for DOCs, from $266-$468 for DPFs, and from $418-$526 for SCRs. Based on the results from the ICCT study, aftertreatment costs were estimated to be $266 + $62 = $328 for a DPF + DOC for under 25 hp engines, representing values for 1.5-liter engines. For the cost of adding SCR NOx aftertreatment to 25 to 75 hp engines, an estimate of $474 was utilized, which represents an average of the cost estimates for 2- and 2.5-liter engines.

The costs for the individual aftertreatment systems can be combined with the engine populations to provide an estimate of the total costs of implementing the aftertreatment

systems. For this estimate, the costs were applied to equipment population estimates of 0 to 75 hp based on CARB emissions inventory estimates, as shown in Table 6-5. The cost estimates for the DPF+DOC can be combined with the engine populations for the <25 hp engines to provide a cost estimate for implementing more stringent regulations on PM emissions in this engine size range. These costs would be applied to 10,448 engines for the 0 to 10 hp category and 125,057 engines for the 10 to 25 hp category. In total the cost of implementing DPF + DOCs for the entire fleet under 25 hp small off-road diesel engines would be $44,445,640. The cost estimates for the SCR systems on 25 to 75 hp engines can be determined using a similar methodology. The total number of engines in the 25 to 50 hp category is 79,622 engines, and the total number of engines in the 50 to 75 hp category is 41,666 engines. With that the total cost of implementing SCR technology for the entire population of 25 to 75 hp engines would be $57,490,512.

Based on the cost estimates developed and emission benefits described above, cost/benefit estimates can be made. A summary of the costs and benefits for enhanced emissions controls for 25 to 75 hp and under 25 hp SORDEs is provided in Table 6-6. Based on these estimates, the cost benefits in $ per lb of emission reduction were $15.29 for PM for the under 25 hp category and range from $0.38 to $0.59 for NOx in the 25 to 75 hp category. For PM, the cost benefits in $ per lb of emission reduction are $23.09 for the 0 to 10 hp category and $14.87 for the 10 to 25 hp category. For the 25 to 50 hp category, the cost benefits in $ per lb of emission reduction range from $0.42 to $0.64 for NOx. For the 50 to 75 hp category, the cost benefits in $ per lb of emission reduction range from $0.33 to

$0.51 for NOx. Overall, these NOx costs are cheaper than approximately 70 to 80% of estimates for previous CARB rulemaking efforts (CARB, 2001, 2004, 2005, 2007).

Table 6-5: Population Breakdown of Small Off-road Diesel Engines under 75 hp in California

Small Off-Road Equipment Category by hp range	population			
	0-10	10-25	25-50	50-75
Total	**10448**	**125057**	**79662**	**41666**
Agricultural Tractors		31511	26029	28229
Transport Refrigeration Units	255	7789	26799	
Lawn & Garden Tractors		42716		
Commercial Turf Equipment		11943		
Welders		3646	5254	
Generator Sets		9890	5102	
Pumps	4305	5572	2233	
Air Compressors		172	1051	
Other Agricultural Equipment		751		
Crushing/Proc. Equipment			213	
Hydro Power Units	55	218		
Pressure Washers		325	122	
Sprayers		290	435	150
Signal Boards	3752	3745	18	
Rollers	806	1141	3967	33
Cement and Mortar Mixers	681	740		
Plate Compactors	429	428		
Other General Industrial/Construction Equipment	165	384	2176	823
Skid Steer Loaders		2554	2747	9324
Aerial Lifts		1241	3518	3106

Table 6-6: Cost-Benefit Analysis

	PM			NO_x					
	(Control efficiency 95%)			(Control efficiency 55%)			(Control efficiency 85%)		
	0-10 hp	10-25 hp	Total	25-50 hp	50-75 hp	Total	25-50 hp	50-75 hp	Total
Cost of DOC/DPF ($)	328	328	NA	NA	NA	NA	NA	NA	NA
Cost of SCR ($)	NA	NA	NA	474	474	NA	474	474	NA
# of Units	10,448	125,057	135,505	79,622	41,666	121,288	79,622	41,666	121,288
Total Incremental Cost ($)	$3,426,944	$41,018,696	$44,445,640	$37,740,828	$19,749,684	$57,490,512	$37,740,828	$19,749,684	$57,490,512
Total Emissions Reduction (tons)*	74.21	1378.82	1453.03	29416.09	19252.67	48668.76	45458.03	29755.91	75213.94
Cost per Ton ($)	$46,176.52	$29,749.17	$30,588.20	$1,283.00	$1,025.82	$1,181.26	$830.23	$663.72	$764.36
Cost per lb. ($)	$23.09	$14.87	$15.29	$0.64	$0.51	$0.59	$0.42	$0.33	$0.38

* Assuming that the turn over of the entire statewide off-road fleet will take 30 years, and that the annual fleet turn over rate is evenly distributed over those 30 year

6.6 Conclusions

The results of this study suggest that it is now feasible to apply more stringent emissions controls for the SORDE category of mobile sources. This would provide important emissions benefits for NOx and PM reductions. This study assessed the impact and deterioration of applying new technology after-treatment systems to 4 engines in the SORDE category. Two engines under 25 hp were tested with a DPF and 2 engines between 25 and 75 hp were tested with an SCR. The DPFs showed >98% PM reductions for a baseline degreened and 1,000-hour aging tests. NOx aftertreatment was demonstrated on two 25 to 50 hp engines in a ride mower and skid steer. The NOx aftertreatment systems provided reduction ranging from 70 to 91% for a steady-state C1 cycle. Lower NOx reductions from 26 to 65% were seen for hot and cold start NRTC tests, as the exhaust temperature was below that required to begin dosing during the initial parts of these cycles. No significant deterioration was seen after the 1,000-hour durability testing with some after-treatment systems providing better emissions reductions after the durability tests.

Emissions inventory estimates suggest that the adoption of new standards can provide a PM reduction of 3.8% and a NOx reduction of 8.8-13.7% for the total off-road equipment emissions inventory. A cost benefit analysis indicated that the price of implementing DPFs on engines below 25hp would cost a total of $15.29 per pound of PM saved, while the price of implementing SCRs on engine between 25-75 hp would cost between $0.38 - $0.59 per pound of NOx saved, which compares very favorably to other rulemakings adopted by CARB. While the results of this study are promising, it should be noted that given the wide

variety of applications for off-road engines, the practicality of implementing such aftertreatment systems could vary between applications depending on the potential to transition to electric motors or gasoline engines, the cost of the aftertreatment system relative to the overall cost of the equipment it is being used in, and the complexity of the controls that would be required to manage the aftertreatment system for different applications.

6.7 References

Anenberg, Susan C., et al. "Impacts and Mitigation of Excess Diesel-Related NOx Emissions in 11 Major Vehicle Markets." *Nature*, vol. 545, no. 7655, 2017, pp. 467–471., doi:10.1038/nature22086.

Bartley, G., 2012, The DAAAC Protocol for Accelerated Aging of Diesel Aftertreatment Systems, 15th Cross-Cut Lean Exhaust Emission Reduction Simulations, Dearborn, MI, April-May.

Biswas, Subhasis, et al. "Physical Properties of Particulate Matter (PM) from Late Model Heavy-Duty Diesel Vehicles Operating with Advanced PM and NOx Emission Control Technologies." *Atmospheric Environment*, vol. 42, no. 22, 2008, pp. 5622–5634., doi:10.1016/j.atmosenv.2008.03.007.

Blakeman, P. G., et al. "Investigations into NOx Aftertreatment with Urea SCR for Light-Duty Diesel Vehicles." *SAE Technical Paper Series*, 2001, doi:10.4271/2001-01-3624.

CARB (2019a) MSEI - Documentation - Off-Road - Diesel Equipment, https://ww2.arb.ca.gov/our-work/programs/mobile-source-emissions-inventory/road-documentation/msei-documentation-road.

CARB (2019b) MSEI - Documentation - Off-Road - Diesel Equipment, Off-Road 2007, https://ww2.arb.ca.gov/our-work/programs/mobile-source-emissions-inventory/road-documentation/msei-documentation-road.

Dallmann, Timothy R., and Robert A. Harley. "Evaluation of Mobile Source Emission Trends in the United States." *Journal of Geophysical Research*, vol. 115, no. D14, 2010, doi:10.1029/2010jd013862.

Guan, Bin, et al. “Review of State of the Art Technologies of Selective Catalytic Reduction of NOx from Diesel Engine Exhaust.” *Applied Thermal Engineering*, vol. 66, no. 1-2, 2014, pp. 395–414., doi:10.1016/j.applthermaleng.2014.02.021.

Haugen, Molly J., and Gary A. Bishop. “Long-Term Fuel-Specific NOx and Particle Emission Trends for In-Use Heavy-Duty Vehicles in California.” *Environmental Science & Technology*, vol. 52, no. 10, 2018, pp. 6070–6076., doi:10.1021/acs.est.8b00621.

Haugen, Molly J., et al. “Evaluation of Heavy- and Medium-Duty On-Road Vehicle Emissions in California’s South Coast Air Basin.” *Environmental Science & Technology*, vol. 52, no. 22, 2018, pp. 13298–13305., doi:10.1021/acs.est.8b03994.

Jiang, Yu, et al. “Characterizing Emission Rates of Regulated Pollutants from Model Year 2012 + Heavy-Duty Diesel Vehicles Equipped with DPF and SCR Systems.” *Science of The Total Environment*, vol. 619-620, 2018, pp. 765–771., doi:10.1016/j.scitotenv.2017.11.120.

Johnson, By Tim. “Diesel Engine Emissions and Their Control.” *Platinum Metals Review*, vol. 52, no. 1, 2008, pp. 23–37., doi:10.1595/147106708x248750.

Koebel, M, et al. “Urea-SCR: a Promising Technique to Reduce NOx Emissions from Automotive Diesel Engines.” *Catalysis Today*, vol. 59, no. 3-4, 2000, pp. 335–345., doi:10.1016/s0920-5861(00)00299-6.

Kumar, K. Senthil, and R. Thundil Karuppa Raj. “Effect of Fuel Injection Timing and Elevated Intake Temperature on the Combustion and Emission Characteristics of Dual Fuel Operated Diesel Engine.” *Procedia Engineering*, 2013, pp. 1191–1198.

Mikulic, Ingo, et al. “Dependence of Fuel Consumption on Engine Backpressure Generated by a DPF.” *SAE International*, 12 Apr. 2010.

Millo, Federico, et al. “Impact on Vehicle Fuel Economy of the Soot Loading on Diesel Particulate Filters Made of Different Substrate Materials.” *Energy*, vol. 86, 2015, pp. 19–30., doi:10.1016/j.energy.2015.03.076.

Misra, Chandan, et al. “In-Use NOxEmissions from Model Year 2010 and 2011 Heavy-Duty Diesel Engines Equipped with Aftertreatment Devices.” *Environmental Science & Technology*, vol. 47, no. 14, 2013, pp. 7892–7898., doi:10.1021/es4006288.

Mokhri, M.A., et al. “Soot Filtration Recent Simulation Analysis in Diesel Particulate Filter (DPF).” *International Symposium on Robotics and Intelligent Sensors 2012 (IRIS 2012), 2012*

Pandya, Robert J, et al. “Diesel Exhaust and Asthma: Hypotheses and Molecular Mechanisms of Action.” *Environmental Health Perspectives*, vol. 110, no. suppl 1, 2002, pp. 103–112., doi:10.1289/ehp.02110s1103.

Pope, C. Arden, and Douglas W. Dockery. “Health Effects of Fine Particulate Air Pollution: Lines That Connect.” *Journal of the Air & Waste Management Association*, vol. 56, no. 6, 2006, pp. 709–742., doi:10.1080/10473289.2006.10464485.

Praveena, V., and M. Leenus Jesu Martin. “A Review on Various after Treatment Techniques to Reduce NOx Emissions in a CI Engine.” *Journal of the Energy Institute*, vol. 91, no. 5, 2018, pp. 704–720., doi:10.1016/j.joei.2017.05.010.

Preble, Chelsea V., et al. “Control Technology-Driven Changes to In-Use Heavy-Duty Diesel Truck Emissions of Nitrogenous Species and Related Environmental Impacts.” *Environmental Science & Technology*, vol. 53, no. 24, 2019, pp. 14568–14576., doi:10.1021/acs.est.9b04763.

Rossomando, B., et al. “Experimental Characterization of Ultrafine Particle Emissions from a Light-Duty Diesel Engine Equipped with a Standard DPF.” *Proceedings of the Combustion Institute*, 2020, doi:10.1016/j.proci.2020.09.011.

Roy, Murari Mohon, et al., “Effect of Engine Backpressure on the Performance and Emissions of a CI Engine” *The 7th Jordanian International Mechanical Engineering Conference (JIMEC’7)*, 2010

Shao, Shushan, et al. “Effects of a DOC+DPF System on Emission Characteristics of China Π Engineering Vehicle Diesel Engine and Influence Factors of Trapping Efficiency of PM for DOC+DPF System.” *Energy Sources, Part A: Recovery, Utilization, and Environmental Effects*, vol. 41, no. 5, 2018, pp. 527–541., doi:10.1080/15567036.2018.1520337.

United States Environmental Protection Agency, 2004, Final Regulatory Analysis: Control of Emissions from Nonroad Diesel Engines, Document # EPA420-R-04-007, May.

United States Environmental Protection Agency, “Air Pollutant Emissions Trends Data.”, 30 Apr. 2020, www.epa.gov/air-emissions-inventories/air-pollutant-emissions-trends-data.

“United States: Nonroad Diesel Engines.” *Emission Standards: USA: Nonroad Diesel Engines*, Dec. 2017, dieselnet.com/standards/us/nonroad.php#tier4.

Vermeulen, Roel, et al. “0374 Exposure-Response Estimates for Diesel Engine Exhaust and Lung Cancer Mortality Based on Data from Three Occupational Cohorts.” *Occupational and Environmental Medicine*, vol. 71, no. Suppl 1, 2014, doi:10.1136/oemed-2014-102362.145.

Welch, W., and Durbin, T.D., 2004. Emissions and Demonstration of an Emissions Control Technology for Small Two-Stroke Utility Engines. *Journal of Air and Waste Management*, vol. 54, 200-206.

White, Jeff J., et al. "Durability of Low-Emissions Small Off-Road Engines." *SAE Technical Paper Series*, 2004, doi:10.4271/2004-32-0058.

Williams, Aaron, et al. "Impact of Fuel Metal Impurities on the Durability of a Light-Duty Diesel Aftertreatment System." *SAE Technical Paper Series*, 2013, doi:10.4271/2013-01-0513.

Yang, Jiacheng. "Impact of Alternative Fuels and Emission Control Systems on Small Engines to Large Ocean Going Vessels." *University of California, Riverside*, 2018.

Zhao, Hong, et al. "Effects of Fuel Sulfur Content and Diesel Oxidation Catalyst on PM Emitted from Light-Duty Diesel Engine." *Energy & Fuels*, vol. 24, no. 2, 2010, pp. 985–991., doi:10.1021/ef900982c.

7. Sources of Air Pollutants from a Tier 2 Ocean-Going Container Vessel and Panamax Tanker Vessel

7.1 Abstract

This study assessed the gaseous and particulate emissions from a Tier 2 oceangoing vessel using two emission control area (ECA) compliant fuels, a very low sulfur marine gasoil (MGO) and a novel ultra-low sulfur heavy fuel oil (ULSHFO). In-use emissions are reported for the main engine when the ship traveled in within California's ECA, whereas emissions for the auxiliary engine and boiler are presented when the ship was at-berth in the port of Long Beach. For the auxiliary boiler, emissions of carbonyl compounds and metallic elements were also characterized. The ULSHFO showed higher nitrogen oxide (NOx) emissions than MGO for both the main and auxiliary engines, but not at statistically significant levels, whereas for the auxiliary boiler the ULSHFO showed statistically significant increases in NOx emissions compared to MGO. NOx emissions for this vessel's main and auxiliary engines were within the certification limits for both fuels. Particulate matter (PM2.5) and black carbon emissions were higher for the ULSHFO and decreased with higher engine load conditions. The main engine PM2.5 composition was dominated by organic carbon and the auxiliary engine PM composition was primarily comprised of elemental carbon. For both engines, there was little contribution of sulfate due to the very low sulfur content in both fuels. Formaldehyde and acetaldehyde were the major aldehyde species in boiler exhaust. Sulfur, vanadium, and iron were the most abundant elements detected in PM2.5 emissions. Overall, this work demonstrated the potential global benefit

of using ultra-low sulfur residual fuels, however, their use near ports will likely increase local emissions compared to middle distillate fuels.

7.2 Introduction

The maritime industry is playing an important role in the transport of goods around the world, with ocean-going vessels being responsible for over 80% of global trade by volume (UNCTAD, 2017). At the same time, the shipping sector is recognized as a major contributing source to air pollution, especially in coastal areas (Corbett, 2003; Petzold et al., 2008). The major air pollutants from the shipping sector are sulfur oxides (SOx), nitrogen oxides (NOx), black carbon, particulate matter (PM), and carbon dioxide (CO_2) (Yau et al., 2012; Zetterdahl et al., 2016). Studies have shown that more than 70% of marine emissions can travel up to 400 kilometers (km) inland, affecting air pollution and human health (Corbett et al., 2007; Viana et al., 2009). Climate change is also affected by international shipping due to the positive radiative forcing of CO_2 and black carbon emissions, and the secondarily formed ozone (Winnes et al., 2015; Eyring et al., 2010). The importance of emissions from the shipping sector to the anthropogenic emission burden and air pollution has been recognized by the International Maritime Organization (IMO) through Annex VI of the International Convention for the Prevention of Pollution from Ships of the MARPOL. These regulations established sulfur emission-controlled areas (SECAs) and set a global limit on fuel sulfur content to 0.5% starting from January 1, 2020 to primarily control SOx emissions. Regarding NOx emissions, four emission-controlled areas (ECAs) have been established by MARPOL, including the North Sea, the

Baltic Sea, the English Channel, and the North America and the US Caribbean coasts. Moreover, Annex VI also imposed a maximum sulfur limit of 0.1% within ECAs.

Ship emissions are influenced by several factors, including ship operation and fuel type. Different operations and speeds have different power requirement and hence different emission profiles. Ships maneuvering in port areas requires slow speeds and transient operation, where engine loads may rapidly change. During cruising conditions in the open sea, the main engines are usually operating at intermediate loads, whereas typically low loads are applied when the ship is maneuvering in the port. Studies have shown that gaseous and particulate emissions are highly dependent on engine operation, with engine load variations affecting combustion conditions and pollutant formation (Petzold et al., 2010; Hountalas et al., 2014; Zhang et al., 2016; Khan et al., 2012a). Chu-Van et al. (2018) found elevated emission factors of carbon monoxide (CO), total hydrocarbons (THC), PM, and particle number during maneuvering at a port of a large bulk carrier compared to cruising conditions. Agrawal et al. (2008) showed higher NOx emissions when they tested an oceangoing container vessel at low speed and low load conditions compared to intermediate engine load at normal cruise speed. Khan et al. (2012b) also showed higher CO and SO_2 emissions at low engine loads from a Tier 1 large container vessel, but lower PM mass emissions at low engine loads.

Fuel type and composition are also important factors in gaseous and particulate emissions formation. Heavy fuel oil (HFO) contains residues and distillates of fuel refining process, such as sulfur, aromatics, and metals, and is mainly used in the main engines used for

propulsion. Significant improvements on fuel quality have been made with the aim to reduce emissions from ships, with fuel switching capabilities when entering the SECA regions being the most important. A number of studies have shown that switching from HFO to marine gas oil (MGO), a middle distillate fuel used in auxiliary and main engines, could potentially result in lower gaseous and particulate emissions (Moldanova et al., 2013; Browning et al., 2012; Mueller et al., 2015; Khan et al., 2012). Gysel et al. (2017) tested an oceangoing vessel operating within ECAs on a novel low-sulfur heavy fuel oil (LSHFO) and a distillate ECA MGO fuel. They found higher NOx emissions with MGO than LSHFO, and higher PM and particle number emissions with LSHFO than MGO. Zetterdahl et al. (2016) found lower emissions of SO_2, PM mass, total volatile organic compounds (VOCs), and polycyclic aromatic hydrocarbons (PAHs) from switching between HFO and distillate fuels on a ship operating in a SECA. Reda et al. (2015) showed increases in carbonyl emissions with HFO compared to a SECA diesel fuel using a single-cylinder diesel research engine, with formaldehyde and heavier carbonyls being predominant in the emissions of HFO. Similarly, Wu et al. (2018) showed higher PM and PAH emissions, as well as higher oxidative activity and cytotoxicity with HFO compared to diesel fuel when they tested emissions from a container ship.

In addition to main and auxiliary engines, ship emissions are also generated from boilers used to produce hot water and steam, but in lower concentrations (Chen et al., 2017). Boilers are typically used when at berth or operating on low main engine loads to meet demands for heating on board (Zenczak, 2013; Starcrest, 2011). Unlike the main and auxiliary engines, regulations applicable to ship boilers are less restrictive, with ship boiler

emissions being indirectly regulating by restricting the fuel sulfur content when used in ports and SECA regions. Hulskotte and Denier van der Gon, (2010) showed that oceangoing vessels, tankers, and container ships consume the greater part of the fuels when at-berth in boilers. Additionally, they showed lower emission factors from boilers compared to reciprocating combustion engines. Agrawal et al. (2008b) investigated the emissions of an auxiliary boiler powered by HFO on a crude oil tanker operating at sea. They found PM and NOx emissions were lower in an auxiliary boiler compared to the main engine, while acetaldehyde was the primary carbonyl in the auxiliary boiler. Cooper, (2003) also showed lower NOx, THC, SO_2, and PAH emissions from boiler use compared to the main or auxiliary engines. Yau et al. (2012) also showed that boilers generally contribute less than 5% of the NOx, PM, and SO_2 emissions from oceangoing vessels in Hong Kong when compared to main and auxiliary engines.

As highlighted above, the body of literature on ship emissions characterization is rich and has primarily focused on older technology engines when operated on fuels with relatively high sulfur contents. The present study provides better understanding on the characterization of gaseous and particulate emissions from a modern Tier 2 oceangoing vessel operating on a new generation ultra-low sulfur HFO suitable for use in SECAs. For the main engine, emissions were measured on-board for both fuels while the vessel was cruising from the Port of Long Beach to the Port of Oakland in California. For the auxiliary engine and the auxiliary boiler, emissions were measured for both fuels while the vessel was at-berth at the Port of Long Beach and during loading and unloading cargo. In addition to the Tier 2 OGV, emissions were also characterized from the auxiliary boiler of a modern

Panamax tanker. The results of this study are discussed as a function of fuel type and engine operation conditions.

7.3 Experimental

7.3.1 Tier 2 Test vessel, main and auxiliary engines, and boiler

The test article was a modern container vessel (Class DNV+1A1 Container Carrier) manufactured by Hyundai Samho Heavy Industries, South Korea, with a deadweight tonnage of 141,550 tons, a net tonnage of 140,979 tons, an overall length of 350 m, and a breadth of 48.2 m. The vessel's service speed was 18 knots, and it was equipped with one main engine, five auxiliary engines, and one auxiliary boiler.

The main engine was a Tier 2 12-cylinder Hyundai MAN-B&W AA4214 72.24 MW SSD two-stroke engine with a total displacement of 21723 L. The auxiliary engines were Tier 2 HiMSEN BA3707-1 2.87 MW medium speed diesel four-stroke engines with a total displacement of 193 L each over 6-cylinders. The auxiliary boiler (model RP-500M) was manufactured by KangRim Heavy Industries Company Ltd., South Korea. It was a vertical boiler with a pressure jet system and a maximum fuel rate heating capacity of 408 kg/hr.

7.3.2 Modern Tanker vessel and Boiler

The test article was 2014 Panamax tanker vessel with a 155,374 dead weight tonnage capacity and overall length of 275m by 48m breadth. The Auxiliary boiler tested was manufactured by Alfa Laval. It was a large capacity boiler with a steam rating of 50,000

kg/h. This is near the highest level of steam production that is commercially offered suggesting the emissions will be of interest to regulators.

7.3.3 Test fuels

Two ECA compliant fuels, a standard low-sulfur MGO and a commercially available ultra-low sulfur HFO (ULSHFO) were utilized for this study. The main fuel properties are shown in Table 7-1. For this campaign, an exemption was granted by the California Air Resources Board (CARB) to allow the main and auxiliary engines, and the auxiliary boiler to be operated in Regulated California Waters (a zone approximately 25 nautical miles seaward of the California baseline) on the ULSHFO instead of the low sulfur MGO, as required by the California Fuel Rule. While both fuels meet ECA low-sulfur fuel requirements, CARB regulations require marine fuels to meet specification for distillate grades, such as MGO. The auxiliary boiler from the Panamax tanker was only tested using MGO fuel.

Table 7-1: Fuel properties for the ULSHFO and MGO

Properties	Test Method	ULSHFO	MGO
Density at 15°C, kg/m^3	ISO 12185	853.2	841.0
Kinematic viscosity at 40°C, mm^2/s	ASTM D445	20.96	3.474
Micro carbon residue, % m/m	ASTM D524	0.5	0.08
Sulfur content, ppm	ASTM D2622	893.4	384.4
Calculated carbon aromaticity index (CCAI)	ISO 8217	761	794
Net specific energy, MJ/kg	ISO 8217	42.99	42.73
Ash content, % m/m	LP 1001	<0.01	<0.01
Pour point, °C	ISO 3016	18	3

7.3.4 Test protocol

Direct drive engines (i.e., main ship engines) are certified per the ISO 8178-4 E3 marine test cycle, whereas constant speed auxiliary engines follow the ISO-8178-4 D2 test cycle. These test cycles include loads that range from idle to 100%. While such loads can readily be achieved on engine dynamometers, there are greater limitations on the load ranges that the engines are subjected to under in-use conditions. For this testing, the maximum allowable main engine load was 43% of the maximum continuous rating (MCR) and 63% MCR for the auxiliary engine. While at sea, the main engine typically operates at 45% load and two auxiliary engines are operated for ship services, hoteling, and maneuvering power (typically at loads from 30% to 60% depending on the vessel's needs). During berth entry and exit maneuvers, the main engine power is reduced to 25% to 30% load, while the auxiliary engines increase in load, but to a point still below 60%. While at berth (loading and unloading goods), the auxiliary engines are used at around 50% load and the main engine is at zero load. Most of the vessel operation is based on at-sea conditions, estimated to be 95% of the vessel operation, while berth exit and entry and dock conditions represent approximately 1% (or less) and 4%, respectively, of the operation. For the main engine, emission measurements were performed at engine loads between 9% to 45%, representing low speed operation, such as vessel speed reduction (VSR) and port maneuvering, and up to cruise speeds, respectively. The auxiliary engine testing followed the ISO-8178-4 D2 test cycle at loads between 25% to 65%. For the auxiliary boilers, emission measurements were made when operated at 60% load and 65% load for the Tier 2 vessel and Panamax tanker, respectively, which is considered as the most representative load for normal

operation since boilers operate at a single load and cycle on and off where the frequency varies with demand.

7.3.5 Emissions analysis

Emissions testing was conducted according to guidelines set forth in the 40 Code of Federal Regulations (CFR) Part 1065, with specific details following ISO 8178-1 for dilution and exhaust gas sampling. For each mode and each combustion source, emissions were measured in triplicate. Emissions of NOx, CO, and SO_2 were obtained with a Horiba PG-350, utilizing a heated chemiluminescence detector for NOx and a non-dispersive infrared absorption for CO and SO_2. PM2.5 emissions were sampled using a partial flow dilution system that was developed based on the ISO 8178-1 protocol. Total PM2.5 mass was collected on 47 mm 2 μm pore Teflon filters (Whatman brand). The filters were measured for net gains using a UMX2 Mettler Toledo ultra-precision microbalance with a buoyancy correction in accordance with the weighing procedure guidelines set forth in the CFR. Before and after collection, the filters were conditioned for a minimum of 24 hours in an environmentally controlled room (RH = 40%, T = 25 °C) and weighed daily until two consecutive weight measurements were within 3 μg. Real-time soot mass or black carbon emissions were measured using an AVL Micro-Soot Sensor (MSS-483). The MSS is an instrument that measures soot mass concentration at a frequency of one Hertz basis using a photo acoustic detection technique, where the light-absorbing PM components (such as soot particles) are exposed to laser light that is periodically modulated at the acoustical resonant frequency.

Elemental and organic carbon samples (EC/OC) were collected in parallel on pre-cleaned QAT Tissuquartz quartz-fiber filters (Pall-Gelman, Ann Arbor, MI, USA). Quartz fiber filters were pre-cleaned to remove carbonaceous contaminants by firing for 5 hours at 600 °C. A Thermal/Optical Carbon Aerosol Analyzer (Sunset Laboratory, Forest Grove, OR) operating using NIOSH (National Institute of Occupational Safety and Health) Method 5040 was used to analyze OC and EC. The ionic sulfate component in the PM was measured with an ion chromatography (IC) method.

Carbonyl emissions and metals were measured for both auxiliary boilers at 60% and 65% load, respectively. Samples for carbonyl analysis were collected on 2,4-dinitrophenylhydrazine (DNPH) coated silica cartridges (Waters Corp., Milford, MA). The DNPH cartridges were eluted with 2 mL of acetonitrile (HPLC grade, EMD Millipore Corporation, Billerica, MA, USA) and analyzed with a high-performance liquid chromatography (HPLC) system (Waters 2690 Alliance System with 996 Photodiode Array Detector) following a modified US-EPA TO-11A method. The HPLC response was calibrated with a certified calibration mixture purchased from AccuStandard Inc. (New Haven, CT 06513, USA). Trace elements and metals were collected onto 47 mm Teflon filters and subsequently analyzed using the X-Ray fluorescence (XRF) method, as per EPA IO-3.3.

7.4 Results and Discussion

7.4.1 Tier 2 Vessel

7.4.1.1 Gaseous emissions

Emissions of NOx, expressed in g/kW-hr, for the main and auxiliary engines, as well as for the auxiliary boiler, expressed in g/kg-fuel are shown in Figure 7-1 (a-b). NOx emission factors (EFs) are also shown in Table 5-3. NOx emissions from the main engine when operated on the ULSHFO ranged from 17.7 to 28.8 g/kW-hr across the different engine loads. NOx emissions with the MGO were found at slightly lower levels (about 5%) than ULSHFO for each engine load point (Figure 1a). The main engine NOx emissions were within the expectations of Tier 2 Category 3 marine engines, given in-use measurement uncertainties of ~20%, and comparable to the certification values for Tier 2 Category 1 marine engines. NOx emissions are largely dependent on combustion temperatures, and thus are expected to be primarily related to engine load. For both fuels, NOx emissions trended lower with increasing engine load for both the main and auxiliary engines. Our results agree with previous studies showing reductions in NOx emissions with higher engine loads (Sippula et al., 2014; Huang et al., 2018; Zetterdahl et al., 2016). The reduced NOx emissions with higher engine loads could be due to the lower availability of oxygen for NOx formation with increased engine load. In addition, other studies have also shown lower NOx emissions with fuel switching from HFO to MGO, even though the present results showed markedly lower reductions than previously reported (Moldanova et al., 2013; Huang et al., 2018; Browning et al., 2012). The slightly higher NOx emissions with

the ULSHFO could be ascribed to its higher nitrogen content compared to middle distillate fuels (although this property was not measured, usually heavy fuel oils contain more nitrogen than middle distillates), which can contribute to the formation of fuel NOx pathways during combustion (Haglind, 2008). Additionally, middle and light distillate fuels, owned to their lower density and viscosity, are associated with shorter ignition delay than HFO, which leads to lower peak flame temperatures and reduced formation of NOx (Ntziachristos et al., 2016).

NOx emissions from the auxiliary engine followed similar patterns to those of the main engine, but at a lower emission rate (Figure 1b). The auxiliary engine NOx emissions ranged from 8.1 to 9 g/kW-hr for the MGO fuel, with some slight increases in NOx emissions (about 3%) for the ULSHFO. It is worth noting that the estimated ISO weighted NOx emissions in this study were found to be lower than the Tier 2 standard (9.8 g/kW-hr) for this size and category engine. In slow-speed, two-stroke diesel engines, thermal NOx formation occurs primarily on the lean side of the flame and increases with the combustion temperature and residence time, as well as oxygen availability. Thus, slow-speed engines produce more NOx than the higher rotational speed auxiliary engines due to the longer combustion process and longer engine stroke, and the more time available for thermal NOx formation (Ntziachristos et al., 2016; Lamas and Rodriguez, 2012).

Boiler NOx emissions at 60 % load averaged 1.68 g/kg-fuel and 2.28 g/kg-fuel for the MGO and ULSHFO, respectively. NOx emissions for the ULSHFO showed an increase of 36% compared to MGO, at a statistically significant level. Agrawal et al. (2008) also

showed lower NOx emissions for an auxiliary boiler compared to the main and auxiliary engines of a crude oil tanker.

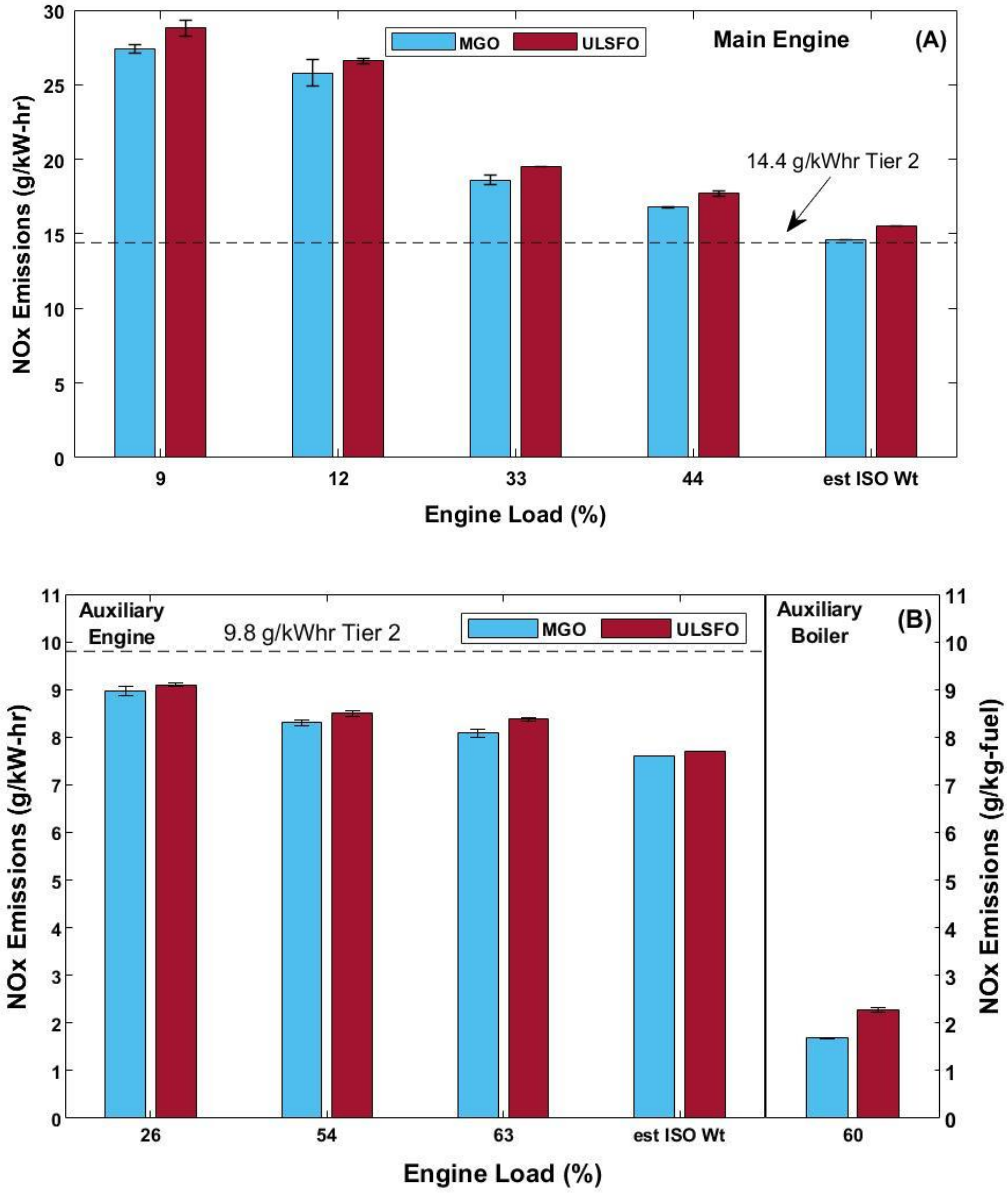

Figure 7-1 (a-b): NOx emissions for the main engine (top panel, A) and the auxiliary engine and boiler (bottom panel, B) for the ULSHFO and MGO; est ISO Wt is the estimated weighted

Table 7-2 presents the CO emissions for the main and auxiliary engines, and the auxiliary boiler for both fuels, whereas CO EFs are shown in Table 7-3. CO emissions depend not only on engine load and engine power, but also on the gradient of engine power. For the main engine, CO emissions were relatively constant as a function of engine load. For the lower loads, CO emissions were higher for the ULSHFO compared to MGO, while for the higher loads the differences in CO emissions between the fuels were insignificant. For the auxiliary engine, CO emissions were the highest at light load and significantly reduced with higher engine loads. At light load, CO emissions showed statistically significant increases for the ULSHFO compared to MGO, whereas CO emissions for the ULSHFO were lower relative to MGO at higher loads. CO emissions from the auxiliary boiler were at lower levels compared to the main and auxiliary engines, with the ULSHFO showing significantly higher CO emissions relative to MGO at 60% load. A number of studies have shown elevated CO emissions at low load conditions, which can be ascribed to the incomplete combustion at low load operation caused by the local fuel-poor regions and the low combustion temperature (Zetterdahl et al., 2016; Jiang et al., 2019; Chu-Van et al., 2019).

CO_2 emissions dominated the gaseous emissions from the main and auxiliary engines and the auxiliary boiler, as shown in Table 7-2. CO_2 EFs are presented in Table 7-3. CO_2 emissions are largely dependent by the engine power, the engine efficiency, and the elemental composition of the fuel, and directly related to fuel consumption (Haglind, 2008). For the main and auxiliary engines, CO_2 emissions were lower at higher engine loads, with the ULSHFO showing higher CO_2 levels than the MGO. The auxiliary engine

showed higher CO_2 emissions than the main engine, as reported in other work (Chu-Van et al., 2018; Celo et al., 2015). These increases could be due to the lower combustion efficiency for the smaller displacement engine and design differences between four-stroke and two-stroke engines, as opposed to differences in carbon-to-hydrogen ratio (distillate fuels generally contain slightly more hydrogen). For the auxiliary boiler, CO_2 emissions were constant for both fuels at about 3180 g/kg-fuel. Our results generally agree with CO_2 emission levels reported in previous studies and with the trend of lower CO_2 emissions with increasing engine load (Chu-Van et al., 2018; Agrawal et al., 2008; Cooper, 2003; Moldanova et al., 2013; Huang et al., 2018).

SO_2 emissions are shown in Table 5-2, while SO_2 EFs are presented in Table 7-3. The amount of SO_2 emissions from ships is directly related by the sulfur content in the fuel. SO_2 emissions for the main and auxiliary engines were lower at higher engine loads as a result to the more efficient combustion that occurs at loads typical for cruising conditions compared to maneuvering at port. The use of ULSHFO resulted in about 2-times higher SO_2 emission levels compared to MGO. This finding is attributed to the ~2.3-times higher sulfur content for ULSHFO relative to MGO (0.089% vs 0.038%). SO_2 emissions from this study were found in significantly lower levels than those reported in previous studies due to the very low sulfur content in both fuels, in comparison with typical HFO fuels that can have sulfur levels between 0.5% to 3% (Chu-Van et al., 2018; Moldanova et al., 2013; Zetterdahl et al., 2016; Agrawal et al., 2008a; Browning et al., 2012; Winnes and Fridell, 2009). We expect that the SO_2 emissions reported here are representative of the current emissions inventory from oceangoing vessels and of future emission scenarios capturing

the decline of SO_2 emissions from ships when operated on ultra-low sulfur fuels. The auxiliary boiler showed higher SO_2 concentrations when compared to the main and auxiliary engines, with ULSHFO being higher than the MGO. This finding suggests that the contribution of SO_2 emissions from an auxiliary boiler when the ship is at-berth will likely be greater than cruising operation at sea. Higher SO_2 emissions from ships at ports will largely contribute to sulfate aerosols and will primarily affect populated communities closely adjacent to ports.

Carbonyl emissions were only measured for the auxiliary boiler at 60% load for both fuels. Carbonyl compounds are not present in the fuel and their formation depends on the partial oxidation of hydrocarbon components during combustion. Consistent with previous studies (Murphy et al., 2009; Reda et al., 2015; Agrawal et al., 2008), formaldehyde, acetaldehyde, and acetone were the most abundant carbonyls in the auxiliary boiler exhaust (Table 2). The dominant aldehyde for ULSHFO was acetaldehyde, while formaldehyde was the dominant aldehyde for MGO. These phenomena could be attributed to the compositional differences between the fuels and the different combustion behavior of these fuels, which affected the formation mechanisms of these saturated aliphatic aldehydes. The formaldehyde emissions ranged from 3.86 mg/kg-fuel for the ULSHFO to 0.69 mg/kg-fuel for the MGO. The acetaldehyde emissions ranged from 0.93 mg/kg-fuel for the ULSHFO fuel to 0.44 mg/kg-fuel for the MGO. While the concentrations of carbonyl compounds were relatively low, they can potentially be an important source of air pollution on a local scale, considering the amount of time ships spend hoteling in ports near populated areas.

Table 7-2: CO, CO_2, and SO_2 emissions for the main and auxiliary engines, and boiler when operated on ULSHFO and MGO as a function to engine load. Carbonyl emissions were only measured for the auxiliary boiler

Main Engine (g/kw-hr)							
Fuel	Load	CO	CO_2	SO_2	Formaldehyde	Acetaldehyde	Acetone
MGO	9%	0.19 ± 0.01	644 ± 3.4	0.15	-	-	-
	12%	0.19 ± 0.00	623 ± 0.0	0.15	-	-	-
	33%	0.20 ± 0.01	588 ± 0.4	0.14	-	-	-
	44%	0.19 ± 0.03	583 ± 0.0	0.14	-	-	-
ULSHFO	9%	0.21 ± 0.01	656 ± 0.2	0.36	-	-	-
	12%	0.20 ± 0.01	634 ± 1.0	0.35	-	-	-
	33%	0.19 ± 0.01	602 ± 0.3	0.33	-	-	-
	44%	0.19 ± 0.01	597 ± 0.3	0.33	-	-	-
Auxiliary Engine (g/kw-hr)							
MGO	26%	2.04 ± 0.03	784 ± 2.3	-0.003	-	-	-
	54%	0.87 ± 0.01	653 ± 0.6	0.001	-	-	-
	63%	0.81 ± 0.03	635 ± 0.8	-0.001	-	-	-
ULSHFO	26%	2.43 ± 0.01	787 ± 1.8	0.042	-	-	-
	54%	0.82 ± 0.01	669 ± 0.5	0.008	-	-	-
	63%	0.74 ± 0.01	651 ± 1.1	0.007	-	-	-
Auxiliary Boiler (g/kg-fuel)							
MGO	60%	0.01 ± 0.00	3174 ± 0.1	0.77	$6.9 \times 10^{-4} \pm 6.9 \times 10^{-5}$	$4.4 \times 10^{-4} \pm 8.0 \times 10^{-5}$	$4.3 \times 10^{-4} \pm 1.8 \times 10^{-4}$
ULSHFO	60%	0.13 ± 0.09	3178 ± 0.2	1.43	$3.9 \times 10^{-3} \pm 4.6 \times 10^{-4}$	$9.3 \times 10^{-4} \pm 1.8 \times 10^{-4}$	$1.1 \times 10^{-3} \pm 6.0 \times 10^{-4}$

Table 7-3: Emission factors (EFs) for the gaseous and particulate pollutants for the main and auxiliary engines, and the auxiliary boiler of the Tier 2 OGV

Main Engine Emission Factors										
Fuel	Engine Load	NOx (g/kg-fuel)	CO (g/kg-fuel)	CO_2 (g/kg-fuel)	SO_2 (g/kg-fuel)	PM2.5 (mg/kg-fuel)	EC (mg/kg-fuel)	Hydrated Sulphate (mg/kg-fuel)	OC (mg/kg-fuel)	Black Carbon (mg/kg-fuel)
MGO	9	135.2 ± 1.0	0.9 ± 0.1	3175 ± 0.4	0.14 ± 0.01	1086 ± 40	15.7 ± 0.0	10.9 ± 0.4	1046 ± 0	19.8 ± 1.3
MGO	12	131.4 ± 4.6	1.0 ± 0.0	3178 ± 0.2	0.13 ± 0.01	1184 ± 95	21.5 ± 2.0	11.8 ± 0.9	1113 ± 30	40.2 ± 2.6
MGO	33	100.8 ± 1.7	1.1 ± 0.2	3180 ± 0.2	0.07 ± 0.01	1263 ± 205	11.6 ± 0.6	12.6 ± 2.0	1026 ± 93	16.2 ± 3.7
MGO	44	91.9 ± 0.2	1.0 ± 0.0	3180 ± 0.3	0.05 ± 0.01	1067 ± 37	5.9 ± 0.4	10.7 ± 0.4	979 ± 68	8.2 ± 0.1
ULSD	9	139.4 ± 2.6	1.0 ± 0.1	3174 ± 1.0	0.19 ± 0.03	1688 ± 40	84.4 ± 2.0	50.6 ± 1.2	1485 ± 33	28.8 ± 1.5
ULSD	12	133.2 ± 1.2	1.0 ± 0.1	3177 ± 0.1	0.13 ± 0.00	1586 ± 53	79.3 ± 2.7	47.6 ± 1.6	1434 ± 45	43.1 ± 1.9
ULSD	33	103.2 ± 0.1	1.0 ± 0.1	3180 ± 0.1	0.07 ± 0.01	1469 ± 38	73.5 ± 1.9	44.1 ± 1.2	1292 ± 9	20.4 ± 1.0
ULSD	44	94.2 ± 0.8	1.0 ± 0.1	3179 ± 0.1	0.07 ± 0.00	1396 ± 17	69.8 ± 0.9	41.9 ± 0.5	1266 ± 5	11.2 ± 3.0
Auxiliary Engine Emission Factors										
MGO	26	36.1 ± 0.5	8.2 ± 0.1	3158 ± 0.2	0.00 ± 0.01	1194 ± 19	730.3 ± 21.6	11.9 ± 0.2	445.5 ± 16	836.8 ± 6.9
MGO	54	40.3 ± 0.5	4.0 ± 0.2	3166 ± 0.2	0.00 ± 0.00	451 ± 12	236.4 ± 3.3	4.5 ± 0.1	314.0 ± 16	268.5 ± 20.5
MGO	63	40.4 ± 0.4	4.2 ± 0.0	3165 ± 0.1	0.01 ± 0.01	563 ± 17	310.8 ± 10.7	5.6 ± 0.2	284.5 ± 21	349.8 ± 4.3
ULSD	26	36.6 ± 0.1	9.8 ± 0.0	3166 ± 0.0	0.17 ± 0.01	1455 ± 363	512.2 ± 190.3	43.7 ± 10.9	702.8 ± 263	779.3 ± 33.5
ULSD	54	40.5 ± 0.3	3.9 ± 0.0	3175 ± 0.1	0.04 ± 0.00	930 ± 30	180.0 ± 13.5	27.9 ± 0.9	675.4 ± 27	193.7 ± 3.8
ULSD	63	40.9 ± 0.1	3.6 ± 0.0	3175 ± 0.0	0.03 ± 0.00	823 ± 10	148.5 ± 14.6	24.7 ± 0.3	596.0 ± 38	153.9 ± 5.1
Auxiliary Boiler Emission Factors										
MGO	60	1.7 ± 0.0	0.0 ± 0.0	3174 ± 0.1	0.08 ± 0.01	39.5 ± 30.3	0.21 ± 0.00	0.39 ± 0.30	34.9 ± 13.0	0.36 ± 0.03
ULSD	60	2.3 ± 0.1	0.1 ± 0.1	3178 ± 0.2	0.14 ± 0.00	28.5 ± 4.2	0.42 ± 0.02	0.86 ± 0.13	15.6 ± 0.5	0.11 ± 0.04

7.4.1.2 Particulate emissions

PM2.5 mass emissions for the main and auxiliary engines, and the auxiliary boiler are shown in Figure 7-2 (a-b), whereas PM2.5 EFs are listed in Table 7-3. For both the main and auxiliary engines, PM2.5 mass emissions were higher for the ULSHFO compared to MGO and decreased with higher engine load. During low load operation the combustion temperature will be reduced, and fuel injection pressure will likely drop, causing large fuel droplets and incomplete combustion of fuel and lubrication oil fragments that contribute to more PM2.5. At higher engine load operation, the higher combustion temperatures will enhance the oxidation of particles and hydrocarbon molecules, leading to reduced PM2.5 emissions. In most cases, for the main engine, the increases in PM2.5 mass for the ULSHFO were statistically significant compared to MGO. For the main engine, PM2.5 mass levels ranged from 0.26 g/kW-hr to 0.35 g/kW-hr for ULSHFO, while for the MGO ranged from 0.20 g/kW-hr to 0.23 g/kW-hr. For the auxiliary engine, PM mass levels ranged from 0.17 g/kW-hr to 0.36 g/kW-hr, while for the MGO ranged from 0.09 g/kW-hr to 0.30 g/kW-hr. Higher PM emissions have been previously reported for slow speed two-stroke diesel engines compared to medium speed auxiliary engines, likely as a result of more unburned hydrocarbons from both the fuel and lubrication oil escaping through the cylinder during the exhaust/intake stroke, and contributing to greater PM formation (Agrawal et al., 2008; Moldanova et al., 2013; Chu-Van et al., 2018).

The higher sulfur content of ULSHFO compared to MGO, which will be oxidized to SO_2 and partly SO_3 and contribute to the total PM2.5 as sulphates, could be one of the factors for the higher PM2.5 emissions for the ULSHFO. However, the sulfate fraction in PM2.5

composition was very small, as it will be discussed later, and other fuel properties played a more dominant role in PM2.5 formation between the fuels. Even though ULSHFO had a lower calculated carbon aromaticity index (CCAI) value than MGO, which is a parameter indicating the ignition quality for residual fuels, it resulted in higher PM2.5 mass emissions than MGO, indicating that the level of fuel aromatics played a rather small role on PM2.5 formation. Properties such as density, kinematic viscosity, and carbon residue appeared to be major contributing factors to PM formation for the ULSHFO compared to MGO. The ULSHFO was more viscous, contained a higher carbon content, and thus heavier than MGO. Fuel viscosity will affect the mean drop size, penetration, and rate of evaporation of the fuel spray (Haglind, 2008). The higher viscosity of the ULSHFO likely increased the tendency to form fuel-rich pockets in the main engine combustion chamber and favored the formation of soot. Higher density fuels are typically high in carbon residue and asphaltenes (a property not measured in this study). This may result in poor combustion characteristics and higher soot formation due to the incomplete burn of the fuel, leaving unburned solid carbon material or coke residue and the generation of solid particle emissions. Additionally, the differences in PM2.5 emissions between the test fuels could also be explained by the higher amount of ash and metals in the ULSHFO compared to MGO, which contribute to the fraction of the PM2.5 originating from non-carbonaceous inorganic material (emissions of metals and elements will be discussed in the next section).

Previous works have also shown higher PM mass emissions with HFO compared to distillate fuels (Sippula et al., 2014; Wu et al., 2018; Moldanova et al., 2013; Zetterdahl et al., 2016; Browning et al., 2012). The PM2.5 mass results reported here were generally

found in considerably lower levels than previous studies, primarily due to the very low sulfur content of both fuels in this study (Agrawal et al., 2008b; Sippula et al., 2014; Murphy et al., 2009), but in similar levels to those of Gysel et al. (2017) where they utilized very low sulfur content fuels when testing a large crude carrier. The PM2.5 mass emissions from the auxiliary boiler were about 50% higher for the MGO compared to the ULSHFO at 60% engine load, at a statistically significant level. This phenomenon could be due to poor optimization of the fuel vaporization parameters for operation with distillate fuels, possibly leading to flame instability and improper combustion.

The PM2.5 composition for both fuels is compared for the three emission sources in Figure 7-3 (a-b), with Table 7-3 showing the EFs. The PM2.5 emissions for the main engine were predominantly comprised of OC (~92-94%), with a smaller contribution from EC (5-6%). OC emissions mostly originated from the partially burned heavy components of the ULSHFO (diffusion combustion), as well as from the engine lubrication oil (scavenging process) because of the large air-fuel ratio of the two-stroke engine (Ntziachristos et al., 2016; Jiang et al., 2019). For the ULSHFO, OC and EC emissions decreased with increased engine load, whereas OC and EC emissions for the MGO showed small changes with engine load. OC emissions for the ULSHFO were higher compared to MGO under all load conditions, similar to the results reported by Zetterdahl et al. (2016). The sulfur in the PM2.5 was calculated as hydrated sulfate (H_2SO_4 x 6.656 H_2O), following methods described in 40 CFR Part 1065. The contribution of hydrated sulfate to the overall PM composition was very little (~1-3%), with the ULSHFO showing higher levels of hydrate sulfate than MGO due to the higher sulfur content of this fuel. Our results agree with other

studies showing the dominance of the OC fraction in PM2.5 emissions from HFO, and more OC at low engine loads (Jiang et al., 2019; Mueller et al., 2015; Wu et al., 2018; Gysel et al., 2017).

For the auxiliary engine, PM2.5 emissions showed a decrease in the OC fraction, but an increase in the EC fraction compared to the main engine, indicating a strong dependence of EC emissions on engine type. For the ULSHFO, the EC levels were 4-7 times higher than when operated on the main engine. Huang et al. (2018) also showed substantially higher EC emissions from a medium speed engine compared to the main engine of a large bulk carrier. For both fuels, the EC and OC fractions were lower with higher engine loads. The ULSHFO showed lower EC emissions compared to MGO. Similar to the main engine, there was a small contribution of hydrated sulfate to the total PM2.5 (~0.8-2.9%). For the auxiliary boiler, the OC emissions were lower for the ULSHFO compared to MGO. The OC fraction represented 98.5% and 93% of the total PM2.5 mass for MGO and ULSHFO, respectively, while the EC fraction was less than 0.5% for the MGO and about 2% for the ULSHFO. Hydrate sulfate was a very minor fraction of the auxiliary boiler PM2.5 because of the very low sulfur content in the fuels, with the ULSHFO showing generally higher hydrate sulfate (~5%) than the main and auxiliary engines.

Black carbon emissions were higher for the ULSHFO compared to MGO for the main engine, and decreased with higher engine loads, as shown in Figure 7-2 (a-b). An exception was observed at 12% load for both fuels, where black carbon emissions showed elevated concentrations compared to the other load conditions. For the main engine, black carbon

emissions ranged from 0.0086 g/kW-hr to 0.0015 g/kW-hr. For the auxiliary engine, black carbon emissions were lower with higher engine loads, but the MGO showed higher concentrations relative to ULSHFO. Our results are consistent with previous studies that have shown lower black carbon emissions at higher engine load conditions as a consequence of higher combustion efficiencies at higher load operation (Zetterdahl et al., 2016; Moldanova et al., 2013; Petzold et al., 2010). Black carbon emission levels for the auxiliary engine were about 20 times higher than those of the main engine. Comparing the main and auxiliary engines, black carbon emissions did not show a consistent trend as a function of sulfur content, since black carbon originated from the pyrolysis of fuel droplets, and sulfur does not participate in black carbon formation pathways. However, the lower black carbon for ULSHFO in the auxiliary engine could be a result of the presence of heavy metals and metal oxides in the residual oil, which may enhance the oxidation of black carbon during combustion (Sippula et al., 2014).

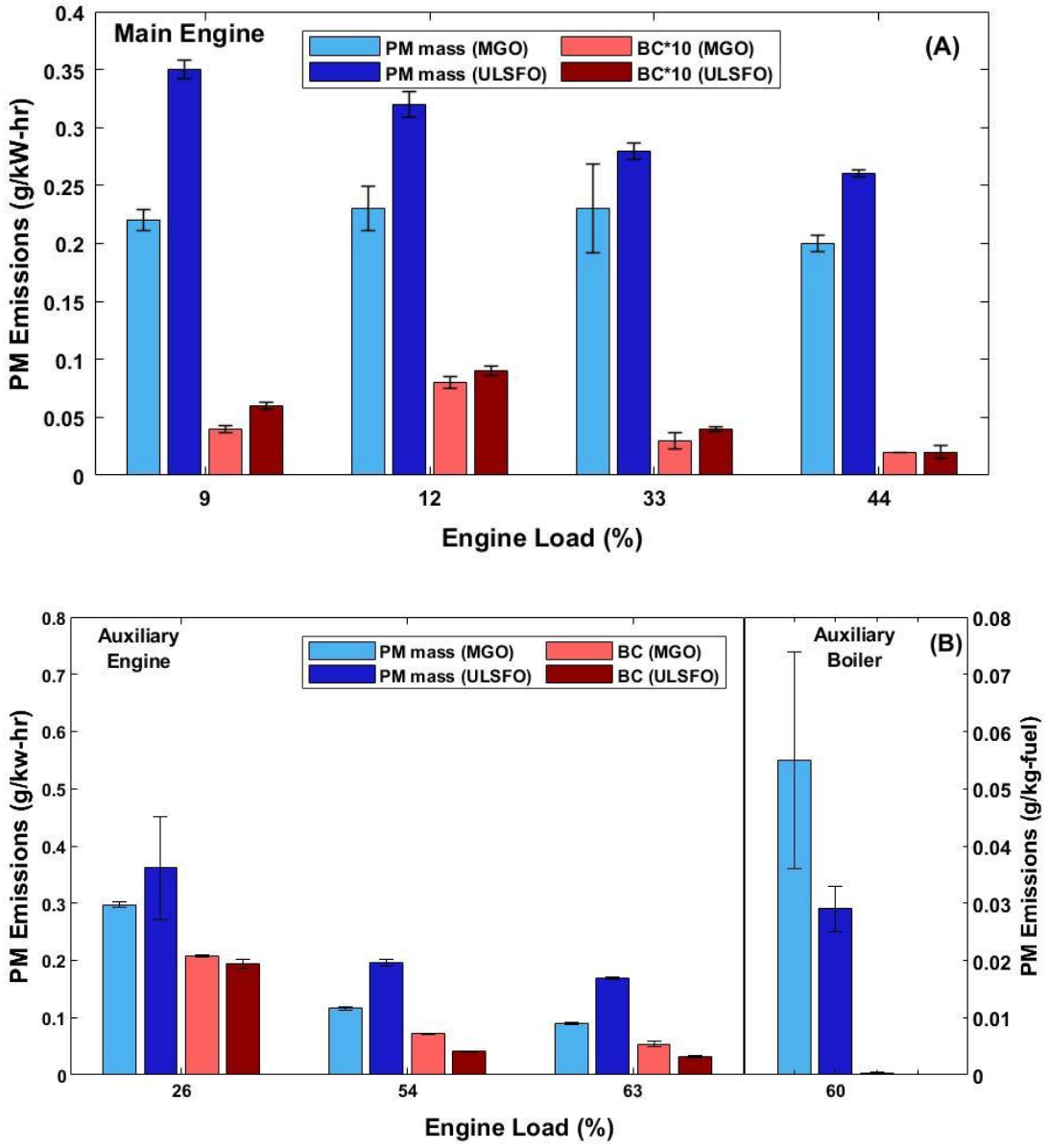

Figure 7-2 (a-b): PM mass and black carbon emissions for the main engine (top panel, A) and the auxiliary engine and boiler (bottom panel, B) for the ULSHFO and MGO

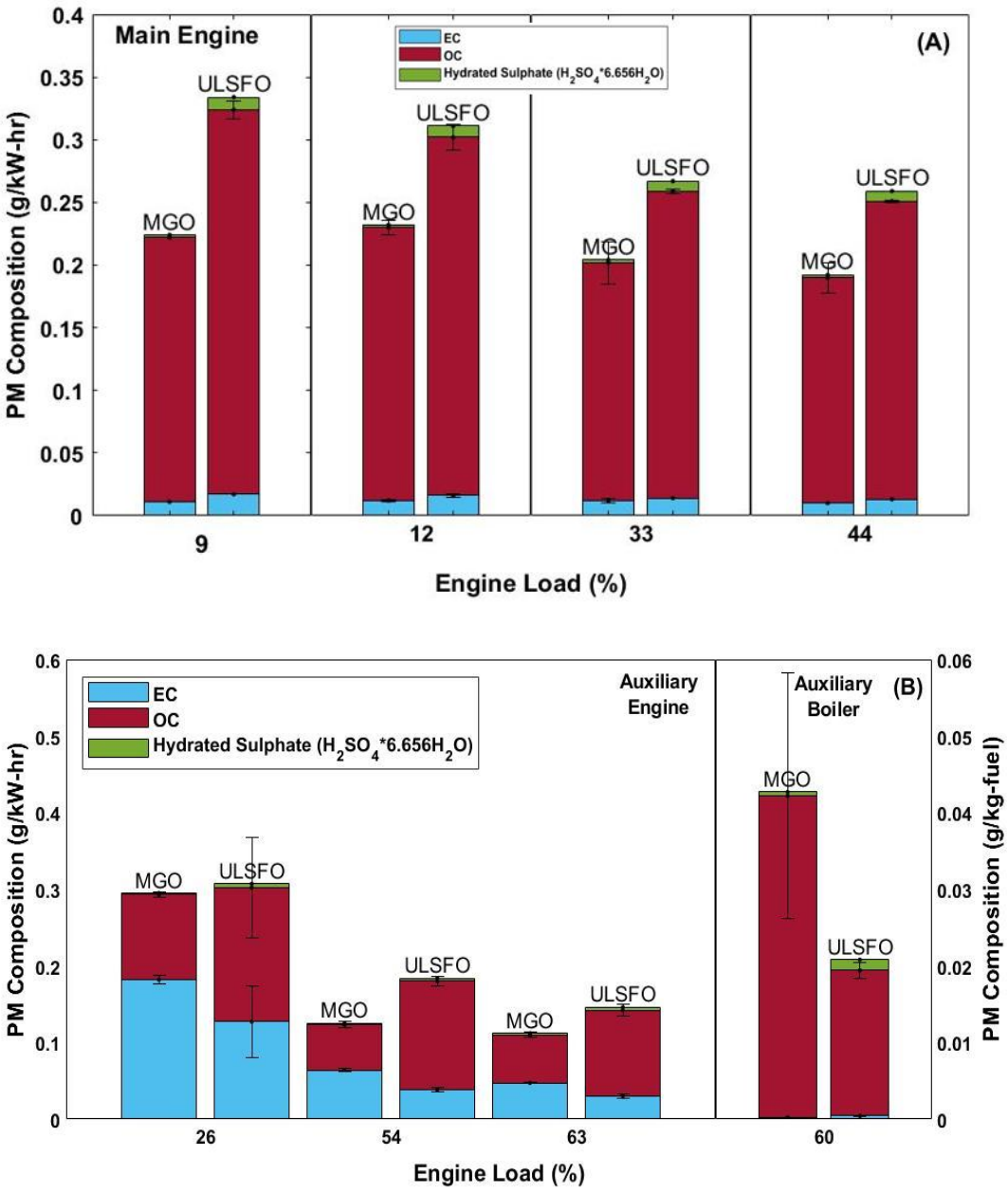

Figure 7-3 (a-b): PM composition including EC/OC fractions and hydrated sulfate for the main engine (top panel, A) and the auxiliary engine and boiler (bottom panel, B) for the ULSHFO and MGO

7.4.1.3 Inorganic composition of PM2.5 from the auxiliary boiler

Metal emissions were only measured for the auxiliary boiler for both fuels and are listed in Table 7-4. Emissions of metals from the combustion of middle distillate and heavy fuel oils are typically related to the content of metals in the fuel. Overall, metals and elements in the ULSHFO were found in much higher concentrations (about 2 times higher) than those in the MGO, which can explain the higher PM2.5 emissions for this fuel due to the contribution of inorganic species. This finding was as expected and is attributed to the crude oil refining process, where the distillation of organic hydrocarbon fractions leads to an enrichment of metals in the residual oil. Our results agree with previous studies that have shown lower metal emissions for middle distillate fuels compared to HFO (Moldanova et al., 2013; Agrawal et al., 2008a; Agrawal et al., 2008b; Zetterdahl et al., 2016; Celo et al., 2015). For both fuels, sulfur (S) was the most abundant element and approximately 2 times higher for ULSHFO relative to MGO. Sulfur is usually sourced from the fuel itself. Although both fuels had very low sulfur contents, we theorize that the larger oxygen content in the PM2.5 of ULSHFO resulted in the presence of more oxidized sulfur species in the PM2.5.

The dominant PM-bounded metals for the ULSHFO were vanadium (V), iron (Fe), and nickel (Ni), which can be linked to their presence in the crude oils. These metals belong to the group of the redox-active transition metals, which are known to induce adverse health effects by generating reacting oxygen species, leading to the oxidative damage of cellular membrane lipids, proteins-enzymes, and DNA (Jomova et al., 2012). Vanadium and Ni in ship exhaust emissions are considered as tracers of the contribution of ships to the ambient

PM2.5 emissions (Corbin et al., 2018). Sodium (Na) was only detected for the ULSHFO and is usually associated with sea water contamination. For the MGO, V was the most abundant metal, followed by lanthanoid elements such as lanthanum (La), cerium (Ce), gadolinium (Gd), and samarium (Sm). These lanthanoids were generally detected in smaller concentrations for the ULSHFO, whereas V emissions were about 10 times lower for the MGO compared to the ULSHFO. Nickel was also detected in significantly lower concentrations for the MGO (about 100 times lower), suggesting that both Ni and V emissions for the MGO were less likely to originate from the fuel and more likely to originate from the boiler parts. While metals composition in both fuels was not measured, typically very low sulfur fuels contain relatively low levels of trace elements, especially V. It is therefore reasonable to assume that the elevated V emissions for both fuels were in the form vanadium oxides (i.e., vanadium pentoxide, V_2O_5), with their levels also trending with the oxygen content in both fuels (Sarvi et al., 2011).

Emissions of trace elements including Fe, Ni, magnesium (Mg), aluminum (Al), silicon (Si), calcium (Ca), phosphorus (P), barium (Ba), and zinc (Zn) are associated with both the fuel and lubrication oil compositions (Sarvi et al., 2011; Moldanova et al., 2013, Sippula et al., 2014). Species such as Al and Si are usually present in marine fuels as a result of catalytic cracking during the crude oil refining process, in which fragments of the catalyst material entrain the refined and residue products. Other elements like Ca, Zn, P, Mg, and Ba originate from the lubrication oil, since some of these elements are part of the detergent and anti-wear additive package in lubrication oils (Sarvi et al., 2011; Zetterdahl et al., 2016; Celo et al., 2015).

Table 7-4: Trace elements and metals in the PM emissions for the tier 2 auxiliary boiler at 60% engine load for the ULSFO and MGO

Compound	MGO (mg/kg-fuel)	ULSHFO (mg/kg-fuel)	Compound	MGO (mg/kg-fuel)	ULSHFO (mg/kg-fuel)
Na	0.00 ± 0.00	0.16 ± 0.09	Y	0.02 ± 0.01	0.00 ± 0.00
Mg	0.17 ± 0.01	0.26 ± 0.01	Zr	0.00 ± 0.00	0.00 ± 0.01
Al	0.02 ± 0.02	0.28 ± 0.04	Nb	0.01 ± 0.01	0.02 ± 0.02
Si	0.18 ± 0.05	0.40 ± 0.03	Mo	0.03 ± 0.00	0.02 ± 0.02
P	0.14 ± 0.00	0.41 ± 0.05	Rh	0.12 ± 0.05	0.02 ± 0.02
S	3.65 ± 0.34	8.78 ± 1.52	Pd	0.03 ± 0.04	0.04 ± 0.01
Cl	0.03 ± 0.01	0.00 ± 0.00	Ag	0.03 ± 0.01	0.08 ± 0.02
K	0.03 ± 0.04	0.00 ± 0.00	Cd	0.08 ± 0.02	0.06 ± 0.02
Ca	0.23 ± 0.01	0.44 ± 0.07	In	0.02 ± 0.03	0.03 ± 0.04
Ti	0.07 ± 0.10	0.00 ± 0.00	Sn	0.08 ± 0.00	0.11 ± 0.08
V	0.16 ± 0.02	2.49 ± 0.49	Sb	0.01 ± 0.01	0.08 ± 0.11
Cr	0.00 ± 0.00	0.00 ± 0.00	Te	0.01 ± 0.02	0.02 ± 0.03
Mn	0.00 ± 0.00	0.00 ± 0.00	Cs	0.00 ± 0.00	0.00 ± 0.00
Fe	0.21 ± 0.02	0.79 ± 0.15	Ba	0.23 ± 0.09	0.23 ± 0.02
Co	0.00 ± 0.00	0.00 ± 0.00	La	0.27 ± 0.28	0.10 ± 0.08
Ni	0.01 ± 0.01	1.05 ± 0.19	Ce	0.30 ± 0.25	0.00 ± 0.00
Cu	0.03 ± 0.02	0.01 ± 0.01	O	0.39 ± 0.28	0.29 ± 0.17
Zn	0.06 ± 0.01	0.07 ± 0.01	Sm	0.23 ± 0.26	0.18 ± 0.09
Ga	0.00 ± 0.00	0.00 ± 0.00	Gd	0.10 ± 0.14	0.25 ± 0.18
Ge	0.00 ± 0.00	0.02 ± 0.00	Pt	0.02 ± 0.01	0.02 ± 0.01
As	0.00 ± 0.00	0.00 ± 0.00	Au	0.03 ± 0.00	0.06 ± 0.03
Se	0.03 ± 0.00	0.01 ± 0.02	Tl	0.02 ± 0.01	0.03 ± 0.01
Br	0.01 ± 0.01	0.01 ± 0.00	Pb	0.02 ± 0.01	0.01 ± 0.01
Rb	0.01 ± 0.01	0.00 ± 0.01	Bi	0.00 ± 0.00	0.01 ± 0.01
Sr	0.03 ± 0.00	0.03 ± 0.03	U	0.04 ± 0.00	0.03 ± 0.03

7.4.2 Panamax Tanker

7.4.2.1 Auxiliary Boiler Gaseous Emissions

Gaseous emissions, including NOx, CO, CO_2 and calculated SO_2, are presented in g/kg-fuel in Figure 7-4. CO_2 emissions, which are largely dependent by the boiler efficiency, and the elemental composition of the fuel, were 3171 g/kg-fuel. This is consistent with the testing of the auxiliary boiler from the Tier 2 vessel, suggesting that both boilers were tested under similar conditions. NOx emissions averaged around 3.0 g/kg-fuel for the Panamax boiler. This is slightly higher than the Tier 2 OGV auxiliary boiler tested, which is likely the result of increased combustion chamber temperatures producing higher levels of thermal NOx emissions. Fuel specific CO and SO_2 emissions were comparable to the Tier 2 boiler testing with emission factors of 0.10 and 0.96 g/kg-fuel, respectively. The SO_2 emissions were over 2 times lower for this boiler compared to the boiler tested on HFO fuel.

Carbonyl emissions are akin to the Tier 2 boiler tested on MGO with Formaldehyde emissions of 0.42 mg/kg-fuel and acetaldehyde emissions of 0.40 mg/kg-fuel. Acrolein was the most abundant carbonyl detected at 1.8 mg/kg-fuel. Acrolein is an unsaturated hydrocarbon chain that is formed when fats are heated to high temperatures and can be seen in diesel combustion (Cahill et al., 2012). Acrolein can be toxic in high concentrations and has been shown to form protein adducts that have been implicated in atherosclerosis and Alzheimer's disease (Faroon et al., 2008). Although the carbonyl emissions are

relatively small, they can still have an impact on the population near ports when the ship is hoteling.

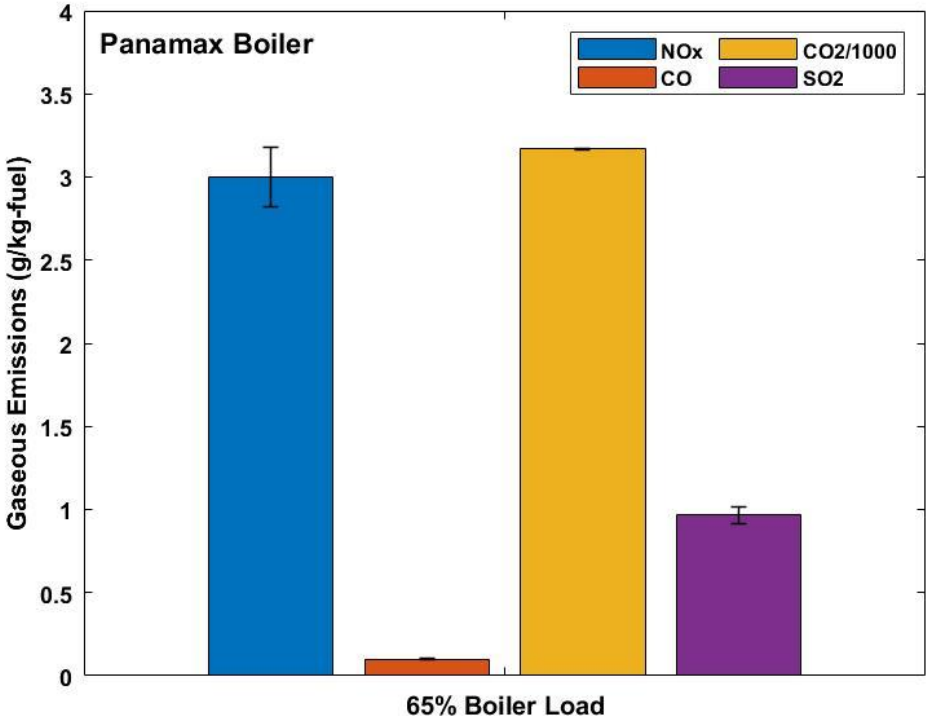

Figure 7-4: Gaseous Emission Rates of Panamax Auxiliary Boiler

Table 7-5: CO, CO_2, SO_2, and Carbonyl emissions for the auxiliary boiler as a function to engine load.

Tanker Auxiliary Boiler (g/kg-fuel)							
Fuel	Load	CO	CO_2	SO_2	Formaldehyde	Acetaldehyde	Acrolein
MGO	65%	0.10 ± 0.00	3170 ± 3.4	0.97	4.2×10^{-4}	3.9×10^{-4}	1.8×10^{-3}

7.4.2.2 Auxiliary Boiler PM2.5 Emissions

The PM2.5 mass emissions are shown in Figure 7-5 in g/kg-fuel. The PM2.5 mass emissions ranged from 0.018 to 0.025 g/kg-fuel for the Panamax boiler. This is slightly lower than the PM2.5 mass emissions from the Tier 2 OGV auxiliary boiler. The higher combustion temperatures of the larger boiler will enhance the oxidation of particles and hydrocarbon molecules, leading to reduced PM2.5 emissions. The OC fraction represented 97% of the total PM2.5 mass emissions, while the EC and Hydrated Sulphate fraction were around 2% and 1%, respectively. The low hydrated sulphate emissions are a consequence of the very low sulfur content in the fuel, as discussed previously. The EC and BC emission levels were very similar, representing around 2-3% of the total PM2.5 mass emissions. The predominance of OC emissions in the PM2.5 is consistent with the Tier 2 auxiliary boiler testing on MGO and is a result of the higher viscosity fuel.

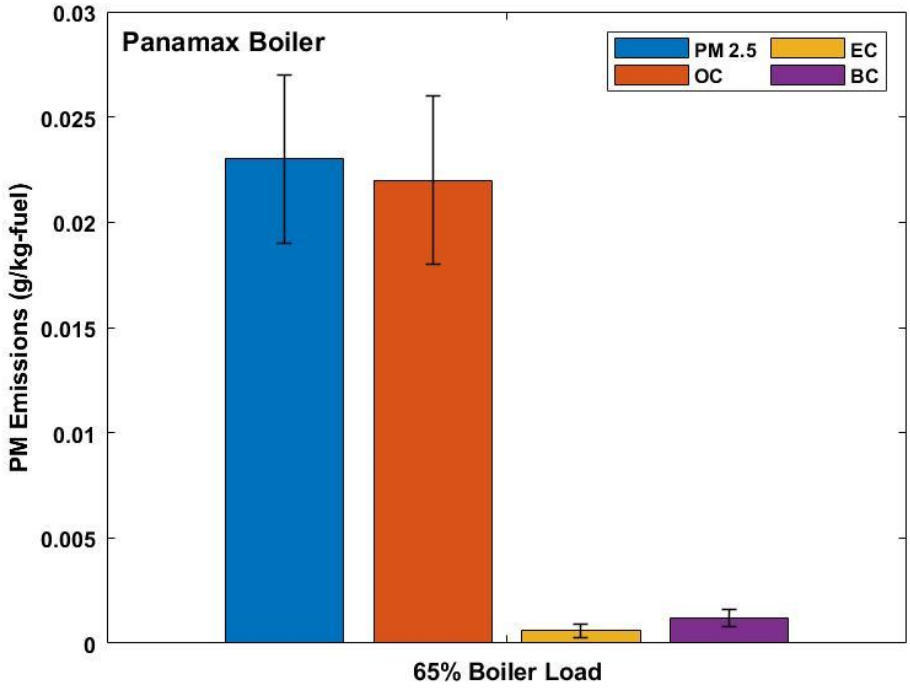

Figure 7-5: PM2.5 emissions in g/kg-fuel

7.4.2.3 Auxiliary Boiler Inorganic composition of PM2.5

The most abundant element in the PM2.5 was sulfur with an emission rate of 3.59 mg/kg-fuel. Similar sulfur emission rates between the two auxiliary boilers when tested on MGO is expected as the sulfur is derived from the fuel itself. Al and Si are also present in the PM2.5 emissions and are a result of the elements being present in the fuel itself. V and Fe were the most abundant PM-bound metals for the Panamax boiler with the emission rates ranging from 0.14 to 0.13 mg/kg-fuel, respectively. Heavy metals such as Vanadium and Nickel, which are typically considered as tracers of the contribution of ships to the ambient PM2.5 emissions, were greatly reduced when comparing to boilers tested on HFO

(Agrawal et al., 2008, Wen et al., 2018). Na was also present with emission rates nearly double that of the previous boiler testing at 0.37 mg/kg-fuel. This is typically linked to sea water contamination as discussed above. Constituents of the fuel oil such as calcium, zinc and phosphorus were also found at levels similar to previous testing (Agrawal et al., 2008). Unlike the previous boiler tested, no lanthanoids were detected in the PM.

Table 7-6: Trace elements and metals in the PM emissions for the Panamax Tanker auxiliary boiler at 65% engine load

Compound	MGO (mg/kg-fuel)	Compound	MGO (mg/kg-fuel)
Na	0.37 ± 0.14	Y	0.00 ± 0.00
Mg	0.03 ± 0.03	Zr	0.00 ± 0.00
Al	0.06 ± 0.01	Nb	0.00 ± 0.00
Si	1.04 ± 0.18	Mo	0.00 ± 0.00
P	0.07 ± 0.01	Rh	0.00 ± 0.00
S	3.59 ± 0.67	Pd	0.00 ± 0.00
Cl	0.01 ± 0.01	Ag	0.00 ± 0.00
K	0.00 ± 0.00	Cd	0.00 ± 0.00
Ca	0.18 ± 0.02	In	0.00 ± 0.00
Ti	0.00 ± 0.00	Sn	0.01 ± 0.01
V	0.14 ± 0.00	Sb	0.00 ± 0.00
Cr	0.02 ± 0.01	Te	0.00 ± 0.00
Mn	0.00 ± 0.00	Cs	0.00 ± 0.00
Fe	0.13 ± 0.04	Ba	0.00 ± 0.00
Co	0.00 ± 0.00	La	0.00 ± 0.00
Ni	0.02 ± 0.00	Ce	0.00 ± 0.00
Cu	0.01 ± 0.00	O	0.00 ± 0.00
Zn	0.06 ± 0.01	Sm	0.00 ± 0.00
Ga	0.00 ± 0.00	Gd	0.00 ± 0.00
Ge	0.00 ± 0.00	Pt	0.00 ± 0.00
As	0.00 ± 0.00	Au	0.00 ± 0.00
Se	0.00 ± 0.00	Tl	0.00 ± 0.00
Br	0.00 ± 0.00	Pb	0.00 ± 0.00
Rb	0.00 ± 0.00	Bi	0.00 ± 0.00
Sr	0.00 ± 0.00	U	0.00 ± 0.00

7.5 Conclusions

In this study, gaseous and particulate emissions were measured from a modern Tier 2 large oceangoing vessel using a low sulfur MGO and a new ultra-low sulfur HFO. Emission measurements were performed on the main and auxiliary engines, as well as on 2 different auxiliary boilers. For the auxiliary boiler testing, carbonyl emissions and the inorganic composition of PM2.5 (i.e., trace metals and elements) were investigated. The results revealed higher NOx and PM2.5 emissions for the main and auxiliary engines. For the auxiliary boiler, NOx emissions showed a statistically significant increase for the ULSHFO compared to MGO. For the larger auxiliary boiler, NOx emissions showed increases of around 50%. The higher PM2.5 emissions for the ULSHFO compared to MGO could be attributed to fuel properties such as viscosity, density, and carbon residue. Low engine load conditions generally resulted in higher NOx, PM2.5, and black carbon emissions. This finding can potentially have important environmental and health implications since marine engines are optimized for higher loads (typically 70-90%) when cruising at-sea. When at-berth or during maneuvering, the required low engine loads will contribute to total emissions and affect local air quality and associated health effects in coastal communities. Formaldehyde and acetaldehyde emissions were the major aldehydes for both auxiliary boilers. Both aldehydes are known for their deleterious health effects, which could have an important contribution to air quality on a local scale when the ship was hoteling. The results also demonstrated that auxiliary boiler PM2.5 composition was dominated by sulfur, vanadium, iron, and nickel, which were derived from the lubrication oil and fuel, and were likely present in the PM2.5 emissions in the form of metal oxides.

7.6 References

Agrawal, H., Malloy, Q.G.J., Welch, W.A., Miller, J.W., Cocker III, D.R. In-use gaseous and particulate matter emissions from a modern ocean going container vessel. Atmospheric Environment 2008a, 42, 5504-5510.

Agrawal, H., Welch, W.A., Miller, J.W., Cocker III, D.R. Emission measurements from a crude oil tanker at sea. Environ. Sci. Technol. 2008b, 42, 7098-7103.

Browning, L., Hartley, S., Bandemehr, A., Gathright, K., Miller, W. Demonstration of fuel switching on oceangoing vessels in the Gulf of Mexico. J. Air Waste Manage Assoc 2012, 62, 1093-10101.

Cahill, Thomas M., and Robert A. Okamoto. "Emissions of Acrolein and Other Aldehydes from Biodiesel-Fueled Heavy-Duty Vehicles." *Environmental Science & Technology*, vol. 46, no. 15, 2012, pp. 8382–8388., doi:10.1021/es301659u.

Celo, V., Dabel-Zlotorzynska, E., McCurdy, M. Chemical characterization of exhaust emissions from selected Canadian marine vessels: The case of trace metals and lanthanoids. Environ. Sci. Technol. 2015, 49, 5220-5226.

Chen, D., Wang, X., Li, Y., Lang, J., Zhou, Y., Guo, X., Zhao, Y. High-spatiotemporal-resolution ship emission inventory of China based on AIS data in 2014. Science of the Total Environment 2017, 609, 776-787.

Chu-Van, T., Ristovski, Z., Pourkhesalian, A.M., Rainey, T., Garaniya, V., Abbassi, R., Jahangiri, S., Enshaei, H., Kam, U.S., Kimball, R., Yang, L., Zare, A., Bartlett, H., Brown, R.J. On-board measurements of particle and gaseous emissions from a large cargo vessel at different operating conditions. Environmental Pollution 2018, 237, 832-841.

Chu-Van, T., Ristovski, Z., Pourkhesalian, A.M., Rainey, T., Garaniya, V., Abbassi, R., Kimball, R., Cong, N.L., Jahangiri, S., Brown, R.J. A comparison of particulate matter and gaseous emission factors from two large cargo vessels during manoeuvring conditions. Energy Reports 2019, 5, 1390-1398.

Cooper, D.A. Exhaust emissions from ships at berth. Atmospheric Environment 2003, 37, 3817-3830.

Corbett, J.J. Updated emissions from ocean shipping. J. Geophys. Res. 2003, 108.

Corbett, J.J., Winebrake, J., Green, E.H., Kasibhatia, P., Eyring, V., Lauer, A. Mortality from ship emissions: a global assessment. Environ. Sci. Technol. 2007, 41, 8512-8518.

Corbin, J.C., Mensah, A.A., Pieber, S.M., Orasche, J., Michalke, B., Zanatta, M., Czech, H., Massabo, D., Buatier de Mongeot, F., Mennucci, C., El Haddad, I., Kumar, N.K.,

Stengel, B., Huang, Y., Zimmermann, R., Prevot, A.S.H., Gysel, M. Trace metals in soot and PM2.5 from heavy-fuel-oil combustion in a marine engine. Environ. Sci. Technol. 2018, 52, 6714-6722.

Eyring, V., Isaksen, I.S.A., Berntsen, T., Collins, W.J., Corbett, J.J., Endresen, O., Grainger, R.G., Moldanova, J., Schlager, H., Stevenson, D.S. Transport impacts on atmosphere and climate: Shipping. Atmospheric Environment 2010, 44, 4735-4771.

Faroon, O, et al. "Acrolein Environmental Levels and Potential for Human Exposure." *Toxicology and Industrial Health*, vol. 24, no. 8, 2008, pp. 543–564., doi:10.1177/0748233708098124.

Gysel, N.R., Welch, W.A., Johnson, K., Miller W., Cocker, D.R. Detailed analysis of criteria and particle emissions from a very large crude carrier using a novel ECA fuel. Environ. Sci. Technol. 2017, 51, 1868-1875.

Haglind, F. A review on the use of gas and steam turbine combined cycles as prime movers for large ships. Part III: Fuels and emissions. Energy Conversion and Management 2008, 49, 3476-3482.

Hountalas, D.T., Papagiannakis, R.G., Zovanos, D., Antonopoulos A. Comparative evaluation of various methodologies to account for the effect of load variation during cylinder pressure measurement of large two-stroke diesel engines. Applied Energy 2014, 113, 1027-1042.

Huang, C., Hu, Q., Wang, H., Qiao, L., Jing, S., Wang, H., Zhou, M., Zhu, S., Ma, Y., Lou, S., Li, L., Tao, S., Li, Y., Lou, D. Emission factors of particulate and gaseous compounds from a large cargo vessel operated under real-world conditions. Environmental Pollution 2018, 242, 667-674.

Hulskotte, J.H.J., Denier van der Gon, H.A.C. Fuel consumption and associated emissions from seagoing ships at berth derived from an on-board survey. Atmospheric Environment 2010, 44, 1229-1236.

Jiang, H., Wu, G., Li, T., He, P., Chen, R. Characteristics of particulate matter emissions from a low-speed marine diesel engine at various loads. Environ. Sci. Technol. 2019, 53, 11552-11559.

Jomova, K., Baros, S., Valko, M. Redox active metal-induced oxidative stress in biological systems. Transition Met Chem 2012, 37, 127-134.

Khan. Y.M., Agrawal, H., Ranganathan, S., Welch, W.A., Miller, J.W., Cocker, D.R. Greenhouse gas and criteria emission benefits through reduction of vessel speed at sea. Environ. Sci. Technol. 2012, 46, 12600-12607

Khan, M.Y., Giordano, M., Gutierrez, J., Welch, W.A., Asa-Awuku, A., Miller, J.W., Cocker, D.R. Benefits of two mitigation strategies for container vessels: cleaner engines and cleaner fuels. Environ. Sci. Technol. 2012, 46, 5049-5056.

Lamas, M.I., Rodriguez, C.G. Emissions from marine engines and NOx reduction methods. Journal of Maritime Research 2012, IX, 77-82.

Luecken, D.J., Hutzell, W.T., Strum, M.L., Pouliot, G.A. Regional sources of atmospheric formaldehyde and acetaldehyde, and implications for atmospheric modeling. Atmospheric Environment 2012, 47, 477-490.

Moldanova, J., Fridell, E., Winnes, H., Holmin-Fridell, S., Boman, J., Jedynska, A., Tishkova, V., Demirdjian, B., Joulie, S., Bladt, H., Ivleva, N.P., Niessner, R. Physical and chemical characterization of PM emissions from two ships operating in European emission control areas. Atmos. Meas. Tech. 2013, 6, 3577-3596.

Mueller, L., Jakobi, G., Czech, H., Stengel B., Orasche, J., Arteaga-Salas, J.M., Karg, E., Elsasser, M., Sippula, O., Streibel, T., Slowik, J.G., Prevot, A.S.H., Jokiniemi, J., Rabe, R., Harndorf, H., Michalke, B., Schnelle-Kreis, J., Zimmermann, R. Characteristics and temporal evolution of particulate emissions from ship diesel engine. Applied Energy 2015, 155, 204-217.

Murphy, S. Agrawal, H., Sorooshian, A., Padro, L.T., Gates, H., Hersey, S., Welch, W.A., Jung, H., Miller, J.W., Cocker, D.R., Nenes, A., Jonsson, H.H., Flagan, R.C., Seinfeld, J.H. Comprehensive simultaneous shipboard and airborne characterization of exhaust from a modern container ship at sea. Environ. Sci. Technol. 2009, 43, 4626-4640.

Ntziachristos, L., Saukko, E., Lehtoranta, K., Ronkko, T., Timonen, H., Simonen, P., Karjalainen, P. Keskinen, J. Particle emissions characterization from a medium-speed marine diesel engine with two fuels at different sampling conditions. Fuel 2016, 186, 456-465.

Petzold, A.; Hasselbach, J.; Lauer, O.; Baumann, R.; Franke, K.; Gurk, C.; Schlager, H.; Weingartner, E. Experimental studies on particle emissions from cruising ship, their characteristic properties, transformation and atmospheric lifetime in the marine boundary layer Atmos. Chem. Phys. 2008, 8, 2387– 2403

Petzold, A., Weingartner, E., Hasselbach, J., Lauer, P., Kurok, C., Fleischer, F. Physical properties, chemical composition, and cloud forming potential of particulate emissions from a marine diesel engine at various load conditions. Environ. Sci. Technol. 2010, 44, 3800-3805.

Reda, A.A., Schnelle-Kreis, J., Orasche, J., Abbaszade, G., Lintelmann, J., Arteaga-Salas, J.M., Stengel, B., Rabe, R., Harndorf, H., Sippula, O., Streibel, T., Zimmermann, R. Gas phase carbonyl compounds in ship emissions: differences between diesel fuel and heavy fuel oil operation. Atmospheric Environment 2015, 112, 370-380.

Sarvi, A., Lyyranen, J., Jokiniemi, J., Zevenhoven, R. Particulate emissions from large-scale medium-speed diesel engines: 2. Chemical composition. Fuel Processing Technology 2011, 92, 2116-2122.

Sippula, O., Stengel, B., Sklorz, M., Streibel, T., Rabe, R., Orasche, J., Lintelmann, J., Michalke, B., Abbaszade, G., Radischat, C., Groger, T., Schnelle-Kreis, J., Harndorf, H., Zimmermann, R. Particle emissions from a marine engine: Chemical composition and aromatic emission profiles under various operating conditions. Environ. Sci. Technol. 2014, 48, 11721-11729.

Starcrest Consulting Group, LLC. Port of Los Angeles inventory of air emissions-2010. Starcrest, 2011.

UNCTAD, Review of Maritime Transport 2017

Viana, M., Amato, F., Alastuey, A., Querol, X., Moreno, T., Dos Santos, S.G., Herce, M.D., Fernandez-Patier, R. Chemical tracers of particulate emissions from commercial shipping. Environ. Sci. Technol. 2009, 43, 7472-7477.

Wen, Jie, et al. "PM2.5 Source Profiles and Relative Heavy Metal Risk of Ship Emissions: Source Samples from Diverse Ships, Engines, and Navigation Processes." *Atmospheric Environment*, vol. 191, 2018, pp. 55–63., doi:10.1016/j.atmosenv.2018.07.038.

Winnes, H., Styhre, L., Fridell, E. Reducing GHG emissions from ships in port areas. Research in Transportation Business & Management 2015, 17, 73-82.

Wu, D., Li, Q., Ding, X., Sun, J., Li, D., Fu, H., Teich, M., Ye, X., Chen, J. Primary particulate matter emitted from heavy fuel and diesel oil combustion in a typical container ship: characteristics and toxicity. Environ. Sci. Technol. 2018, 52, 12943-12951.

Yau, P.S., Lee, S.C., Corbett, J.J., Wang, C., Cheng, Y., Ho, K.F. Estimation of exhaust emission from ocean-going vessels in Hong Kong. Science of the Total Environment 2012, 431, 299-306.

Zenczak, W. The possibilities of limiting the toxic compound emission from diesel engines and boilers during ship's stay in harbour. Scientific Journals 2013, 36, 190-195.

Zetterdahl, M., Moldanova, J., Pei X., Pathak, R.K., Demirdjian, B. Impact of the 0.1% fuel sulfur content limit in SECA on particle and gaseous emissions from marine vessels. Atmospheric Environment 2016, 145, 338-345.

Zhang, F., Chen, Y., Tian, C., Lou, D., Li, J., Zhang, G., Matthias, V. Emissions factors for gaseous and particulate pollutants from offshore diesel engine vessels in China. Atmos. Chem. Phys. 2016, 16, 6319-6334.

8. Conclusions

The main objective of chapters two to three in this research was the evaluate the PM, Gaseous, and toxic emissions from alternative fuel sources, namely HVO and HVO biodiesel fuel blends, as well as the impact of combustion. Chapter two focused on the combustion and pollutant formation of neat HVO fuel in a light duty diesel engine. Chapter 3 focused on the pollutant formation and toxic emissions of HVO and HVO biodiesel blends in on-road and off-road heavy duty diesel engines. Chapters four to five in this research was to investigate the emissions of light duty and heavy-duty vehicles during real world driving conditions. Chapter four focused on the emissions of GDI vehicles and the reduction efficiencies of GPFs. Chapter six investigated the possibility of implementing new stringent standards on SORDEs. The objective of chapter seven was to evaluate the emissions benefits of newer low sulfur fuels use in OGVs.

Chapter 2 demonstrated the emissions benefits of utilizing HVO, a second-generation biodiesel fuel source, in a light duty diesel engine. It was found that the use of HVO can provide NOx, PM, and PN reductions over standard driving cycles. During high load conditions the use of HVO showed interesting results including a double pilot injection and increased fuel injection evident by the increase in CO_2 emissions. The lower volumetric energy content of HVO would mean that more fuel would need to be injected at high loads to keep up with the power demand. In general however, the reduction in gaseous emissions were slight due to the pilot injection mitigating the fuel effects seen by other researchers.

Chapter 3 evaluated the emission benefits of neat HVO and HVO biodiesel fuel blends in one on-road heavy-duty diesel engine and one off-road heavy-duty diesel engine. Benefits in PM, PN, and soot were seen with neat HVO and increase biodiesel blends for both engines. Gaseous emissions of CO, and THC also showed decreases for HVO and HVO biodiesel fuel blends. The on-road engine benefits were not as pronounced do to the DPF and DOC aftertreatment systems mitigating some of the fuel effects. NOx emissions generally decreased with neat HVO, however NOx emissions showed no changes or increases when utilizing HVO biodiesel fuel blends. Toxic emissions such as carbonyls, BTEX, PAHs, and metals generally showed decrease with increase biodiesel in the fuel source.

Chapter four examined the gaseous and PM emissions from 3 GDI vehicles operating in real world conditions. Two of the three vehicles were retrofitted with a catalyzed GPF after initial testing to investigate the potential benefits of using GPFs for PM control in GDI engines. PM emissions were highest during urban driving routes which can have important implications of the exposure for densely populated areas. The use of a catalyzed GPF provided PM and PN reductions under all driving conditions. A NOx benefit was also seen with the use of a catalyzed GPF due to the increase in catalytic surface area. Generally, no CO_2 impacts were seen with the use of a catalyzed GPF suggesting that wide-spread adoption would not affect fuel economy.

Chapter five compared gaseous emissions measurements of 50 heavy-duty vehicles from 5 different vocations during typically daily operation. Emission measurements were made

on school buses, transit buses, refuse haulers, goods movement trucks, and delivery trucks operating on diesel with and without and SCR, CNG, LPG, and diesel-electric hybrid powertrains. SCR operation is limited by exhaust temperatures which can be difficult to achieve during real world driving conditions. As such the newer technologies such as, CNG, LPG, and diesel-electric hybrids showed NOx emission benefits compared to diesel vehicles. All vehicles tested showed on average higher in use NOx emissions compared to the certification limits. This has important implications as more improvements need to be made for future NOx emission standards to be fully realized.

Chapter 6 evaluated the efficiency, durability, and cost benefit of implementing regulations that require the use of SCRs and DPFs on off-road engines under 75 hp. Emission standards for SORDEs have not been updated since 2004 and results of this study suggest that it is now feasible for the emission standards to be updated and require aftertreatment systems on all SORDEs. No significant deterioration was seen on the aftertreatment systems after 1,000 hours of in use testing with some aftertreatment systems showing additional benefits during post durability tests. DPFs showed PM reductions greater than 98% while SCR showed reductions in NOx ranging from 26%-91% dependent on the cycle and aftertreatment temperatures. Enforcing new regulations could potentially provide a PM reduction of 3.8% and a NOx reduction of 8.8-13.7% for the total off-road equipment emissions inventory in California. The cost benefit analysis showed the costs of impleting a DPF would cost $15.29 per pound of PM saved while the cost of implementing a SCR would cost $0.38 to $0.59 per pound of NOx saved.

Chapter seven investigated the emissions from 2 OGVs utilizing new ULSHFO and distillate fuel MGO. Emissions measurements were made on the main engine, auxiliary engine, and auxiliary boiler of a tier 2 container vessel running on ULSHFO and MGO, as well as the auxiliary boiler of a panama tanker operating on MGO. The results suggest that implementation of newer fuels would lead to NOx, SO_2, and PM emissions benefits compared to older high sulfur heavy fuel oils. MGO provided additional NOx, SO2, and PM emissions benefits compared to ULSHFO in general which could be attributed to fuel properties such as viscosity, density, and carbon residue. Emissions generally increased with decreasing engine loads which can have many implications on communities near ports since engine are operated at low loads while the vessel is at berth or hoteling.